“Investigation of The Effects of Inorganic Nitrate on Blood Pressure-dependent and -independent Cardiac Dysfunction”

LORNA CLAIRE GEE

Queen Mary, University of London

Submitted in partial fulfilment of the requirements of the Degree of Doctor of Philosophy

Statement of Originality

I, Lorna Claire Gee, confirm that the research included within this thesis is my own work or that where it has been carried out in collaboration with, or supported by others, that this is duly acknowledged below and my contribution indicated. Previously published material is also acknowledged below.

I attest that I have exercised reasonable care to ensure that the work is original, and does not to the best of my knowledge break any UK law, infringe any third party's copyright or other Intellectual Property Right, or contain any confidential material.

I accept that the College has the right to use plagiarism detection software to check the electronic version of the thesis.

I confirm that this thesis has not been previously submitted for the award of a degree by this or any other university.

Signature: LORNA GEE
Date: 05/12/19

Details of collaboration and publications:

Gee, L.C. & Ahluwalia, A., 2016. Dietary Nitrate Lowers Blood Pressure: Epidemiological, Pre-clinical Experimental and Clinical Trial Evidence. *Current hypertension reports*, 18(2), pp.2224–14.

Gee, L.C. et al., Under review - submitted for publication
Inorganic nitrate attenuates BP-dependent and independent cardiac dysfunction in mice and reduces oxidative stress.

Funding:

This work was supported by **The British Heart Foundation.**

Grant Number - **MCPG1J4R.**

Abstract

Introduction: Constitutive NO (synthesized by eNOS) is an endogenous vasodilator and independent modulator of cardiac hypertrophy. Hypertension accounts for approximately 50% of morbidity, alongside other risk factors such as ischaemic heart disease and obesity. Inorganic nitrate, through sequential reduction *in vivo* to NO, exerts potent BP lowering effects. However, its effects on cardiac hypertrophy/HF independent of BP lowering remain unknown. Thus, we investigated the effects of dietary nitrate in BP-dependent (ANGII) and independent (isoprenaline) models of cardiac dysfunction.

Methods: C57Bl6 mice underwent minipump infusion of ANGII or isoprenaline and received 15 mM KNO_3 or KCl drinking water. Echocardiographic, BP telemetry, organ bath, histological and molecular assessments were made. Furthermore, as some benefits of nitrate appeared dependent on xanthine oxidoreductase (XOR), *Xdh* knockout (KO) mice underwent cardiovascular phenotyping with and without ANGII infusion, to further investigate the influence of XOR in health and disease.

Results: Inorganic nitrate attenuated ANGII-induced endothelial dysfunction, hypertension, left ventricular (LV) hypertrophy and fibrosis, and reduced H_2O_2 and superoxide generation, whilst increasing nitrite reductase capacity. Furthermore, nitrate prevented isoprenaline-induced decline in ejection fraction, reduced cardiac fibrosis and superoxide generation.

Increased physiological BP, and trends towards increased LV hypertrophy and reduced ejection fraction were observed in *Xdh* Heterozygous KO (Het) mice compared to littermate controls. Despite higher baseline BPs, *Xdh* Hets were protected from ANGII-induced hypertension and associated cardiac dysfunction.

Conclusions: Inorganic nitrate improved cardiac remodelling both directly (by attenuating fibrosis and reducing superoxide generation) and indirectly (through BP-lowering), demonstrating that dietary nitrate may offer a therapeutic option for BP-dependent and -independent HF. Furthermore, XOR helped maintain physiological BP in wildtype mice (as a nitrite reductase), but upon ANGII infusion was detrimental (as a superoxide generator). *Xdh* Hets were protected from further BP increases and resulting cardiac dysfunction, highlighting the complexity of XOR's role in health and disease.

Acknowledgements

Without the funding of the British Heart Foundation and Professor Ahluwalia's extensive knowledge and lab resources this project would not have been possible. For the weekly meetings, encouragement when things were challenging, and support through raising a family whilst completing a PhD there must be a huge thank-you! Everyone in the Ahluwalia lab who have come and gone during my time there have added so much to the experience (and most at some point have helped with feeding my seemingly endless supply of mice), so thank-you!

However, special thanks must go to the ever-present Rayomand Khambata (my secondary supervisor and patient teacher with regards to telemetry surgery and organ bath) and Gianmichelle Massimo (who has been especially important in helping pull this project together with his input regarding molecular assays).

Heartfelt thanks also go to Sven van Eijl (lab manager and ozone chemiluminescence extraordinaire), Alexander Hamers (fellow PhD student and font of RT-PCR knowledge), Federica Filomena (fellow PhD student and long-suffering mouse feeding and tail cuff companion), Alison Goddard and Daniel Fernandes who helped with Langendorff and organ bath experiments at times when I had to juggle tissue harvesting and other assays, and Krishnaraj Rathod for helping start me off with XO and nitrite reductase assays.

My final and most heartfelt acknowledgement must go to my amazing family who have supported me through this – my patient and supportive husband (Matt), daughter (Zoey) and parents who have made personal and financial sacrifices to help get me to the point of submitting my thesis. Without their encouragement I would not have got to where I am today, and this achievement would not mean nearly as much.

Table of Contents

List of Tables

Abbreviations

Abbreviation	
ANGII	Angiotensin II
BP	Blood pressure
BP probes	Blood pressure telemetry probes
d	Diastole
DBP	Diastolic blood pressure
DMSO	Dimethyl sulfoxide
HBSS	Hank's balanced salt solution
Het	Heterozygote
HFpEF	Heart failure with preserved ejection fraction
HFrEF	Heart failure with reduced ejection fraction
HR	Heart rate
HW:BW	Heart weight (mg): body weight (g)
IP	Intraperitoneally
IVS	Intraventricular septum diameter
KCl	Potassium chloride
KNO_3	Potassium nitrate
KO	Knockout
LECL	Lucigenin-enhanced chemiluminescence
LV	Left ventricle
LV:BW	Left ventricle weight (mg): body weight (g)
LVID	Left ventricle internal dimension
LVM	Left ventricular mass
LVPW	Left ventricle posterior wall diameter
MAP	Mean arterial blood pressure
MQ water	Milli-Q filtered water
NADH	Nicotinamide adenine dinucleotide
NADPH	Nicotinamide adenine dinucleotide phosphate
PBS	phosphate buffered saline
PP	Pulse pressure
RAAS	Renin-angiotensin-aldosterone system
ROS	Reactive oxygen species
RT-PCR	Real-time quantitative reverse transcription–polymerase chain reaction
s	Systole
SBP	Systolic blood pressure
SC	Subcutaneously
SHR	Spontaneously hypertensive rat
SNP	Sodium nitroprusside
TAC	Trans-aortic Constriction
WT	Wildtype
XOR	Xanthine oxidoreductase

Reagent and Equipment Sources

Equipment/Reagent	Source
(R)-(-)-Phenylepherine Hydrochloride	Sigma Aldrich®, UK Product code: P6126-50G
0.2 ml Thermo-tubes	Thermo Scientific, UK Product code: AB-0621
10 mM dNTP Mix	Life Technologies, UK Product 18427-013
4-0 coated VICRYL™ resorbable sutures	ETHICON*, UK Product code: W9443
5-0 Sofsilk™ non-resorbable sutures	COVIDEN™, UK Product code: S-182
7900 HT Realtime PCR System	Applied Biosystems®, Life Technologies, UK Product code: 4329001
96-well Cellstar tissue culture-treated plate	Greiner Bio-One, UK Product code: 655098
Absolute qPCR SYBR green ROX mix	Thermo Scientific Abgene, UK Product code: PCR-575-020V
Acetic acid 100%	AnalaR NORMAPUR, VWR, UK Product code: 20104.334
Acetylcholine chloride	Sigma Aldrich®, UK Product code: A6625-25G
AEBSF	Sigma Aldrich®, UK Product code: A76307
Allopurinol	Sigma Aldrich®, UK Product code: A8003
Angiotensin II human	Sigma Aldrich®, UK Product code: A9525
Antipain	Sigma Aldrich®, UK Product code: A6191
Aprotinin	Sigma Aldrich®, UK Product code: A1153
Aqua Gel® Lubricating Gel	CIVCO Medical Solutions, USA Product code: 610-920
Ascorbic Acid	Sigma Aldrich®, UK Product code: A2174-100G
Benzamidine	Sigma Aldrich®, UK Product code: B6506
Bradykinin	Bachem, Switzerland Product code: H1970
C57Bl6 mice	Charles River, UK
$CaCl_2$	VWR - AVS TITRINORM, UK Product code:190464K
cGMP enzyme immunoassay	GE Healthcare, UK Product Code RPN226
CODA 2 animal machine	Kent Scientific Corporation, US
Cryolys	Bertin Technologies, FR, Product code: EQ05068.200.RD000.0
Dimethyl sulfoxide	Sigma Aldrich®, UK Product code: 41640-500ML
Diphenyleneiodonium	Sigma Aldrich®, UK Product code: D2926
Febuxostat	Cambridge Bioscience, UK Product code: F1607
First Strand Buffer, 2 µl 0.1 M DTT, 1 ul M-MLV	Life Technologies, UK Product code: 28025-013
Gluteraldehyde solution	Fluka Analytical, Sigma Aldrich®, UK Product code: 49629-250ML
HBSS	Sigma Aldrich®, UK Product code: 55037C
Heat box	Clinipath Ltd, UK

Rectal thermometer heating pad	Physitemp Instruments Inc., USA Model: TCAT-2LV
HEPES	Sigma Aldrich®, UK Product code: H3375-100G
Hydrex® Pink	ECOLAB, UK
Hydrochloric acid	Sigma Aldrich®, UK Product code: 30721-1L
IBMX (3-Isobutyl-1-methylxanthine)	Sigma Aldrich®, UK Product code: I5879
Isoprenaline Hydrochloride	Sigma® Life Science, UK Product code: I5627-25G
Krebs ringer solution	Sigma Aldrich®, UK Product code: K0507
Langendorff krebs filter paper	Fischer Scientific, UK Product code: 1841-047
Leupeptin	Sigma Aldrich®, UK Product code: L0649
Lucigenin	Cambridge Bioscience, UK Product code: 14872
L-NAME (N-nitro L-arginine methyl ester hydrochloride)	Sigma Aldrich®, UK Product code: N5751-25G
MILLEX® GP 0.22µm Filter	MERCK MILLIPORE, UK Product code: SLGP033RS
Milli-Q purified water	Merck Millipore filtration system, UK
Molecular grade H_2O	5PRIME, UK Product code: 2500010
Mouse restrainers	Harvard Apparatus, UK Product code: 340012
NADH	Sigma Aldrich®, UK Product code: N8129
NADPH	Sigma Aldrich®, UK Product code: N1630
NanoDrop ND-1000 UV/Vis Spectrophotometer	NanoDrop Technologies, US. Serial no. 7334
Osmotic minipumps	ALZET® Osmotic Pumps, 1004 model, Durect Corporation, USA
Pepstatin A	Sigma Aldrich®, UK Product code: P5318
Perkin Elmer Wallac 1420 Victor2 Plate Reader	Perkin Elmer, USA
Phosphate buffered saline	Sigma Aldrich®, UK Product code: P4417-100TAB
Pierce® BCA Protein Assay Kit	Thermofisher, UK Product code: 23225
Potassium chloride	Sigma Aldrich®, UK Product code: P9333-500G
Potassium iodide	Sigma Aldrich®, UK Product code: 22, 194-5
Potassium nitrate	Sigma Aldrich®, UK Product code: 12648-1KG
Precellys®	Bertin Technologies, FR, Product code: EQ03119.200.RD000.0
Precellys® CK28 (2ml) Tubes	Bertin Technologies, FR, Product code: KT03961-1-002.2
Press'n Seal®	GLAD®, USA
Protein LoBind Tube	Eppendorf, UK Product code: C152107M
PTC-225 Peltier Tetrad Thermal Cycler	MJ Research, US
Random Hexamers	Life Technologies, UK Product code: 48190-011

Redux Crème	Parker Laboratories, Inc., USA Product code: 66-04
RNase OUT Recombinant Ribonuclease Inhibitor	Life Technologies, UK. Product code: 10777-019
Rneasy® Fibrous Tissue Minikit	Qiagen Ltd, UK Product code: 74704
RT-PCR Primers	Thermofisher, UK
Saturated aqueous picric acid	Sigma Aldrich®, UK Product code: P6744
SDS 2.3 Software	Applied Biosystems®, Life Technologies, UK
Sievers 280i Nitric Oxide Analyzer	Sievers, USA
Sirius red (Direct Red 80)	Sigma Aldrich®, UK Product code: 365548
Slide scanner (NanoZoomer)	Hamamatsu, Japan
Sodium citrate	Sigma Aldrich®, UK Product code: S1804-500G
Sodium fluoride	Sigma Aldrich®, UK Product code: 1614002-1G
Sodium hydroxide	Sigma Aldrich®, UK Product code: S5881-500G
Sodium nitrate	Sigma Aldrich®, UK Product code: S8170-250G
Sodium nitrite	Sigma Aldrich®, UK Product code: S2252-500G
Sodium nitroprusside dihydrate	Sigma Aldrich®, UK Product code: 71778:25G
Sodium orthovanadate	Sigma Aldrich®, UK Product code: S6508-10G
Spermine NONOate	CAYMAN CHEMICAL COMPANY, USA Product code: CAY82150
Sterile saline	Baxter, UK Product code: FE1307
Sterile saline vehicle	B. BRAUN, UK Product code: 3627667
TA11PA-C10 radiotelemetric probes	Data Sciences International, USA
U46619	CAYMAN CHEMICAL COMPANY, USA Product code: CAY16450
Vanadium (III) chloride	Sigma Aldrich®, UK Product code: 208272-25G
Veet® For Men Hair Removal Gel Cream	Veet® (available from Boots, UK)
Vevo 770 imaging system	FujiFilm VisualSonics Inc., Netherlands
Vevo mouse-handling platform	FujiFilm VisualSonics Inc., Netherlands
Vivaspin 500 filter eppendorfs	Sartorius stedim biotech, SA, Vivaspin 500; 3,000 MWCO PES
Xanthine	Sigma Aldrich®, UK Product code: X7375

CHAPTER ONE -

Introduction

1. CHAPTER ONE - Introduction

1.1. Heart failure epidemiology

Heart failure is an incurable, lifelong condition that is a significant burden on medical resources in both developed and developing countries (Callender et al. 2014). In the UK alone, nearly one million individuals are currently estimated to be living with heart failure (NICE 2018), with approximately 200,000 new diagnoses made each year (Conrad et al. 2018). An individual's condition can deteriorate rapidly following diagnosis, with data suggesting that approximately 50% of patients diagnosed with heart failure can be expected to die within 5 years (Mozaffarian et al. 2016).

1.2. Risk factors for heart failure development

1.2.1. Hypertension and heart failure risk

It has long been recognised that the two main predisposing factors for heart failure development are coronary heart disease and chronic hypertension (Ho et al. 1993). Chronic hypertension increases an individual's risk of developing heart failure 2-3 fold (Levy et al. 1996) and is the most common risk factor shared by patients with heart failure. In hypertensive individuals, the heart initially adapts to increased load by increasing heart muscle mass, particularly by increasing wall thickness of the left ventricle (LV). This is thought to occur in order to maintain healthy cardiac function and minimize wall stress (compensated growth). However, if blood pressure (BP), and therefore cardiovascular load and wall stress, remain increased cardiac hypertrophy is likely to become accompanied by heart dilation, increased interstitial fibrosis and myocyte death (Levy et al. 1990; Cohn et al. 1997; Bernardo et al. 2010). This ultimately results in the onset of progressive cardiac dysfunction, with stiffening of the heart walls, reduced contractile function and reduced LV ejection fraction (Levy et al. 1987; Levy et al. 1990; Drazner et al. 2004; de Simone et al. 2008).

One example of the impact of hypertension on heart failure risk is evidence demonstrating that at the age of 30, individuals with raised BP (i.e. ≥140/90 mmHg) have a lifetime risk of heart failure of 63% compared to 46% for normotensive 30-year olds. The at risk individual develops cardiovascular disease, on average, 5 years earlier, with heart failure and stable angina responsible for the largest proportion of life years lost (Rapsomaniki et al. 2014). Hypertension is currently estimated to affect 27% people in

the UK, with more than half of them not receiving effective treatment (BHF, 2019). Such high levels of incidence have caused some to refer to it as an 'epidemic' (Lloyd-Sherlock et al. 2014).

With estimates that hypertension precedes heart failure in 66-90% of cases (Chobanian et al. 2003; Dunlay et al. 2009), hypertension is a significant risk factor for death caused by heart failure, including its complications such as arrhythmias and sudden death (Rapsomaniki et al. 2014). Meta-analyses have shown that controlling high BP effectively, it is possible to reduce one's risk of developing heart failure by ≈52% (Meredith & Ostergren 2006). The SPRINT study has further emphasised the importance of BP lowering, as the degree to which BP could be lowered (even below traditional target BP of <140mmHg) had a significant effect on the incidence of heart failure in this population. In an 'intensive' treatment group with target BP <120 mmHg, individuals had 38% lower relative risk of heart failure development compared to the individuals with a traditional treatment target of <140 mmHg (SPRINT Research Group et al. 2015).

1.2.2. **Other risk factors for heart failure development**

However, hypertension is by no means the only risk factor for heart failure development. Other significant risk factors include coronary heart disease, obesity and smoking (Dunlay et al. 2009), as well as increasing age.

The incidence of heart failure increases significantly with age; affecting approximately 1.5% of individuals in the US aged between 40 and 59 years old, 6% aged between 60-79 and 12.5% over the age of 80 (Benjamin et al. 2019). It is therefore highly likely that with people living longer, and with incidences of hypertension, obesity and smoking so prevalent in the western world, heart failure rates will also increase. In addition to this, improved therapies and faster treatment times for patients suffering cardiac insults, such as acute MI, mean more individuals survive the initial event (Gibson et al. 2008; Rosamond et al. 1998) and these patients are also highly likely to go on to develop heart failure (Velagaleti et al. 2008) – increasing heart failure morbidity further still. Projections, based on data in the US, have estimated that the prevalence of heart failure will increase by 46% between 2012 and 2030 (Heidenreich et al. 2013). This projection is unfortunately proving to be somewhat correct – with the American Heart Association confirming that a prevalence of 6.2 million was reported in the US between 2013–2016,

compared to 5.7 million between 2009–2012 - a 9% rise in just 4 years (E. J. Benjamin et al. 2019).

1.3. **The role of superoxide in hypertension and heart failure**

Over the last two decades, numerous clinical and experimental studies have shown that oxidative stress is implicated in the progression of a number of CVD pathologies, including cardiac hypertrophy (Li et al. 2002; Satoh et al. 2006) and heart failure (Lakshmi et al. 2009; Tsutsui et al. 2011). Studies in isolated cardiomyocytes have shown that by reducing oxidative stress using treatments such as vitamin E, hydroxyanisole and catalase, the pro-hypertrophic effects of ANGII and TNF-α on neonatal cardiac myocytes could be prevented (Nakamura et al. 1998). *In vivo* models of chronic heart failure have also demonstrated progressive increases in myocardial xanthine oxidoreductase (XOR) levels, and associated oxidative stress, which can be reduced in the presence of the XOR inhibitor allopurinol (Amado et al. 2005; Ekelund et al. 1999).

In addition to this, the aforementioned risk factors for heart failure development are all also associated with increased levels of oxidative stress generation, highlighting at least one pathway through which these risk factors may be actively contributing towards heart failure development and progression. For example, with regards to endothelial dysfunction and subsequent hypertension, although numerous influential factors have been implicated in its development, superoxide generation, by enzymes such as NAD(P)H oxidase and XOR, represents a major causative factor (Cai & Harrison 2000). Not only does the presence of superoxide reduce NO levels, by reacting to form peroxynitrite (ONOO-), but it also oxidizes tetrahydrobiopterin (BH_4), a crucial cofactor for endothelial NO synthase (eNOS) activity.

With superoxide generation implicated in so many pathological pathways associated with cardiac hypertrophy, heart failure and their risk factors, it is not surprising that attempting to reduce oxidative stress in patients would be of interest. Unfortunately, however, translation of the use of antioxidants to patients has not been straightforward and no clear benefits have been observed in clinical trials using traditional antioxidants (Myung et al. 2013). It is important to note however that reducing oxidative stress and accumulating superoxide damage via other, more specific downstream mechanisms, with targeted treatments, could still be beneficial.

1.4. Current therapies and therapeutic targets for heart failure

1.4.1. Preventative measures

With many environmental factors capable of significantly increasing an individual's risk of developing cardiac hypertrophy/heart failure, it is important initially for clinicians to carefully manage each individual's risk. For example, risk factors such as hypertension, reduced glucose tolerance, increased total cholesterol:HDL ratio, obesity and cigarette smoking all increase one's risk of developing heart failure (Kannel & Belanger 1991). However, they are all factors, which are generally modifiable, either by lifestyle changes, or with medical intervention. It is therefore extremely important for all individuals to be made aware of, and aim to adjust, such modifiable factors accordingly, particularly those who also have non-modifiable risk factors, such as having suffered MI, which put them at substantially greater risk of developing heart failure. However, for patients who have already shown signs of developing cardiac hypertrophy/heart failure, what options are currently available in terms of treatment?

1.4.2. Treating cardiac hypertrophy/heart failure

One way in which many currently available treatments (discussed further below) aim to reduce pathological hypertrophy is by reducing BP. In experimental models, cardiac hypertrophy caused by increased haemodynamic load can be decreased by ≈25% after just 1 week of reducing this load (Hill & Olson 2008). Regression of left ventricular hypertrophy (LVH) in patients has been demonstrated following treatment with a variety of drugs which reduce haemodynamic load, as well as by life-style modifications (Liebson et al. 1995; Xing et al. 2017). However, it is worth noting that whilst many successful heart failure drugs are anti-hypertensives, not all anti-hypertensives reverse cardiac hypertrophy to the same degree, despite perhaps producing similar reductions in BP (Ferreira Filho et al. 2010). BP severity is therefore considered not to be the only factor important in cardiac hypertrophy development and progression, with other hormonal and cell signalling pathways also implicated.

1.4.3. Renin-angiotensin system (RAS) therapeutics

ANGII is a vital component of the RAAS and plays a key role in regulating BP and fluid balance in the body. ANGII is a peptide produced by enzymatic cleavage of angiotensinogen → ANGI → ANGII (see **Figure 1.1**). Some of the known effects of ANGII

on the cardiovascular system include vasoconstriction and water retention when bound to ANGII type I receptors (AT_1 receptor), resulting in increased BP (de Gasparo et al. 2000), as well as inducing smooth muscle cell proliferation (Daemen et al. 1991).

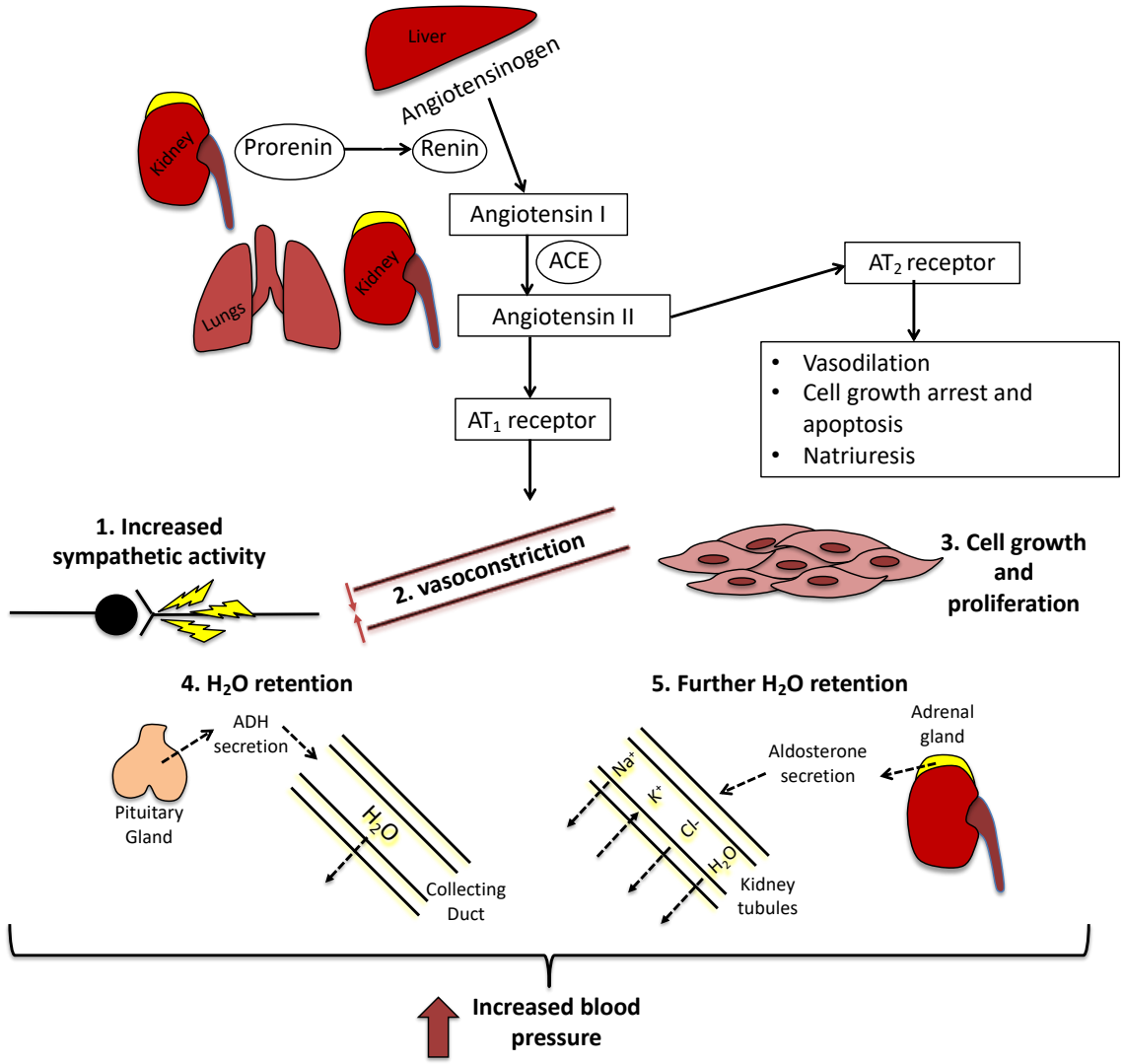

Figure 1.1 Key pathways of the renin-angiotensin aldosterone system (RAAS).
Schematic diagram illustrating the key components of the RAAS and the physiological changes that can result, highlighting angiotensinogen cleavage by renin to give angiotensin I (ANGI), and ANGI cleavage by angiotensin converting enzyme (ACE) to give angiotensin II (ANGII). Physiological changes shown include those resulting from ANGII binding to ANGII type 1 receptors (AT_1 receptors) and ANGII type 2 receptors (AT_2 receptors). AT_2 receptors are highly expressed in foetal tissues, with expression greatly decreasing following birth. It is therefore primarily the AT_1 receptors that responds to ANGII in adult tissues (Li et al., 2012).

Studies have shown that heterozygous (Het) and homozygous AT1 knockout (KO) mice have decreased BP compared to controls (Ito et al. 1995). Moreover, several studies show that restricting ANGII activity therapeutically (both in patients and animal models) reduces BP, cardiac hypertrophy and ventricular remodelling (reviewed recently by (Ferrario 2016)). Competitive ANGII receptor antagonists such as losartan, as well as ACE inhibitors, are used to treat heart failure, since they reduce left ventricular mass (LVM) in hypertrophic patients, as well as significantly reducing BP (Ferrario 2016). Meta-analyses of clinical trial data have also shown angiotensin converting enzyme (ACE)

inhibitors reduce LVM more effectively than other well established hypertensive treatments, such as diuretics and β-blockers (Dahlöf 2001). These drugs also significantly reduce death and hospital administration rates for heart failure and re-infarction in patients with MI-induced left-ventricular dysfunction or heart failure (Flather et al. 2000). The mechanisms through which RAS-targeted drugs are likely to act, to ameliorate cardiac hypertrophy, are both indirect (through decreasing BP) and direct (through moderating ANGII signalling in hypertrophic and oxidative stress pathways in the vasculature and myocardium). These mechanisms of ANGII activity will be discussed further below, but ultimately, the multiple mechanisms through which ANGII acts in the body to worsen cardiac and vascular dysfunction highlight why RAAS therapeutics have been relatively successful in treating both hypertension and cardiac hypertrophy.

1.4.4. **β-adrenergic receptor blockers**

Other widely used therapeutics for treating cardiac hypertrophy are β-adrenergic receptor blockers. These are anti-hypertrophic, reduce LVM (Dahlöf 2001), increase exercise capacity of patients (Vyssoulis et al. 1995) and reduce mortality (Doughty et al. 1997). It is thought that in addition to being anti-hypertensive, the anti-oxidant and anti-proliferative properties of β-blockers such as carvedilol may be responsible for enhancing the beneficial effects of these drugs (Moser & Frishman 1998). A recent meta-analysis has further highlighted β-blocker efficacy in regressing LVH, finding that regression following use of β-blockers in hypertensive cardiac hypertrophy patients was comparable to that in patients using ACE inhibitors or ANGII receptor blockers, and was greater than in those using diuretics or calcium channel blockers (Xing et al. 2017).

1.4.5. **Diuretics**

Diuretics have been used for some time as symptomatic treatment for heart failure, and act by effectively reducing blood volume (and thus BP) by increasing excretion of ions (such as Na^+) and water through the kidneys. However, they are generally used in combination with other treatments such as ACE inhibitors, ANGII receptor blockers or β-blockers. Thiazide diuretics (which increase excretion of sodium by blocking resorption in the kidney via the electroneutral sodium-chloride co-transporter (NCCT)) are most commonly used for this purpose (Blowey 2016). Tolerance to diuretics can be particularly problematic, and can occur both in the short and long-term by differing

mechanisms (Brater 1998). This is therefore one major disadvantage to their use, in addition to the risks of severe electrolyte imbalances (Clayton et al. 2006) and potential worsening of kidney function (Reungjui et al. 2008). Due to these potential side effects, and the fact that other interventions, such as those discussed above, have generally proved to be more efficacious in treating cardiac hypertrophy, they are rarely used as a first line therapy. More often, diuretics are added to the treatment regimen later on, only if deemed necessary (Blowey 2016).

1.4.6. **Natriuritic peptides and neprysilin inhibitors**

Natriuretic peptides are endogenous signalling molecules which are of particular interest with regards to heart failure. Despite the presence of brain natriuretic peptide (BNP) widely being used clinically as a marker of heart failure, rather than being a negative signalling molecule, this peptide family (comprising atrial natriuretic peptide (ANP), BNP and c-type natriuretic peptide (CNP)) is in fact regarded as having potential positive impacts on cardiac structure and function. The natriuretic peptides have the ability to help counter regulate the increases in RAAS signalling which often occur in heart failure. Administration of exogenous natriuretic peptides such as Nesiritide (recombinant human BNP), showed promise in early trials with regards to haemodynamics and natriuresis (Publication Committee for the VMAC Investigators (Vasodilatation in the Management of Acute CHF) 2002). However, in a large-scale randomised controlled trial, there was no significant improvement in patient outcome (O'Connor et al. 2011).

ANP, BNP, CNP are broken down and deactivated by an enzyme called neprilysin. Logically, by inhibiting this enzyme it would be hoped that increases in natriuretic peptides would follow – and in turn an improvement in outcome. Racecodotril (an oral neprilysin inhibitor) and Candoxatrilat (an IV formulation), did successfully increase natriuresis and excretion of ANP. However, in a long-term study using the candoxatril pro-drug, BP reduction was not sustained (Bevan et al. 1992). Later, it was found that neprilysin, in addition to natriuretic peptides, also breaks down ANGII (Richards et al. 1992). Therefore, by inhibiting neprilysin not only are the natriuretic peptides being increased, but so are ANGII levels. It is therefore understandable that neprilysin

inhibition is likely to result in counter-intuitive actions from the build-up of resulting peptides (Dalzell et al. 2014).

1.4.7. **Combination therapies**

Whilst various combinations of pre-existing single drugs (for example thiazide diuretics and RAAS inhibitors mentioned above) are often used in patients to treat heart failure, one particularly successful recent example of a novel combination therapy is sacubitril/valsartan. Sacubitril/valsartan harnesses the benefits of both neprilysin inhibition (building up natriuretic peptide levels as mention above) and RAAS inhibition (preventing the counterintuitive ANGII build up).

The 'Prospective comparison of ARNI with ACEI to Determine Impact on Global Mortality and morbidity in Heart Failure' trial (PARADIGM-HF) tested whether sacubitril/valsartan was superior to enalapril in reducing the primary end point of CV death or HF hospitalisation (McMurray et al. 2014). This trial was terminated early, on the recommendation of the Data Monitoring Committee, due to a sustained and highly significant reduction in the risk of the primary composite end point (CV death or HF hospitalisation) and in CV mortality in the sacubitril/valsartan group compared with the enalapril group. At the end of the trial, there was a 20% relative risk reduction in the primary end point and each of its components, as well as a 16% reduction in all-cause mortality. Both sudden death and death from worsening HF, were equally reduced, and both first hospitalisations for HF and total hospitalisations were reduced (21% and 23%, respectively) (Packer et al. 2015). Hypotension was significantly more common with sacubitril/valsartan than with enalapril (14% vs 9% in the in the sacubitril/valsartan and enalapril groups respectively, $p<0.001$), although this rarely led to study-drug discontinuation. Conversely, renal dysfunction, hyperkalaemia and cough were less common with sacubitril/valsartan than with enalapril. Furthermore, it has recently been reported that changes in $\log_2$–NT-proBNP concentrations over 12 months in study participants correlated with changes in left ventricular (LV) ejection fraction ($r = -0.381$), LV end-diastolic volume index ($r = 0.320$), LV end-systolic volume index ($r = 0.405$), left atrial volume index ($r = 0.263$), and ratio of early diastolic filling/early diastolic annular velocity ($r = 0.269$) (Januzzi et al. 2019).

1.5. **Limitations of current therapies**

Whilst some patients benefit from the treatments discussed above, a significant proportion of patients remain resistant to their effects (even following combination therapies). It must also be noted that RAAS therapeutics have particular limitations with regards to efficacy in certain patient populations (specifically black patients) (Saunders et al. 1990; Rahman et al. 1997; Cushman et al. 2000; Exner et al. 2001; ALLHAT Collaborative Research Group 2002), which means they are somewhat restrictive in terms of application. It must also be considered that ACE is not the only enzyme capable of converting ANGI → ANGII, and in recent years, the pathways involved in the RAAS have been found to be more complex than the key pathways shown in **Figure 1.1** (Ferrario et al. 2014). The potential compensatory, or tissue specific, alternative pathways for ANGII formation, involving enzymes such as chymase, represents a further limitation to such therapies for heart failure patients, as simply inhibiting ACE may not be the most optimal treatment method for the long term (Ihara et al. 1999; Arakawa & Urata 2000).

Unfortunately, the above treatment options and findings also refer specifically to patients classified as having heart failure with reduced ejection fraction (HFrEF). Unfortunately, patients with heart failure with preserved ejection fraction (HFpEF) do not respond in the same way to these treatments, and no effective treatment has yet been found for this patient population (Ilieșiu & Hodorogea 2018).

Crucially, it must also be noted that even in responsive patients, cardiac hypertrophy/heart failure may be improved but it is never truly reversed. Progression of the condition can still occur, albeit at a potentially slower rate, leaving prognosis largely uncertain. Ultimately, when heart failure has progressed beyond a point of current therapies being efficacious, with blood flow to the rest of the body highly compromised, a heart transplant is the only viable option for patients. The wait for a suitable donor can be lengthy and patients with a particularly poor chance of survival may have to undergo invasive surgery to implant a left ventricular assist device (LVAD) in order to restore cardiac function until a heart becomes available (NICE, 2019). Therefore, despite current treatments often helping to control hypertrophy and heart failure to some degree, there is a constant quest to develop more effective and safe treatments for patients in the hope that the number of patients requiring LVAD and

heart transplantation procedures in the future can be significantly reduced.

1.6. **Developing new treatments**

Relative success in the implementation of various available treatments resulted in improved prognosis for heart failure patients over a decade - with 6 month mortality rates decreasing from 26% to 14% between 1995 and 2005 (Mehta et al. 2009). However, unfortunately despite this improvement, 5-year mortality in 2016 is estimated to be approximately 50% (Mozaffarian et al. 2016) and heart failure remains considered an incurable, lifelong condition, with current therapies focusing on prolonging and improving life quality for patients as much a possible (Al-Mohammad et al. 2010), but not actively curing the disease.

With no current therapies proven to be effective in the HFpEF patient population, and heart failure morbidity on the increase there is a significant unmet need for, and thus a requirement to develop, novel therapeutics. For this to happen, it is vital to better understand the pathophysiology and molecular mechanisms responsible for development of cardiac hypertrophy and heart failure, with the hope of identifying potential new therapeutic targets. With increased hemodynamic stress, directly associated with hypertension, an important physiological determinant in the development of LVH and heart failure (Devereux et al. 1983), research into such mechanisms may ultimately help uncover potential new targets in the search for prevention and possibly cure.

1.7. **The potential of inorganic nitrate**

1.7.1. **Nitric oxide in vasculature**

Nitric Oxide (NO), derived from the endothelium via endothelial NO synthase (eNOS), is critical in maintaining healthy vascular homeostasis, acting as a vasodilator (maintaining healthy systemic BP). NO also mediates multiple other beneficial cardiovascular effects proposed to be mediated by activation of soluble guanylyl cyclase (sGC) and subsequent elevation of cyclic guanosine monophosphate (cGMP) (Napoli & Ignarro 2001; Loscalzo 2001; Napoli et al. 2006) (see **Figure 1.2**).

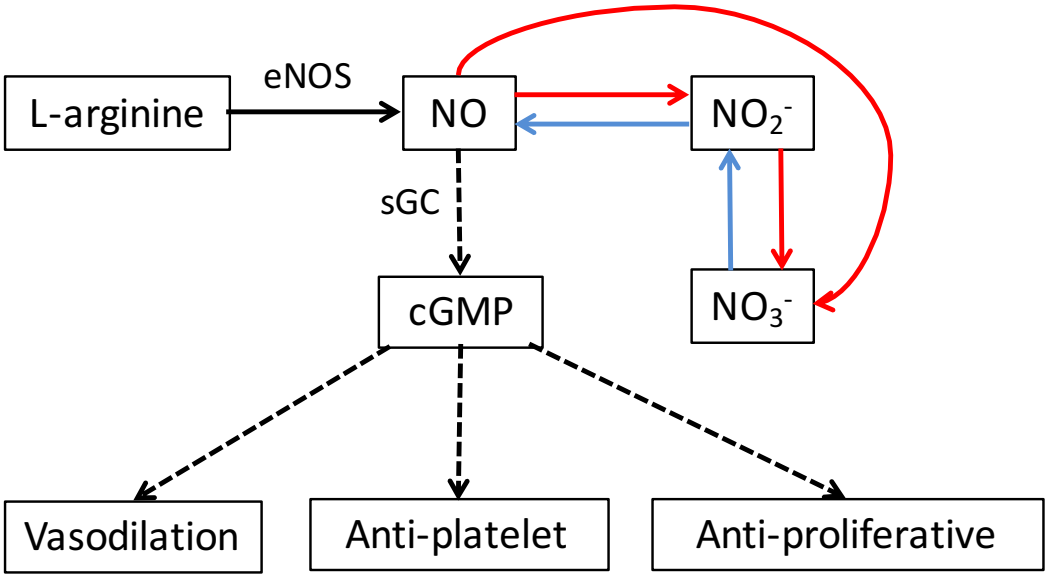

Figure 1.2 L-arginine-NO and nitrate-nitrite-NO reaction pathways and key biological effects exerted by resulting NO.
Schematic illustrating the production of NO via the L-arginine-NO (eNOS) (black) and the nitrate-nitrite-NO (blue) pathways. Figure also highlights some key beneficial effects of NO exerted through sGC-mediated increases in cGMP signaling (---), such as vasodilation, anti-platelet and anti-proliferative effects. The conversion of NO to nitrite (NO_2^-) and nitrate (NO_3^-) by oxidation is also highlighted (red).

A failure of endothelial cells to produce sufficient bioactive NO in the vasculature, for example as a result of endothelial dysfunction and eNOS uncoupling, is therefore harmful in a number of ways and has been implicated in the pathogenesis of hypertension and LVH – both cardiovascular morbidities which are significant risk factors for developing heart failure (Brunner et al. 2005; Katholi & Couri 2011; Panza et al. 1990; Treasure et al. 1993). Furthermore, New York Heart Association (NYHA) class III heart failure patients exhibit significantly blunted flow-mediated dilatation (FMD) responses (Smith et al. 1996), and heart failure patient serum contains reduced levels of NO metabolites and cGMP (a biomarker of NO activity), compared to age-matched controls (Bhushan et al. 2014). These findings support the view that NO deficiency is likely occurring in these patient populations and may be implicated in heart failure pathogenesis and disease progression.

Not only could NO deficiency increase the risk of LVH development indirectly (due to reduced vasodilation, contributing to chronically raised BP, but constitutive NO is also considered a direct negative-modulator of cardiac hypertrophy. Reduced NO bioavailability and endothelial dysfunction has been associated with hypertension in a number of animal models (Lockette et al. 1986; Tesfamariam & Halpern 1988), in humans with hypertension, as well as patients with LVH and long-term coronary heart

disease (Panza et al. 1990; Panza et al. 1993; Treasure et al. 1993; Schächinger et al. 2000).

In addition to this, loss of constitutive NO production has been identified as an important modulator of cardiac hypertrophy directly. For example, in animal models chronic inhibition of endogenous NO synthesis using the NO synthase inhibitor L-nitroarginine methyl ester (L-NAME) has been associated with increased myocardial fibrosis in rats without any other stimulus (Pechánová et al. 1999), also leading to enhanced cardiac fibrosis development in rats co-dosed with a low dose ANGII regimen, which alone did not cause cardiac fibrosis (Hou et al. 1995).

Both nNOS and eNOS KO mice have also been shown to develop cardiac hypertrophy spontaneously, with double KO mice developing yet more severe cardiac hypertrophy (McNamara et al. 2003). In eNOS KO mice, an increased cardiac hypertrophic response and worse cardiac function compared to wildtype (WT) mice has been reported following transverse aortic constriction (TAC) (Ichinose et al. 2004; Buys et al. 2007). Although it must be noted that in models where pressure-overload is yet more severe, and eNOS uncoupling occurs (where monomeric eNOS begins to produce O_2^- instead of NO), more extreme cardiac hypertrophy/fibrosis and worsening of cardiac function has been reported (Takimoto et al. 2005).

In patients with heart failure, a genetic variant of eNOS, resulting in shortened enzyme half-life, is also associated with increased mortality (McNamara et al. 2003). The low-level expression of NO produced by nNOS and eNOS therefore appears protective in cardiac hypertrophy, with significant antihypertrophic effects. It is therefore thought that the loss of low-level constitutive NO generation from eNOS in the cardiovascular system, as a result of endothelial dysfunction, may result in the loss of a crucial braking mechanism of cardiac hypertrophic pathways.

My PhD hypothesis therefore postulates that providing NO therapeutically, through replacement of lost endogenous NO, will prevent/slow development of cardiac hypertrophy/heart failure via both blood-pressure dependent and BP-independent mechanisms.

1.7.2. **How can we provide NO therapeutically?**

Traditionally, delivering NO therapeutically (for example in angina, where the aim is to treat periods of acute cardiac ischaemia by rapidly dilating coronary blood vessels) has been achieved using organic nitrates (such as nitroglycerin (GTN)). Additionally, organic nitrates are used in acute decompensated heart failure, when sudden worsening of heart failure symptoms occurs (Alzahri et al. 2016). However, due to the development of tolerance to NO donors such as GTN (Münzel et al. 2005), and with these donors even capable of inducing endothelial dysfunction following prolonged exposure (Gori et al. 2010), their protective effects are short-lived and chronic treatment for CVD with such therapies are not suitable. It has therefore been the focus of numerous research groups to develop novel NO donors that are capable of exerting beneficial effects on the vasculature *in vivo* without the development of tolerance. However, even in potentially promising compounds, proposed to act via alternative mechanisms to the traditional organic nitrates (using cytochrome YP3A4 metabolism as opposed to cytochrome P450/XOR/glutathione-S-transferase and/or aldehyde dehydrogenase 2), tolerance has still been observed in clinical trials (Knox et al. 2016). Thus, alternative approaches, which provide sustained, long-term NO delivery to the vasculature are still highly sought after. One such approach that has gained support over the last decade is that of the nitrate-nitrite-NO pathway.

1.7.3. **Nitrate→ Nitrite→ NO**

It has recently been demonstrated that upon provision of dietary inorganic nitrate (NO_3^-), both healthy volunteers and hypertensive individuals exhibit increased plasma nitrate, nitrite (NO_2^-) and cGMP levels, with significant decreases in BP (Larsen et al. 2006; Webb et al., 2008a; Ghosh et al. 2013; Kapil et al. 2014).

The efficacy of nitrate in these individuals is explained by the enterosalivary circuit (**Figure 1.3**). Food containing inorganic nitrate, or oral nitrate salt supplementation, once consumed and digested makes the nitrate available for absorption across the surface of the upper intestine into the circulation. Nitrate then circulates in the blood, and whilst a substantial proportion of this is excreted, a significant amount is extracted from the blood by the salivary glands (Tannenbaum et al. 1976). This is an active process that relies on exchange via the sialin transporter (Qin et al. 2012) and results in a nitrate

concentration up to 10x that found in plasma accumulating in the saliva (Lundberg & Govoni 2004; Spiegelhalder et al. 1976). When this nitrate-rich saliva is released into the oral cavity, facultative bacteria here reduce nitrate to nitrite (Xie et al. 2009), which is then swallowed and absorbed across the gut wall into the circulation, increasing plasma nitrite levels (Webb, Patel, Loukogeorgakis, Okorie, Aboud, Misra, Rashid, Miall, Deanfield, N. Benjamin, Macallister, A. J. Hobbs & Ahluwalia 2008a). Disruption of this enterosalivary circuit is sufficient to prevent increases in plasma nitrite ordinarily seen following oral inorganic nitrate supplementation, and prevents the beneficial effects on BP which would normally be seen (Kapil et al. 2013; Webb, Patel, Loukogeorgakis, Okorie, Aboud, Misra, Rashid, Miall, Deanfield, N. Benjamin, Macallister, A. J. Hobbs & Ahluwalia 2008a). Following increases in plasma nitrite, endogenous nitrite reductases in the circulation, such as Xanthine Oxidoreductase (XOR), reduce this nitrite further to produce bioactive NO (H. Li et al. 2001; Lundberg, Weitzberg & Gladwin 2008a; Lundberg & Weitzberg 2010a; Modin et al. 2001). NO can then exert its beneficial effects on the cardiovascular system. This means of delivering NO has thus far proved to be effective in a wide variety of both acute and chronic studies (Gee & Ahluwalia 2016), with no side-effects reported after up to 17 months of supplementation (Hezel et al. 2015).

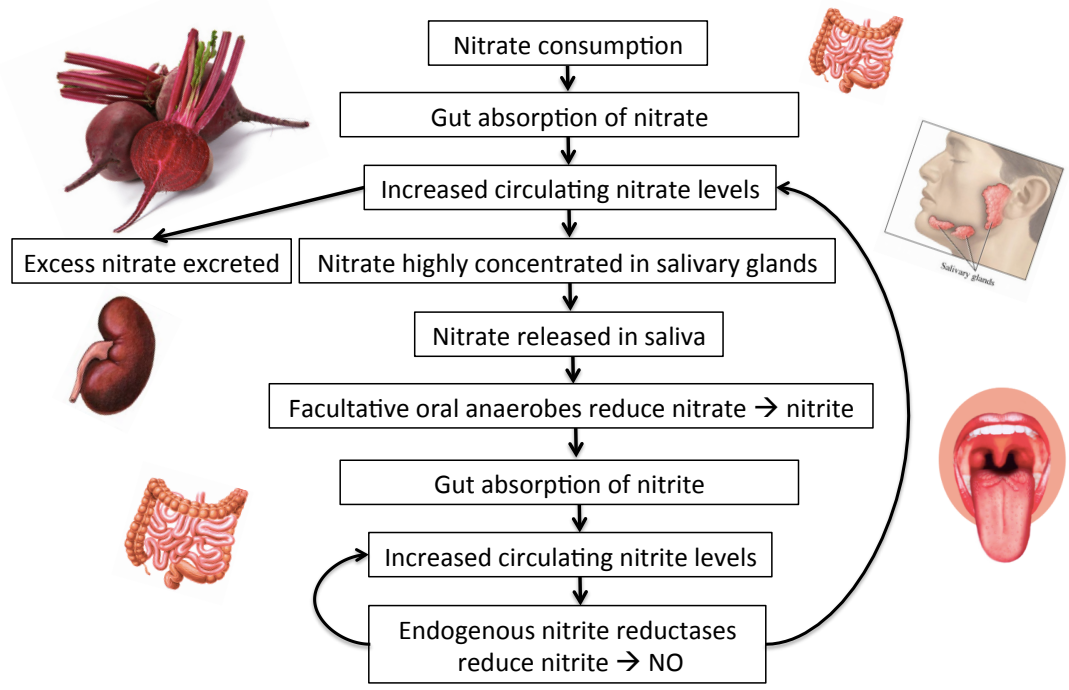

Figure 1.3 The enterosalivary circuit.
Schematic illustrating the critical steps of the enterosalivary circuit, describing how conversion of Nitrate → Nitrite → NO occurs following consumption of dietary inorganic nitrate.

1.7.4. **Postulated benefits of Nitrate supplementation in cardiac dysfunction**

1.7.4.1. **BP reduction**

Whilst some studies in certain patient subpopulations have not shown reductions in BP with inorganic nitrate (Bondonno et al. 2014; Bondonno, A. H. Liu, Croft, Ward, Shinde, Moodley, Lundberg, Puddey, Woodman & Hodgson 2015a; Gilchrist et al. 2013), it is widely accepted that in the majority of studies in healthy individuals and hypertensive individuals without further comorbidities, inorganic nitrate significantly reduces BP (Gee & Ahluwalia 2016; Siervo et al. 2013).

It is possible that a reduction in BP as a result of inorganic nitrate treatment could potentially reduce the extent of cardiac hypertrophy/dysfunction observed. Anti-hypertensive medications including RAAS therapeutics and calcium channel blockers have both been shown to induce some degree of reverse remodelling in the hypertrophic heart (Yui et al. 2010), and as previously discussed, clinical trials demonstrate clear benefits of anti-hypertensives in heart failure patients. Thus, it is possible that via a similar mechanism the same could be true of inorganic nitrate. Although BP reduction in itself is unlikely sufficient to reverse the condition entirely, particularly in cases of advanced disease, it may still be capable of reversing remodelling to some extent and slowing disease progression.

1.7.4.2. **Reducing cardiac hypertrophy directly**

As previously mentioned, deletion of the eNOS and/or nNOS genes in mice, or pharmacological inhibition of NO synthesis, for example using L-NAME, can independently lead to development of, or further exacerbate, cardiac hypertrophy, fibrosis and worsen cardiac function (Hou et al. 1995; Pechánová et al. 1999; Scherrer-Crosbie et al. 2001; Barouch et al. 2002; Barouch et al. 2003; Ichinose et al. 2004; Dawson et al. 2005; Buys et al. 2007).

Conversely, genetic overexpression of eNOS specifically in mouse cardiomyocytes improves post-MI survival, improves cardiac output and fractional shortening, and limits ventricular remodelling (Janssens et al. 2004).

In vitro studies in neonatal rat cardiomyocytes, have shown that exogenous treatment with NO via s-nitroso-N-acetyl-D,L-penacillamine (SNAP) is capable of inhibiting

noradrenaline-induced hypertrophy; an effect mediated by cGMP signalling (Calderone et al. 1998). Since these observations there have been a variety of studies indicating that increased cGMP signalling is capable of reducing cardiac hypertrophy and remodelling (Hammond & Balligand 2012). The NO donor spermine NONOate (SNO), when applied to cardiomyocytes isolated from C57Bl6 WT mice, was also found to have a negative ionotropic effect when applied in addition to isoprenaline. However this effect was not seen in cells isolated from sGC α_1 KO mice, further supporting that sGC signalling is likely an important mediator of NO reducing noradrenaline-induced cardiac hypertrophy (Cawley et al. 2011). These effects have so far been supported clinically by recent observations in HFrEF patients with sGC activator vericiguat in phase IIb studies. Exploratory analyses in this study highlighted a clinically significant reduction in NT-proBNP in the vericiguat treated patients (Gheorghiade et al. 2015). Such findings were not replicated in a similar study in HFpEF patients, however quality of life metrics were significantly improved in this patient population (Pieske et al. 2017). Vericiguat Phase III trials are now underway in HFrEF patients (the Vericiguat Global Study in Subjects With HFrEF (VICTORIA) study) (Armstrong et al. 2018).

Such results support the importance of NO as a down-regulator of hypertrophy and fibrosis, and both *in vitro, in vivo* and clinical studies suggest that these beneficial effects are likely to be both as a result of direct and indirect signalling mechanisms. Endothelial dysfunction, where eNOS fails to produce endogenous NO in the vasculature, is therefore likely a key regulator of cardiac hypertrophy, not only by causing an increase in BP via reduced vasodilatory responses, but also by direct signalling in the myocardium. It is therefore possible that by utilising inorganic nitrate to provide NO therapeutically, by impacting these signalling pathways, in addition to reducing BP, this could potentially prevent cardiac hypertrophy development/worsening. Inorganic nitrate has already been shown to successfully reduce lung fibrosis in a mouse model of pulmonary hypertension (Baliga et al. 2012) and we therefore postulate that it may be possible for inorganic nitrate to reduce cardiac fibrosis in a mouse model of cardiac dysfunction.

1.7.4.3. **Down-regulation of AT1R**

It has previously been shown that the NO donor SNAP can down-regulate expression of AT_1 receptors in vascular smooth muscle cells (Ichiki et al. 1998). AT_1 receptors are

responsible for many of the adverse effects of prolonged ANGII signalling, including development of hypertension, oxidative stress and cardiovascular remodelling (Dasgupta & Zhang 2011). Not only may this contribute to any potential reduction in BP in ANGII-infused mice receiving nitrate supplementation (in addition to the direct vasodilatory effect of NO) but it may also be worth considering whether inorganic nitrate may also be capable of down-regulating these receptors in these, and other cell types. As ANGII causes cardiac hypertrophy development both indirectly (through increasing BP via vasoconstriction), and indirectly through ANGII triggering hypertrophic pathways in cardiomyocytes (Kurdi & Booz 2011), down-regulation of its receptors through NO delivery could potentially reduce the extent of hypertrophy observed in cases where increased ANGII signalling is occurring. Whilst ANGII is not considered to be the only driver of hypertension, cardiac hypertrophy and heart failure development by any means, it's involvement in concert with inflammatory, hormonal and oxidative stress mechanisms is considered to contribute significantly to heart failure pathophysiology (Zablocki & Sadoshima 2013). The general success of RAAS therapeutics for heart failure, as discussed in section 1.4.3, further highlights the importance of pathways involving ANGII in the progression of heart failure, and the potential for clinical improvement through pathways which involve reductions in RAAS signalling.

1.7.4.4. **Reducing superoxide damage and repurposing of XOR**

As previously mentioned, studies in isolated cardiomyocytes have indicated that by reducing oxidative stress using anti-oxidants, hypertrophy of these cells could be attenuated (Nakamura et al. 1998). Moreover, in cultured vascular smooth muscle cells exposed to ANGII, transfection with antisense p22phox (a crucial component of NADH/NADPH oxidase) significantly reduced H_2O_2 accumulation, and overexpression of catalase, as well as superoxide dismutase inhibition reduced the extent of hypertrophy observed (Zafari et al. 1998). Whilst translation of the use of antioxidants to the clinic has not been straightforward (Myung et al. 2013), it should not be ruled out that reducing oxidative stress and accumulating superoxide damage via downstream mechanisms, with other specifically targeted treatments, may still be beneficial. In this regard, it has been reported that targeting the nitrate-nitrite-NO pathway therapeutically may be beneficial in models of renal and cardiovascular disease by

reducing the oxidative stress and increasing NO bioavailability (Carlstrom et al. 2011; Ling et al. 2018; Peleli et al. 2016; Tripatara et al. 2007).

In vivo models of chronic heart failure have demonstrated progressive increases in myocardial XOR levels, and associated oxidative stress (Amado et al. 2005; Ekelund et al. 1999). Accordingly, XOR has been implicated in the superoxide generation in cardiovascular pathology (Berry & Hare 2004). The enzyme is extremely complex, demonstrating varying activities depending on substrate/binding site, oxidation state and availability of terminal electron acceptors (for a comprehensive review on XOR in pathology see (Battelli et al. 2014)).

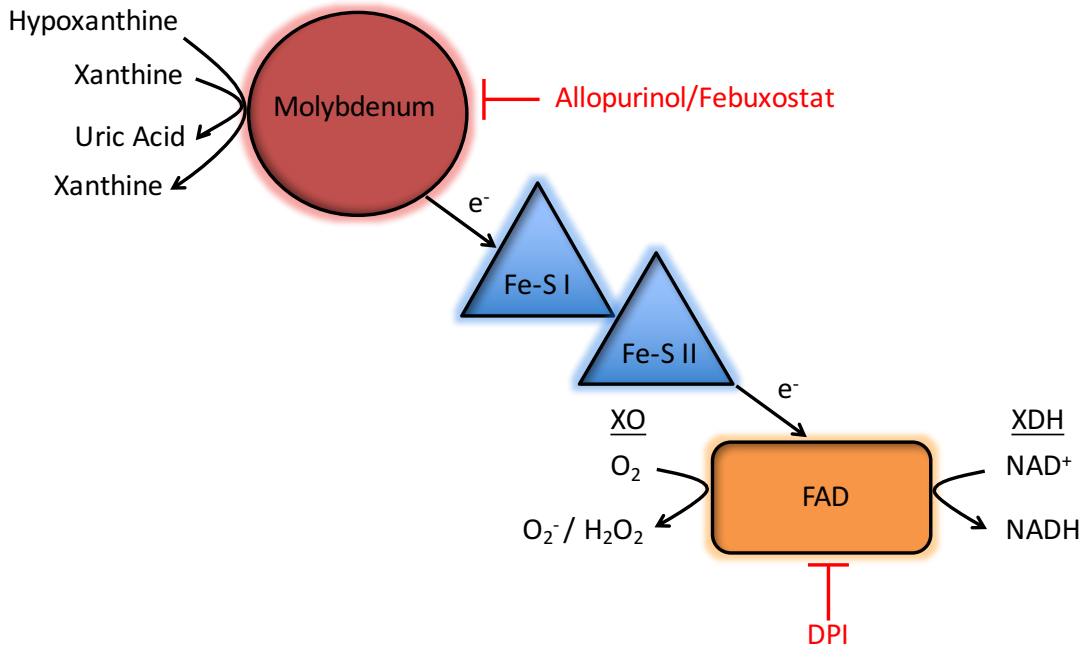

Figure 1.4 Biochemistry and electron flux in a single XOR monomer.
Schematic illustrating potential flows of electrons (e^-), shown by arrows, during purine catabolism in an XOR monomer, with the FAD subunit in either XO or XDH form. As XO, the reduced FAD site reacts with molecular oxygen to form superoxide (O_2^-) or hydrogen peroxide (H_2O_2), depending on whether FADH or $FADH_2$ are utilised respectively. As XDH the reduced FAD site reacts with NAD^+ to form NADH. Key subunits within the XOR monomer include: the molybdenum binding site, two iron sulphur units (Fe-S) and a single FAD binding site. Binding at the molybdenum site can be inhibited using Mo-directed inhibitors allopurinol and febuxostat (as shown in the diagram), and binding at the FAD site inhibited using FAD-directed inhibitor diphenyleneiodonium (DPI).

It has been understood for some time that the molybdenum-binding subunit of XOR is responsible for catalysing oxidation of hypoxanthine to xanthine, and xanthine to uric acid. It is also known that XOR exists in two interconvertible states - XDH (the reduced form of the enzyme) and XO (the oxidised form). The principal form present under physiological conditions *in vivo* is *XDH*, but this can be converted to XO by either sulfhydryl oxidation (reversible) or proteolysis (irreversible) (Stirpe & Corte 1969; Enroth et al. 2000). The importance of this oxidation state is critical following the hydroxylation

of purines at the molybdenum site as, regardless of oxidation state, electrons are generated here and go on to be used at the FAD site. However, depending on the oxidation state of the FAD site, the resulting products will differ. XDH typically uses NAD^+ as its terminal electron acceptor (and molecular oxygen only in times of NAD^+ deficiency). However, XO utilizes only oxygen as a terminal acceptor, resulting in substantial superoxide formation (Hille & Massey 1981), contributing to the accumulated oxidative stress present in pathological conditions such as heart failure (Tsutsui et al. 2011). The electron flux in XOR and reactions of XO and XDH are summarised in **Figure 1.4**.

Particularly importantly for this study, XO has also been known for some time to catalyse the reduction of nitrite → NO (Millar et al. 1998; Zhang et al. 1998; Godber et al. 2000; H. Li et al. 2001) and does so optimally in the presence of reducing substrates NADH and/or xanthine. Under hypoxia and acidosis however, the capacity of XO to reduce nitrite is further increased, which is thought to help explain the success of nitrite infusion in ischaemia reperfusion (IR) injury (Webb et al. 2004; D. A. Jones et al. 2015). Nitrite reduction to NO can be inhibited using allopurinol (molybdenum-directed inhibitor) or DPI (FAD-directed inhibitor). It is therefore thought that NADH acts as an electron donor at the FAD site, whilst nitrite binds to the molybdenum site where it is reduced, releasing NO (Zhang et al. 1997). The functional importance of the nitrite reductase capacity of XOR was first demonstrated in a study by Webb et al., (2004) where sodium nitrite perfusion reduced infarct size following IR injury in the rat heart in *ex vivo* Langendorff heart preparation. This effect was dependent on XOR activity, and importantly suggested that both xanthine and NADH can facilitate nitrite reduction. Also, in a study investigating the effects of nitrite on BP in the spontaneously hypertensive rat (SHR) model, significant reductions in BP were observed with dietary nitrite supplementation. Importantly, this effect was also prevented by the addition of XOR inhibitor allopurinol, highlighting the importance of this enzyme in these beneficial effects of nitrite (Ghosh et al. 2013). Interestingly, in these studies, this activity of XOR was evident under physiological conditions i.e. normoxia and neutral pH. The authors suggest that the increased XOR expression and activity in hypertension increased the role of XOR in its biological activity in this setting.

With XOR's known capacity to act as a nitrite reductase, in the presence of high

concentrations of nitrite, it may be possible to re-direct enzyme activity towards favourable nitrite reduction and away from generating harmful superoxide. It has therefore been postulated that by providing abundant nitrite (via diet as inorganic nitrate or nitrate salt supplementation), the beneficial effects on the cardiovascular system may be two-fold. Not only could the resulting NO be of benefit in terms of encouraging blood vessel dilation and reducing hypertrophy, smooth muscle cell proliferation, platelet reactivity, and inflammatory cell activation/recruitment, but with nitrite acting as a substrate for XO, the ability of XOR to generate superoxide may also be reduced due to a 'repurposing' of the enzyme (discussed in (Khambata et al. 2015)). The reduction of nitrite to NO and 'repurposing' of XOR are summarised in **Figure 1.5.**

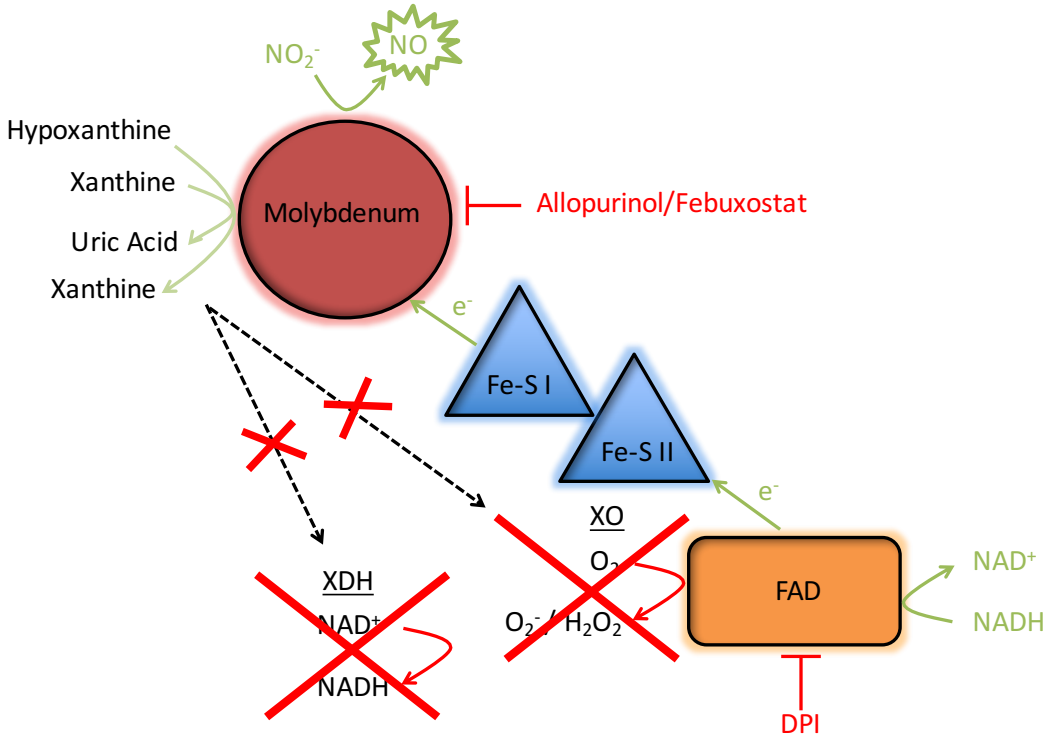

Figure 1.5 Nitrite reduction to NO – biochemistry, electron transfer and repurposing or XOR.
Schematic illustrating the reduction of nitrite (NO_2^-) to NO by XOR, occurring optimally in the presence of NADH as the reducing substrate and in hypoxia. Electrons (e^-) during nitrite reduction are shown to flow (green) from NADH at the FAD site through iron-sulphur subunits (Fe-S) to nitrite at the molybdenum site. In essence this process is the opposite to that which occurs during purine catabolism, where electrons flow (red) from hypoxanthine/xanthine at the molybdenum subunit to O_2 or NAD^+ at the FAD site. By utilising the nitrite reductase pathway it has been postulated that with high concentrations of nitrite present, a 'repurposing' of the enzyme could potentially occur, resulting in reduced superoxide formation, at the same time as increasing NO release (i.e. with electron transfer following the direction of the green arrows instead of red).

1.7.4.5. Improving exercise and muscle performance and cardiac contractility

Recently, significant evidence has been generated supporting the view that inorganic nitrate supplementation exerts beneficial effects on aerobic exercise endurance in heart failure. Exercise endurance in patients with HFpEF was increased by ≈24% following 6.1

mmol/day KNO_3 supplementation in the form of beetroot juice (compared to patients receiving placebo control juice). The same effect, however, was not seen following a single 6.1 mmol KNO_3 dose, suggesting that beneficial effects require a longer-term dosing regimen (Eggebeen et al. 2016). Exercise endurance was also improved in a similar study where HFpEF patients received 6 mmol KNO_3 supplementation three times daily and in addition to observing improvements in exercise in endurance, quality of life scores for patients were also improved (Zamani et al. 2017).

Zamani et al., (2015) deduced that improvements in HFpEF patient exercise performance induced by dietary nitrate likely do not occur as a result of increased O_2 uptake, but are due to improved exercise-induced vasodilation, cardiac output reserve, diastolic function and limited remodelling (as suggested by reduction in arterial wave reflections) (Zamani et al. 2015). These successes in treating HFpEF patients, however, have not been so clearly demonstrated in HFrEF. In a study by Hirai et al., (2017) nitrate supplementation failed to improve exercise tolerance assessed by low and high intensity cycle testing in patients with HFrEF (Hirai et al. 2017). However, in a different study, increased knee extensor power was observed in HFrEF patients following 11.2 mmol KNO_3 supplementation (Coggan et al. 2015)

A study investigating the effects of nitrate supplementation on mouse skeletal muscle found significantly higher concentrations of Ca^{2+} released following electrical stimulation in fast twitch muscle fibres in mice fed 1 mM $NaNO_3$. This increase in Ca^{2+} translated to a significant increase in contractile force, with contraction rate being ≈35% faster in the nitrate fed mice. Also observed were increases in Ca^{2+} handling proteins as measured by western blot (Hernández et al. 2012). Further research has mirrored these findings in mouse cardiac muscle, with increased left ventricle pressure measured in Langendorff experiments and increased *in vitro* contractility of cardiomyocytes following $NaNO_3$ dietary supplementation, as well as increases in free Ca^{2+} and Ca^{2+} handling protein expression (Pironti et al. 2016). *In vitro* experiments using mouse cardiomyocytes have also shown NO increases contractility, with local NO signalling from nNOS implicated in cardiomyocyte mechanotransduction (Jian et al. 2014) indicating how on a subcellular level, NO may have potential to impact cardiomyocyte contractility, therefore having an effect on cardiac performance as a whole.

Inorganic nitrate has also been found to have beneficial effects on mitochondrial energy efficiency, with mouse skeletal muscle mitochondria exhibiting improved oxidative phosphorylation following dietary nitrate supplementation (Larsen et al. 2011) and improved haemodynamics have been observed in healthy rats and those with MI-induced heart failure (Ferguson et al. 2013; Ferguson et al. 2016).

Such findings, help explain some of the benefits on muscle performance observed following nitrate supplementation, but further understanding is required to elucidate why these changes are sufficient to improve cardiac output and exercise performance in HFpEF but not HFrEF. Ultimately, further investigation into mitochondrial, muscle and haematological dynamics will be required to further understand the effects of NO on cardiac muscle structure and function in health, and also in these two similar, yet disparate diseases.

1.7.5. **Particular hope for HFpEF?**

However, particularly with regards to HFpEF, it can be postulated that inorganic nitrate/NO delivery appears to have huge potential as an effective therapeutic. This may be by improving cardiac remodelling via direct pathways such as those discussed above (e.g. AT1R expression etc), or by improving exercise capacity, muscular performance and haemodynamics, and perhaps in turn encouraging remodelling indirectly. The relative contributions of each of these mechanisms to the clinical improvements observed in patients remains to be deduced. During my PhD studies we carried out BP-dependent and -independent models of cardiac dysfunction, to address some of these issues.

1.8. **Mouse models of cardiac dysfunction**

There are multiple animal models of cardiac dysfunction which we could have utilised to investigate pre-clinical potential of inorganic nitrate as a treatment in heart failure (Houser et al. 2012). Mouse models are often popular due to the ever-increasing number of genetically modified strains available. It is for this reason that we primarily focus on mouse models in our lab – as proteins of interest which might identified as a result of a study have the potential to have genetically modified mouse variants generated (or are already widely available). Comparable studies can then we carried out in future genetically modified mouse models. The most popular mouse models of cardiac dysfunction are described below.

1.8.1. **Pressure overload of the heart using surgical banding**

Surgical banding of the abdominal, ascending or transverse aorta is a frequently used model for cardiac dysfunction. This model is considered to most closely represent the clinical features of cardiac dysfunction caused by aortic stenosis (AS) in humans and clear benefits of this model include the ability to use this in both small and large animals. In large animals onset can be developed to be gradual, and more representative of the human condition (Tagawa et al. 1998; Ye et al. 2001). However, in small animals (rats and mice) trans-aortic constriction (TAC) causes an abrupt increase in LV afterload and high incidence of post-operative mortality (Sakata et al. 1998). This makes the mouse model less similar to the clinical manifestation of AS, and thus whilst a popular model, is by no means an ideal comparison to the human condition.

1.8.2. **Coronary artery ligation**

Another popular surgical method used for inducing cardiac dysfunction in mice is coronary artery ligation. Dilated cardiomyopathy in particular can be modelled in animals using ischaemic injury induced by surgical coronary artery ligation (Pfeffer et al. 1979; Prabhu et al. 2000). The coronary artery is tied either temporarily or permanently, and the degree of LV remodelling and dysfunction in this model are directly proportional to the infarct size (Fletcher et al. 1981). With this in mind, this model takes time to perfect in order to get equivalent dysfunction in different treatment/control groups.

1.8.3. **Osmotic minipump infusion of drugs**

Osmotic minipumps are a particularly effective way to deliver consistent drug doses over medium to long term in small animals.

1.8.3.1. **ANGII model of BP-dependent cardiac dysfunction**

ANGII plays a major role in regulating BP and fluid balance in the body. ANGII is a peptide produced by enzymatic cleavage of angiotensinogen → ANGI → ANGII (see **Figure 1.1**). Some of the known effects of ANGII on the cardiovascular system include vasoconstriction when bound to AT_1 receptors, resulting in increased BP as well as inducing smooth muscle cell proliferation (reviewed extensively in (de Gasparo et al. 2000)). As well as the RAAS being implicated in BP control and fluid homeostasis, the local RAAS of the heart is also known to be activated during times of hemodynamic

stress, for example during pressure overload (Sadoshima et al. 1993; Lijnen & Petrov 1999).

1.8.3.1.1. Previous studies using ANGII infusion

ANGII has been used for some time as a mouse model of cardiac dysfunction. In previously reported studies, doses of between 1.4 and 2.8 mg/kg/day of ANGII have been shown to rapidly and significantly increase BP in mice, raising systolic BP from approximately 115 mmHg to 170 mmHg (Francois et al. 2004; Kawano et al. 2005; Crowley et al. 2006). Doses between 1.5 and 2.8 mg/kg/day have also been shown to induce cardiac hypertrophy and remodelling, measured using echocardiography, histology, heart weight:body weight ratios and molecular markers of hypertrophy (Kawano et al. 2005; Crowley et al. 2006; Zhong et al. 2010; Becher et al. 2012; Mori et al. 2012).

Such studies use osmotic minipumps to chronically deliver ANGII for between 3 and 4 weeks by osmotic infusion. Therefore, for my PhD I have used a dose of 2 mg/kg/day ANGII to be infused by Alzet® osmotic minipumps (Durect Corporation, USA) for 3 weeks.

1.8.3.1.2. ANGII-induced mechanisms of cardiac dysfunction

The majority of ANGII-induced cardiac hypertrophy is considered to occur through BP-dependent mechanisms. ANGII increases BP through a number of pathways, including direct vasoconstriction, stimulating the sympathetic nervous system and increasing aldosterone synthesis (which helps control ion and water uptake in the kidneys) (Kim & Iwao 2000). In addition to this, ANGII induces smooth muscle cell growth, migration and proliferation, as well as increases collagen (type I and II) synthesis in fibroblasts. These effects can therefore lead to thickening and stiffening of blood vessel walls (Fyhrquist et al. 1995).

The ANGII model of cardiac dysfunction is therefore thought to reflect, fairly accurately, the development of hypertension-induced cardiac hypertrophy/heart failure in humans, where the heart initially adapts to increased load by increasing heart muscle mass, increasing wall thickness of the LV in order to maintain healthy cardiac function and minimize wall stress (often referred to as compensated growth). However, if BP (and

therefore cardiovascular load and wall stress) remain increased, cardiac hypertrophy is likely to become accompanied by heart dilation, increased interstitial fibrosis and myocyte death (Levy et al. 1990; Weber et al. 1993; Cohn et al. 1997; Bernardo et al. 2010). This ultimately results in stiffening of the heart walls, reducing contractile function and LV ejection fraction, causing cardiac dysfunction and an increased risk of heart failure, arrhythmias and sudden death (Levy et al. 1987; Levy et al. 1990; Drazner et al. 2004; de Simone et al. 2008).

However, it is also worth noting that direct ANGII signalling in the heart can cause increased synthesis of collagen in fibroblasts, as well as enhancing cardiomyocyte growth and proliferation in vitro (McEwan et al. 1998) It is, therefore, likely that ANGII may also encourage pathological cardiac hypertrophy by enhancing fibrosis of the myocardium directly. Thus, BP independent mechanisms of cardiac hypertrophy caused by ANGII are also likely to occur to some degree in this model.

As previously mentioned, inhibition of NO synthesis (and therefore increasing BP) using L-NAME leads to exacerbated cardiac fibrosis in rats concomitantly receiving low dose ANGII, which alone was insufficient to cause increases in BP or cardiac fibrosis (Hou et al. 1995). Myocyte hypertrophy and inflammatory cell recruitment in ANGII+L-NAME treated mice was found to not be entirely dependent on BP, as these effects were not observed in rats given only L-NAME, despite exhibiting a similar increase in BP. Thus, suggesting that the additional ANGII stimulus had an effect on cardiovascular signalling and remodelling other than by increasing BP.

One study by Mazzolai et al., 1998 found that normotensive transgenic mice over-expressing ANGII specifically in the cardiomyocytes showed some degree of mild hypertrophy (categorized by enlarged myocytes) at 20 weeks of age. However, the degree of hypertrophy was far greater, and observed in mice as young as 8 weeks old when mice were hypertensive. Also, in a study by Xu et al., (2010), using similar transgenic mice treated with deoxycorticosterone acetate salt to suppress the systemic RAS, when hemodynamic conditions remained unchanged, ANGII expressed in cardiac tissue failed to change heart size or cardiac output. However, in hypertensive mice, the cardiac expression of ANGII significantly enhanced inflammation, oxidative stress and cell death.

From these studies, it therefore appears that ANGII has a direct effect on the heart and that this can contribute to the extent of cardiac hypertrophy. However, this appears to occur primarily in the presence of a stimulus such as increased BP and hemodynamic stress (Mazzolai et al. 1998; J. Xu et al. 2010). Therefore, the use of ANGII infusion seems an appropriate model of BP-induced hypertrophy for the purpose of this study.

1.8.3.2. Isoprenaline model of cardiac dysfunction

Isoprenaline, also known as isoproteranol hydrochloride, is a synthetic, non-selective β-adrenergic agonist, which acts in a similar way to endogenous signalling hormone epinephrine (adrenaline). The chemical structure of isoprenaline is shown in **Figure 1.6**.

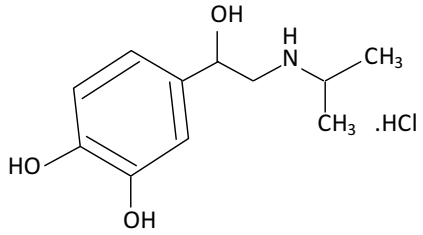

Figure 1.6 Schematic illustrating the chemical structure of isoprenaline hydrochloride.

Figure 1.7 illustrates the signalling cascade induced by isoprenaline binding to β1-adrenergic receptors. Isoprenaline binding to β1 adrenoreceptors induces positive chronotropic, dromotropic and ionotropic effects. In other words, isoprenaline increases cardiac output as a result of increased heart rate, increased electrical impulse conduction from the AV node, and increased strength of cardiac contractions as well as increasing rate of cardiomyocyte relaxation. For these reasons, isoprenaline has been used in the clinic to treat conditions such as bradycardia (slow heart rate) and heart block (irregular heartbeat). In addition to this, β1 binding by isoprenaline reduces peripheral vascular resistance (afterload) (Granata et al. 1970) and increases the return of blood to the heart (preload).

It has been discovered that in mice, due to the extra strain put on the heart, chronic doses of isoprenaline (15-60 mg/kg/day for 1-2 weeks) result in increased heart size and weight:body weight ratios, increased ventricle wall thickening (as measured by echocardiography), decreased ejection fraction, fractional shortening and BP and increased cardiac fibrosis (Friddle et al. 2000; Bueno et al. 2002; Oudit 2003; Nakayama et al. 2009).

As a result of these effects, chronic isoprenaline dosing is therefore a commonly used model of BP-independent cardiac dysfunction. For my BP-independent model of cardiac dysfunction, I therefore used a dose of 15 mg/kg/day isoprenaline hydrochloride, infused by Alzet® osmotic minipumps (Durect Corporation, USA) for 3 weeks.

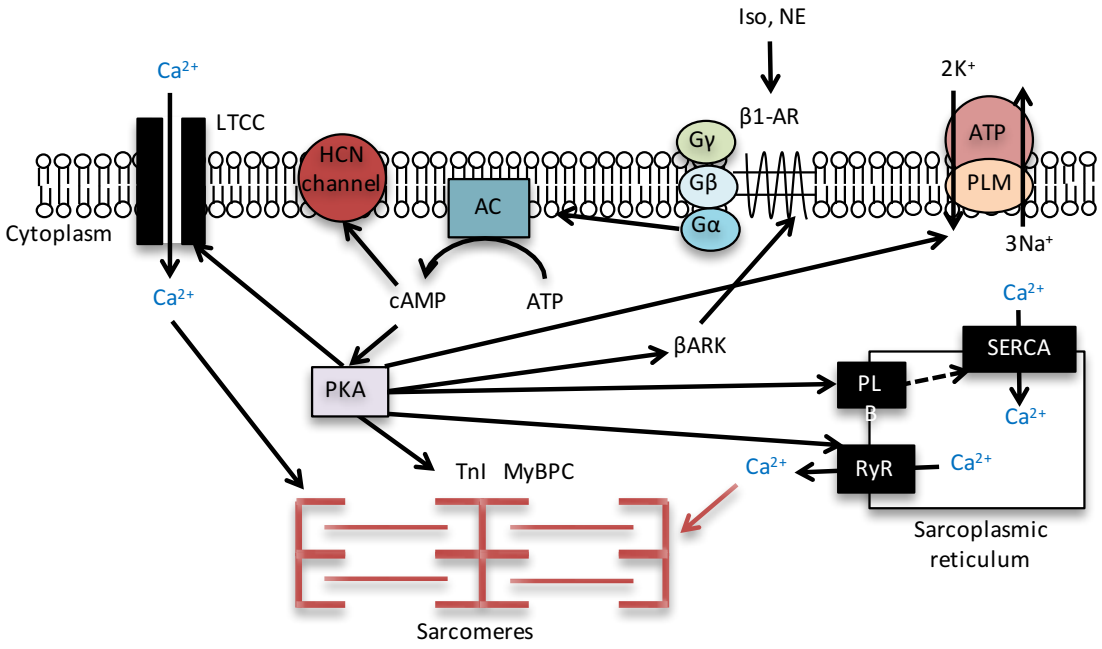

Figure 1.7 β1 adrenergic signaling cascade mediating changes in cardiac contractility by isoprenaline.
Schematic illustrating the signaling cascade initiated by β1-adrenergic agonist (e.g. isoprenaline (Iso) and norepinephrine (NE)) binding to β1-adrenergic receptors (β1-AR), resulting in changes in cardiac contractility. β-adrenergic agonist binding to β1-AR GPCR results in the activation of stimulatory G-proteins, which stimulate adenylyl cyclase (AC) generation of 3',5'-cyclic monophosphate (cAMP) from adenosine triphosphate (ATP). Increased levels of cAMP can alter activity of HCN voltage-gated K^+ channels (known as 'pacemaker channels') as well as increasing the activity of cAMP-dependent protein kinase A (PKA) which mediates a series of phosphorylation events in a variety of intracellular substrates including L-type Ca^{2+} channels (LTCC), phospholemman (PLM), sarcoplasmic phospholamnan (PLB) and ryanodine receptors (RyR) and sarcomeric proteins troponin I (TnI) and cardiac myosin-binding protein C (MyBPC). Such phosphorylation events each contribute to the increased contractility of cardiac muscle and enhanced repolarization. PKA also phosphorylates β-adrenergic receptor kinase (βARK) which in turn phosphorylates β1-AR, acting as a feedback signaling mechanism. Adapted from Triposkiadis et al., 2009 and Feldman et al., 2005.

1.9. Experimental aims

For my PhD studies I have used two experimental mouse models to investigate the effects of nitrate supplementation on cardiac dysfunction – a BP-dependent model and a BP-independent model. In both of these models I investigated whether dietary inorganic nitrate has any effect on cardiac performance and remodelling by comparing heart weight:body weight ratios, cardiac histology and echocardiographic measurements such as LV wall thickness and ejection fraction. For the BP-dependent and BP-independent models of cardiac dysfunction I used osmotic minipump infusions of ANGII and isoprenaline respectively. This allowed me to maintain consistency in the methodology used, with the only variable altered being the drug administered.

Using both a BP-dependent and BP-independent model of cardiac dysfunction enable determination of the potential direct cardiac effects of dietary nitrate versus any cardiac improvements secondary to BP changes. To further tease apart mechanisms in these models I have:

- Investigated the effects of inorganic nitrate on ANGII-induced increases in BP using BP telemetry probes and organ bath pharmacology to assess blood vessel reactivity in response to vasorelaxants and vasoconstrictors.
- Assessed whether nitrate alters cardiac structure and function using echocardiography, and cardiac histology - staining for the presence of collagen by picrosirius red.
- Assessed changes in mRNA expression in the heart using RT-PCR to assess fibrotic, inflammatory and ANGII signaling pathways.
- Assessed changes in protein expression using western blot to assess XOR and NADPH oxidase pathways.
- Assessed NO bioactivity by measuring plasma nitrite and nitrate levels (using ozone chemiluminescence) and cGMP protein levels following treatment with nitrate supplementation versus controls.
- Assessed changes in oxidative stress markers using lucigenin chemiluminescence.
- Examined the impact of XOR in cardiac dysfunction by using an *Xdh* KO mouse model.

CHAPTER TWO -

Methods

2. CHAPTER TWO – Methods

2.1. C57Bl6 mice: sourcing and husbandry

Male C57Bl6J mice were sourced from Charles River Laboratories (UK) at 6-7 weeks of age and were individually housed upon arrival. Mice were kept in Individually Ventilated Cages (IVCs) with food and water available *ad libitum* throughout studies. Room lighting was on a 07:00 – 19:00 GMT schedule and humidity and room temperature monitored according to Home Office regulations (maintained at 55±10% and 19-23°C respectively). A total of 361 animals were used. All animal experiments were conducted according to The Animals (Scientific Procedures) Act 1986.

Mice were manually randomised to water feeding treatment groups upon arrival to the facility. For randomization of individual mice to ANGII or control treatment, this was done using http://www.randomization.com random permutation of integers. Due to having to maintain reliable water changing schedules, and the fact that some control mice had no minipump implanted, blinding to treatment was not possible in all situations when carrying out echocardiography or tail cuff protocols. However, during data analysis, or ex vivo studies, blinding was ensured so as not to allow bias with regards to the more critical stage of analysing results.

Mice were weighed three times weekly, with food and water weights recorded, allowing food and water consumption to be calculated.

2.2. KNO_3 and KCl supplemental feeding

For inorganic nitrate vs. control water feeding, mice received 15 mM KNO_3 (treatment) or 15 mM KCl (control) in replacement of their usual drinking water. This treatment regimen was based upon previous studies demonstrating this to be an effective method for elevating circulating plasma nitrite and nitrate levels compared to control mice (Baliga et al. 2012). With C57Bl6 mice drinking approximately 6 ml/day (Bachmanov et al. 2002), this equates to consuming approximately 90 µmol of nitrate per day, and resulted in a rise of 0.3 µM plasma nitrite in studies by Baliga et al (2012). In clinical studies, average increases in plasma nitrite concentrations of 0.3 and 0.5 µM were observed following consumption of a single 250 ml dose of beetroot juice, and resulted in demonstrable clinical reductions in BP (Kapil et al. 2010; Kapil et al. 2015). Using a 15

mM KNO_3 dose in mouse drinking water is therefore expected to result in a rise in plasma nitrite similar to that reported in human studies where healthy volunteers or hypertensive patients ingested 250 ml/day of beetroot juice.

15 mM KCl was used as a placebo control in this study in order to provide an equimolar salt load. Potassium, rather than a sodium salt, was used since this better simulated dietary interventions delivering NO_3^-, which often contain a substantial concentration of potassium (Webb et al., 2008a). In addition, since potassium has been suggested to be responsible for some of the BP lowering effects of diets rich in fruit and vegetables (Whelton et al. 1997; Geleijnse et al. 2003; Haddy et al. 2006), using KCl as a placebo, controls for any potential effects we may see from potassium.

2.3. Measuring nitrate/nitrite concentrations in supplemental drinking water

2.3.1. Tap vs. Milli-Q (MQ) filtered water

In this study it was essential that the amount of nitrate ingested by the mice was carefully controlled. Therefore, the nitrite and nitrate content of MQ filtered water (Merck Millipore filtration system, UK) and tap water were compared using ozone chemiluminescence (see section 7.19) to ensure the tap water typically used to feed mice in the animal unit did not contain excessive levels of nitrite or nitrate which could influence experimental results.

1 ml aliquots of MQ filtered water and tap water were therefore collected across a number of different days. These were stored at -20 °C until defrosted and ozone chemiluminescence utilised for measurement of nitrite and nitrate concentrations.

2.3.2. Changes in nitrate/nitrite over time in running tap water

In order to maintain consistency of 15 mM KNO_3 and KCl water formulations, tap water was also tested for fluctuations in nitrite and nitrate concentrations after different lengths of running time. 1 ml tap water samples were collected at $T_{0\ secs}$, $T_{30\ secs}$, $T_{120\ secs}$, $T_{240\ secs}$ and $T_{360\ secs}$ after turning the tap on. These samples were then stored at -20 °C until analysed using ozone chemiluminescence (see section 7.19).

2.3.3. **15 mM KNO_3 stability**

In order to measure the stability of nitrate in drinking water over time, a 15 mM KNO_3 stock was made up in tap water. 1 ml aliquots were then collected on days 0, 3, 4, 5, 6 and 7 following formulation. These aliquots were stored at -20 °C until analysed using ozone chemiluminescence (see section 7.19).

2.3.4. **Measuring nitrate/nitrite present in other experimental components**

For surgical and echocardiographic methods, a variety of gels and creams are used, some for a prolonged period of time. There is little evidence to suggest that nitrite and/or nitrate can be absorbed through skin. However, it has been suggested in some case studies, for example in burns victims, that it may be possible for nitrate to be absorbed through the skin (Harris et al. 1979).

Therefore, in order to ensure mice were not being exposed to high nitrite/nitrate levels through these products, these gels/creams were formulated into aqueous solutions so that nitrite and nitrate concentrations could be measured using ozone chemiluminescence (see section 7.19). Gels/creams tested included Aqua Gel® Lubricating Gel (CIVCO Medical Solutions, USA), Redux Crème (Parker Laboratories, Inc., USA) and Veet® For Men Hair Removal Gel Cream (Boots, UK).

For nitrite and nitrate measurements, Aqua Gel was diluted 1:10, Redux Crème 1:100 and Veet® 1:1000 in MQ filtered water.

2.4. **Implantation of osmotic minipumps for subcutaneous infusion of ANGII and isoprenaline**

2.4.1. **Minipump filling**

ANGII or Isoprenaline was infused using ALZET® model 1004 osmotic minipumps (Durect Corporation, USA), shown in **Figure 2.1**, releasing 2 mg/kg/day ANGII SC (Sigma Aldrich®, UK) or 15 mg/kg/day isoprenaline respectively.

Mice were weighed on the day of minipump filling and an average mouse weight calculated. Weight increase throughout the duration of the study was taken into account using mouse weight predictions for C57Bl6J mice of various ages (**Table 2.1**). The estimated average mouse weight at the midpoint of the study was used for

calculating the drug concentration required for filling minipumps.

Age (weeks)	Male		Female	
	Mean	St Dev	Mean	St Dev
3	9.7	1.9	9.3	1.7
4	15.7	2.2	14.1	1.8
5	19.4	1.8	16.9	1.2
6	21.1	1.5	17.5	1.0
7	22.9	1.5	18.2	1.1
8	24.0	1.5	18.7	1.2
9	25.0	1.6	19.3	1.2
10	25.6	1.7	19.8	1.3
11	26.7	1.7	20.2	1.4
12	27.7	1.7	20.7	1.4
13	28.4	1.9	21.7	1.5
14	29.1	1.9	22.0	1.6
15	29.7	2.2	22.3	1.7
16	30.1	2.1	22.6	1.8
17	30.7	2.2	22.6	2.0
18	31.1	2.3	23.0	2.1
19	31.4	2.4	23.5	2.3
20	31.8	2.5	23.6	2.3

Table 2.1 Typical C57Bl6J mouse weights.
Table shows average mouse weights from 400 - 500 mice obtained at weaning from three different barrier levels (standard, high, maximum) from two Jackson Laboratory facilities (The Jackson Laboratory, 2014). Mice were fed a typical laboratory diet (6% fat) and were weighed the same day each week until 20 weeks of age. No statistically significant difference was found between facility or barrier level groups. This table was used to help estimate expected weight gain by mice at certain ages in our experiments.

For example, if the average mouse weight at 10 weeks old was 25.6 g, and a minipump was scheduled to be implanted for 3 weeks, mice would be estimated to gain approximately 2.8 g between 10 weeks and 13 weeks of age (JAX, 2019). Therefore, at 11.5 weeks old weight can be estimated as approximately 25.6+1.4 = 27 g. A weight of 27 g would therefore be used to calculate the drug concentration required for filling the minipumps.

The drug concentration required for filling minipumps is determined by the pump model, pump flow rate, and average mouse weight. A 'Drug Concentration Calculator' is available on the ALZET® website (ALZET, 2019) and essentially calculates the concentration of drug required using the following equations:

$$\textbf{Equation 1}: mass\ flow\ (\mu g/hr) = volume\ flow\ rate\ (\mu l/hr)\ \ x\ concentration\ (\mu g/\mu l)$$

$$\textbf{Equation 2}: mass\ flow\ (\mu g/hr) = \frac{\left(dose\ (\mu g/kg/day)\ x\ mouse\ weight\ (kg)\right)}{24(hrs)}$$

For a predicted mouse weight of 27 g:

$$mass\ flow\ (\mu g/hr) = \frac{2000 \mu g/kg/day}{24hrs}\ x\ 0.027kg = 2.25 \mu g/hr$$

With a volume flow rate of 0.12 µl/hr (standard for an ALZET® osmotic minipump, model 1004) and desired mass flow of 2.25 µg/hr for a 27 g mouse:

$$concentration\ (\mu g/(\mu l) = \frac{2.25 \mu g/hr}{0.12 \mu l/hr} = 18.75\ \mu g/\mu l$$

A drug concentration of 18.75 µg/µl would therefore need to be formulated. Minipump fill volumes were calculated by recording the weight of empty minipumps, then recording the weight again after filling. The fill volume was then calculated assuming that 1 mg = 1 µl of ANGII drug solution:

$$\textbf{Equation 3}: Drug\ solution\ (\mu l) = Filled\ pump\ weight\ (mg) - Empty\ pump\ weight\ (mg)$$

Minipumps were primed at 37°C in 5 ml sterile saline in a 15 ml tube for 48-72 hours. Until implantation, and during surgery preparation, minipumps were maintained at this temperature in surgical theatre using a heat box set at 37°C.

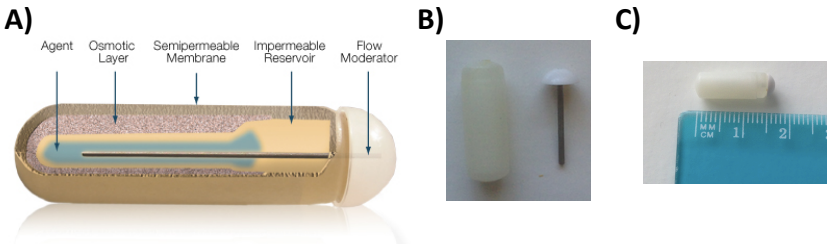

Figure 2.1 A cross-sectional view of an ALZET® minipump (Durect Corporation, 2014a) and photographic images of an ALZET® model 1004 minipump prior to and after filling.
Figure illustrating A) A cross-sectional schematic diagram of the internal structures of an ALZET® osmotic minipump, including the drug formulation (agent), osmotic layer, semipermeable membrane, impermeable reservoir and the flow regulator (Durect Corporation, 2014a), and photographic images showing B) the pump and flow regulator as supplied before filling, and C) the scale of an ALZET® model 1004 minipump when filled, prior to implantation.

2.4.2. Minipump implantation surgery

Anaesthesia was induced using 5% Isofluorane/0.4 litre min^{-1} O_2 in an induction box and maintained using approximately 2.5% Isofluorane/0.4 litre min^{-1} O_2 through a nose cone, with the mouse in a prone position. Vetergesic (100 µl of 3 µg/ml SC) was administered upon anaesthesia induction to give sufficient post-surgery analgesia.

A region of hair approximately 2 cm^2 was removed from the base of the neck and shoulders of the mouse using Veet® For Men Hair Removal Gel Cream (Boots, UK) and the area rinsed with sterile saline. The mouse was covered with Press'n Seal® (GLAD®, USA) draping and a hole cut in the draping for surgical access before applying Hydrex Pink disinfectant (Ecolab, UK) to the exposed skin. Mouse temperature was maintained using a rectal thermometer and Physitemp TCAT-2LV thermostatic heating pad (Physitemp Instruments Inc., USA).

A transverse incision of approximately 1 cm was made across the base of the neck and a subcutaneous pocket created by blunt dissection. The pocket was lubricated with sterile saline before removing the minipump from its 15 ml tube, wiped over with 70% IMS and implanted (flow moderator first). The incision was then sutured closed using 4-0 coated VICRYL™ resorbable sutures (ETHICON*, UK) and 0.5 ml sterile saline (Baxter, UK) administered SC before ceasing anaesthesia and recovering the animal in a heated cage.

2.5. BP telemetry

2.5.1. Telemetry probe implantation

TA11PA-C10 radiotelemetric probes (Data Sciences International, USA) were surgically implanted to allow individual BP recording in freely moving, conscious mice over the course of 3-4 weeks. A schematic illustrating the approximate dimensions of a BP probe can be seen in **Figure 2.2A**. Implantation surgery was performed on 9-week old C57Bl6J mice under aseptic conditions in accordance with Home Office regulations.

Prior to implantation, the tips of BP probes were re-gelled and the baseline pressure of probes measured using Dataquest A.R.T™ acquisition software (Data Sciences International, USA). Probes were sterilised in 2% Gluteraldehyde solution (Fluka Analytical, Sigma Aldrich®, UK (diluted 1:25 in MQ filtered water)) for approx. 30 minutes then rinsed in sterile saline (Baxter, UK) immediately before implantation.

Anaesthesia of mice was induced using 5% Isoflurane/0.4 litre min^{-1} O_2 and maintained using approximately 2.5% Isoflurane/0.4 litre min^{-1} O_2. 100 µl of Vetergesic (3 µg/ml SC) was administered to give sufficient post-surgery analgesia and mouse core temperature was maintained during surgery using a rectal thermometer and Physitemp TCAT-2LV thermostatic heating pad (Physitemp Instruments Inc., USA).

With the mouse laid vertically (head downwards) in a supine position, fur was removed from the neck and upper chest using Veet® For Men Hair Removal Gel Cream (available from Boots, UK) and the area rinsed with sterile saline. The surgical site was covered with Press'n Seal® (Glad®, USA) draping and a hole cut in the draping for surgical access before applying Hydrex Pink disinfectant (Ecolab, UK) to the exposed skin.

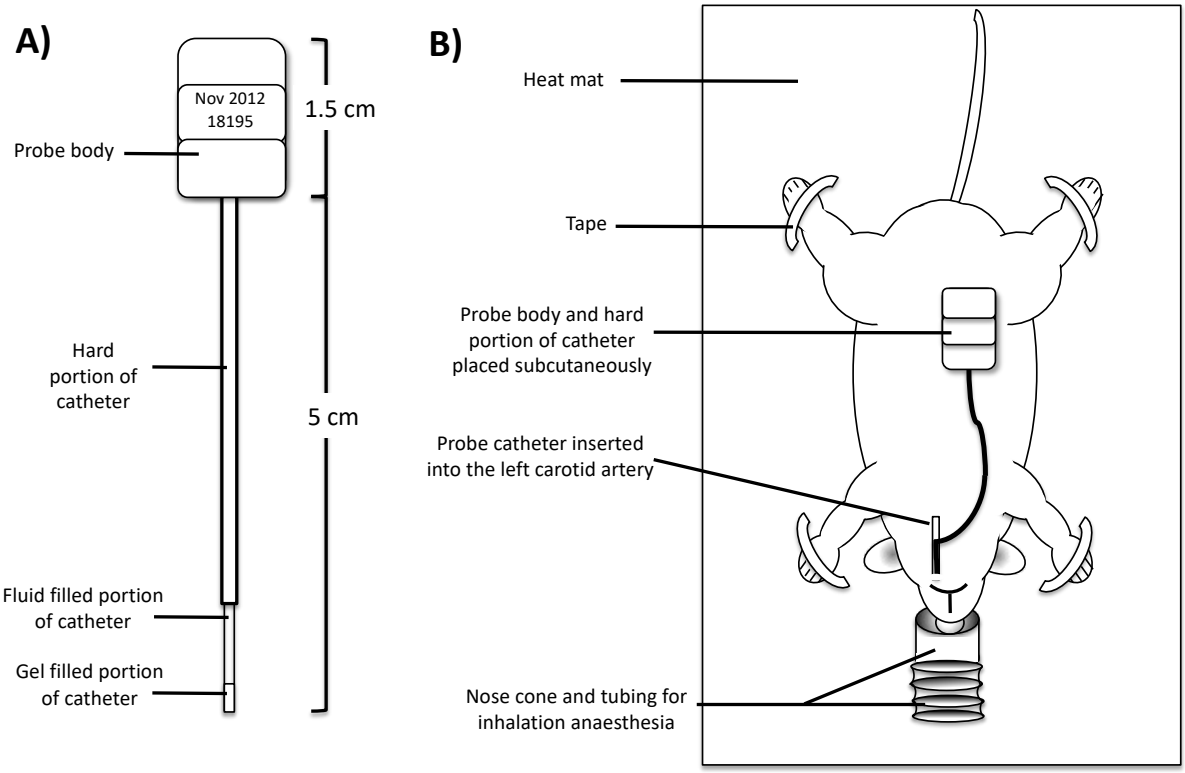

Figure 2.2 Schematic of a BP telemetry probe and BP telemetry probe implantation surgery.
Schematic diagram illustrating A) the approximate dimensions of a BP probe and B) the set-up of a mouse during BP probe implantation surgery, with mouse laid vertically in a supine position, secured using tape. Anaesthesia was maintained during the procedure using 2.5% Isofluorane/0.4 litre min^{-1} O_2 inhaled through a nose cone and temperature maintained using a rectal thermometer and Physitemp TCAT-2LV thermostatic heating pad (Physitemp Instruments Inc., USA). The probe catheter was inserted into the left carotid artery and held in place by sutures. The probe body was implanted subcutaneously, as illustrated, along with the portion of the probe catheter which isn't fed into the carotid artery.

A ventral midline incision was made between the submandibular area and the sternum and stretched by blunt dissection to approximately 2 cm wide. The salivary glands were separated, and the left carotid artery identified and separated from the vein and the vagus nerve. Two lengths of 5-0 Sofsilk™ non-resorbable suture (Coviden™, UK) were tied loosely around the artery, and stretched to extend the artery until blood flow temporarily ceased. Sterile saline was added to the body cavity and the BP probe inserted into a small incision made in the artery. The probe was secured firmly in position using a third 5-0 Sofsilk™ non-resorbable sutures (Coviden™, UK). The initial sutures, which had been placed to prevent blood flow, were then used to further secure the probe in position. The salivary glands could then be placed back into position.

A subcutaneous pouch was then made for the telemeter body, where the battery could lie on the right-hand side of the abdomen, below the ribs. With the telemeter body in place, the salivary glands were pulled back together, and the incision closed using 4-0

coated VICRYL™ resorbable sutures (Ethicon*, UK). 0.5 ml sterile saline (Baxter, UK) was then administered SC before recovering the mouse in a heated cage.

A schematic illustrating the positioning of the mouse for surgery and the approximate positioning of a BP probe subcutaneously can be seen in **Figure 2.2B.**

2.5.2. **Telemetry recording**

Mice were recovered for 7-10 days post-surgery before recording BP data. After recovery, baseline BP readings were taken before osmotic minipumps were implanted. Mice were then recovered prior to beginning further BP recordings. To switch on the telemetry probe and begin data acquisition, a magnet was held close beneath the cage near the belly of the mouse, until a signal and live BP measurement could be observed on the computer programme. Each probe comes with a finite battery life. Therefore, when recording was complete after a 24-hour recording window, the magnet was used to switch off the probe again until the next recording period.

For one day of BP recording, BP was recorded continuously for 24 hours starting at 13:00 GMT. Mean arterial BP (MAP), systolic BP (SBP), diastolic BP (DBP), heart rate (HR), pulse pressure (PP) and mouse activity were recorded, with data points collected once every 15 seconds for 2 minutes at 15-minute intervals across a 24-hour period.

2.6. **Tail cuff BP measurement**

In a subset of study mice, tail cuff BP data was collected using a CODA mouse BP set up (Kent Scientific Corporation, US). For each time point data were averaged from 4 consecutive days of sampling. On each of these days, mice were placed in a restrainer and left to acclimate in a custom-made heat box (Clinipath Ltd, UK) with an ambient temperature of 30 °C for 10 mins prior to beginning recordings. Mice were subjected to 5 acclimation cycles followed by a further 10 cycles of data acquisition. Average MAP, SBP and DBP were calculated to generate a single n for each mouse.

A priori exclusion criteria were: any individual cycles which had readings of ± 15 mmHg from the mouse's daily average were excluded; If a mouse had a day where the average was ± 15 mmHg from that mouse's average for that time point, then the day was

excluded; Any mice whose readings were ± 15 mmHg from the group average at the end of the study were excluded.

2.7. **Echocardiography**

Baseline echocardiographic data was obtained using 7 control, untreated C57Bl6J male mice aged 12-13 weeks. Data from these mice were compared to that published previously to ensure our methods produced data consistent with similar studies. In the ANGII pre-treatment and reversal, and isoprenaline pre-treatment studies, transthoracic echocardiography was performed using a Vevo 770 imaging system with an RMV-707B 30-MHz transducer (FujiFilm VisualSonics Inc., Netherlands). In the *Xdh* KO mouse studies, the Vevo 3100 system was used for measurements of cardiac structure and function. For both machines the standard practical protocols remained the same, but with the Vevo 3100 we were also able to measure doppler flow of the pulmonary artery and aortic arch.

In both cases, anaesthesia was induced using 5% Isofluorane/0.4 litre min^{-1} O_2 and maintained using 1.5 - 2% Isofluorane/0.4 litre min^{-1} O_2. Redux Crème (Parker Laboratories, Inc., USA) was placed on the back of each paw and the mouse secured in a supine position, on a Vevo mouse-handling platform (FujiFilm VisualSonics Inc., Netherlands), with paws taped to electrodes allowing observation of ECG and breathing rate. Body temperature was monitored using a rectal probe, and was maintained between 36.8 – 37.2°C using a heated stage and a heat lamp when required. A schematic illustrating the positioning of the mouse for echocardiography imaging can be seen in **Figure 2.3.**

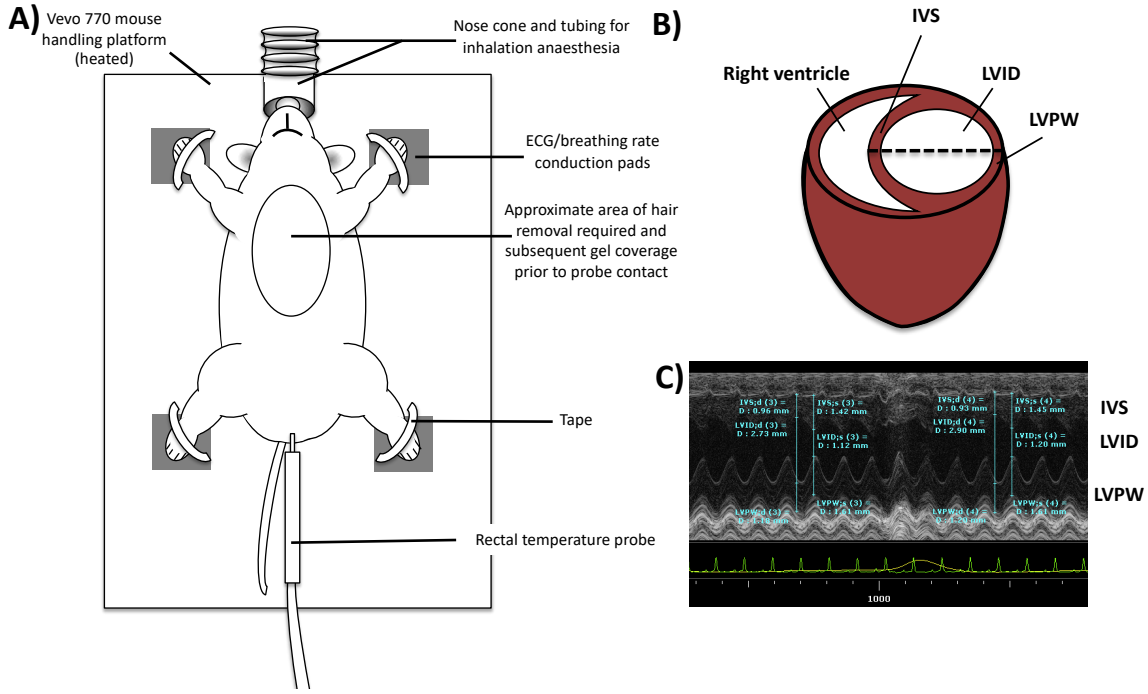

Figure 2.3 Mouse echocardiography set-up, plane of m-mode imaging and example echocardiography trace. Schematic diagrams illustrating A) the set-up of a mouse during echocardiography, with the mouse in a supine position, secured using tape, with paws positioned on pads measuring ECG and breathing rate and B) the plane of echocardiography imaging for m-mode traces (- - -) and C) an example of an m-mode trace recorded from a control C57Bl6J mouse. Anaesthesia was maintained during the procedure using 1.5 - 2% Isofluorane/0.4 litre min^{-1} O_2 inhaled through a nose cone. Temperature was monitored using a rectal temperature probe. IVS = Intraventricular Septum, LVID = Left Ventricule Internal Dimension, LVPW = Left Ventricle Posterior Wall.

Chest fur was removed using Veet® For Men Hair Removal Gel Cream (available from Boots, UK) and Aqua Gel® Lubricating Gel (CIVCO Medical Solutions, USA) applied liberally to the chest. Three two-dimensional M-mode images were obtained for each mouse, from the same short-axis view. These images were then used for taking measurements of intraventricular septum (IVS) diameter, left ventricle internal dimension (LVID) and left ventricle posterior wall (LVPW) diameter in both systole (s) and diastole (d). From these measurements, left ventricle ejection fraction and left ventricle fractional shortening were calculated. For each mouse, 6 measurements of IVSs, LVIDs, LVPWs, IVSd, LVIDd and LVPWd were taken (blind) from M-mode images acquired during echocardiographic imaging. Calculations for ejection fraction (EF) and fractional shortening (FS) were made by the Vevo software using the following equations:

$$\textbf{\textit{Equation}}\ \mathbf{4}\text{: } EF(\%) = \left(\frac{(end\ diastolic\ volume - end\ systolic\ volume)}{end\ diastolic\ volume}\right) x\ 100$$

$$\textbf{\textit{Equation}}\ \mathbf{5}\text{: } FS(\%) = \left(\frac{LVIDd - LVIDs}{LVIDd}\right) x\ 100$$

Six measurements of each parameter were averaged for each mouse to generate a single n.

2.7.1. **ANGII and isoprenaline study echocardiography**

Echocardiography was conducted on all mice in the ANGII pre-treatment and reversal studies using the Vevo 770 on the day prior to mouse sacrifice and tissue collection. For isoprenaline studies, echocardiography was carried out on the Vevo 770 sequentially during the study, with data collected at baseline (the day prior to minipump implantation) and at weeks 1, 2 and 3 to determine cardiac function.

2.7.2. ***Xdh* WT (+/+) vs. Het (+/-) echocardiography**

For the *Xdh* WT (+/+) vs. Het (+/-) study, echocardiographic measurements were carried out on the Vevo 3100 machine at 8, 12 and 16 weeks of age. In mice undergoing ANGII infusion, imaging at 12 weeks of age was used as baseline data, with 16-week imaging carried out following 4 weeks of ANGII infusion. In addition to the aforementioned cardiac measurements, it was also possible to collect doppler flow data within the aortic arch from these mice.

2.8. **End of study blood collection under terminal anaesthesia**

At the end of our studies, mice had terminal anaesthesia induced using 5% Isofluorane/0.4 litre min^{-1} O_2, maintained with 2.5-3% Isofluorane/0.4 litre min^{-1} O_2. Sodium citrate (Sigma Aldrich®, UK) was used to create a 3.8% (w/v) solution by dissolving 7.6 g sodium citrate in 20 ml MQ filtered water. 80 µl of 3.8% sodium citrate was used in a 1 ml syringe for blood collection, acting as an anti-coagulant for blood draws. Blood was taken by cardiac puncture, or when hearts were to be used for histology, from the thoracic aorta (at the branch point to the left kidney), using a 23G needle and 1 ml syringe Note: Most *Xdh* mice were used for Langendorff and therefore blood was not collected from these mice.

3-Isobutyl-1-methylxanthine (IBMX) was added to a 300 µl aliquot of whole blood collected prior to centrifugation in order to prevent phosphodiesterase (PDE) inhibitors breaking down cGMP in samples. This would allow measurement of cGMP in frozen plasma samples using a cGMP assay. To achieve this, a 100 mM stock of 3-Isobutyl-1-methylxanthine (Sigma Aldrich®, UK) was made up in dimethyl sulfoxide (Sigma Aldrich®,

UK). This stock was then diluted 1:9 in sterile saline to give a 10 mM working solution. 3 µl of this 10 mM solution was used per 300 µl blood to give a final concentration of 100 µM IBMX.

The remaining blood was placed in an empty 1.5 ml tube. Both tubes were centrifuged for 5 minutes at 13,000 *g* at 4°C before IBMX-treated and untreated plasma were removed and aliquoted from their respective tubes and stored separately from the cell pellets. All plasma and cell pellet samples were snap frozen in liquid nitrogen then stored at -80°C.

2.9. **Tissue extraction**

After blood collection the following tissues were dissected: heart, thoracic aorta, aortic arch, lungs, liver, kidneys, spleen, tongue, salivary glands and mesentery. All tissues were rinsed briefly in phosphate buffered saline (PBS) and placed in 1.5 ml microcentrifuge tubes, snap frozen in liquid nitrogen and stored at -80°C.

2.10. **Plasma nitrite and nitrate concentrations determined by ozone chemiluminescence**

Ozone chemiluminescence was used to determine the concentration of nitrite and nitrate present in samples of plasma. Prior to chemiluminescence measurement of plasma, samples were deproteinated using Vivaspin 500 filter columns (Sartorius Stedim Biotech, SA). Each column was washed twice with 200 µl MQ filtered water by centrifuging at 14,000 *g* for 15 minutes at room temperature, to remove any possible pre-existing nitrite/nitrate contamination. Following this, each plasma sample was centrifuged through a Vivaspin 500 filter at 14,000 *g* for 60 minutes at 4°C. Samples were then snap frozen in liquid nitrogen and stored at -80°C until used in an ozone chemiluminescence assay. As healthy urine does not contain any protein, defrosted urine samples could be used directly in ozone chemiluminescence without being filtered.

2.10.1. **Ozone chemiluminescence**

Ozone chemiluminescence is an assay based on the reaction between NO and ozone (O_3), which generates Nitrogen Dioxide (NO_2), some of which exists in an excited state with unstable electrons (NO_2*). When this excited form returns to ground state, a

photon (hv) of light will be emitted, which can be detected and measured quantitatively. Equation 6 and Equation 7 describe the chemical reactions which are occurring:

$$\boldsymbol{Equation\ 6}: NO + O_3 \rightarrow NO_2^* + O_2$$

The reaction between NO and O_3 occurs in the gas phase.

$$\boldsymbol{Equation\ 7}: NO_2^* \rightarrow NO_2 + hv$$

For nitrite and NO_x quantification a Sievers 280i Nitric Oxide Analyzer (Sievers, USA) was used. In order to quantify levels of nitrite or NO_x in a sample, the metabolite in question can be reduced to NO in order to allow direct quantification by the resulting light emission following its reaction with O_3.

2.10.2. Nitrite measurements

A schematic illustrating the equipment setup for nitrite measurement is shown in **Figure 2.4.** All nitrite measurements were conducted at room temperature. To allow quantification of nitrite present in a sample it must be chemically reduced to NO. The purge vessel therefore contains a reducing agent, 1% (w/v) potassium iodide (Sigma Aldrich®, UK) in glacial acetic acid (AnalaR Normapur, VWR, UK). 5 ml of reducing agent was added to the purge vessel and nitrogen bubbled through for 10 minutes prior to starting measurements in order to remove all oxygen.

A standard curve was generated by preparing a 1 mM sodium nitrite ($NaNO_2$) stock solution by dissolving 0.069 g $NaNO_2$ (Sigma Aldrich®, UK) in 1 L of MQ filtered water. The nitrite concentration of MQ water was tested first, by injecting 25 µl into the purge vessel (a peak should not be seen). Then 0.1 µM, 1 µM and 10 µM dilutions of the 1 mM $NaNO_2$ stock were used to construct a calibration curve for nitrite measurements. 20 µl, 40 µl and 50 µl of each dilution was used in turn, beginning with the smallest volume of the most dilute sample. Once a satisfactory calibration curve had been created (see **Figure 2.5**), the concentrations of nitrite in an unknown sample could be tested. For filtered plasma samples, 30 µl of each sample was injected into the purge vessel. When samples are added to the vessel, the following reaction occurs:

$$\boldsymbol{Equation\ 8}: I^- + NO_2^- + 2H^+ \rightarrow NO + \frac{1}{2}I_2 + H_2O$$

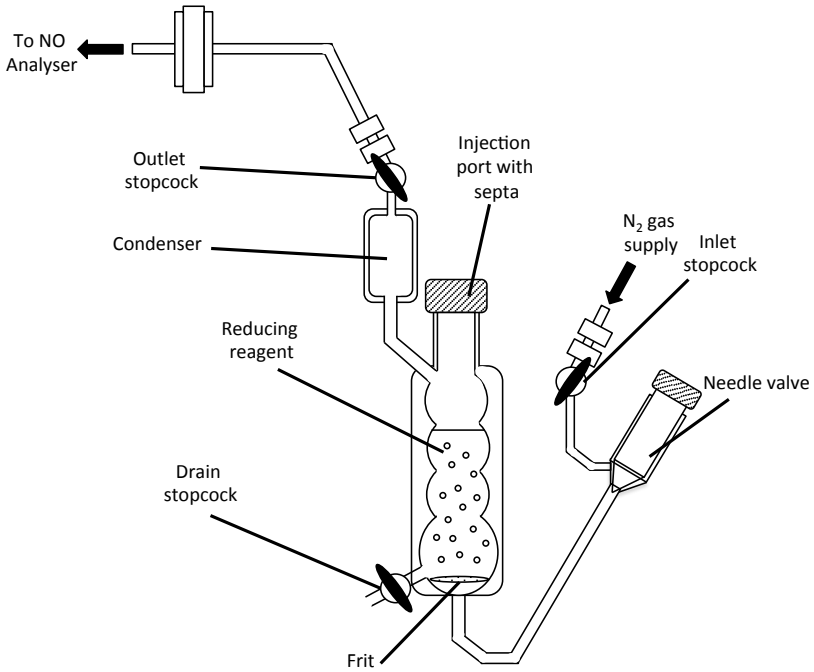

Figure 2.4 Schematic of ozone chemiluminescence equipment set-up for nitrite measurements
Schematic diagram illustrating the set-up of equipment for ozone chemiluminescence nitrite measurements in water and filtered plasma samples.

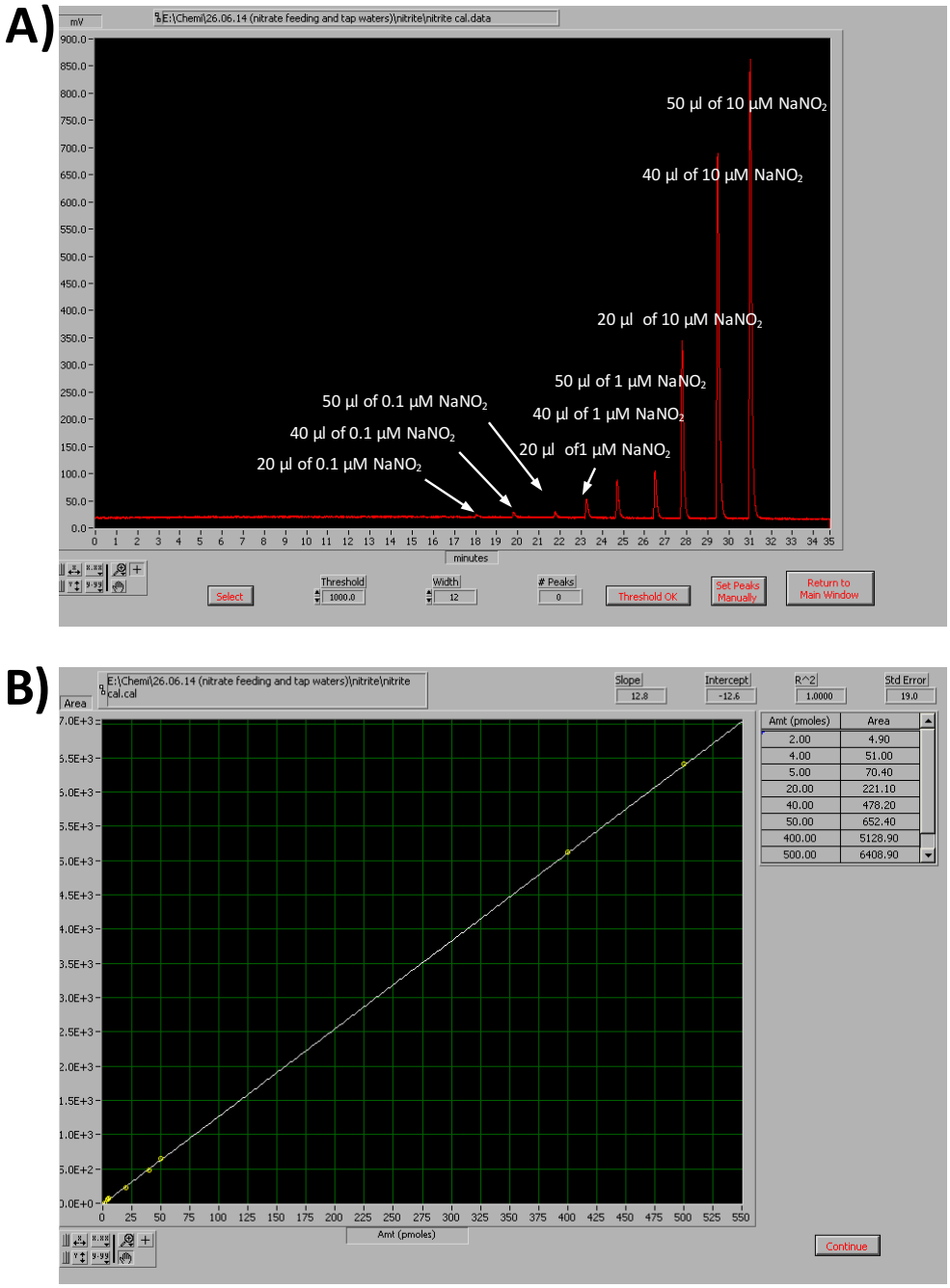

Figure 2.5 A typical nitrite calibration curve in ozone chemiluminescence experiments.
Figure illustrating A) peaks observed following injections of nitrite standard concentrations (20, 40 and 50 µl injections of 0.1 µM, 1 µM and 10 µM $NaNO_2$) and B) the resulting standard concentration curve.

2.10.3. <u>NO_x measurements</u>

A schematic illustrating equipment setup for NO_x measurement is shown in **Figure 2.6**. In order to measure nitrate levels in a sample, the equipment was adjusted and reducing agent changed to 0.1 M vanadium (III) chloride (Sigma Aldrich®, UK) in 1 M hydrochloric acid (Sigma Aldrich®, UK). This was refluxed in the purge vessel at 95°C under nitrogen. These reducing conditions cause nitrate and nitrite to be converted NO (which is measured upon reaction with O_3). A gas bubbler filled with 1 M sodium hydroxide

(NaOH) was attached between the purge vessel and the NO analyser to prevent vapour damage to the analyser.

Equation 9 illustrates the reduction of nitrate to NO:

$$\boldsymbol{Equation\ 9}: 2NO_3^- + 3V_3 + 2H_2O \rightarrow 2NO + 3VO_2^+ + 4H^+$$

The measurement of nitrite and nitrate concentrations in a sample is referred to as 'NO_x'. To calculate the concentration of specifically nitrate in a sample, it is therefore necessary to measure both nitrite and NO_x concentrations, then use the following equation:

$$\boldsymbol{Equation\ 10}: [NO_x] - [NO_2^-] = [NO_3^-]$$

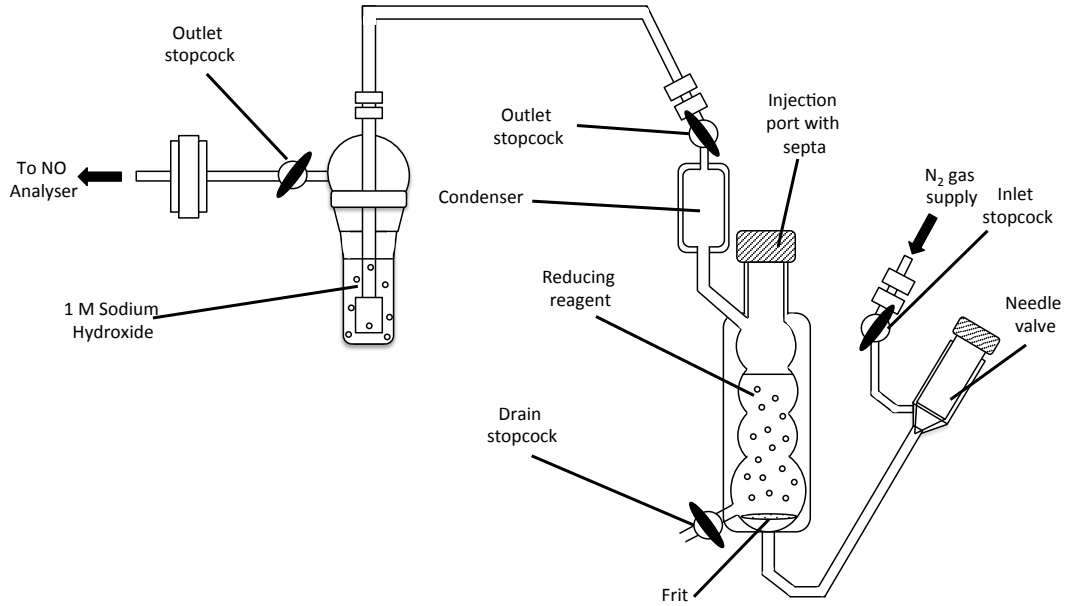

Figure 2.6 Schematic of ozone chemiluminescence equipment set-up for nitrate measurements.
Schematic diagram illustrating the set-up of equipment for ozone chemiluminescence nitrate measurements in water and filtered plasma samples.

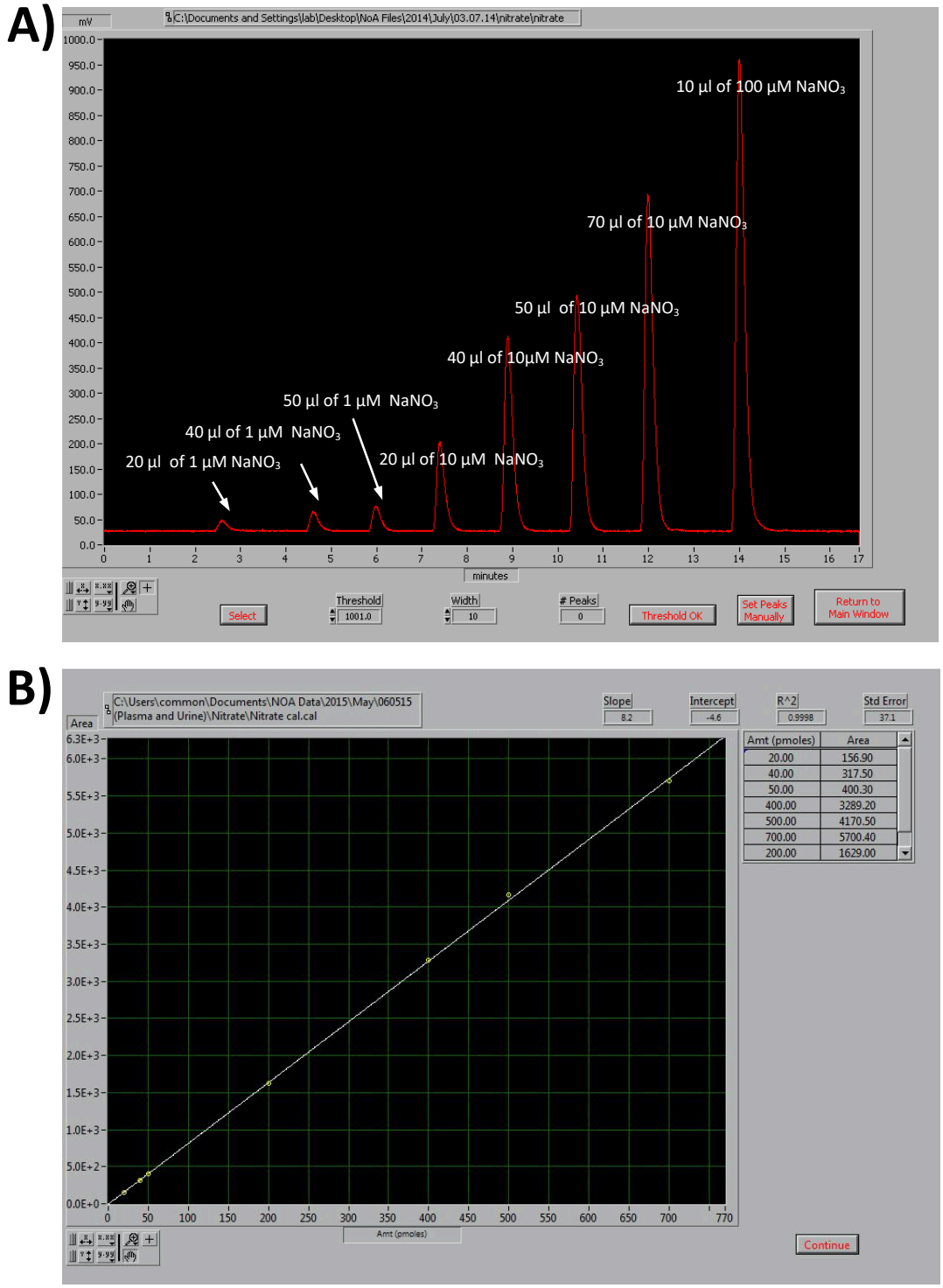

Figure 2.7 A typical NO_x calibration curve in ozone chemiluminescence.
Figure illustrating A) peaks observed following injections of nitrate standard concentrations (20, 40 and 50 µl injections of 1 µM $NaNO_3$, then 20, 40, 50 and 70 µl injections of 10 µM $NaNO_3$ and 10 µl of 100 µM $NaNO_3$) and B) the resulting standard concentration curve.

A 1 mM sodium nitrate ($NaNO_3$) stock solution was prepared by dissolving 0.085 g $NaNO_3$ (Sigma Aldrich®, UK) in 1 L of MQ filtered water. For constructing a NO_x calibration curve, 1 µM, 10 µM and 100 µM dilutions were made. Again, before creating a NO_x calibration curve, MQ water was tested as a blank sample. Then 20 µl, 40 µl then 50 µl of 1 µM $NaNO_3$ were added to the purge vessel in turn, followed by 20 µl, 40 µl,

50 µl then 70 µl of 10 µM $NaNO_3$. Finally, 10 µl of 100 µM $NaNO_3$ was added. See **Figure 2.7** for a typical nitrate calibration curve trace.

When measuring NO_x in water samples, original samples were diluted 1:1000 (first 1:10, then 1:100) for NO_x measurements. 10µl of each sample was then injected into the purge vessel in turn. Plasma sample dilutions are shown in **Table 2.2**. When sufficient sample volume was available, injections were carried out in duplicate and average concentrations calculated to generate a single value.

Treatment Group	Dilution
KNO_3 Control	1:10
KCl Control	n/a
ANGII + KNO_3 Pre	1:10
ANGII +KCl Pre	n/a
ANGII + KNO_3 Rev	1:10
ANGII +KCl Rev	n/a
Iso + KNO_3 Pre	1:10
Iso + KCl Pre	n/a

Table 2.2 Plasma dilutions for ozone chemiluminescence. Table shows dilutions used for mouse plasma and urine samples during ozone chemiluminescence measurement of NO_X.

2.11. cGMP assay

A cGMP assay was carried out in mouse plasma using a commercially available Biotrak cGMP enzyme immunoassay kit (GE Healthcare, UK). This is a competitive enzymeimmunoassay, where cCAMP peroxidase competes with cGMP for substrate binding to a rabbit anti-cGMP antibody. Therefore, the level of colour developed by cCAMP peroxidase as a result of antibody binding, and the subsequent reaction with substrate mix, is inversely proportional to the concentration of cGMP present in the sample. Thus, the greater the amount of cGMP in the unknown (or standard), the less colour generated upon addition of the enzyme substrate. Protocol 2 from the instruction manual was used for determination of cGMP concentrations in plasma.

3 µl of a 10 mM IBMX solution (formulation described in section 2.8) was added to 300 µl whole blood upon collection prior to spinning down to separate plasma and blood pellet. This was to inhibit breakdown of cGMP by phosphodiesterases. The plasma aliquot collected was snap frozen and stored -80°C before being used for the cGMP assay.

2.11.1. Reagent preparation

Prior to beginning the assay, reagents were equilibrated to room temperature. To prepare the assay buffer the bottle contents (10 ml) were transferred to a 500 ml glass cylinder and made up to 500 ml with MQ water. To prepare the acetylation standard 2.5 ml of diluted assay buffer was added to the acetylation standard bottle and mixed until completely dissolved. To prepare the antibody 11 ml diluted assay buffer was added to the antibody bottle, and the contents gently mixed until dissolved. To prepare the cGMP conjugate 11 ml diluted assay buffer was added to the bottle and the contents gently mixed until dissolved. To prepare the wash buffer, the contents were transferred to a 500 ml measuring cylinder and made up to 500 ml with MQ water.

2.11.2. **Preparation of standards and samples**

Standards had to be used within 1 hour of preparation, so were made up accordingly. 9 microcentrifuge tubes were labelled 2, 4, 8, 16, 32, 64, 128, 256, 512 (referring to the fmol amount of cGMP standard which will be present in the final well). 500 µl diluted assay buffer was added to all tubes except the 512 fmol tube. 500 µl of standard (10.24 pmol/ml) was added to the 512 tube, and 500 µl also added to the 256 tube. Serial dilutions were then made up by transferring 500 µl of each stock in turn, beginning with transferring 500 µl from the 256 tube to the next tube (128). This was repeated for the rest of the tubes to give 1:2 dilutions. For the zero standard, only 500 µl diluted assay buffer was present. 500 µl of each unknown sample was required for the assay. For each plasma sample we used diluted 1:200 assay buffer.

2.11.3. **cGMP assay protocol**

After having prepared the assay reagents at room temperature, the acetylation reagent was prepared by mixing 1 volume acetic anhydride with 2 volumes trimethylamine in a glass vessel. This was kept covered with parafilm and prepared under a fume hood to protect against the fumes. The volume required was determined by the number of samples to be run - with 50 µl of acetylation reagent required per standard/unknown.

50 µl of acetylation reagent was added to each standard and unknown's microcentrifuge tube. When adding the acetylation reagent, the pipette tip was placed in contact with the microcentrifuge tube to allow fluid to run down the side. The sample was then vortexed immediately after addition.

100 µl of antiserum was added into all wells of a 96 well plate (except for the blank and NSB well). Starting with the most dilute, 50 µl of all standards and unknowns were pipetted into the appropriate wells according to the plate template in **Figure 2.8**. 150 µl of assay buffer was added to non-specific binding (NSB) well. The plate was covered and gently mixed, then incubated at 4°C for 2 hours. At this point the conjugate was removed from the fridge to equilibrate to room temperature. After the 2-hour incubation step, 100 µl of diluted conjugate was added into all wells except the blank. The lid was replaced, and plate incubated for 60 minutes at 4°C. At this point the wash buffer was taken out of the fridge to equilibrate to room temp, and TMB was taken out after 30 min to equilibrate to room temp.

The contents of all wells were aspirated and washed 4 times with wash buffer, with the plate blotted on tissue to remove any residual buffer. 200 µl of enzyme substrate was added into all wells, the plate covered and mixed for 30 min at room temp. 100 µl 1M sulphuric acid was added to all wells and the plate read at 450 nm using the TECAN Sunrise 96 well plate reader.

<>	1	2	3	4	5	6	7	8	9	10	11	12
A	Blank	Blank	64	64	A115	A115	A112	A112	Is77	Is77	Is76	Is76
B	NSB	NSB	128	128	A117	A117	A116	A116	Is79	Is79	Is78	Is78
C	0	0	256	256	A119	A119	A118	A118	Is83	Is83	Is86	Is86
D	2	2	512	512	A121	A121	A120	A120	Is91	Is91	Is90	Is90
E	4	4	A107	A107	A123	A123	A122	A122	Is95	Is95	Is92	Is92
F	8	8	A109	A109	A125	A125	A126	A126	Is97	Is97	Is94	Is94
G	16	16	A111	A111	A108	A108	A128	A128	Is99	Is99	Is100	Is100
H	32	32	A113	A113	A110	A110	Is75	Is75	Is101	Is101	Is102	Is102

Figure 2.8 Example plate layout for cGMP immunoassay.
All standards and unknown samples were plated in duplicate (white and blue). NSB = non-specific binding. Samples denoted by A = angiotensin study mice and Is = isoprenaline study mice.

2.12. Heart weight:body weight and left ventricle:body weight ratios

At the end of the study, mice were weighed before blood/tissue extraction. In cases where minipumps and/or probes were removed from the mouse, these were also weighed and the weight subtracted from the total mouse weight to give an acurate mouse weight. When the heart was removed from the mouse, this was rinsed, blotted on tissue paper and weighed. In samples where the heart did not have to remain whole for histology or other assessments, the left and right ventricle were also seperated and weighed individually. Heart weight: body weight (mg/g) ratio (HW:BW) and/or left ventricle: body weight ratio (LV:BW) could then be calculated for each mouse.

2.13. Heart histology

Picrosirius red PSR staining identifies areas of connective tissue deposition, with collagen showing red, and muscle/other tissue elements yellow. At the end of studies whole hearts were fixed in 10% Formalin solution (5ml) and embedded in paraffin at Blizzard Institute Core Pathology Facility (UK) prior to PSR staining. Hearts were randomly assigned to be sectioned in either the transverse or dorsal plane. 4 µm sections were cut using a microtome (Thermo Scientific, UK) and heart sections stained with PSR; 0.1 g sirius red F3BA ((Direct red 80), Sigma Aldrich, UK) in 100 ml saturated aqueous picric acid (Sigma Aldrich, UK). Images were acquired using a NanoZoomer slide scanner (Hamamatsu) and viewed using NDP View software. 3 left ventricle, 3 intraventricular septum and 3 right ventricle fields of view were randomly selected at x20 magnification (see **Figure 2.9**) and PSR staining quantified using manual thresholding techniques in ImageJ software. Manual thresholds were set for each image at which the red collagen deposition could be clearly distinguished from the yellow

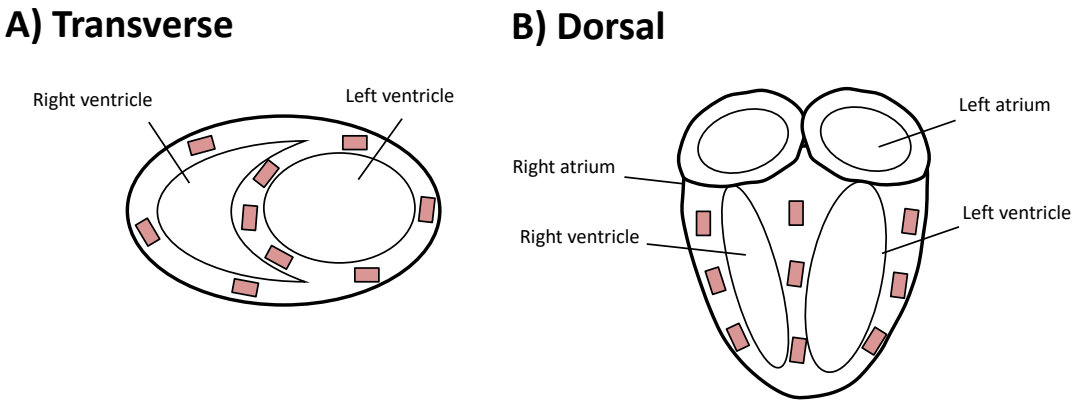

tissue. The area of red staining, relative to the area of yellow was quantified. An average of all 9 fields of view was calculated for each mouse to give a single n value. Quantification was conducted blind to treatments.

Figure 2.9 Fields of view selected at x20 magnification for histology.
Schematic illustrating examples of the fields of view selected at x20 magnification for histology analysis. Images of 4 µm thick heart sections stained with Picrosirus Red were acquired using a NanoZoomer slide scanner (Hamamatsu) and viewed using NDP View software. 3 left ventricle, 3 intraventricular septum and 3 right ventricle fields of view were randomly selected from all samples. Hearts were sectioned either in the A) transverse or B) dorsal plane.

2.14. Organ bath pharmacology

At the end of the study, aortae from a subset of study mice were used in organ bath assays in order to characterize vasoreactivity in response to various vasodilators and vasoconstrictors. Thoracic aortae were dissected from mice and fat and connective tissue were carefully removed whilst immersed in Krebs solution. The aorta was cut into

rings ~3 mm long with 3 or 4 rings typically generated from each mouse. Rings were then mounted onto the wires of the organ bath, with care taken not to damage the endothelium during the mounting process. Organ baths had a total fill volume of 10 ml and contained Krebs solution (see section 7.19.1) heated to 37**°**C and bubbled with 95% O_2, 5% CO_2. A schematic illustrating the organ bath equipment and set-up is shown in **Figure 2.10**.

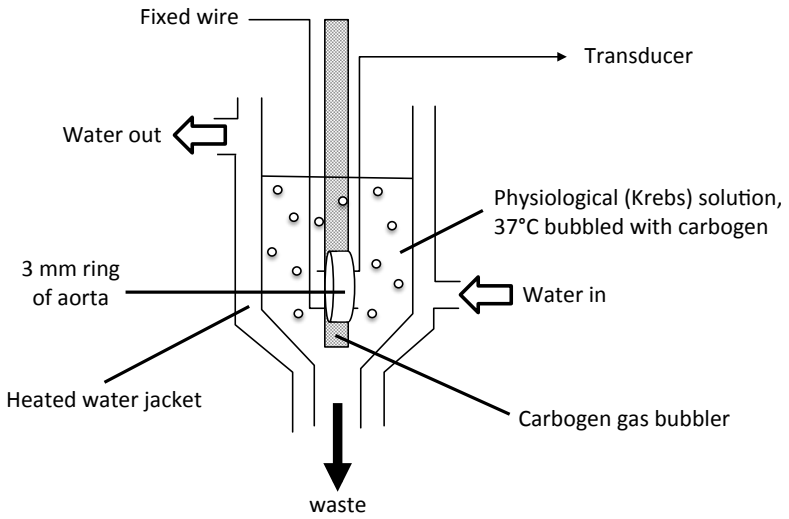

Figure 2.10 Thoracic aorta organ bath set-up.
Schematic diagram illustrating the set-up of a typical organ bath with a 3 mm ring of thoracic aorta mounted on the wires. The vessel is mounted in physiological (Krebs) solution, maintained at 37°C by the heated water jacket, and bubbled with carbogen. Total organ bath volume is 10 ml.

Post mounting, tension of aortic rings was set at 0.3 g and rings left to equilibrate for 45 minutes, washed every 15 minutes (with each wash consisting of 2 repeat washes) and tension adjusted back to 0.3 g when necessary. Following this equilibration period, rings were contracted with 48 mM KCl (adding 120 µl of 4 M KCl to the bath). Once the contraction had plateaued, rings were washed once every 10 minutes for 30 minutes (with each wash consisting of 2 repeat washes) and the KCl contraction repeated again. After maximal contraction had again been reached, rings were washed once every 10 minutes for 30 minutes (with each wash consisting of 2 repeat washes).

To test endothelial integrity, rings were pre-contracted with 10^{-5} M phenylephrine (PE) and once a stable level of contraction had been reached, 10^{-5} M ACh added to induce vessel relaxation. When maximal relaxation in response to acetylcholine (ACh) had occurred, rings were washed once every 10 minutes for 30 minutes (with each wash consisting of 2 repeat washes).

1 of 3 randomly assigned concentration-response curves was then constructed in each vessel. A cumulative contraction concentration response curve to PE (10^{-9} – 3 x 10^{-5} M), or in PE-pre-contracted vessels, a relaxation curve to ACh (10^{-9} – 3 x 10^{-5} M) or Spermine NO-NOate (SNO) (10^{-9} – 3 x 10^{-5} M) was constructed.

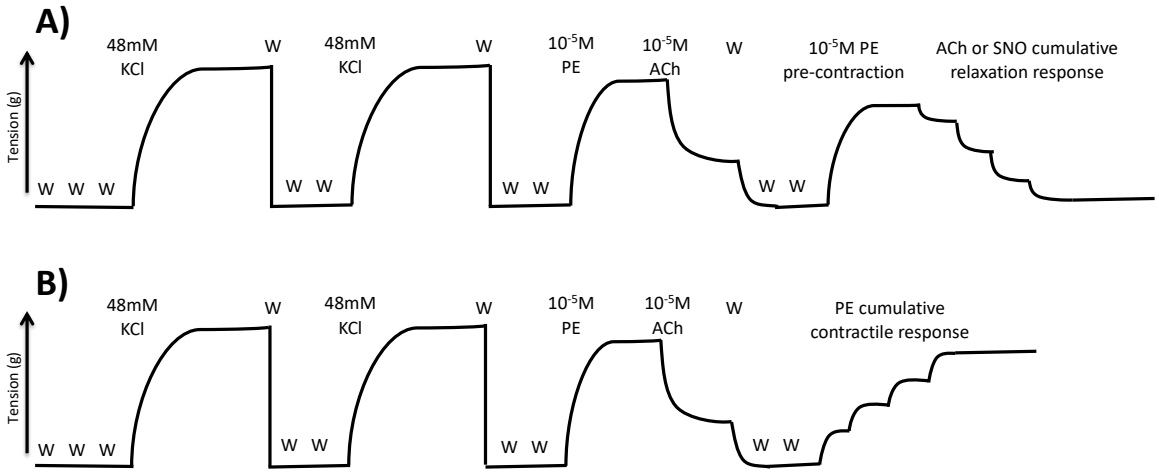

Figure 2.11 Typical organ bath experimental design.
Schematic illustrating examples of typical organ bath experiments conducted on mouse aortas at the end of this study. Experiments comprise two 48 mM KCl contraction responses and a 10^{-5} M ACh relaxation response followed by either A) a cumulative ACh or SNO relaxation curve following precontraction with 10^{-5} M PE, or B) a cumulative PE contractile concentration response curve. Each treatment is interspersed with wash steps (W), with tension returned to baseline of 0.3 g at these points.

For PE pre-contractions of both ACh and SNO curves, one of two conditions were used. Some rings were pre-contracted with a standard concentration of 10^{-5} M PE – ensuring all aortae received an equal concentration of vasoconstrictor prior to inducing relaxation. This condition is likely to more accurately mimic *in vivo* conditions of aortic vessels, where equal levels of vasoconstrictive stimulation would be expected to be present in these mice. Alternatively, PE concentration was titrated until vessel tension reached EC_{75} of KCl maximal contraction. This condition allowed comparison of response to ACh and SNO when the level of pre-contracted vessel tone is equal in all vessels.

Figure 2.11 shows a typical example of an organ bath experiment, and a table of volumes and drug concentrations used for single concentrations and cumulative concentrations can be found in **Table 2.3**.

	Working Concentration (M)	Final concentration in bath	Cumulative concentration response (µl)	Single concentr (µl)
-9	10^{-6}	**10^{-9}** (1nM)	10	10
-8.5	10^{-6}	**3 x 10^{-9}** (3nM)	20	30
-8	10^{-5}	**10^{-8}** (10 nM)	7	10
-7.5	10^{-5}	**3 x 10^{-8}** (30 nM)	20	30
-7	10^{-4}	**10^{-7}** (100 nM)	7	10
-6.5	10^{-4}	**3 x 10^{-7}** (300 nM)	20	30
-6	10^{-3}	**10^{-6}** (1 µM)	7	10
-5.5	10^{-3}	**3 x 10^{-6}** (3 µM)	20	30
-5	10^{-2}	**10^{-5}** (10 µM)	7	10
-4.5	10^{-2}	**3 x 10^{-5}** (30 µM)	20	30
-4	10^{-1}	**10^{-4}** (100 µM)	7	10
-3.5	10^{-1}	**3 x 10^{-4}** (300 µM)	20	30
-3	10^{-0}	**10^{-3}** (1 mM)	7	10
-2.5	10^{-0}	**3 x 10^{-3}** (3 mM)	20	30

Table 2.3 Table showing working concentrations (M) and final concentrations in a 10 ml organ bath resulting from either a cumulative concentration response (µL) or a single concentration (µL) of these working concentrations.

Data Analysis:

Any aortic ring from control mice with a relaxation of <50% in response to 10^{-5} M ACh was excluded from data analysis, as this suggests that the endothelium has been damaged during dissection/mounting. However, as it is possible that endothelial dysfunction may occur in ANGII-infused animals, all rings from ANGII-infused animals (regardless of their endothelial response), were used for data analysis.

PE contraction was represented relative to maximal 48 mM KCl contraction, using the following equation:

$$\textbf{\textit{Equation 11}}: \frac{tension\ observed - basal\ tension}{KCl\ contraction - basal\ tension}\ x\ 100$$

ACh and SNO relaxation was calculated using the following equation:

$$\textbf{\textit{Equation 12}}: \frac{precontracted\ tension - tension\ observed}{precontracted\ tension - basal\ tension}\ x\ 100$$

Concentration response curves could then be plotted, and EC_{50} values for each curve calculated. Vessel contraction in response to 48 mM KCl and 10^{-5} M PE, and relaxation in response to 10^{-5} M ACh was also calculated for each ring.

2.14.1. **Krebs and drug formulations**

A working concentration of Krebs Ringer Solution containing: 6.9 g/L sodium chloride, 0.35 g/L potassium chloride, 0.29 g/L magnesium sulphate, 0.16g potassium dihydrogen orthophosphate, 2.1 g/L anhydrous sodium hydrogen carbonate and 2 g/L D-glucose, was prepared by diluting a 10x stock (Sigma Aldrich®, UK) 1:10 with MQ filtered water. This was bubbled through with carbogen and 2.5 ml/L of 1 M Calcium chloride ($CaCl_2$)

(VWR - AVS Titrinorm, UK) added. Stock solutions of 10^{-2} M PE, ACh and SNO were made freshly by dissolving (R)-(-)-PE hydrochloride (Sigma Aldrich®, UK), ACh chloride (Sigma Aldrich®, UK) or SNO (Cayman Chemical Company, USA) in MQ filtered water. These were then serially diluted to yield 10^{-3}, 10^{-4}, 10^{-5} and 10^{-6} M solutions.

2.15. Langendorff ex-vivo heart prep

In some experiments, hearts from mice were excised and mounted used in a Langendorff perfusion system. A 5x stock of Krebs was made up in MQ water and refrigerated until use. 5x stock contained 34.63g/L NaCl, 1.76g/L KCl, 1.48g/L $MgSO_4$, 0.82g/L KH_2PO_4, 10.8g/L Glucose, 10.5g/L $NaHCO_3$, 1.1g/L Sodium Pyruvate. This stock was diluted to a 1x solution on day of experiment. 1 x Krebs solution was filtered using Whatman microfibre 1μm filter paper (Fischer Scientific, UK) and bubbled with carbogen before 1.7 ml/L of $CaCl_2$ (1.7 mM) was added. The pH was measured and maintained at pH7.4 ± 0.05 by adjusting carbogen bubbling as required.

2.15.1. Langendorff set-up

The water bath temperature was set so that the Krebs in the reservoir system was 37 ± 0.5°C. The heart was perfused at a flow rate of 2 ± 0.5 ml/min. Briefly, 100 μL of heparin (5000 iu/ml, IP) was given prior to induction of anaesthesia with 5% isoflurane, 0.4 ml/min oxygen. Anaesthesia was maintained with 3% isoflurane, 0.4 ml/min oxygen. An incision was made just below the sternum, the heart removed and washed in a modified ice-cold Krebs solution (see section 2.15).

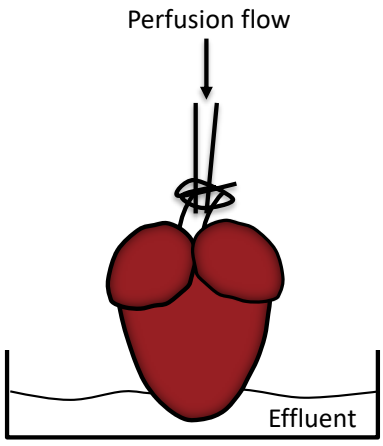

Figure 2.12 Schematic illustrating the mounting of a mouse heart in the Langendorf set up, with perfusion flow in through the aorta.

In a petri dish, the aortic arch was visualised, and fat, connective tissue and thymus trimmed as required. The aorta was isolated and then tied to the perfusion set-up as depicted in **Figure 2.16**. The apex of the heart was submerged in effluent Krebs. Following mounting, the afterload pressure was gradually increased to 100 mmHg to achieve a coronary perfusion pressure (CPP) of approximately 75-120 mmHg. Under these conditons, the spontaneous heart rate is 300-400 BPM. Hearts not achieving 300 BPM were excluded. Following a 15 min period of CPP stabilisation the experimental protocol was carried out. Concentration response curves were created with 0.01, 0.1

and 1 nmol SNP, and 0.1, 1 and 10 nmol bradykinin, as shown in **Figure 2.13**. This was then followed by a 15 min response to 300 μM L-NAME.

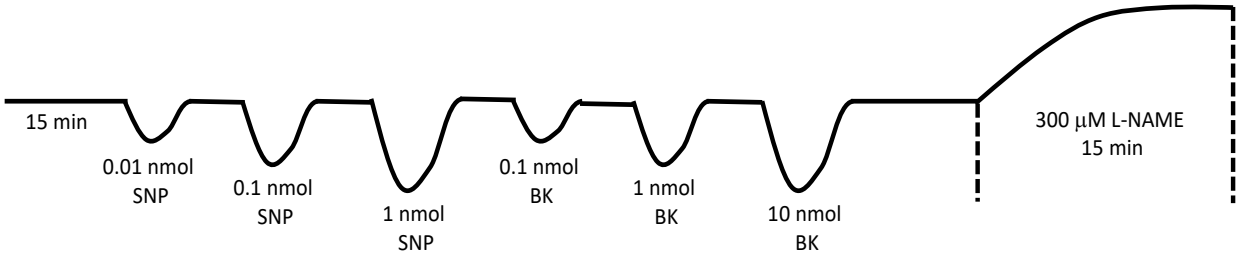

Figure 2.13 Typical Langendorff experimental design.
Schematic illustrating the time course of a typical Langendorff experiment, with a 15-minute equilibration period, concentration responses to sodium nitroprusside (SNP) and bradykinin (BK), and a 15-minute response to L-NAME.

2.15.2. Drug formulation

2.15.2.1. Sodium nitroprusside (SNP)

Approximately 1.5 mg of SNP (Sigma Aldrich, UK) was used to make a 10 mM stock solution of SNP in MQ. Serial dilutions were generated to give 0.1 mM, 0.01 mM and 0.001 mM working concentrations. Injections of 10μL each would result in 1 nmol, 0.1 nmol and 0.01 nmol respectively.

2.15.2.2. Bradykinin

0.5 ml of a 10 mM stock of Bradykinin (Bachem, Switzerland) was made up in Lobind tubes (5.3 mg in 0.5 ml). This was divided into 10 μL aliquots in Lobind tubes and stored at -20 °C. Frozen stocks were then used to make serial dilutions 1:10 (10μL stock:90μL MQ water) to get working concentrations of 1 mM, 0.1 mM and 0.01 mM. Injections of 10μL into the Langendorff would result in 10, 1 and 0.1 nmol respectively.

2.15.2.3. L-NAME

1 ml of 300 mM stock of L-NAME (Sigma Aldrich, UK) was required, so 80.91 mg was weighed and dissolved in 1 ml MQ water. This stock was diluted 1:1000 by adding 0.5 ml stock to 499.5ml Krebs to give a 300 μM solution. This L-NAME solution was then perfused through the heart for 15 mins (time from L-NAME actually reaching the heart).

2.16. Quantitative reverse transcription polymerase chain reaction (RT-PCR)

Expression of key molecular markers of cardiac hypertrophy were determined in mouse heart tissue using RT-PCR. Genes selected for analysis were: AT1Ra, BNP, CTGF, Col1a, Col3, NLRP1, NLRP3, TGFβ and XOR. The primer sequences used are shown in **Table 2.4**.

Gene	FWD 5'-3'	RVS 5'-3'	BLAST Results	Reference
18S	AGCCTGCGGCTTAATTTGAC	CAACTAAGAACGGCCATGCA	121bp	Villar, I.C. et al., 2011
AT1Ra	AACAGCTTGGTGGTGATCGTC	CATAGCGGTATAGACAGCCCA	135 bp	Zhou et al., 2011
BNP	TATCTGTCACCGCTGGGAGG	TTGTGAGGCCTTGGTCCTTC	151bp	Gaspar-Pereira, S. et al., 2012
COL1A	TCCTGCTGGTGAGAAAGGAT	TCCAGCAATACCCTGAGGTC	103bp	Villar, A.V. et al., 2013
COL3	TCGGAACTGCAGAGACCTAAA	CCCCAGTTTCCATGTTACAGA	122 bp	van Bilsen et al., 2014
CTGF	CACAGAGTGGAGCGCCTGTTC	GATGCACTTTTTGCCCTTCTTAATG	163 bp	van Bilsen et al., 2014
NLRP1	ATGTGGACCCAACCTTCAAA	GTACGTGCTCCTGGAAAGGT	108 bp	Sand et al., 2018
NLRP3	TGCTCTTCACTGCTATCAAGCCCT	ACAAGCCTTTGCTCCAGACCCTAT	85 bp	Kaushik et al., 2012
TGFβ1	GGATACCAACTATTGCTTCAGCTCC	AGGCTCCAAATATAGGGGCAGGGTC	156bp	Sullivan, D.E. et al., 2009
XDH	GGTTGTTTCCACTTCCTCCA	TTCCAAGGAAACCTCTGTCG	103 bp	Yang et al., 2009

Table 2.4 Primer sequences to be used for RT-PCRs on mRNA from mouse hearts.
Table shows primer sequences used for RT-PCRs investigating mRNA expression of various genes often implicated in cardiac hypertrophy/heart failure signaling, including: Angiotensin receptor type 1 (AT1Ra), brain natriuretic peptide (BNP), type I collagen (COL1A), type 3 collagen (COL3), connective tissue growth factor (CTGF), NLR Family Pyrin Domain Containing 1(NLRP1), NLR Family Pyrin Domain Containing 3 (NLRP3), transforming growth factor β (TGFβ) and xanthine oxidoreductase (XDH). 18S ribosomal RNA (18S) was used as an internal control 'housekeeping gene'. BLAST results for each primer pair show the predicted product length and references show papers where these sequences have been used previously.

2.16.1. RNA extraction from heart tissue

For RNA isolation, whole mouse hearts were each placed in 594 µl of RLT buffer from the RNeasy® Fibrous Tissue Minikit (Qiagen Ltd, UK) with 6 µl ß-mercaptoethanol in a CK-28 2 ml tube (Bertin Technologies, FR) and homogenised using a Precellys®24 homogeniser with protocol: 6000 (rate) for 15 seconds (x2) with a 5 second pause. A Cryolys® machine was used to maintain sample temperatures of 4 - 10°C during homogenisation. All further procedures were conducted at room temperature unless otherwise specified.

Once homogenised, 150 µl of homogenate was added to 590 µl of RNase free water with 10 µl of proteinase K, and incubated at 55°C for 10 minutes. This sample was then centrifuged at 10,000 *g* for 3 min and supernatant transferred to a new tube. 375 µl of 100% ethanol was added and pipetted repeatedly to mix. 700 µl of the resulting sample was added to an RNeasy® mini column (in a 2 ml collection tube) and centrifuged for 15 secs at 10,000 *g.* The flow-through was discarded and process repeated with the remainder of the lysate. 350 µl Buffer RW1 was then added to the column and centrifuged for 15 secs at 10,000 *g* and flow-through discarded. The RNeasy® DNase stock solution was diluted 1:7 in Buffer RDD, and 80 µl added to each RNeasy® membrane, and incubated for 15 min at room temp. 350 µl Buffer RW1 was then added to the column and centrifuged for 15 secs at 10,000 *g.* Flow-through was discarded, then

500 µl Buffer RPE added and centrifuged for 15 secs at 10,000 *g.* Another 500 µl Buffer RPE was added and centrifuged for 2 min at 10,000 *g.* The entire collection tube was discarded with flow-through, and the RNeasy® column placed in a new 2 ml tube and centrifuged at full speed for 1 min to dry membrane. The collection tube was discarded with flow-through and RNeasy® column placed in a new 1.5 ml microcentrifuge tube. 50 µl RNase-free water was added to the membrane and centrifuged for 1 min at 10,000 *g* to elute RNA. Resulting RNA concentration was measured using a ND-1000 UV/Vis NanoDrop spectrophotometer (NanoDrop Technologies, US). This concentration was then used to calculate the volume of RNA solution required to give 1 µg of RNA in the RNA to cDNA conversion reactions below. The 50 µl RNA eluate was split into two 25 µl aliquots for snap freezing and stored at -80°C until used for RNA to cDNA conversion.

2.16.2. **RNA to cDNA conversion**

RNA was converted to cDNA by first making a 'RT1 mix' in a 0.2ml Thermo-tube (Thermo Scientific, UK), comprising 1 µg RNA, 2 µl random hexamers (Life Technologies, UK, Product number: 48190-011), 1 µl 10 mM dNTP mix (Life Technologies, UK Product 18427-013) and made up to 12 µl total volume with molecular grade H_2O (5Prime, UK). This mixture was heated to 65°C for 5 minutes in a PTC-225 Peltier Tetrad Thermal Cycler (MJ Research, US), then removed and placed on ice. This step allows optimal primer annealing.

'RT2 mix,' comprising 4 µl First Strand Buffer, 2 µl 0.1 M Dithiotreitol (DTT), 1 µl Moloney Murine Leukaemia Virus (M-MLV) reverse transcriptase (Life Technologies, UK) and 1 µl RNase OUT Recombinant Ribonuclease Inhibitor (Life Technologies, UK. Product code: 10777-019) was then added to each tube. With RT2 mix added, tubes were heated again in the PTC-225 Peltier Tetrad Thermal Cycler (MJ Research, US) under the conditions shown in **Table 2.5**.

Assuming approximate conversion of 1 µg of RNA to 1 µg of cDNA, the resulting cDNA was diluted 1:10 in H_2O to give 5 ng/µl. This cDNA was then aliquoted and stored at -80°C until used in RT-PCR assays.

Step	Temperature	Time
Extension	25°C	10 min
Reverse transcription	37°C	50 min
Enzyme deactivation	70°C	15 min
Storage	4°C	Forever

Table 2.5 Table illustrating the stages of RNA to cDNA conversion reaction: with step description, temperature and length of time used.

2.16.3. RT-PCR assay

RT-PCR assays were conducted using SYBR green ROX mix (Thermo Scientific Abgene, UK) in 384 well plates, with primers (**Table 2.4**) sourced from Thermo Fischer Scientific. Each RT-PCR well contained 10 µl of SYBR green mix (Thermo Scientific Abgene, UK), 0.2 µl of 10 µM forward and 0.2 µl of 10 µM reverse primers (Thermo Fisher Scientific, UK), and 5.6 µl H_2O (5Prime, UK). Cycling conditions are shown in **Figure 2.14**. An ABI7900 HT Realtime PCR System (Applied Biosystems®, Life Technologies, UK), with SDS 2.3 computer software, was used to run and analyse plates. All samples were run in duplicate and gene expression was measured relative to internal control 18S and expressed relative to KCl fed controls using ΔΔCT analysis (Livak & Schmittgen 2001).

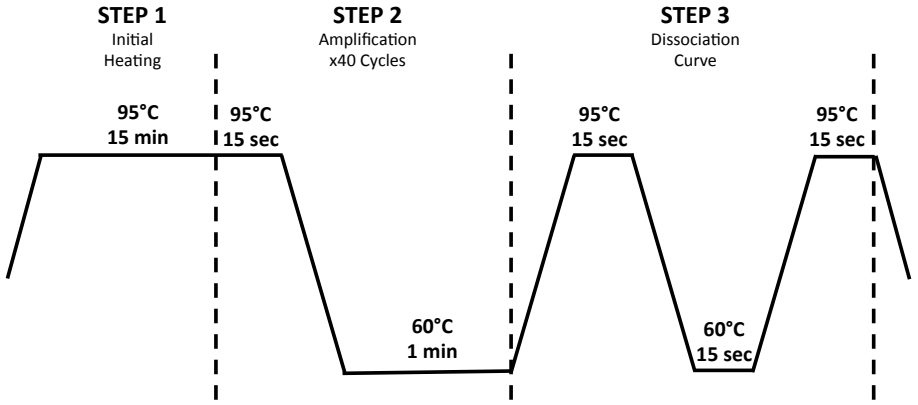

Figure 2.14 RT-PCR cycling conditions.
Schematic illustrating the cycling conditions used for RT-PCR assays in an ABI7900 HT Realtime PCR System (Applied Biosystems®, Life Technologies, UK).

2.17. Pierce® Bicinchoninic Acid (BCA) Protein Assay

Protein samples were diluted as required (previously determined to be 1:100 for liver protein, and 1:50 for heart) in leftover protease inhibitor cocktail following the homogenisation protocol used each particular assay. Specific protease inhibitor formulations are described in the appropriate methods sections below. Standard protein concentrations were prepared for a standard curve, using bovine serum albumin (BSA) provided in the BCA kit (Thermofisher, UK). A typical standard curve is shown in **Figure 2.15**. BSA was diluted in the same protease inhibitor cocktail used for tissue homogenisation.

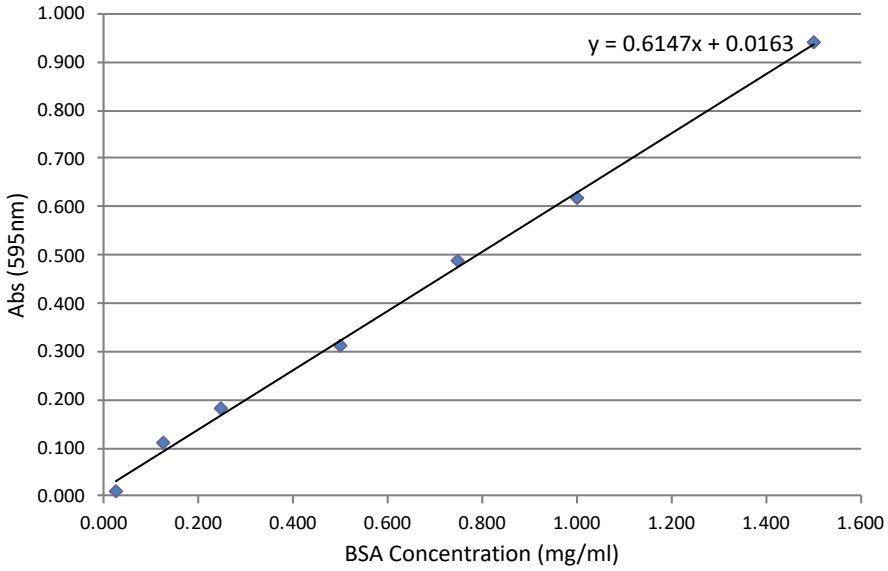

Figure 2.15 A typical standard curved from a Pierce®BCA protein assay as described in section 2.17.

The BCA working reagent mix was made according to manufacturer's instructions and in a 96-well plate, 25 µl of each standard or unknown were added to wells in duplicate followed by 200 µl of working reagent. The plate was then incubated at 37° C for 30 minutes and read using a TECAN sunrise plate reader, at a wavelength of 595 nm.

2.18. Measurement of xanthine oxidase activity

Xanthine oxidase activity was measured in liver homogenates using a commercially available colorimetric XO assay kit (abcam, UK). The assay measures levels of hydrogen peroxide (H_2O_2) produced by XO enzyme following oxidation of xanthine. The H_2O_2 produced reacts stoichiometrically with the OxiRed Probe in the reaction mix, generating a change in colour intensity, which is detected by a plate reader at 570 nm and is proportional to the level of XO activity.

Livers were homogenized in CK-28 2 ml tubes using a Cryolys® and Precellys®24 homogeniser (Bertin Technologies, FR) in a 1:4 ratio (tissue weight (mg): buffer volume (µl)) in the XO assay buffer supplied with the kit. This homogenate was then centrifuged at 16,000 *g* for 10 minutes. A standard curve was generated using 0, 0.1, 0.2, 0.3, 0.4 and 0.5 nmol/well of H_2O_2 standards. Liver samples were diluted 1:3 (50 µl sample: 150 µl XO assay buffer) and 50 µl of this added to the plate in triplicate. Two of these sample wells were used for the XO reaction, with full reaction buffer added. The remaining sample well had negative control buffer added.

XO reaction buffer consisted of 44 µl assay buffer, 2 µl xanthine substrate mix, 2 µl enzyme mix and 2 µl Oxired probe, per standard/unknown. Negative control buffer consisted of 46 µl assay buffer, no xanthine substrate mix, 2 µl enzyme mix and 2 µl Oxired probe mix, per standard/unknown.

The colour was measured using a Dynex MRX Revelation plate reader (Dynex Technologies Limited, UK) at 25°C, taking readings every 2 minutes for 3 hours at 570 nm. The point at which XO activity was observed during this period was determined by establishing when absorbance readings rose above that of the negative control. A 10-minute period from this time was then analysed, using the same 10-minute period for both treatment groups. A reading at T1 (activity = A1) was used and again at T2 (activity = A2) after incubation for 10 minutes. The signal generated by XO activity during this period is:

$$\boldsymbol{Equation\ 13}: \Delta A = A1 - A2$$

Background control signal was subtracted from all readings before calculation of ΔA, then ΔA used on the standard curve to gain B nmol of H_2O_2 (generated between T_1 and T_2 by XO). XO activity was then calculated as:

$$\boldsymbol{Equation\ 14}: XO\ Activity = \frac{(B\ x\ Dilution\ Factor)}{(T2 - T1)\ x\ V} = nmol/min/ml = mU/ml$$

One unit of XO is defined as the amount of enzyme that catalyzes the oxidation of xanthine, yielding 1 µmol of uric acid and H_2O_2 per minute at 25°C.

A typical standard curve is shown in **Figure 2.16**. The protein concentration of each sample determined using a Pierce® BCA Protein Assay Kit (Thermoscientific, UK) was used to correct the assay results retrospectively for variations in protein loading.

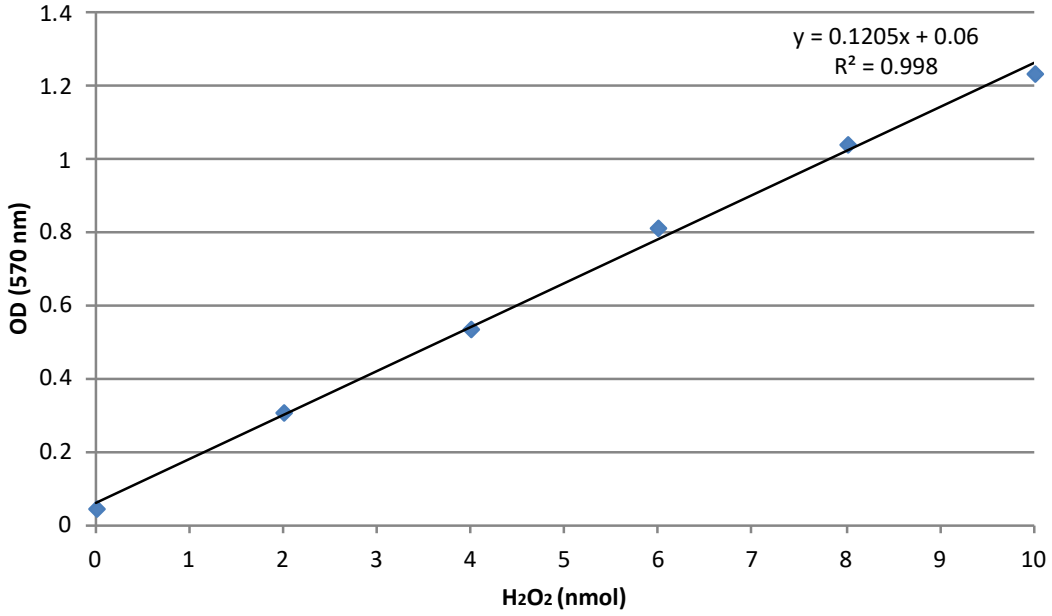

Figure 2.16 A typical standard curve from an XO assay as described in section 2.18.

2.19. Measurement of nitrite reductase activity

Nitrite reductase activity was measured in both heart and liver homogenates using gas phase chemiluminescence, as described previously (Webb et al. 2004). Heart and liver samples were homogenised in a 1:4 and 1:2 ratio respectively (tissue weight (mg): buffer volume (µl)) in buffer consisting of PBS with the protease inhibitors listed in **Table 2.6**.

Protease Inhibitor	Stock Concentration	Volume Added to 10 ml PBS	Final Concentration
Benzamidine	1mg/ml	10 µl	5.7 µM
Antipain	1mg/ml	10 µl	1.5 µM
Aprotinin	1 mg/ml	10 µl	0.15 µM
Leupeptin	1 mg/ml	20 µl	4.2 µM
Pepstatin A	0.7 mg/ml	10 µl	1.5 µM
AEBSF	100 mg/ml	10 µl	400 µM

Table 2.6 Details of protease inhibitors added to 10 ml PBS buffer for tissue homogenisation for nitrite reductase and lucigenin-enhanced chemiluminescence assays.
Table shows stock concentrations of protease inhibitors formulated and the volume to be added to 10 ml of buffer in order to acquire the final concentrations shown. Benzamidine was made up fresh on day of experiment, but other protease inhibitors were made as stocks, aliquoted and stored at -20 °C.

The protein concentration of the homogenate was determined using a Pierce® BCA Protein Assay Kit (Thermo Fisher Scientific, UK), as described in section 2.17. Experiments were performed in a sealed 10-ml glass reaction chamber containing citric

acid/Na_2HPO_4 buffer at pH 7.4 (physiological levels) or pH 6.8 (representing acidosis), and KNO_2 (10-1000 µM) in a total volume of 1 ml. This solution was bubbled with nitrogen gas (100%) via an NO scrubbing air filter (Sievers, USA). Headspace NO concentration was measured in parts per billion by continuous sampling using a 280A Nitric Oxide Analyzer (Sievers, USA). The impact of biological tissue on NO production from NO_2^- was determined by the addition of heart or liver supernatant (150 and 200 µg of protein respectively) and measurement of NO over 2 min, calculating the rate of NO production (nmol per g of tissue per s) from the area under the curve.

2.20. Oxidative stress quantification - lucigenin-enhanced chemiluminescence (LECL)

Bis-N-methylacridinium nitrate (lucigenin) is a cell-permeable chemiluminescent probe, which acts specifically to detect superoxide generation. Lucigenin is reduced by superoxide initially to become a lucigenin radical cation, which can go on to react with a second superoxide to form lucigenindioxetane. This molecule is unstable and as it breaks down into two *N*-methylacridone molecules, one of these contains an excited electron and emits a photon of light energy as it returns to ground state (Lee et al. 2012). We used a LECL protocol to measure superoxide generation in cardiac tissue collected from mice following 3 weeks of either ANGII or isoprenaline infusion, to investigate whether dietary nitrate exerted any influence over superoxide generation.

For the LECL assay, hearts were weighed and snap frozen immediately following collection. On the day of the LECL assay, hearts were homogenised in CK-28 2 ml tubes using a Cryolys® and Precellys®24 homogeniser (Bertin Technologies, FR) in a 1:5 ratio (tissue weight (mg): homogenisation buffer (µl)). The resulting homogenate was centrifuged at 4°C for 2 mins at 9000 RCF and supernatant collected for the assay. The protein concentration of supernatant was determined using a Pierce® BCA Protein Assay Kit (Thermoscientific, UK).

The LECL assay was performed in a 96-well Cellstar clear, flat-bottomed, tissue culture-treated plate (Greiner Bio-one, UK) with a final volume of 200 µl per well. All treatment groups for one heart sample were run simultaneously (**Figure 2.17**). 100 µg protein was used per well with LECL Assay Buffer volumes calculated to make a well volume of 200

µl with experimental substrate(s) xanthine, NADPH or NADH added at 100µM per well, followed by 10µM lucigenin.

The LECL reagents were prepared as follows:

LECL Homogenization Buffer LECL Homogenization Buffer was made fresh on day of experiment, consisting of PBS with 20 mM monobasic potassium phosphate and 1 mM EGTA. Protease inhibitors were added in the concentrations shown in **Table 2.6**.

LECL Assay Buffer LECL Assay Buffer consisted of a 1:1 (10 ml: 10 ml) mix of Buffer A and Buffer B with final pH adjusted to 10.4 using HCl. Buffer A consisted of 80ml of 0.1 M Sodium Carbonate (Na_2CO_3) and 20 ml of 0.1 M Sodium Bicarbonate ($NaHCO_3$), pH 11.5. Buffer B consisted of Hank's Balanced Salt Solution (HBSS - without red phenol (Sigma Aldrich®, UK)) with 1 mM HEPES (Sigma Aldrich®, UK) added, pH 7.4.

Diphenyleneiodonium chloride (DPI) A 20 mM solution of DPI (Sigma Aldrich®, UK) was formulated in DMSO, then diluted 1:100 by serial dilution in LECL Assay Buffer to give 200 µM working solution.

Allopurinol A 20 mM solution of allopurinol (Sigma Aldrich®, UK) was formulated in DMSO, then diluted 1:100 by serial dilution in LECL Assay Buffer to give 200 µM working solution.

Febuxostat A 20 mM solution of febuxostat (Cambridge Bioscience, UK) was formulated in DMSO, then diluted 1:1000 by serial dilution in LECL Assay Buffer to give 20 µM working solution.

Xanthine A 200 mM solution of xanthine (Sigma Aldrich®, UK) was formulated in 1 M NaOH, then diluted 1:100 by serial dilution in LECL Assay Buffer to give 2mM working solution.

NADH and NADPH NADH and NADPH (Sigma Aldrich®, UK) were each dissolved directly into LECL Assay Buffer as 20mM and then diluted to 2mM.

Lucigenin A 20mM solution of lucigenin (Cambridge Bioscience, UK) was formulated directly into LECL Assay Buffer, then serially diluted to 200µM. This was prepared 15-20 minutes before starting the assay in dark-adapted conditions.

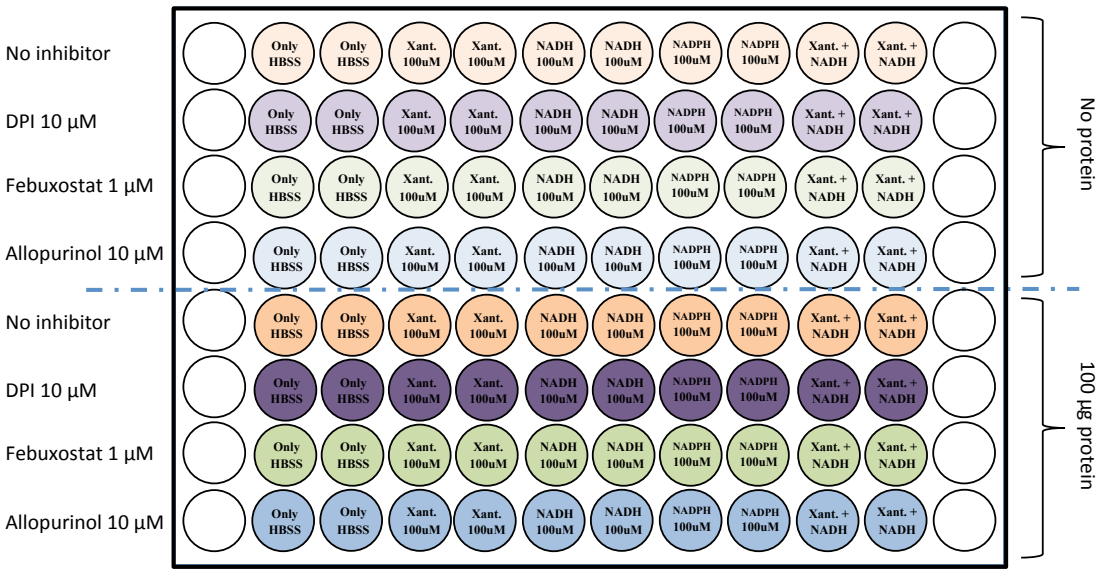

Figure 2.17 Plate layout for Lucigenin-enhanced Chemiluminescence assay.
Schematic illustrating the plate layout used for a 96 well plate in a Lucigenin-enhanced Chemiluminescence (LECL) assay on protein from one mouse heart. Final well volume = 200 µl, and wells containing protein were loaded with 100 µg protein per well. Control wells with no protein had their well volume adjusted accordingly using LECL Assay Buffer. Substrates and inhibitors were added in the configurations shown above, and the concentrations illustrated here reflect final well concentrations. For each added substrate/inhibitor, suitable working stocks were made so that 10 µl of each solution could be added to acquire the final well concentrations shown in the template. Abbreviations are as follows: HBSS = Hank's Balanced Salt Solution (red phenol-free), Xant = Xanthine, NADH = nicotinamide adenine dinucleotide, NADPH = nicotinamide adenine dinucleotide phosphate, DPI = diphenyleneiodonium chloride.

Working solutions were formulated so that 10µl could be added to appropriate wells according to the protocol (See **Figure 2.17** for typical plate layout). Plating was conducted as follows: LECL Assay Buffer (calculated to make well volume up to 200 µl), protein (100 µg protein per well), DPI/febuxostat/no inhibitor (incubated plate for 30 minutes on ice), experimental substrate(s) (xanthine/NADPH/NADH) then lucigenin. The plate was immediately read following addition of lucigenin using a Perkin Elmer Wallac 1420 Victor2 plate reader (Perkin Elmer, USA), with the chamber warmed to 37 °C. Luminescence was measured for 50 repeat readings with 30 seconds of interval between each repeat.

2.21. XOR immunoblotting in liver

Liver samples were snap frozen upon collection and were later defrosted and homogenised in a 1:2 ratio (tissue weight (mg): homogenisation buffer volume (µl)). Homogenisation buffer and protease inhibitors are shown in **Table 2.7** and **Table 2.8.**

	Molecular Weight	g per 200 ml MQ H_2O	Final Concentration
Tris-HCl	157.6	0.3152	5.7 µM
Sodium Chloride	58.44	0.5844	1.5 µM
Sodium Pyrophosphate	446.1	2.6766	0.15 µM
EDTA	292.2	0.1168	4.2 µM

Table 2.7 Table showing recipe for making the homogenisation buffer used for western blot tissue homogenisation. The buffer above was made up in MQ water and adjusted to pH7.4 prior to addition of protease inhibitors shown in **Table 2.8**.

	Stock Concentration	Volume Added to 10 ml Buffer	Final Concentration
Benzamidine	1mg/ml	10 µl	5.7 µM
Antipain	1mg/ml	10 µl	1.5 µM
Aprotinin	1 mg/ml	10 µl	0.15 µM
Leupeptin	1 mg/ml	20 µl	2.1 µM
Pepstatin A	0.7 mg/ml	10 µl	1.5 µM
AEBSF	100 mg/ml	10 µl	400 µM
Sodium orthovanadate	37 mg/ml	50 µl	1 mM
Sodium fluoride	21 mg/ml	1 ml	50 mM
Triton-X	n/a	100 µl	1%

Table 2.8 Details of protease inhibitors and detergent added to 10 ml homogenisation buffer for tissue homogenisation in preparation for western blot assays.
Table shows stock concentrations of protease inhibitors formulated and the volume to be added to 10 ml of buffer in order to acquire the final concentrations shown. Benzamidine was made up fresh on day of experiment, but other protease inhibitors were made as stocks, aliquoted and stored at -20 °C.

The resulting homogenate was centrifuged at 4°C for 2 mins at 9000 RCF and the supernatant collected. The protein concentration of supernatant was determined using a Pierce® BCA Protein Assay Kit (Thermoscientific, UK), as previously described in 2.17. Samples were subjected to SDS/PAGE (0.1% w/v) immunoblotting analysis using the following rabbit antibodies to XOR (1:2000, RRID: 133268) and β-actin (1:5000, RRID: 16039) and visualised using Clarity™ Western ECL Substrate (Bio-Rad, US). Chemiluminescence was automatically recorded and analysed with the FluorChem E imager (Protein Simple, US). Primary and secondary antibodies were purchased from Abcam (UK).

2.22. Power calculations

Preliminary data from the ANGII pre-treatment study (n=4) showed early trends towards differences in LVPW thickness between ANGII-infused mice with KNO_3 compared to KCl pre-treatment when m-mode assessments of LV wall thickness were compared. Thus, with indications that there may indeed be an effect of nitrate on cardiac wall thickness (ANGII+KCl: 0.81±0.14 mm (mean ± SD) ANGII+KNO_3: 1.3 ± 0.4), power calculations based on this data were carried out. Power calculations indicated that with an effect size of 1.6, n = 12 would be required to detect statistical differences with 95% power (**Figure 2.18**). This is within the range reported in a previous study by Matsumoto et al., using ANGII infusion to induce cardiac hypertrophy. Here, a significant difference in LVPW (~0.9 mm compared to 1.2 mm), was detected with n = 7-15 (Matsumoto et al. 2013). Because of some unanticipated deaths caused by both ANGII and isoprenaline infusion in our models, additional n values were added to account for some of these deaths in order to result in n = 12-13 for echocardiography data.

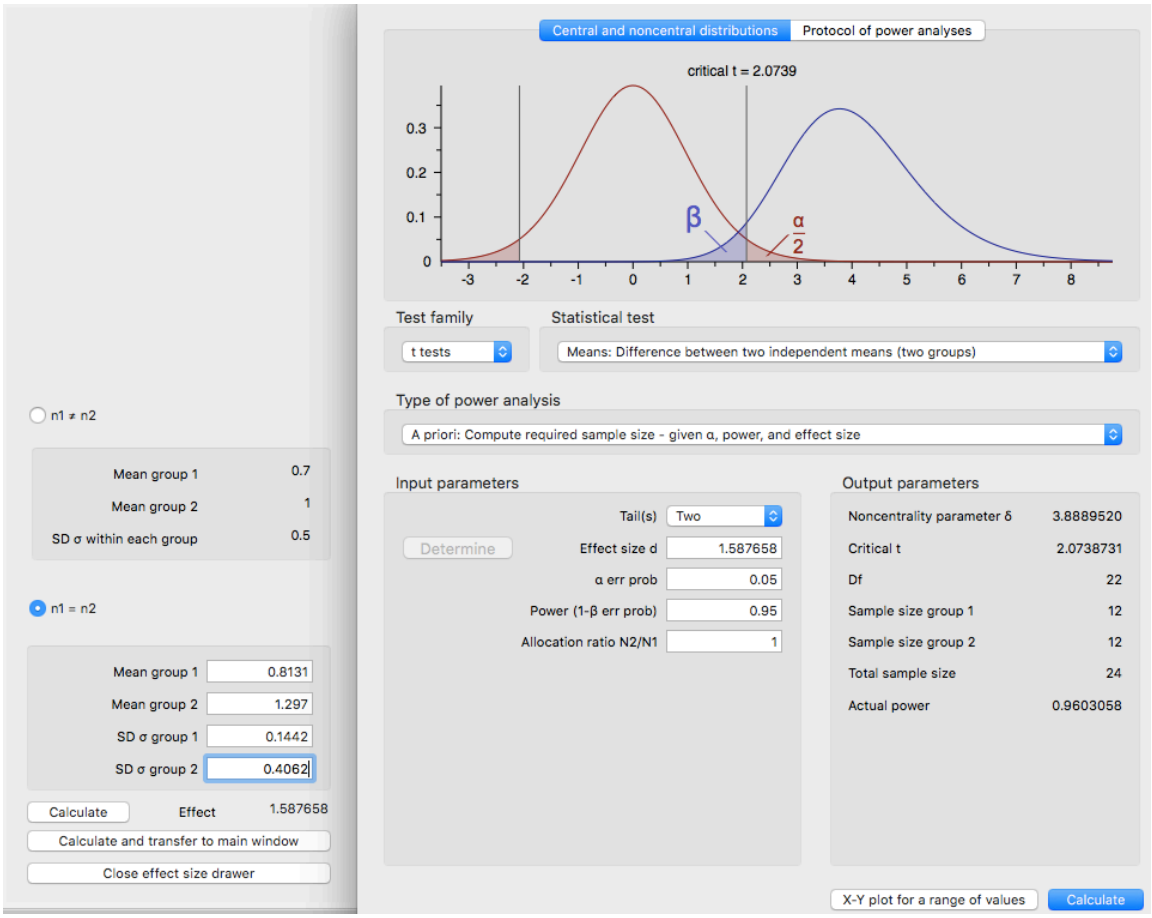

Figure 2.18 G*Power results for power calculations based on preliminary data from ANGII-infused mice receiving KNO_3 (group 1) or KCl (group 2) pre-treatment.

CHAPTER THREE -

The Effect of Dietary Nitrate on a BP-dependent Model of Cardiac Dysfunction

3. CHAPTER THREE - The effect of dietary nitrate on a BP-dependent model of cardiac dysfunction

With dietary nitrate widely recognised as having BP lowering affects in both clinical and animal studies (Gee et al., 2016), and hypertension being one of the most signifcant risk factors in cardiac hypertrophy and heart failure development (Chobanian et al., 2003; Dunlay et al., 2009; Ho et al., 1993; Levy et al., 1996), our primary aim was to establish whether dietary nitrate was capable of reducing BP sufficiently to attenuate cardiac hypertrophy in a BP-dependent model of cardiac dysfunction. To investigate this, both 3-week and 5-week ANGII mouse models were adopted, with either nitrate/control pre-treatment or reversal treatments respectively.

3.1. BP-dependent model of cardiac dysfunction – ANGII

Upon delivery, mice were randomly assigned to one of 6 treatment groups – KNO_3 control, KCl control, ANGII + KNO_3 pre-treatment, ANGII + KCl pre-treatment, ANGII + KNO_3 reversal or ANGII + KCl reversal (see **Figure 3.1A** and **Figure 3.1B**).

Controls - Mice received 15 mM KNO_3 or 15 mM KCl water *ad libitum* for 5 weeks. This dose was chosen since it has previously been shown to be effective in raising both plasma nitrite and nitrate concentrations compared to KCl controls (Baliga et al. 2012; Ghosh et al. 2013). Average nitrate intake for all mice was determined through assessment of water consumption.

ANGII Pre-treatment - Mice received 15 mM KNO_3 or 15 mM KCl water *ad libitum* for 2 weeks prior to beginning a 3-week subcutaneous (SC) infusion of 2 mg/kg/day ANGII (Sigma Aldrich®, UK) in saline, from ALZET® 1004 osmotic minipumps (Durect Corporation, USA). Drinking water treatments were continued throughout the remainder of the study, alongside ANGII infusion. After 3 weeks of ANGII infusion, echocardiography was used to determine cardiac structure and function, including measurements of LV wall thickness, ejection fraction and fractional shortening (see section 2.7 for further details). Prior to ANGII infusion, some pre-treatment study mice also underwent surgery to implant BP telemetry probes (model TA11PA-C10, Data Sciences International, USA) to allow conscious BP measurement during the study (see section 2.5 for further details). Another subset of mice underwent tail cuff BP

measurements during the final week of ANGII infusion (see section 2.6 for further details).

ANGII Reversal - Mice underwent surgery to implant an ALZET® 1004 osmotic minipump (Durect Corporation, USA) releasing 2 mg/kg/day ANGII (Sigma Aldrich®, UK) in saline, SC. After 2 weeks, this pump was surgically replaced with a new pump, releasing 2 mg/kg/day ANGII for a further 3 weeks. Mice therefore received ANGII for a total of 5 weeks. During the final 2 weeks of ANGII infusion mice concomitantly received 15 mM KNO_3 or 15 mM KCl in their drinking water *ad libitum*. At the end of the study, echocardiography was used to determine a range of cardiac measurements.

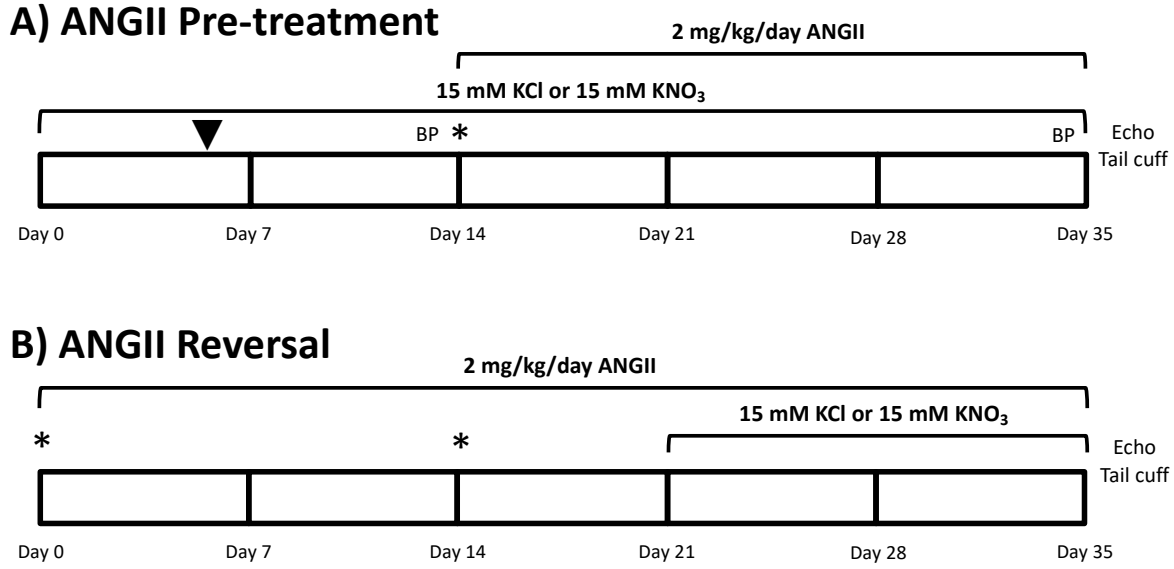

Figure 3.1 Experimental Design for ANGII studies.
Schematic illustrating the experimental design for A) ANGII pre-treatment and B) ANGII reversal studies. Schematics illustrate the duration of 15mM KCl (control) or 15mM KNO_3 (treatment) feeding and ANGII infusion. The points of osmotic minipump (*) and BP telemetry probe implantation (▼) are marked, and days on which BP telemetry (BP), echocardiography (Echo) and tail cuff BP (tail cuff) measurements were taken are indicated.

3.2. **ANGII formulation**

For the filling of osmotic minipumps, ANGII (Sigma Aldrich®, UK) was dissolved under sterile conditions to yield a 25 mg/ml stock solution in sterile saline. This 25 mg/ml stock was then diluted accordingly in LoBind tubes (Eppendorf, UK) for minipump filling according to mouse weights and pump specifications. 25 mg/ml ANGII was stored at 4°C for up to 3 days or at -20°C for up to 1 month. If stored at -20°C, ANGII was not freeze-thawed more than twice.

3.3. KNO_3 and KCl supplemental feeding

3.3.1. Tap vs. MQ filtered water

Prior to formulating supplemental feeding waters, ozone chemiluminescence was used to determine what the levels of nitrate and nitrite were in tap water and MQ filtered water (**Figure 3.2**). Samples were collected across a number of days, and at varying times of day.

Results show there were significantly higher concentrations of both nitrite (P=0.0005) and nitrate (P=0.0006) in tap water compared to MQ filtered water (**Figure 3.2**). However, whilst this difference was evident, the concentrations measured in tap water were low, and deemed highly unlikely to influence our experiments with regards to increasing mouse nitrite/nitrate consumption to a level that would significantly affect circulating plasma levels. Tap water was therefore used to formulate all feeding waters for our studies.

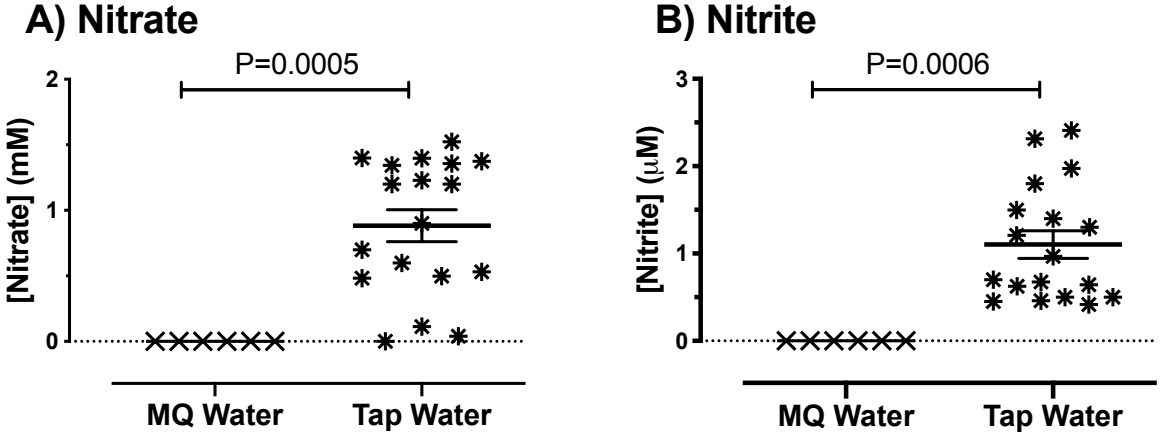

Figure 3.2 Nitrite and nitrate concentrations in Milli-Q (MQ) filtered water and tap water.
Graphs show A) nitrate (mM) and B) nitrite (μM) concentrations measured using ozone chemiluminescence in MQ filtered and tap water. Data are shown as mean ± SEM with n = 9 and n = 18 respectively. Differences between groups were tested for statistical significance using Student's T-tests, with p-values shown in the graphs.

3.3.2. Changes in nitrate/nitrite over time in running tap water

Having decided to use tap water for treatment formulations, ozone chemiluminescence was then used to determine whether there was a significant change in nitrite and nitrate concentrations when running tap water over a set period of time. Tap water samples were collected at $T_{0\ secs}$, $T_{30\ secs}$, $T_{120\ secs}$, $T_{240\ secs}$, $T_{360\ secs}$ on 3 different days and nitrite and nitrate concentrations were measured (**Figure 3.3**).

There were no significant differences in nitrite or nitrate concentrations across this 6-minute period when means of each of the time points were compared using one-way ANOVA. Thus, when generating drinking water interventions, it was decided that it did not matter when tap water was collected.

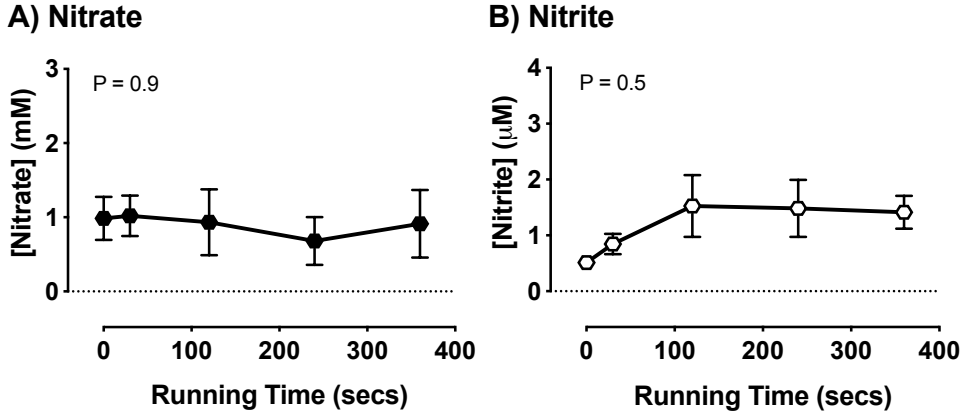

Figure 3.3 Nitrate and nitrite concentrations in tap water at T_0 secs, T_{30} secs, T_{120} secs, T_{240} secs and T_{360} secs.
Graphs show A) nitrate (mM) and B) nitrite (μM) concentrations measured using ozone chemiluminescence in tap water collected at time points T_0 secs, T_{30} secs, T_{120} secs, T_{240} secs and T_{360} secs after starting water flow. Data are shown as mean ± SEM with n = 5 at each time point. Data were tested for statistical significance using a one-way ANOVA with Dunnet's post-hoc analysis (comparing all time points to T_0 secs). P-values are shown in the graphs - no significant differences were found.

3.3.3. 15 mM KNO_3 stability

In order to ensure a supplemental water change schedule of 2 – 3 times per week was sufficient for this study to maintain a consistent dose of nitrate, ozone chemiluminescence was used to determine the stability of a 15mM KNO_3 solution made in tap water. Samples were taken on days 0, 3, 4, 5, 6 and 7 following 15 mM KNO_3 formulation, and nitrite and nitrate concentrations measured. There was no significant difference when mean concentrations of nitrite and nitrate from these days were compared using a one-way ANOVA (**Figure 3.4**).

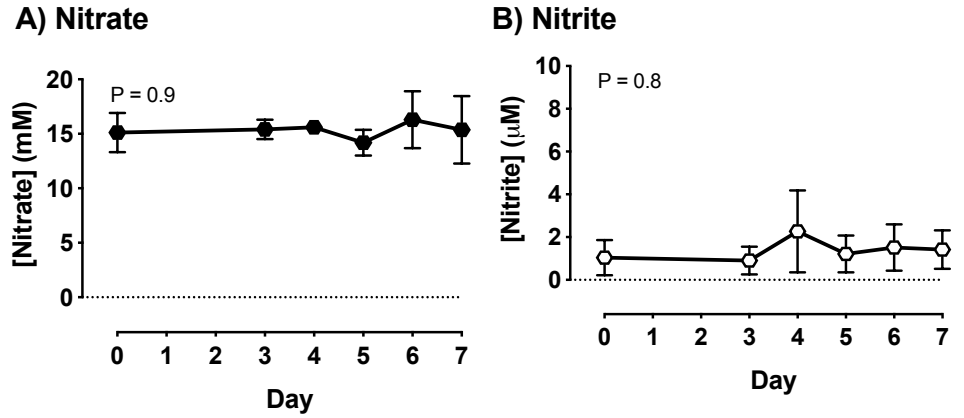

Figure 3.4 Nitrate and nitrite concentration over a one-week period in a 15 mM KNO_3 solution.
Graphs show A) nitrate (mM) and B) nitrite (μM) concentrations measured using ozone chemiluminescence in samples of a 15 mM KNO_3 solution (formulated in tap water), taken periodically over the course of one week on days 0, 3, 4, 5, 6 and 7. Data are shown as mean ± SEM with n = 5 for each day. Data were tested for statistical significance using a one-way ANOVA with Dunnet's post-hoc analysis (comparing all time points to Day 0). P-values are shown in the graphs - no significant differences were found.

3.3.4. **15mM KNO_3 and 15 mM KCl sample verification**

On 20 random days throughout the feeding study, when supplemental waters were changed, samples of freshly made 15 mM KNO_3 and 15 mM KCl waters were taken and ozone chemiluminescence used to confirm formulations (**Figure 3.5**).

There was no significant difference between mean nitrite concentrations in 15 mM KNO_3 and 15 mM KCl water formulation (P=0.7). However, as expected, there was a significantly higher nitrate concentration in 15 mM KNO_3 compared to 15 mM KCl water (P<0.0001), with average nitrate concentrations of 15.5 mM and 0.6 mM respectively.

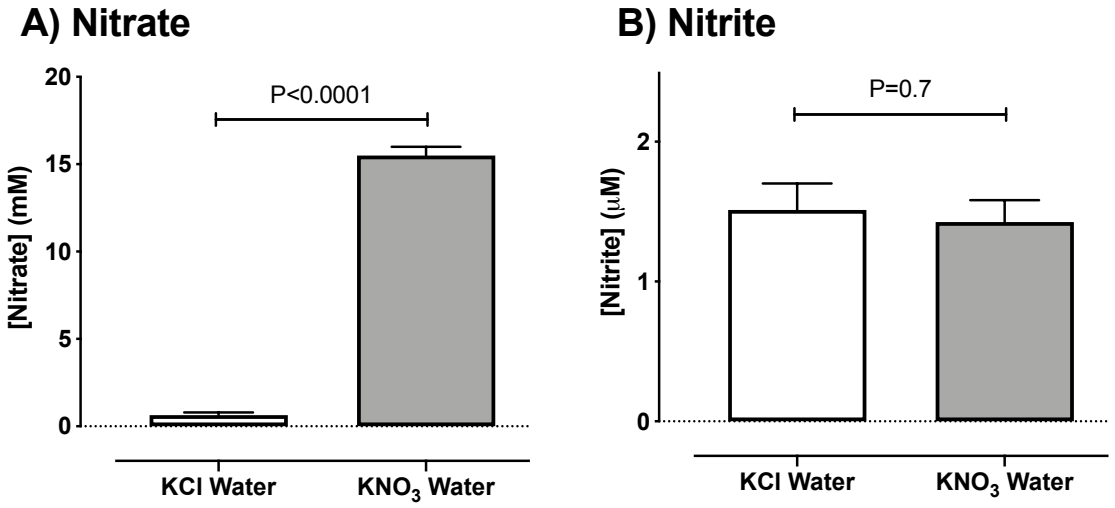

Figure 3.5 Nitrate and nitrite concentrations in 15 mM KNO_3 and 15 mM KCl feeding waters.
Graphs show A) nitrate (mM) and B) nitrite (μM) concentrations measured using ozone chemiluminescence in samples of 15 mM KNO_3 and 15 mM KCl solutions, formulated in tap water, for feeding mice. Water samples were taken periodically throughout the course of the study. Data are shown as mean ± SEM with n = 20 (15 mM KNO_3) and n = 17 (15 mM KCl). Differences between groups were tested for statistical significance using Student's T-tests, with p-values shown in the graphs.

3.3.5. **Nitrite/Nitrate levels of other experimental components**

Ozone chemiluminescence was also used to determine the nitrite and nitrate concentrations of a variety of gels/creams, which would be used during surgery and/or echocardiography. Figure 3.6 shows results obtained, with nitrite and nitrate concentrations of these gels/creams compared to concentrations measured in tap water.

Aqua Gel (used on mice during echocardiography imaging) went easily into solution when diluted with MQ filtered water. A 1:10 dilution was therefore used for nitrite and NO_x measurements. However, Redux Crème (used on the paws of mice for ECG conduction during echocardiography) and Veet (used to remove hair from mice during

surgery and echocardiography) were less water-soluble. The highest concentration achieved in solution was 1:100 for Redux Crème and 1: 1000 for Veet.

Ozone chemiluminescence results show that the various gels and creams used during experimental protocols did not contain substantial amounts of nitrite or nitrate, and all gels/creams had similar or significantly lower concentrations than those of tap water (**Figure 3.6**). These experimental components were therefore highly unlikely to contaminate the mice in our study.

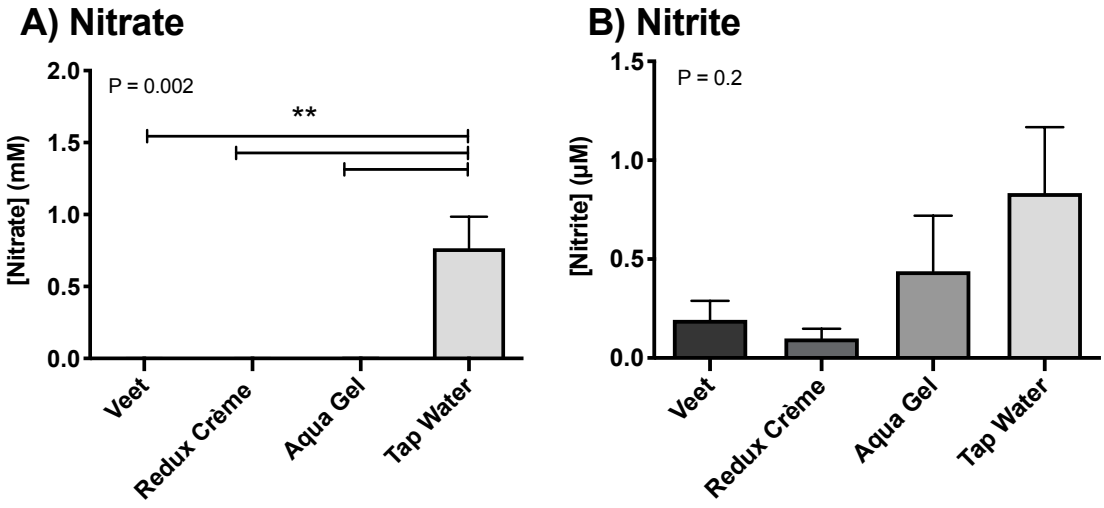

Figure 3.6 Nitrate and nitrite concentrations in gels and creams used in experimental protocols.
Graphs show A) nitrate (mM) and B) nitrite (µM) concentrations measured using ozone chemiluminescence in a variety of gels/creams used in surgical and echocardiography protocols, including: Veet (hair removal cream), Redux Crème (ECG conducting gel) and Aqua Gel (for echocardiographic imaging). For reference, these are shown compared to nitrate/nitrite concentrations measured in tap water. Data are shown as mean ± SEM with n = 5. Data were tested for statistical significance using a one-way ANOVA with Dunnett's post-hoc analysis (comparing all groups to tap water). P-values for one-way ANOVA are shown in the graphs and stars represent statistical significance determined by post-hoc analyses:
** = P <0.01

3.3.6. Plasma nitrite and nitrate concentrations are increased by 15 mM KNO_3 feeding in controls and ANGII infused mice

Ad libitum 15 mM KNO_3 feeding through drinking water significantly raised plasma nitrate in both controls and ANGII-infused mice (**Figure 3.7A** and **Figure 3.7B**). Furthermore, a significant increase in plasma nitrite concentrations were measured in control mice fed KNO_3 vs. KCl (1.5 ± 0.2 vs. 1.0 ± 0.08, mean ± SEM) and in ANGII infused mice, both on pre-treatment (2.5 ± 0.3 vs. 0.9 ± 0.08) and reversal protocols (3.4 ± 0.5 vs. 0.8 ± 0.05) – **Figure 3.7C** and **Figure 3.7D**. The significant increase in nitrite concentration in the plasma is particularly important from a mechanistic point of view, as it highlights that the enterosalivary circuit in these mice is intact. It is noteworthy however, that the rise in plasma nitrate and nitrite with KNO_3 treatment was greater in

ANGII infused mice compared to control mice (i.e. ~10-fold and ~2-fold higher respectively).

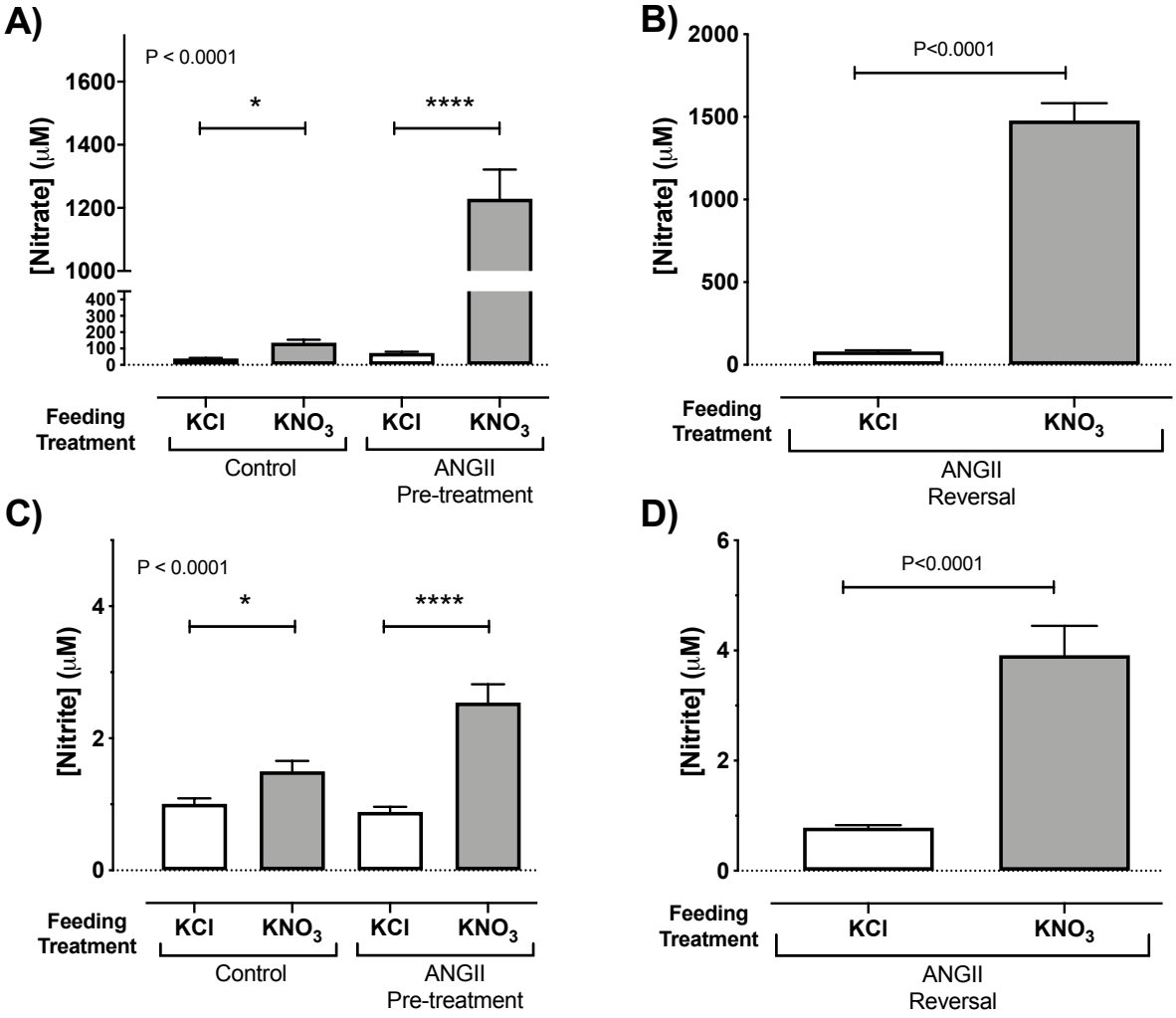

Figure 3.7 Nitrate and nitrite concentrations in plasma of ANGII pre-treatment and reversal study mice.
Graphs show A) and B) nitrate (mM) and C) and D) nitrite (μM) concentrations in plasma of control, ANGII pre-treatment and ANGII reversal mice, fed either 15 mM KNO_3 or KCl water. Data are represented as mean ± SEM with n ≥ 18. Data were tested for statistical significance using a one-way ANOVA with Sidak's post-hoc analysis (A and C) or Student's T-tests (B and D). P-values for one-way ANOVAs and T-tests are shown in the graphs. Stars represent statistical significance determined by post-hoc analyses:
* = P<0.05, **** = P<0.0001

3.4. The effect of ANGII infusion on mouse weight, and food and water consumption

3.4.1. Water and nitrate consumption

In mice treated with ANGII, water consumption in both KNO_3 and KCl-fed mice was significantly greater than in controls (**Table 3.2**). Increased water consumption in these treatment groups therefore resulted in an increase in the estimated dose of nitrate being delivered to ANGII+KNO_3 treated mice, when compared to KNO_3-fed controls (**Table 3.2**).

3.4.2. **Body weight**

There were no significant differences between treatment groups when body weights of mice at baseline were compared (**Table 3.1**). However, when change in body weight from the start to the end of each study was compared, this was significantly different between groups when compared using a one-way ANOVA ($P<0.0001$). Sidak's post-hoc analysis showed that ANGII treatment caused a reduction in weight gain over time compared to control mice (**Table 3.1**). Comparison of KCl to KNO_3 treatment within groups demonstrated no difference between drinking water treatments.

3.4.3. **Food consumption**

There was no significant difference in food consumption in ANGII-infused mice compared to controls, but food consumption was significantly increased in isoprenaline-infused mice. KNO_3 feeding treatment had no significant effect on this increase (**Table 3.1**).

Treatment	Water Consumption (ml/day)			Nitrate Consumption (mmol/kg/day)			Nitrate Consumption (mg/kg/day)			n
	Average	Before Pump	With Pump	Average	Before Pump	With Pump	Average	Before Pump	With Pump	
KNO_3 Control	4.7 ± 0.2	4.7 ± 0.2	4.7 ± 0.2	2.9 ± 0.1	2.9 ± 0.1	2.9 ± 0.1	176.8 ± 4.1	177.4 ± 4.1	179.9 ± 5.1	18
KCl Control	4.5 ± 0.1	4.7 ± 0.2	4.5 ± 0.1	0.1 ± 0.0	0.1 ± 0.0	0.1 ± 0.0	6.9 ± 0.2	7.1 ± 0.2	6.9 ± 0.2	20
ANGII + KNO_3 Pre	8.2 ± 0.3****	4.5 ± 0.1	10.5 ± 0.5****	5.7 ± 0.2****####	3.1 ± 0.1**####	7.2 ± 0.4****####	351.4 ± 15.0	191.8 ± 4.4	448.6 ± 21.9	19
ANGII + KCl Pre	8.3 ± 0.4****	4.7 ± 0.2	10.3 ± 0.6****	0.2 ± 0.0	0.1 ± 0.0	0.3 ± 0.0	14.3 ± 0.7	8.1 ± 0.3	17.5 ± 1.1	20
ANGII + KNO_3 Rev	14.2 ± 0.9****	n/a	14.2 ± 0.9****	9.6 ± 0.6****####	n/a	9.6 ± 0.6****####	596.2 ± 39.6	n/a	596.2 ± 39.6	18
ANGII + KCl Rev	13.3 ± 0.6****	n/a	13.3 ± 0.6****	0.4 ± 0.0	n/a	0.4 ± 0.0	22.8 ± 1.3	n/a	22.8 ± 1.3	18

Table 3.1 Table illustrating mouse water consumption of mice, and therefore resulting nitrate (NO_3^-) dose delivered, during ANGII studies.

Average water and nitrate dose were calculated from water weights recorded 3 times weekly. Dose delivered is shown for KNO_3 and KCl control mice (with no ANGII), ANGII + KNO_3 and KCl pre-treatment (Pre) and reversal (Rev) mice. Data are broken down into average consumption, before pump consumption and with pump consumption. Data are represented as mean ± SEM with n ≥ 18. Pre = pre-treatment study where nitrate treatment was initiated 2 weeks prior to ANGII infusion. Rev = reversal study where nitrate treatment initiated 3 weeks following ANGII infusion.

Differences between treatment groups were tested for statistical significance using a one-way ANOVA and Sidak's post-hoc analysis.

* = significantly different from KNO_3 or KCl control mice with no ANGII infusion.

= KNO_3 fed mice significantly different from KCl fed mice under the same ANGII regimen.

*/# = P<0.05, **/## = P<0.01, ***/### = P<0.001 and ****/#### = P<0.0001

Treatment	Mouse Weight (g)				Food Consumption (g/day)			n
	Average	Start of Study	End of Study	Weight Gain	Average	Before Pump	With Pump	
KNO_3 Control	25.2 ± 0.4	23.1 ± 0.5	26.7 ± 0.4	3.6 ± 0.5	3.6 ± 0.1	3.6 ± 0.1	3.6 ± 0.1	18
KCl Control	25.7 ± 0.5	23.6 ± 0.6	27.3 ± 0.5	3.7 ± 0.4	3.5 ± 0.1	3.5 ± 0.1	3.6 ± 0.1	20
ANGII + KNO_3 Pre	22.6 ± 0.3****	22.4 ± 0.4	23.6 ± 0.3****	1.3 ± 0.3 **	3.3 ± 0.1	3.3 ± 0.1	3.3 ±0.2	19
ANGII + KCl Pre	22.6 ± 0.2****	22.3 ± 0.3	23.5 ± 0.3****	1.2 ± 0.3***	3.2 ± 0.1	3.2 ± 0.1	3.3 ± 0.1	20
ANGII + KNO_3 Rev	23.2 ± 0.4**	23.4 ± 0.5	24.4 ± 0.3***	1.0 ± 0.5***	3.7 ± 0.1	n/a	3.7 ± 0.1	18
ANGII + KCl Rev	23.1 ± 0.4****	23.7 ± 0.5	23.5 ± 0.4****	-0.2 ± 0.5****	3.6 ± 0.1	n/a	3.6 ± 0.1	18

Table 3.2 Table illustrating mouse weights and food consumption of mice during ANGII studies.

Average mouse weights are shown at the start and end of studies for KNO_3 and KCl control mice (with no ANGII), ANGII + KNO_3 or KCl pre-treatment (Pre) and reversal (Rev) mice. Average food consumption was calculated both before and during ANGII infusion, from food weights recorded 3 times weekly. Data are represented as mean ± SEM with n ≥ 18.

Differences between treatment groups were tested for statistical significance using a one-way ANOVA and Sidak's post-hoc analysis.

* = significantly different from KNO_3 or KCl control mice with no ANGII infusion

= KNO_3 fed mice significantly different from KCl fed mice under the same ANGII regimen.

*/# = P<0.05, **/## = P<0.01, ***/### = P<0.001 and ****/#### = P<0.0001

3.5. **cGMP expression**

cGMP, a significant downstream molecule in NO signalling pathways was measured using a cGMP enzyme immunoassay. Despite there being a significant increase in plasma nitrite concentrations measured using ozone chemiluminescence in all nitrate-fed mice, unfortunately there was no detectable difference in plasma cGMP compared in ANGII-infused mice fed KCl or KNO_3 pre-treatment (**Figure 3.8**).

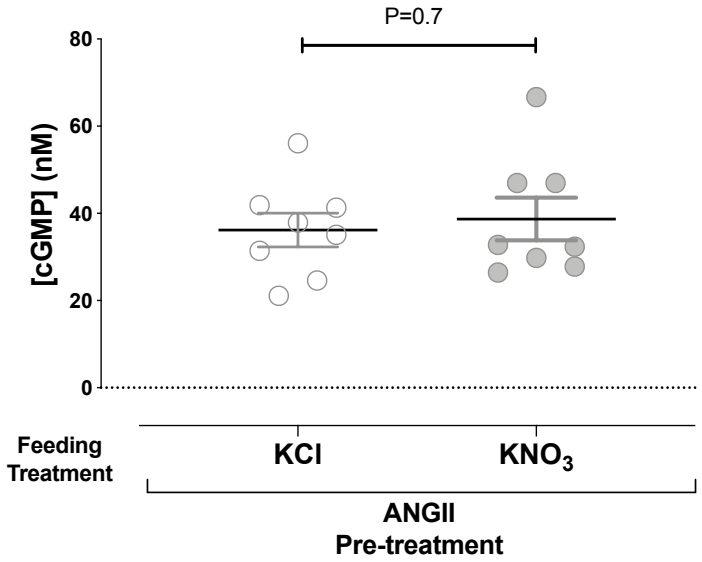

Figure 3.8 cGMP enzyme immunoassay results in ANGII-infused mice with KCl or KNO_3 pre-treatment.
Data are represented as mean ± SEM with n = 8. P-value shows there was no statistical significance of results when data were compared using Student's T-test.

3.6. **Mortality**

Overall mortality in the ANGII model was recorded as 10.4% and 8.2% for KCl and KNO_3 pre-treated mice respectively. This was not statistically significant when the two groups when compared using the Gehan-Breslow-Wilcoxon test (**Figure 3.9**).

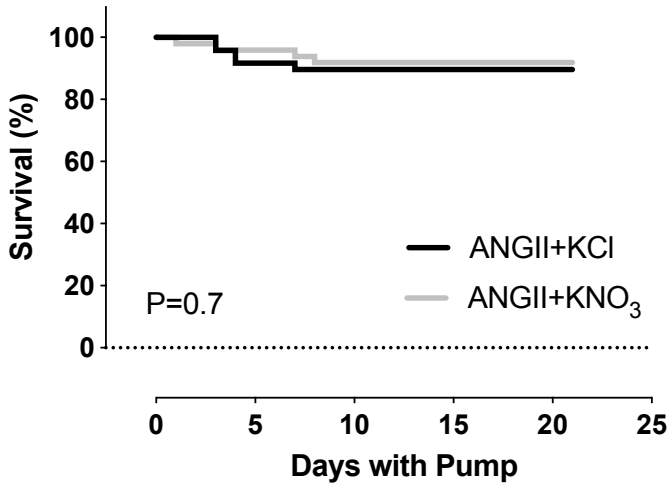

Figure 3.9 Mortality in ANGII-infused mice with KCl or KNO_3 pre-treatment.
Kaplan-Meier mortality curves for ANGII-infused mice with KCl or KNO_3 pre-treatment, n = 43 and 45 respectively. P-value shows there was no statistical significance of results when curves were compared using Gehan-Breslow-Wilcoxon test.

3.7. Control C57Bl6 echocardiography – comparison to literature

Echocardiography was carried out on C57Bl6 mice in order to ensure that the experimental protocol used resulted in data consistent with that published in the literature. **Table 3.3** compares standard cardiac parameters of IVS (mm), LVPW (mm) and LVID (mm) (in diastole (d) and systole (s)) and ejection fraction (%) and fractional shortening (%), obtained from control C57Bl6 mice, compared to values obtained for each parameter which have been reported in literature using a similar experimental protocol (Ram et al. 2011). A typical echocardiographic trace from preliminary echocardiography imaging on a control C57Bl6 mouse, and the measurements taken, can be seen in **Figure 3.10**.

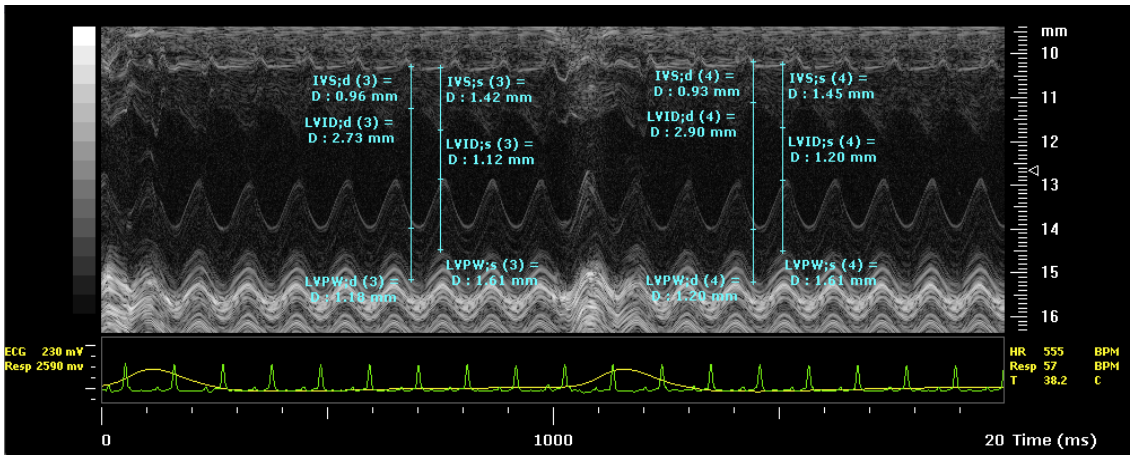

Figure 3.10 Example of a typical echocardiographic image from a C57Bl6 control mouse.
Figure shows an example of an M-mode image, acquired using Vevo 770 echocardiography software and equipment, of a C57Bl6 mouse under ≈2% isofluorane inhalation anaesthetic. Measurements of the intra-ventricular septum (IVS), left ventricle posterior wall diameter (LVPW) and left ventricle internal dimension (LVID) were taken during diastole (d) and systole (s) respectively. Mouse ECG is shown in green and respiration rate in yellow. The image represents a total of 20ms of echocardiographic recording.

Cardiac Parameters Measured	Values Obtained in C57Bl6 Controls	Values Obtained By Ram et al., 2011
IVSs (mm)	1.3 ± 0.03	1.3 ± 0.02
IVSd (mm)	0.9 ± 0.03	0.8 ± 0.1
LVPWs (mm)	1.2 ± 0.03	1.2 ± 0.02
LVPWd (mm)	0.7 ± 0.04	0.7 ± 0.01
LVIDs (mm)	1.8 ± 0.21	1.6 ± 0.04
LVIDd (mm)	3.3 ± 0.22	3.1 ± 0.03
Ejection Fraction (%)	76.1 ± 3.7	81 ± 1
Fractional Shortening (%)	45.0 ± 3.4	49 ± 1

Table 3.3 C57Bl6 echocardiography measurements obtained alongside data reported by Ram et al., 2011.
Table shows intra-ventricular septum diameter (IVS), left ventricle posterior wall diameter (LVPW) and left ventricle internal dimension (LVID) measurements during diastole (d) and systole (s), as well as ejection fraction and fractional shortening of C57Bl6 mice. Data were obtained using a Vevo 770 machine and software, with C57Bl6 mice under ≈2% isofluorane inhalation anaesthetic. Values are shown as mean ± SEM, with n = 7 for in house data and n = 36 for Ram et al., 2011.

3.8. ANGII model verification

3.8.1. Tail cuff BP measurements

To confirm that ANGII induced a significant rise in BP, creating a BP-dependent model of cardiac hypertrophy, tail cuff BP measurement was used (**Figure 3.11**). ANGII significantly increased BP in C57Bl6 mice from 143 ± 3 to 175 ± 5 mmHg (P<0.001). In addition to the fact that there was no significant rise detected in heart rate in ANGII-infused mice (see section 4.4).

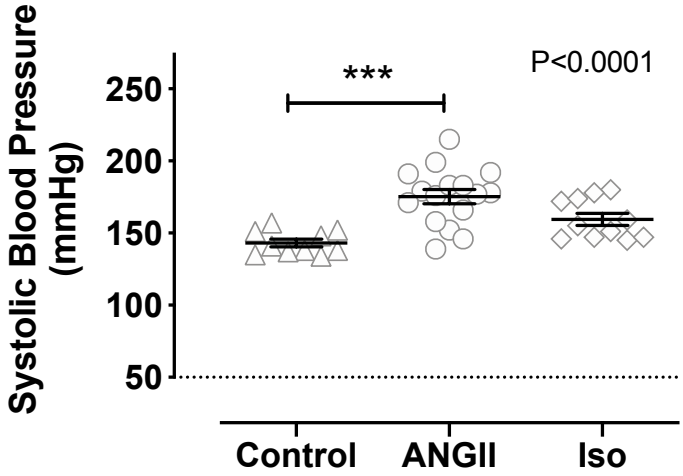

Figure 3.11 Tail cuff BP data from controls, ANGII and isoprenaline study mice.
Figure shows Systolic tail cuff BP measured in control mice and mice infused with 2 mg/kg/day ANGII. Tail cuff data was obtained using a modified CODA tail cuff setup (Kent Scientific), with data averaged from 4 days of recording. Each day consisted of 5 acclimation cycles and 10 recorded data cycles. Data are represented as mean ± SEM with n = 10-16. Data were tested for statistical significance using a one-way ANOVA with Sidak's post-hoc analysis. P-values for one-way ANOVA are shown in the graphs and stars represent statistical significance determined by post-hoc analyses: *** = P<0.001.

3.8.2. Cardiac hypertrophy

In addition to the aforementioned increase in BP, with no significant rise in heart rate of ANGII-infused mice (see section 4.4), cardiac hypertrophy was observed in ANGII treated mice both visually (**Figure 3.12**) and by increases in heart weights (

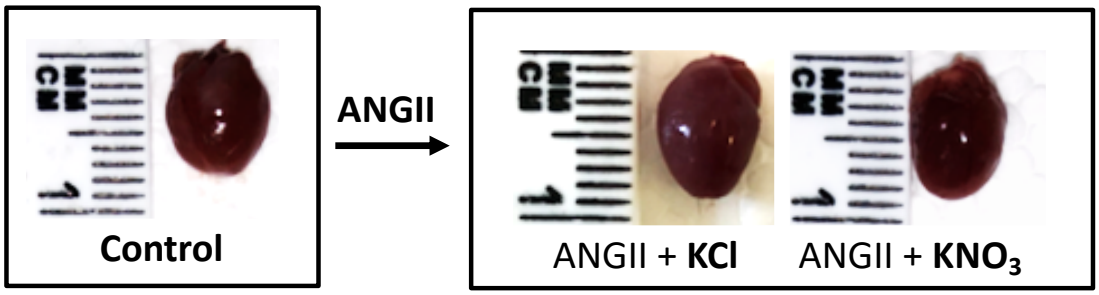

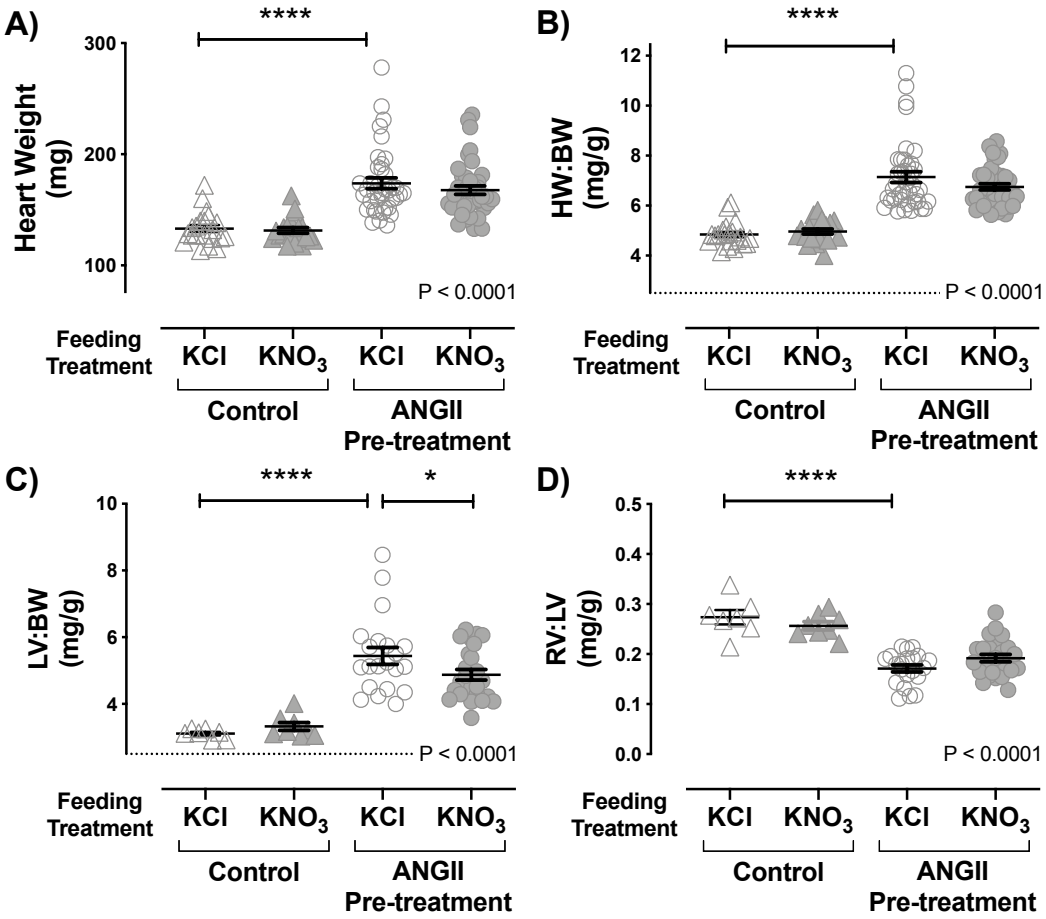

Figure 3.13). These results verify the suitability of the primarily BP-dependent nature of this model.

Figure 3.12 Heart images from mice harvested after 3 weeks of ANGII infusion.
Figure shows photographs of hearts with a 1 cm scale from control mice and mice infused with 2 mg/kg/day ANGII with either 15 mM KCl or KNO_3 pre-treatment.

3.9. Dietary nitrate pre-treatment in ANGII-infused mice

3.9.1. The effect of nitrate pre-treatment on heart weight

ANGII infusion increased overall heart weight, HW:BW ratios and LV:BW ratios (P<0.0001,

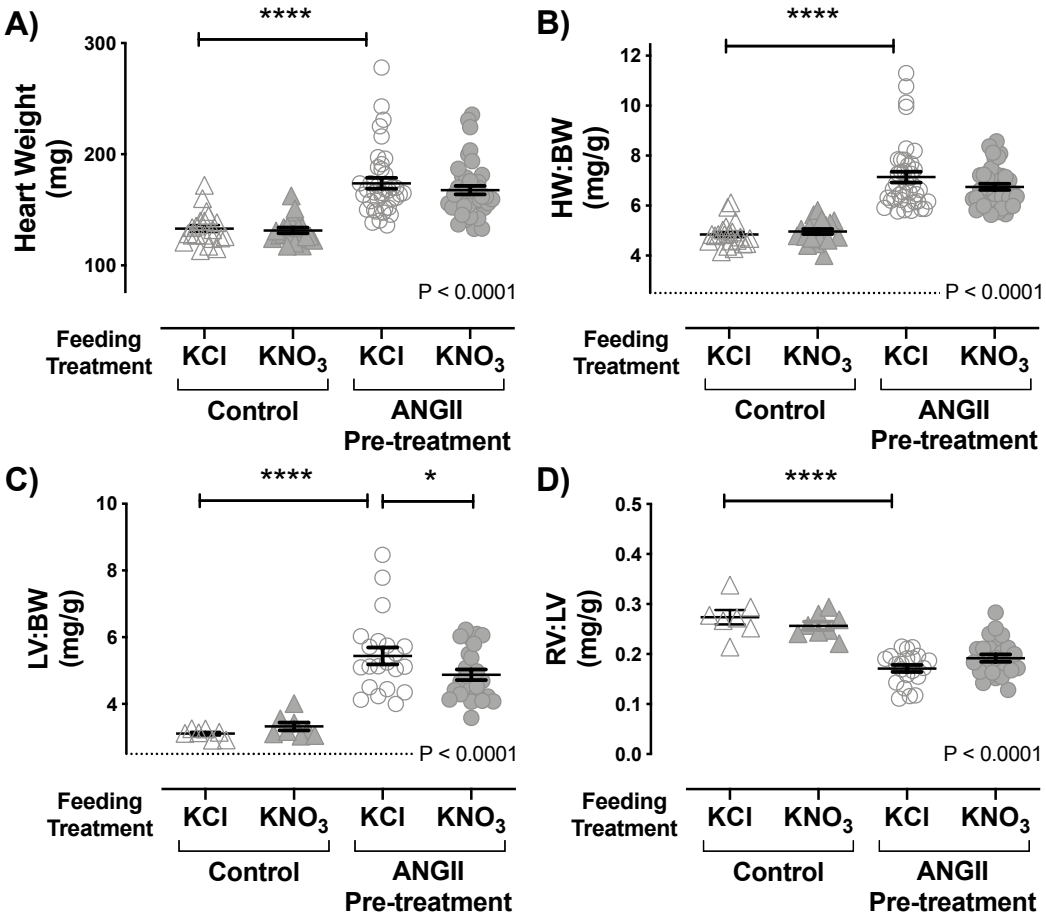

Figure 3.13A-C), and significantly reduced RV:LV ratios (P<0.0001) highlighting the development of LV hypertrophy (

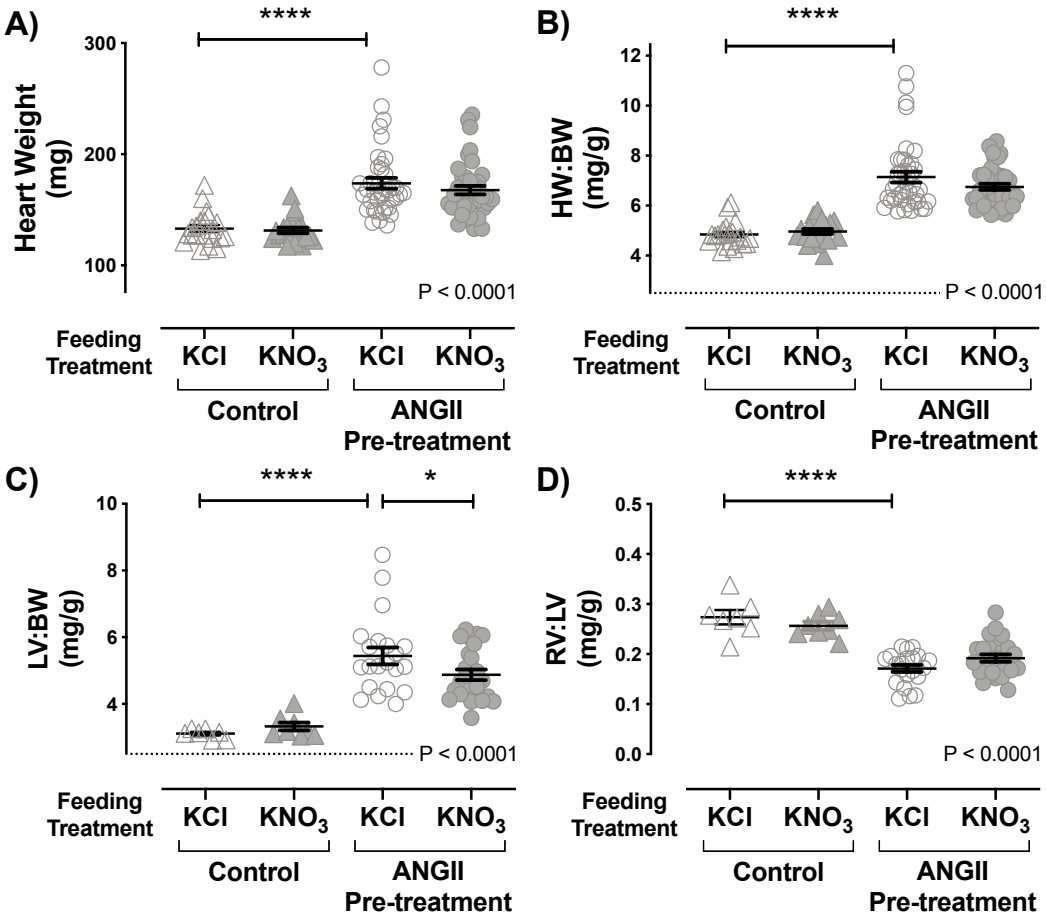

Figure 3.13D). LV:BW ratios were slightly, but significantly, attenuated by dietary nitrate pre-treatment (ANGII+KCl: 5.4 ± 0.3; ANGII+KNO_3 Pre: 4.9 ± 0.2, P<0.05). However, whilst overall heart weight, HW:BW ratios and LV:BW ratios showed trends towards attenuation in ANGII-infused mice, these were not statistically significant.

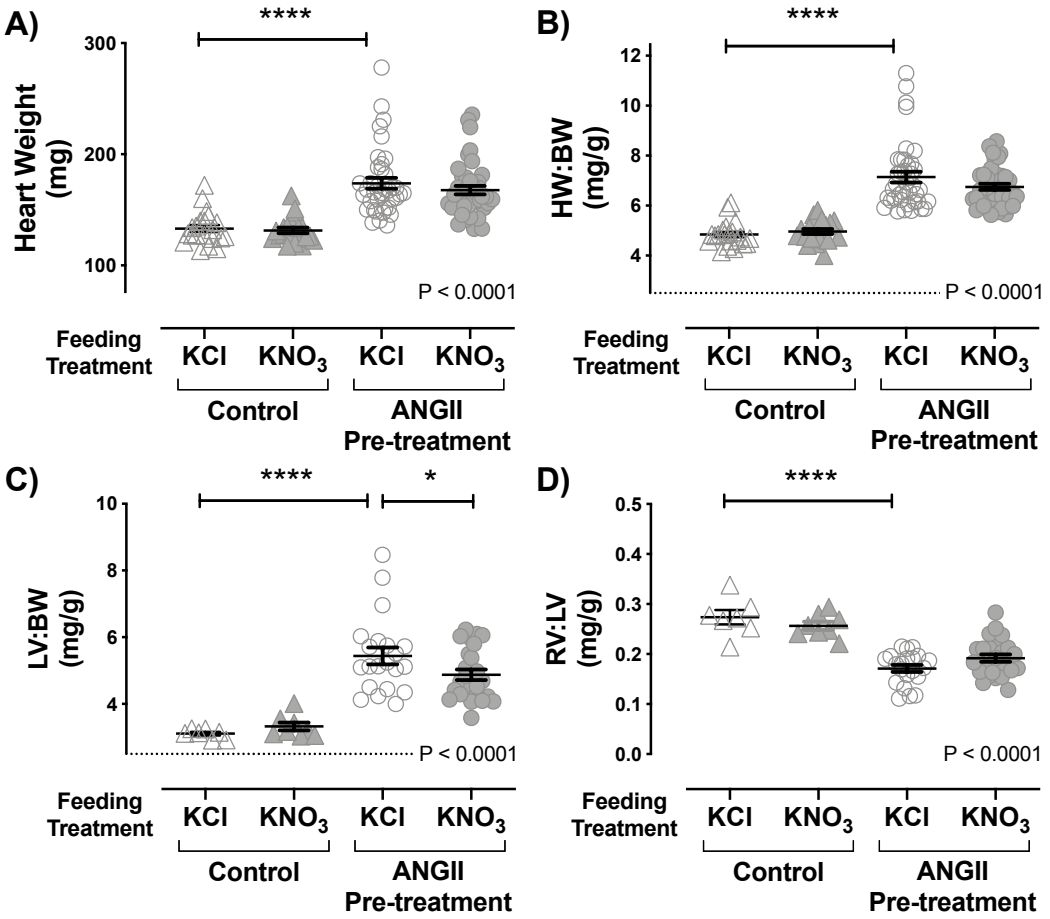

Figure 3.13 Heart weight data from ANGII study mice.
Figure shows A) whole heart weights as well as B) heart weight: body weight, C) left ventricle: body weight and D) right ventricle: left ventricle ratios for control mice and ANGII pre-treatment study mice fed either 15 mM KNO_3 or KCl. Data are represented as mean ± SEM. Data were tested for statistical significance using a one-way ANOVA with Sidak's post-hoc analysis. P-values for one-way ANOVA are shown in the graphs and stars represent statistical significance determined by post-hoc analyses: * = P<0.05, **** = P<0.0001.

3.9.2. **Oral nitrate reduces ANGII-induced LV wall thickening measured by echocardiography**

Echocardiography was performed at the end of each ANGII study in controls, ANGII pre-treatment and ANGII reversal mice fed KNO_3 or KCl. ANGII infusion caused a significant increase in LVPWd thickness in ANGII-infused mice with KCl pre-treatment when compared to KCl controls (KCl control: 0.8 ± 0.03 mm; ANGII+KCl Pre: 1.3 ± 0.09 mm; P<0.0001, **Figure 3.14E**) - representative M-mode images in **Figure 3.14A and Figure 3.14C**.

KNO_3 pre-treatment significantly reduced the level of hypertrophy observed (P<0.0001), with LVPWd in this group similar to that of controls (KNO_3 control: 0.7 ± 0.03 mm;

ANGII+KNO_3 Pre: 0.8 $\pm$ 0.04 mm, **Figure 3.14E**) – see representative M-mode images in **Figure 3.14C and Figure 3.14D**. The same findings were also true of LVPWs dimensions (**Figure 3.14F).**

IVS thickness and predicted LV mass were also increased by ANGII infusion (P<0.01 and P<0.0001 respectively), and significantly reduced by KNO_3 pre-treatment (P<0.0001 and P<0.01) - see **Figure 3.14G** and **Figure 3.14H**.

ANGII infusion also resulted in a reduction in ejection fraction (KCl control: 76 $\pm$ 2%; ANGII+KCl Pre: 57 $\pm$ 1.8%), which was not significantly changed by KNO_3 feeding treatment (**Figure 3.14L**). There were no significant differences in LVIDd or LV end diastolic volumes when compared between treatment groups using one-way ANOVA (**Figure 3.14I and Figure 3.14J)**.

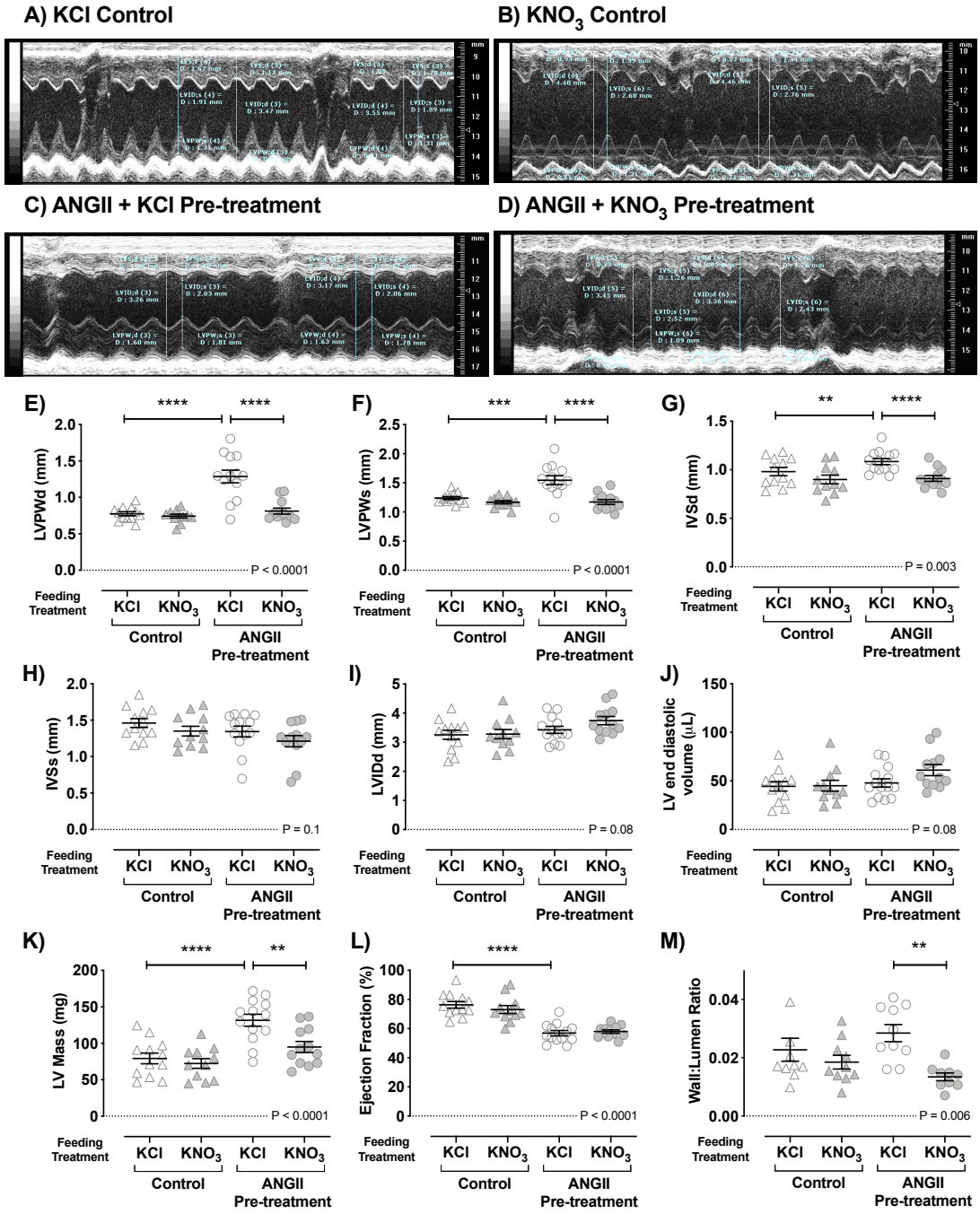

Figure 3.14 End of study echocardiography measurements from ANGII pre-treatment and control study mice. Figure shows representative M-mode images, acquired using Vevo 770 echocardiography software and equipment from A) KNO_3 control B) KCl control C) ANGII + KNO_3 pre-treatment and D) ANGII + KCl pre-treatment mice. Images were acquired under ~2% isofluorane inhalation anaesthetic. Measurements of the intra-ventricular septum (IVS), left ventricle posterior wall (LVPW) and left ventricle internal dimension (LVID) were taken during diastole (d) and systole (s). The image represents a total of 20ms of echocardiographic recording. Resulting LVPWd, LVPWs, IVSd, IVSs, LVIDd dimensions, LV end diastolic volume, LV mass, ejection fraction and wall:lumen ratios are shown in E), F) G), H), I), J), K), L) and M) respectively. Data are represented as mean ± SEM with n = 11-13. Data were tested for statistical significance using a one-way ANOVA with Sidak's post-hoc analysis. P-values for one-way ANOVA are shown in the graphs and stars represent statistical significance determined by post-hoc analyses:
** = P<0.01, *** = P<0.001 **** = P<0.0001.

3.9.3. Effect of oral nitrate on cardiac fibrosis in ANGII-infused mice, measured by PSR staining

3-week ANGII infusion caused a significant increase in fibrosis as measured by PSR staining in formalin-fixed mouse hearts (P<0.001, **Figure 3.15A**). Dietary nitrate

significantly attenuated the fibrosis observed in ANGII-infused mice when compared to KCl-fed controls under the same ANGII regimen (P<0.001).

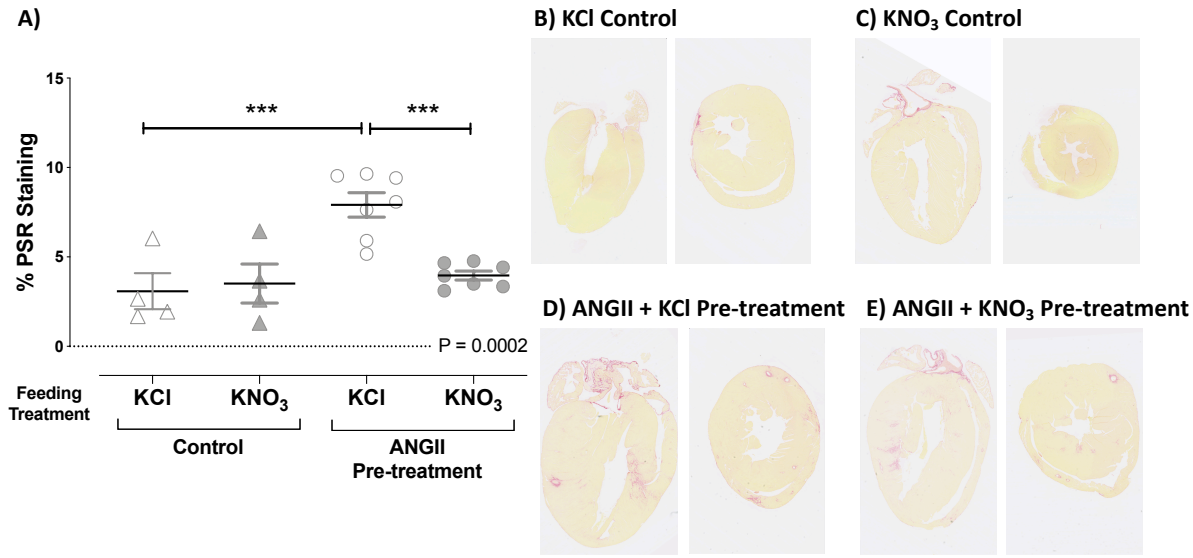

Figure 3.15 Collagen deposition as quantified by PSR staining in ANGII pre-treatment study mouse hearts. Figure shows PSR staining carried out on 4 µm sections of formalin fixed hearts, embedded in paraffin. Hearts were randomly assigned to be sectioned in either the transverse or dorsal plane and stained with PSR to identify areas of connective tissue deposition. Images were acquired using a NanoZoomer slide scanner (Hamamatsu) and viewed using NDP View software. Three left ventricle, three intraventricular septum and three right ventricle fields of view were randomly selected at x20 magnification and PSR staining quantified using manual thresholding techniques in ImageJ software. Figure shows A) quantification of staining in controls and ANGII-infused mice with KNO_3 or KCl pre-treatment. Sections B) – E) shown representative staining images at x 1.25 magnification in all treatment groups. Data are represented as mean ± SEM with n = 4-7. Data were tested for statistical significance using one-way ANOVA with Sidak's post-hoc analysis, with P-value shown in the graphs Stars represent statistical significance determined by post-hoc analyses: *** = P<0.001

3.9.4. Effect of oral nitrate on ANGII-induced BP Increases, measured by radiotelemetry

Radiotelemetric probes were used to record BP of ANGII pre-treatment study mice at baseline and on Day 21 of ANGII infusion with KNO_3 or KCl pre-treatment. At baseline, oral nitrate significantly reduced MAP (P<0.001) and DBP (P<0.0001), but had no significant effect on SBP or HR (**Table 3.4**). On Day 21 of ANGII infusion, although both KNO_3 and KCl fed mice exhibited increases in BP compared to baseline, mice receiving KNO_3 exhibited significantly lower DBP (P<0.0001) and HR (P<0.001) compared to KCl fed mice. However, there was no significant difference in MAP and there was in fact a significant increase in SBP (P<0.001) compared to KCl fed mice (**Table 3.4**).

However, it should also be noted that oral nitrate treatment, both at baseline and on Day 21 of ANGII infusion, resulted in a significant increase in mouse locomotor activity (P<0.0001, **Table 3.4**, **Figure 3.16D** and **Figure 3.16H**). As intensity of locomotor activity has a direct impact on murine BP (Adlam et al. 2011), this finding led us to normalize BP and HR data according to mouse activity level at corresponding time points. When

compared relative to activity level, MAP, DBP, SBP and HR all showed a significant reduction across the 24-hour recording window, both during ANGII infusion and at baseline (24-hour data traces shown in **Figure 3.16A- Figure 3.16J** with averages shown in **Figure 3.17A - Figure 3.17D**).

		Baseline				Day 21 ANGII		
		KNO_3	KCl	n		KNO_3	KCl	n
Mean BP	↓	106.1 ± 2.8 ***	109.2 ± 5.8	6	**NS**	141.1 ± 5.8	141.8 ± 3.5	8
Systolic BP	**NS**	119.8 ± 3.6	119.9 ± 5.7	6	↑	166.8 ± 7.2 ***	161.8 ± 4.1	8
Diastolic BP	↓	91.8 ± 2.3 ****	98.8 ± 6.7	6	↓	119.5 ±5.3 ****	124.5 ±3.2	8
Activity	↑	6.8 ± 0.9 ****	4.7 ± 0.7	6	↑	7.6 ±1.5 ****	5.6 ±1.2	8
Heart Rate	**NS**	588.9 ± 4.6	598.7 ± 19.8	6	↓	579.7 ±16.6 ***	599.0 ± 17.0	8

Table 3.4 24-hour average BP measurements from ANGII pre-treatment study mice at baseline and on day 21 of ANGII infusion.

Table shows mean, systolic and diastolic BP, activity and heart rates at baseline and on Day 21 of ANGII infusion in mice pre-treated with either 15 mM KNO_3 or KCl water. Data were acquired using TA11PA-C10 radiotelemetric probes (Data Sciences International, USA), allowing BP recording in freely moving, conscious animals. Data are expressed as averages from across a 24-hour period of telemetric monitoring with mean ± SEM. n-numbers for each treatment group are shown in the table and arrows indicate direction of change with KNO_3 treatment. Stars show statistical significance of results when 24-hour traces from KNO_3 treated mice were compared to KCl treated mice using Two-way ANOVA:

*** = P<0.001, **** = P<0.0001 and NS = Not Significant

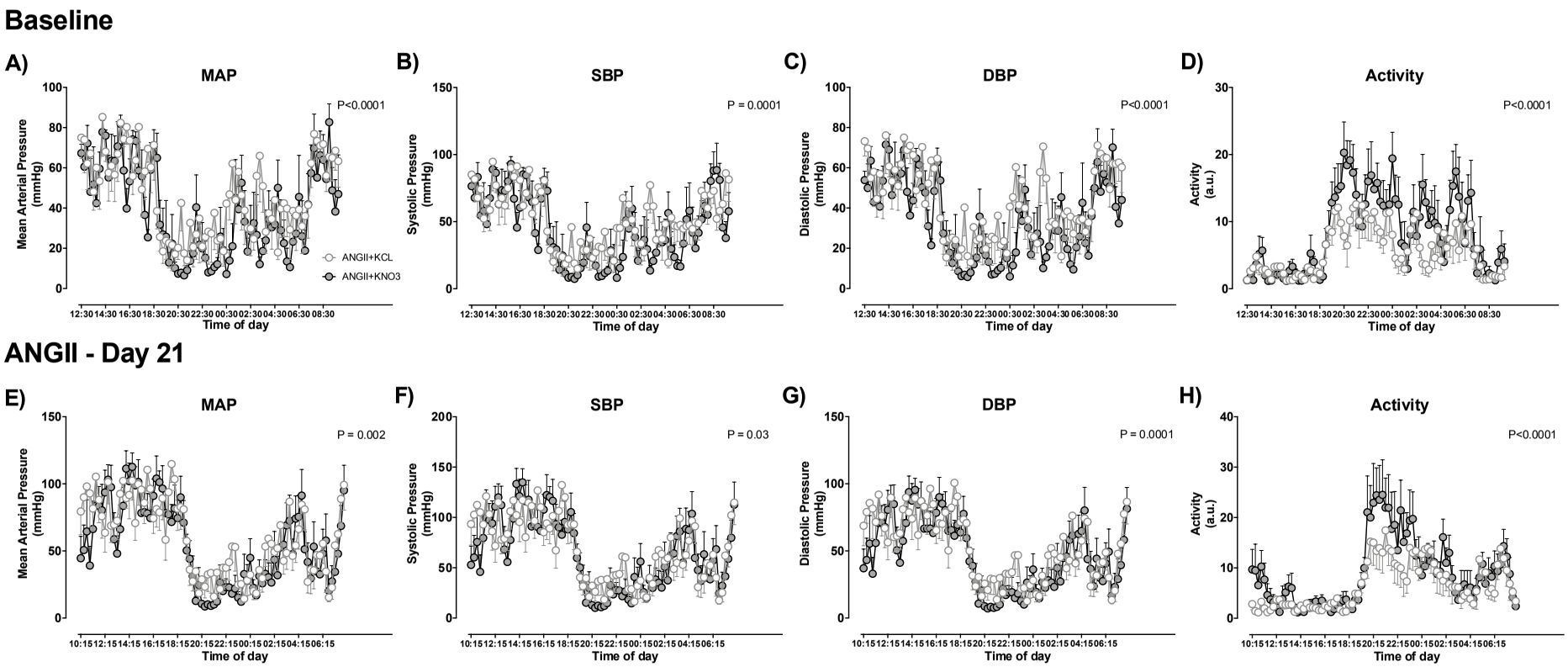

Figure 3.16 BP telemetry data traces from ANGII pre-treatment study mice, normalised to activity level.
Graphs show mean, systolic and diastolic BP (normalised to activity level), and activity data at baseline (A-D) and on Day 21 of ANGII infusion (E-H) in mice pre-treated with either 15 mM KNO_3 or KCl. Data are represented as mean ± SEM with n = 5-6 (baseline) and n = 8 (Day 21).
Stars show statistical significance of results when compared using Two-way ANOVA. P-values show statistical significance when curves were compared with two-way ANOVA.

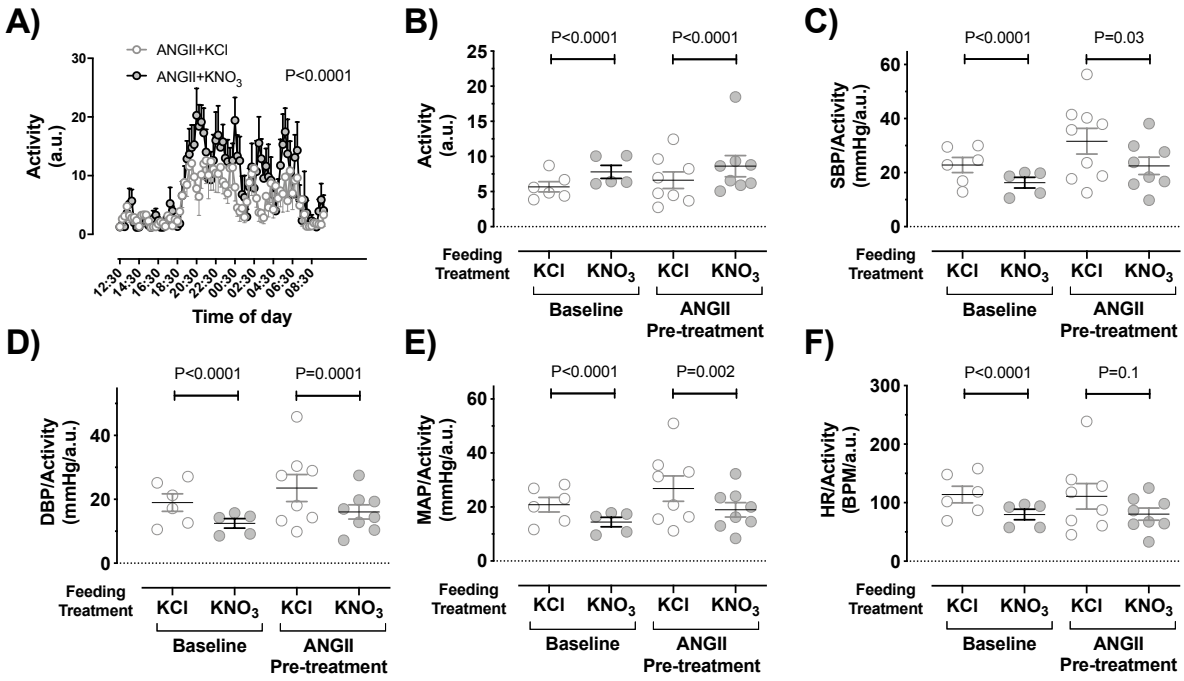

Figure 3.17 BP telemetry data from ANGII pre-treatment study mice, normalised to activity level
Figure shows mouse A) 24-hour traces and B) averages of activity level. Also shown are C) mean, D) systolic and E) diastolic BP and F) hearts rate normalised to activity. Data are shown at baseline and on Day 21 of ANGII infusion in mice with 15 mM KNO_3 or KCl pre-treatment. Data are presented as averages of 24-hour data from telemetric monitoring, with mean ± SEM and n = 8. P-values show statistical significance when data are compared across a 24-hour period using Two-way ANOVA.

3.9.5. Effect of oral nitrate on organ bath pharmacology in ANGII-infused mice

Organ bath assays were carried out to compare the effects of oral nitrate treatment on the vasoreactivity of mouse aortas from controls and ANGII infused mice. In aortic rings from ANGII infused mice, pre-contracted with 10^{-5} M PE, both ACh and SNO concentration-dependent relaxation-response curves were rightward shifted (approximately 3-fold and 1.5-fold shift respectively) in KCl pre-treated mice, compared to tap water fed controls. However, this effect was significantly attenuated in KNO_3 pre-treated mice (P<0.001, **Figure 3.18D**). ANGII infusion also suppressed the maximum response to ACh (but not SNO) in KCl fed mice. When concentration response curves of KNO_3 and KCl pre-treated mice were compared using a two-way ANOVA, the effect of KNO_3 treatment was found to be significant in both ACh (P<0.01) and SNO (P<0.001) curves. KNO_3 pre-treatment had no significant effect on SNO concentration-response curves in control mice (**Figure 3.18B**) but caused a slight leftward shift in ACh curves in controls (P<0.05, **Figure 3.18A**).

Dietary nitrate also had no significant effect on PE concentration-response curves in control mice (**Figure 3.18C** and **Figure 3.18F**).

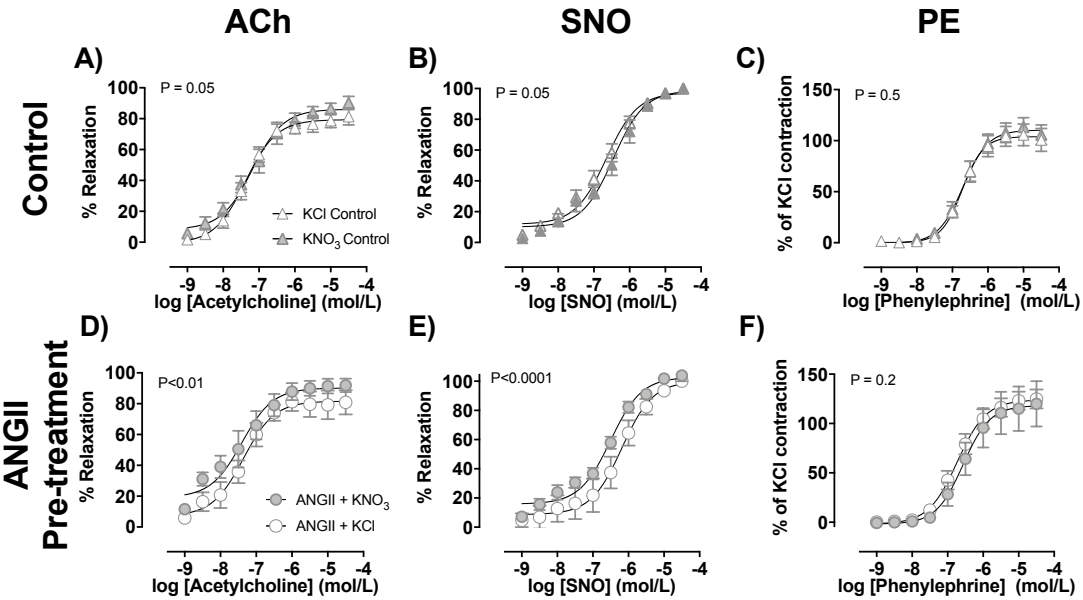

Figure 3.18 Organ bath vessel reactivity of thoracic aortas from control and ANGII pre-treatment study mice fed 15 mM KNO_3 or KCl.

Graphs show A) and D) acetylcholine-induced (ACh) relaxation and B) and E) spermine NONOate-induced (SNO) relaxation concentration-responses with 10^{-5} M phenylephrine (PE) pre-contraction and C) and F) PE-induced contraction concentration-response of aortic rings. Data are shown from control, ANGII pre-treatment and ANGII reversal study mice fed either 15 mM KNO_3 (grey) or 15 mM KCl (white) pre-treatment. Data are shown as mean ± SEM, with n ≥ 5. Mice were sacrificed aged 13-15 weeks. P-values show statistical significance when curves were compared with two-way ANOVA.

3.9.6. Effect of nitrate on mRNA markers in ANGII-infused mice

3.9.6.1. TGFβ, CTGF, Col1 and Col3

A significant increase in CTGF mRNA expression was measured in heart homogenates from ANGII-infused mice when compared to KCl control mice using RT-PCR. This increase was significantly attenuated by KNO_3 pre-treatment (**Figure 3.19B)**. There was also a trend towards increased Col1a expression, which again appeared to be attenuated by KNO_3 pre-treatment (**Figure 3.19C**). However, this did not reach statistical significance with the sample size which was available.

Col3 mRNA also showed a trend towards being increased by ANGII infusion, but with no apparent effect from KNO_3 pre-treatment (**Figure 3.19D**).

Despite no clear results, there seemed to be a slightly greater increase in TGFβ expression in KNO_3 fed ANGII-infused mice compared to ANGII + KCl-fed mice in the pre-treatment study (**Figure 3.19A**). But again, this was not statistically significant.

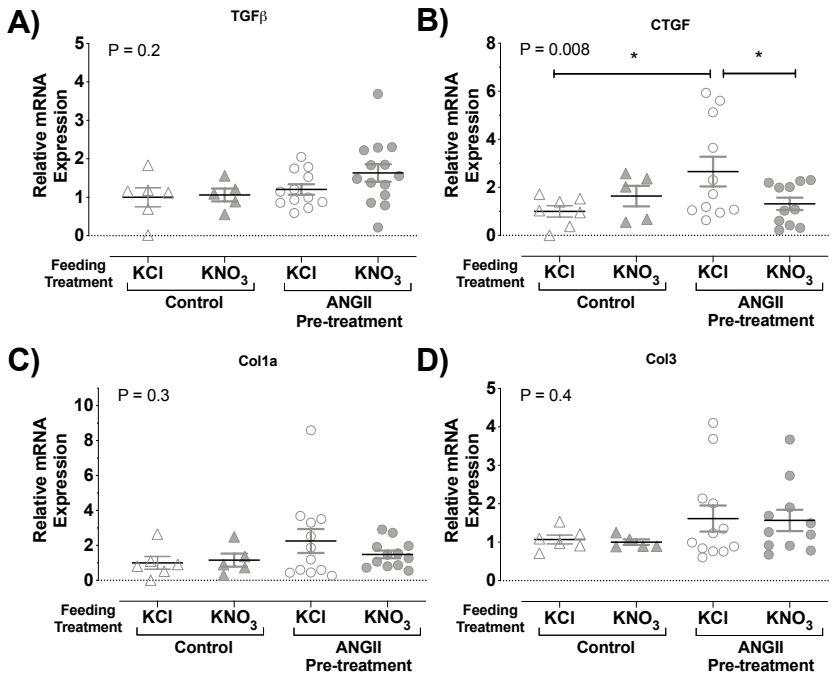

Figure 3.19 mRNA expression of TGBFβ, CTGF, Col1 and Col3 in heart tissue from control and ANGII pre-treatment study mice.

Figure shows mRNA expression of A) transforming growth factor β (TGFβ) B) connective tissue growth factor (CTGF), C) type I collagen (Col1a) and D) type III collagen (Col3) in whole heart homogenate from controls and ANGII pre-treated mice fed 15 mM KNO_3 or KCl. For RT-PCR, all samples were plated in duplicate, with gene expression measured relative to internal control 18S. Results are expressed relative to KCl fed controls using ΔΔCT analysis. Data are expressed as mean ± SEM with n = 6-12. Data were tested for statistical significance using one-way ANOVA with Sidak's post-hoc analysis. P-values for one-way ANOVA are shown in the graphs and stars represent statistical significance determined by post-hoc analyses: * = P<0.05.

3.9.6.2. **AT1Ra and BNP**

AT1Ra mRNA showed a trend towards being increased by ANGII infusion in both KCl and KNO_3 fed mice, with no apparent effect from KNO_3 pre-treatment (**Figure 3.20A**). BNP mRNA showed a trend towards being increased by ANGII infusion in both KCl and KNO_3 fed mice, with no clear effect from KNO_3 pre-treatment (**Figure 3.20B**).

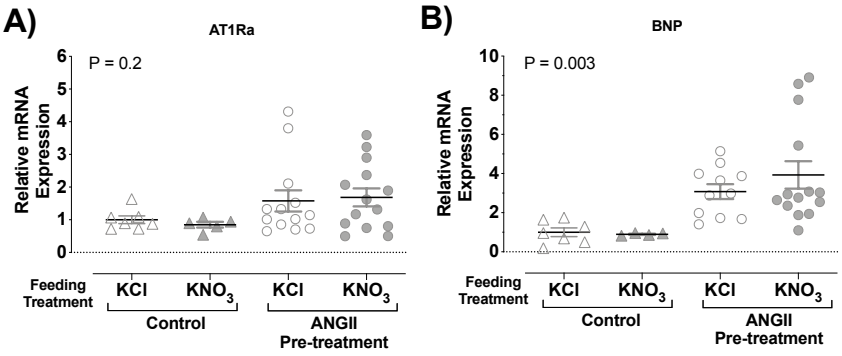

Figure 3.20 mRNA expression of AT1Ra and BNP in heart tissue from control and ANGII pre-treatment study mice.

Figure shows mRNA expression of A) angiotensin type 1 receptor (AT1Ra) and B) brain natriuretic peptide (BNP) in whole heart homogenate from controls and ANGII pre-treated mice fed 15 mM KNO_3 or KCl. For RT-PCR, all samples were plated in duplicate, with gene expression measured relative to internal control 18S. Results are expressed relative to KCl fed controls using ΔΔCT analysis. Data are expressed as mean ± SEM with n = 6-12. Data were tested for statistical significance using one-way ANOVA with Sidak's post-hoc analysis. P-values for one-way ANOVA are shown in the graphs and stars represent statistical significance determined by post-hoc analyses.

3.9.6.3. XDH, NLRP1 and NLRP3

There was no clear effect of either ANGII infusion, or KCl or KNO_3 feeding on XDH mRNA expression in the ANGII pre-treatment study (**Figure 3.21A**).

There was no clear effect of either ANGII infusion, or KCl or KNO_3 feeding on NLRP1 and NLRP3 mRNA expression in the ANGII pre-treatment study (**Figure 3.21B** and **Figure 3.21C**).

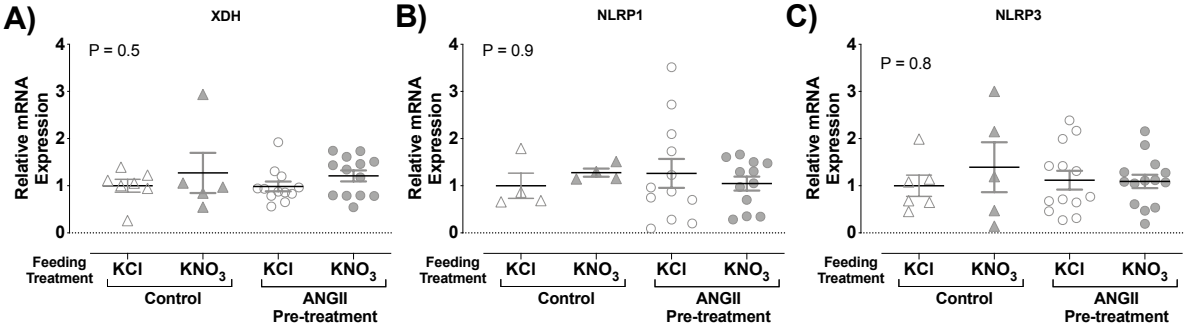

Figure 3.21 mRNA expression of AT1Ra and BNP in heart tissue from control and ANGII pre-treatment study mice. Figure shows mRNA expression of A) xanthine oxidoreductase (XDH), B) NLR family pyrin domain containing 1 (NLRP1) and C) NLR family pyrin domain containing 3 (NLRP3) in whole heart homogenate from controls and ANGII pre-treated mice fed 15 mM KNO_3 or KCl. For RT-PCR, all samples were plated in duplicate, with gene expression measured relative to internal control 18S. Results are expressed relative to KCl fed controls using ΔΔCT analysis. Data are expressed as mean ± SEM with n = 6-12. Data were tested for statistical significance using one-way ANOVA with Sidak's post-hoc analysis. P-values for one-way ANOVA are shown in the graphs and stars represent statistical significance determined by post-hoc analyses.

3.9.7. Effect of oral nitrate on oxidative stress in hearts from ANGII pre-treatment mice

Whole heart homogenates from ANGII-infused mice were incubated with substrates, including xanthine, NADH and NADPH, and resulting superoxide generation measured using lucigenin chemiluminescence quantification.

Inorganic nitrate significantly reduced baseline oxidative stress generation in mouse heart homogenates from ANGII-infused mice (P=0.04), as well as oxidative stress generated in the presence of xanthine (P=0.01), NADH (P=0.09) and NADPH (P=0.02, **Figure 3.22**).

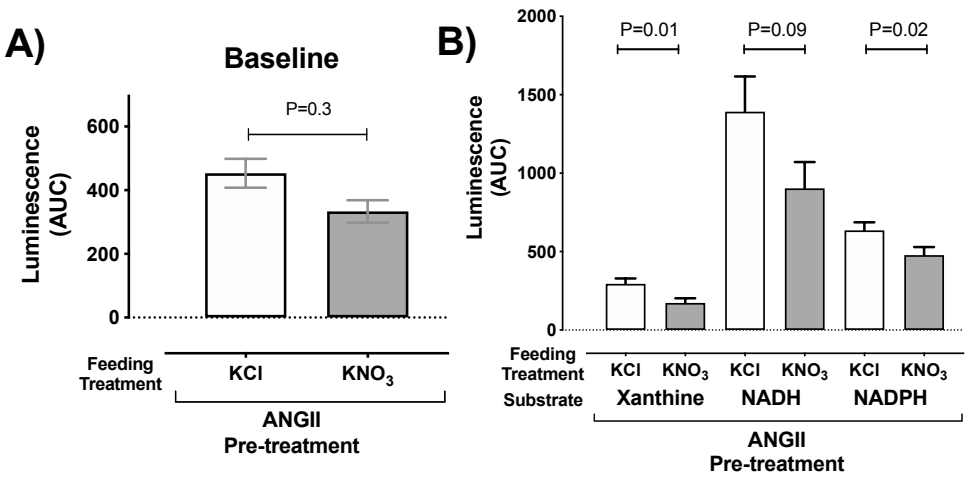

Figure 3.22 Superoxide generation quantified by lucigenin chemiluminescence in heart homogenates from ANGII study mice.
Figure shows superoxide generation in mouse heart homogenates from ANGII-infused mice with either 15 mM KNO_3 or KCl pre-treatment. Superoxide generation was measured by quantifying lucigenin chemiluminescence generated at baseline or upon homogenate incubation with substrates including Xanthine, NADPH, NADH. Data are represented as mean ± SEM with n = 13. P-values show statistical significance of results when data are compared to KCl fed mice under the same ANGII regimen using Student's T-tests.

3.9.8. The effects of dietary nitrate on XOR protein expression in control and ANGII-infused mice

ANGII-infusion resulted in a significant increase in XOR protein expression in mouse livers as measured by western blot immunoassay. There was no significant attenuation of this increase in mice with dietary nitrate pre-treatment (**Figure 3.23**).

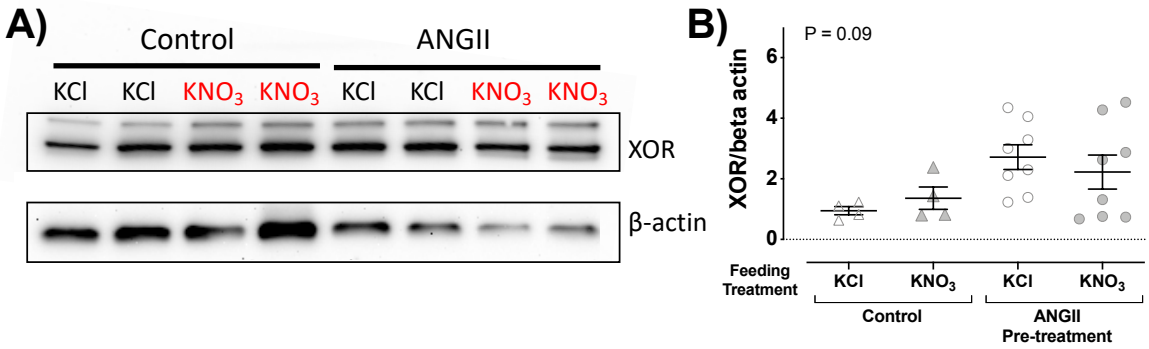

Figure 3.23 The effects of dietary nitrate on XOR protein expression in control and ANGII-infused mice.
Figure shows A) an example blot with XOR and beta-actin protein expression measured in liver homogenates by western blot analysis and B) XOR data normalised to beta actin expression. Data are expressed as mean ± SEM, with n = 4-8. Data were tested for statistical significance using one-way ANOVA with Sidak's post-hoc analysis. The P-value for one-way ANOVA is shown in the graph but there were no significant differences according to post-hoc analyses.

3.9.9. Enhanced XOR activity in ANGII mice pre-treated with KCl compared to ANGII mice pre-treated with KNO_3

ANGII-infusion increased the H_2O_2 generating capacity of XOR in mouse liver homogenates ($P<0.0001$, **Figure 3.24**). There were significantly lower levels of conventional XOR activity measured in pre-treatment study mice fed KNO_3 compared to KCl-fed mice under the same ANGII regimen ($P<0.001$, **Figure 3.24**).

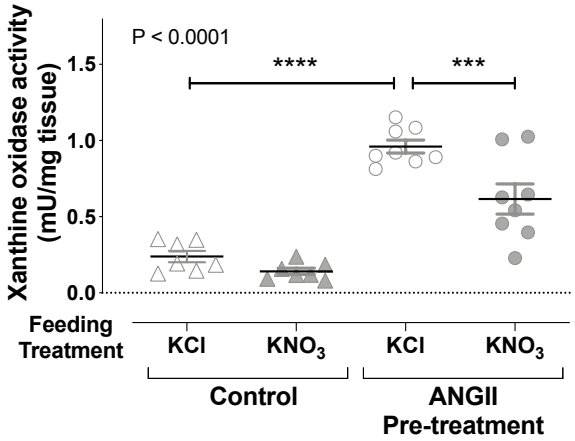

Figure 3.24 XO activity in liver homogenates from control, ANGII pre-treatment and reversal study mice.
Figure shows level of conventional XO activity present in mouse liver homogenates from control and ANGII infused mice with either 15 mM KNO_3 or KCl pre-treatment or reversal treatment. XO activity was measured by quantifying H_2O_2 generation using a commercially available kit. Data are represented as mean ± SEM with n = 8. Data were tested for statistical significance using one-way ANOVA with Sidak's post-hoc analysis (A) or Student's T-tests (B). P-values for one-way ANOVAs and T-tests are shown in the graphs. Stars represent statistical significance determined by post-hoc analyses: *** = P<0.001 and **** = P<0.0001.

3.9.10. The effects of dietary nitrate on nitrite reductase activity in control and ANGII-infused mice

Nitrite reductase capacity, as measured by gas phase ozone chemiluminescence, in mouse heart homogenate was significantly greater in mice receiving dietary nitrate compared to KCl-fed mice in both control (P=0.005, **Figure 3.25A**) and ANGII-infused mice (P=0.004, **Figure 3.25B**).

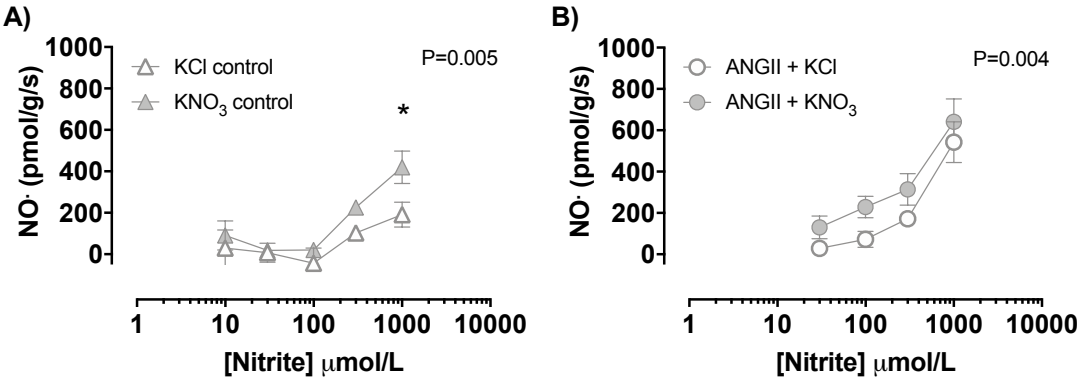

Figure 3.25 The effect of dietary nitrate on nitrite reductase capacity of heart tissue in a chemiluminescence assay.
Cardiac nitrite reductase activity was measured by ozone chemiluminescence at pH 7.4 by incubating heart homogenate with nitrite at incremental doses. Data are represented as mean ± SEM with n = 6-7. P-values show statistical significance when curves were compared with two-way ANOVA. Stars represent statistical significance with Sidak's post-hoc analysis: * = P<0.05.

3.9.11. The effects of dietary nitrate on Nox2 protein expression in ANGII-infused mice

The expression of Nox2 protein was quantified by western blot analysis in mouse aortas. Due to the restricted number of available samples, and the fact that XOR was of more significant interest to our studies, this preliminary data was obtained only in ANGII pre-

treatment mice. There was a trend towards reduced expression of Nox2 in nitrate fed ANGII-infused mice compared to KCl fed controls under the same ANGII regimen. However, this was not statistically significant (**Figure 3.26**).

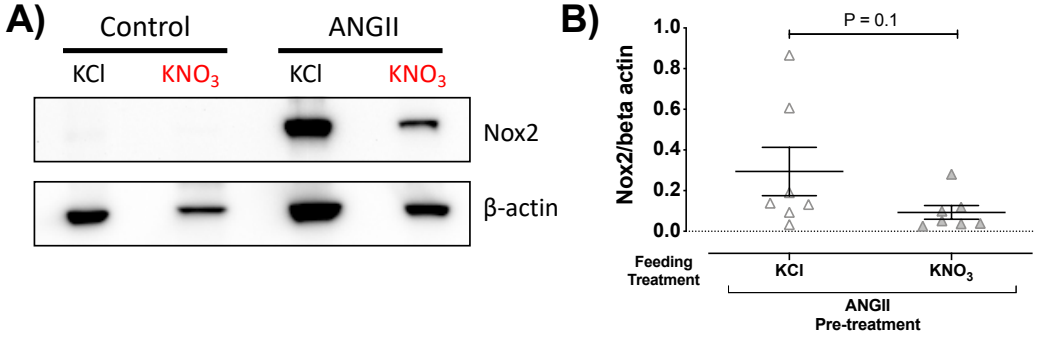

Figure 3.26 The effects of dietary nitrate on Nox2 protein expression in ANGII-infused mice.
Figure shows Nox2 protein expression measured in aorta homogenates by western blot analysis, with protein levels normalised to beta actin expression. Data are represented as mean ± SEM with n = 7. Data were tested for statistical significance using Students' T-test and the P-values is shown in the graph.

3.10. Nitrate reversal treatment in ANGII infused mice

3.10.1. The effect of nitrate on heart weights in ANGII-pretreated mice

Although HW:BW ratios, overall heart weight and LV:BW ratios showed subtle, but consistent, trends towards attenuation in ANGII-infused mice with KNO_3 reversal treatment (**Figure 3.27**), these were not statistically significant when compared to KCl-fed mice.

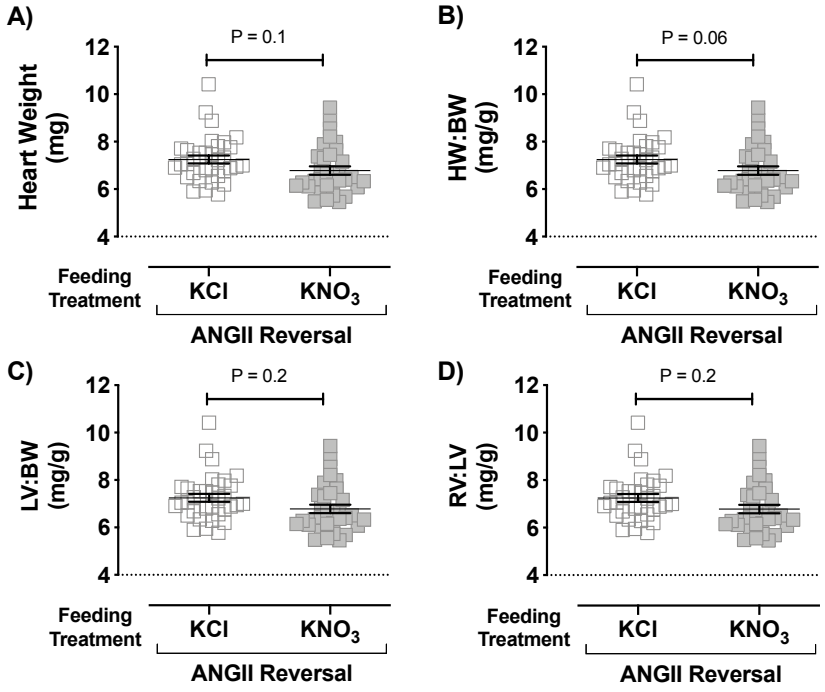

Figure 3.27 Heart weight data from ANGII study mice.
Figure shows A) whole heart weights as well as B) heart weight: body weight, C) left ventricle: body weight and D) right ventricle: left ventricle ratios for control mice and ANGII pre-treatment study mice fed either 15 mM KNO_3 or KCl. Data are represented as mean ± SEM. Data were tested for statistical significance using a one-way ANOVA with Sidak's post-hoc analysis. P-values for one-way ANOVA are shown in the graphs and stars represent statistical significance determined by post-hoc analyses: * = P<0.05, **** = P<0.0001.

3.10.2. Nitrate reversal treatment reduces ANGII-induced LV wall thickening measured by echocardiography

Echocardiography was performed at the end of the study in ANGII reversal mice fed KNO_3 or KCl. LVPWd thickness was significantly reduced in mice fed KNO_3 reversal treatment when compared to KCl fed mice under the same ANGII regimen (ANGII+KCl: 1.2 ± 0.09 mm; ANGII+KNO_3 Pre: 1.0 ± 0.04 mm; P=0.02) – see representative M-mode images in **Figure 3.28A and Figure 3.28B**, and data in **Figure 3.28C**. The same findings were also true of LVPWs dimensions (**Figure 3.28D**). LV mass was also significantly reduced in mice fed KNO_3 reversal treatment when compared to KCl fed mice ($P<0.05$, **Figure 3.28I**). Ejection fraction was not significantly changed by KNO_3 reversal treatment in ANGII-infused mice (**Figure 3.28G**).

There were also no significant differences in IVSd, IVSs, LVIDd, LV end diastolic volumes or wall:lumen ratios when compared between treatment groups using one-way ANOVA (**Figure 3.28E-H and Figure 3.28K**).

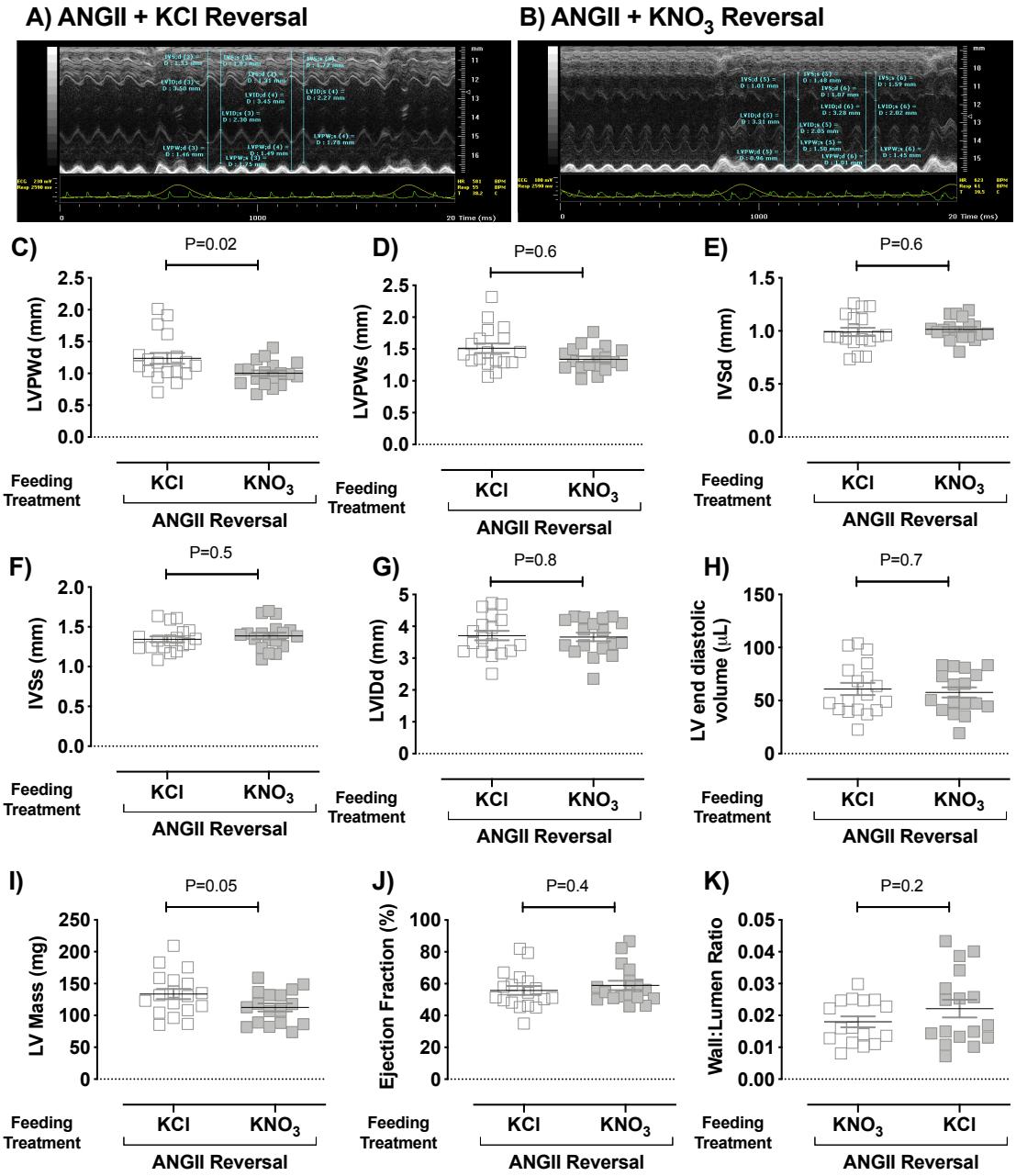

Figure 3.28 End of study echocardiography measurements from ANGII reversal study mice.
Figure shows representative M-mode images, acquired using Vevo 770 echocardiography software and equipment from A) ANGII + KNO_3 reversal and B) ANGII + KCl reversal mice. Images were acquired under 1.5-2% isofluorane inhalation anaesthetic. Measurements of the intra-ventricular septum (IVS), left ventricle posterior wall (LVPW) and left ventricle internal dimension (LVID) were taken during diastole (d) and systole (s). The image represents a total of 20ms of echocardiographic recording. Resulting LVPWd, LVPWs, IVSd, IVSs, LVIDd dimensions, LV end diastolic volume, LV mass, ejection fraction and wall:lumen ratios are shown in C), D) E), F), G), H), I), J) and K) respectively. Data are represented as mean ± SEM with n = 17-18. Data were tested for statistical significance using Student's T-test, and p-values shown in the graphs.

3.10.3. Effect of nitrate reversal treatment on cardiac fibrosis, measured by PSR staining

There was no significant attenuation of fibrosis with oral nitrate in ANGII reversal mice (P = 0.7, **Figure 3.29A**).

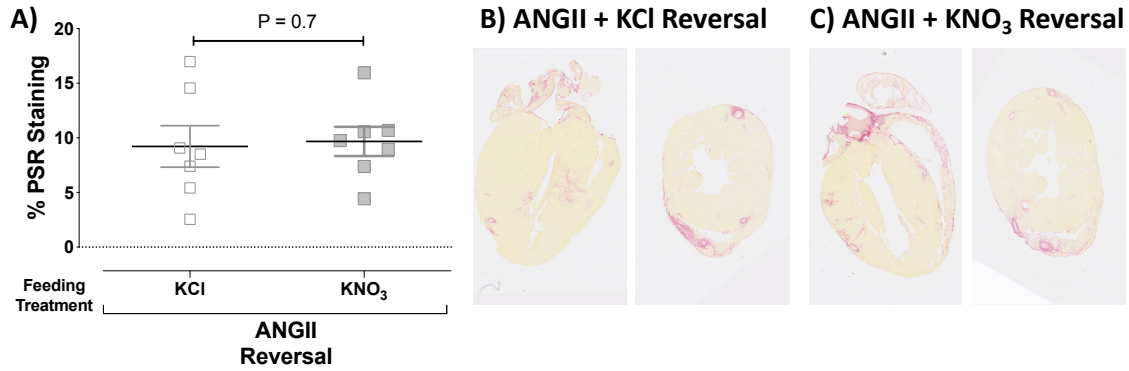

Figure 3.29 Collagen deposition as quantified by PSR staining in ANGII reversal study mouse hearts.
Figure shows PSR staining carried out on 4 µm sections of formalin fixed hearts, embedded in paraffin. Hearts were randomly assigned to be sectioned in either the transverse or dorsal plane and stained with PSR to identify areas of connective tissue deposition. Images were acquired using a NanoZoomer slide scanner (Hamamatsu) and viewed using NDP View software. Three left ventricle, three intraventricular septum and three right ventricle fields of view were randomly selected at x20 magnification and PSR staining quantified using manual thresholding techniques in ImageJ software. Figure shows quantification of staining in ANGII-infused mice with KNO_3 or KCl reversal treatment. Sections B) and C) show representative staining images at x 1.25 magnification in all treatment groups. Data are represented as mean ± SEM with n = 7. Data were tested for statistical significance using Student's T-test, with resulting P-value shown in the graph.

3.10.4. Effect of nitrate reversal treatment on organ bath pharmacology

KNO_3 reversal treatment had no significant effect on ACh, SNO or PE concentration-response curves in ANGII-infused mice (**Figure 3.30**).

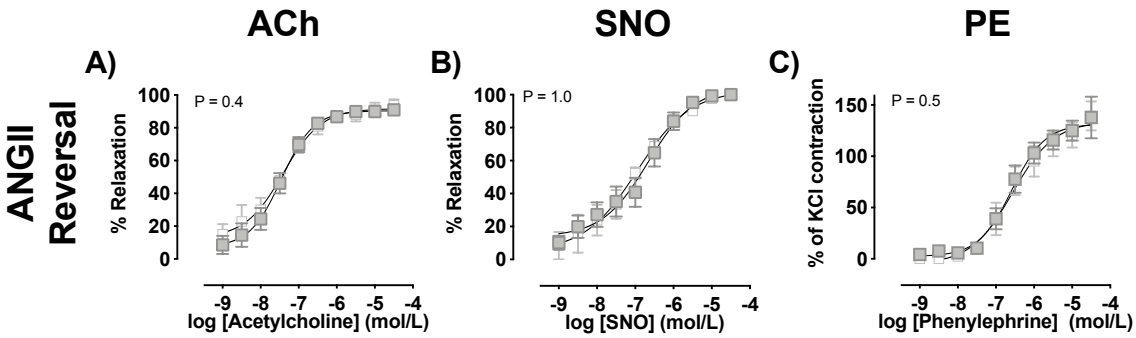

Figure 3.30 Organ bath vessel reactivity of thoracic aortas from ANGII reversal study mice fed 15 mM KNO_3 or KCl.
Graphs show G) acetylcholine-induced (ACh) relaxation and H) spermine NONOate-induced (SNO) relaxation concentration-responses with 10^{-5} M phenylephrine (PE) pre-contraction and I) PE-induced contraction concentration-response of aortic rings. Data are shown from control, ANGII pre-treatment and ANGII reversal study mice fed either 15 mM KNO_3 (grey) or 15 mM KCl (white) pre-treatment. Data are shown as mean ± SEM, with n ≥ 5. Mice were sacrificed aged 13-15 weeks. P-values show statistical significance when curves were compared with two-way ANOVA.

3.10.5. Effect of nitrate on mRNA markers in ANGII-infused mice

3.10.5.1. TGFβ, CTGF, Col1 and Col3

There was a slight, but non-significant increase in TGFβ expression with KNO_3 feeding in the ANGII reversal study compared to KCl fed mice (**Figure 3.31D**), and there was a significant increase in Col3 expression (P=0.04, **Figure 3.31D**). There was no significant

effect of KNO_3 reversal treatment on CTGF or Col1a mRNA expression in ANGII-infused mice (**Figure 3.31B** and **Figure 3.31C**).

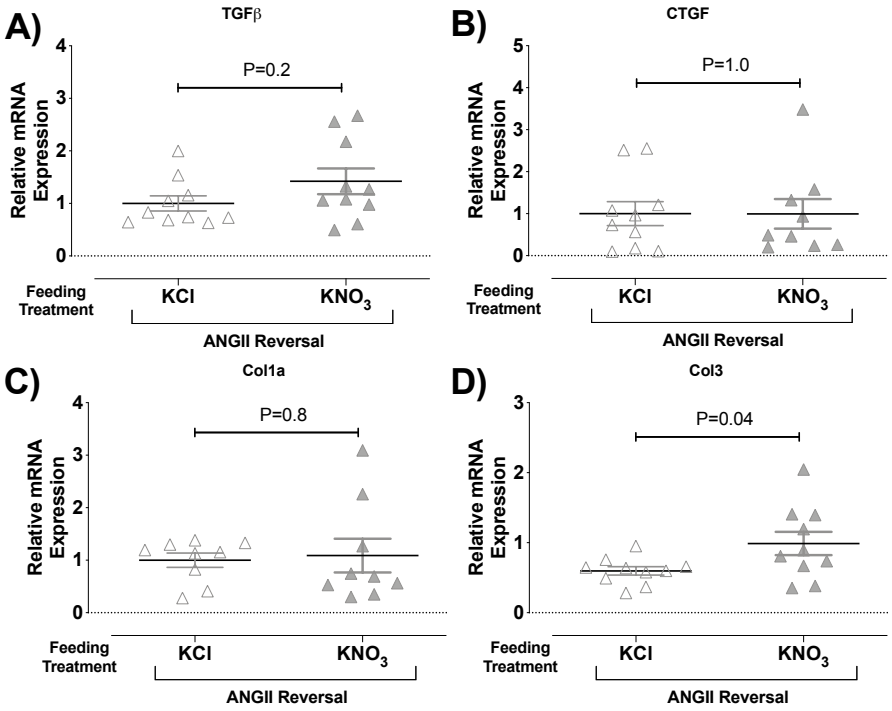

Figure 3.31 mRNA expression of TGBFβ, CTGF, Col1 and Col3 in heart tissue from ANGII reversal study mice.
Figure shows mRNA expression of A) transforming growth factor β (TGFβ) B) connective tissue growth factor (CTGF), C) type I collagen (Col1a) and D) type III collagen (Col3) in whole heart homogenate from ANGII reversal study mice treated with 15 mM KNO_3 or KCl. For RT-PCR, all samples were plated in duplicate, with gene expression measured relative to internal control 18S. Results are expressed relative to KCl fed controls using ΔΔCT analysis. Data are expressed as mean ± SEM with n = 10-11. Data were tested for statistical significance using one-way ANOVA with Sidak's post-hoc analysis. P-values for one-way ANOVA are shown in the graphs and stars represent statistical significance determined by post-hoc analyses: * = P<0.05.

3.10.5.2. **AT1Ra and BNP**

There was no difference in AT1Ra mRNA expression when KNO_3 and KCl ANGII reversal mice were compared (**Figure 3.32A**), but there was a significant increase in BNP expression with KNO_3 reversal treatment (P<0.02, **Figure 3.32B**).

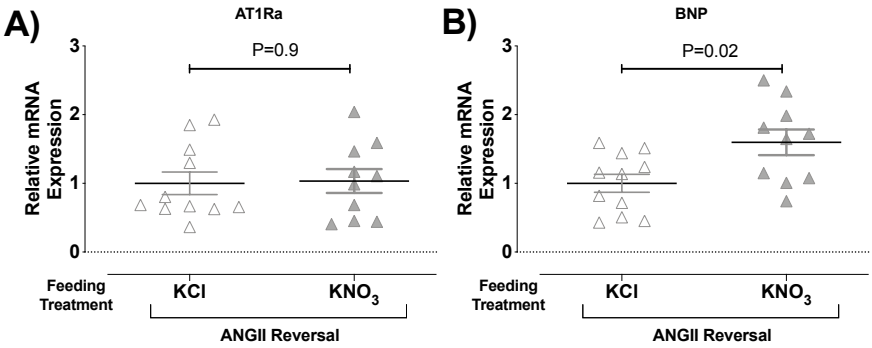

Figure 3.32 mRNA expression of AT1Ra and BNP in heart tissue from ANGII reversal study mice.
Figure shows mRNA expression of A) angiotensin type 1 receptor (AT1Ra) and B) brain natriuretic peptide (BNP) in whole heart homogenate from ANGII reversal study mice treated with 15 mM KNO_3 or KCl. For RT-PCR, all samples were plated in duplicate, with gene expression measured relative to internal control 18S. Results are expressed relative to KCl fed controls using ΔΔCT analysis. Data are expressed as mean ± SEM with n = 10-11. Data were tested for statistical significance using one-way ANOVA with Sidak's post-hoc analysis. P-values for one-way ANOVA are shown in the graphs and stars represent statistical significance determined by post-hoc analyses.

3.10.5.3. **XDH, NLRP1 and NLRP3**

There was no difference in XDH or NLRP1 mRNA expression when KNO_3 and KCl ANGII reversal mice were compared (**Figure 3.33A and Figure 3.33B**), but there was a significant increase in NLRP3 expression with KNO_3 reversal treatment (**Figure 3.33C**).

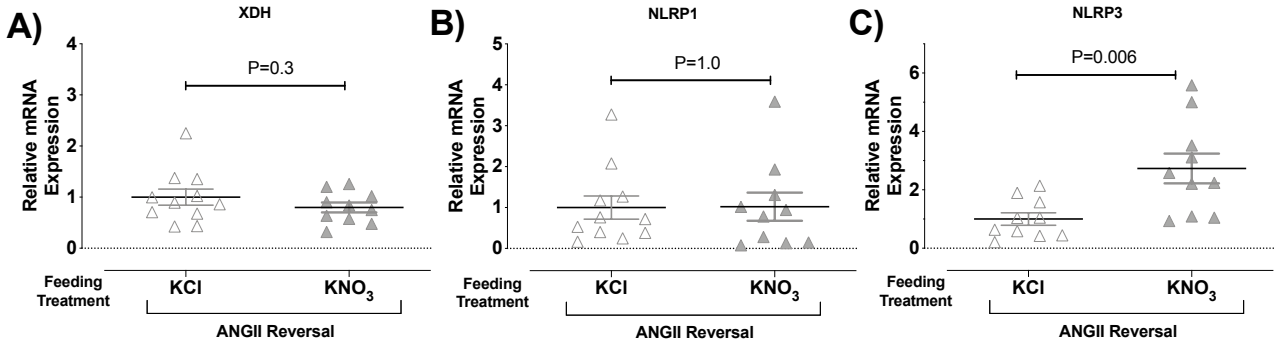

Figure 3.33 mRNA expression of XDH, NLRP1 and NLRP3 in heart tissue from ANGII reversal study mice.
Figure shows mRNA expression of A) xanthine oxidoreductase (XDH), B) NLR family pyrin domain containing 1 (NLRP1) and C) NLR family pyrin domain containing 3 (NLRP3) in whole heart homogenate from ANGII reversal study mice treated with 15 mM KNO_3 or KCl. For RT-PCR, all samples were plated in duplicate, with gene expression measured relative to internal control 18S. Results are expressed relative to KCl fed controls using ΔΔCT analysis. Data are expressed as mean ± SEM with n = 6-12. Data were tested for statistical significance using one-way ANOVA with Sidak's post-hoc analysis. P-values for one-way ANOVA are shown in the graphs and stars represent statistical significance determined by post-hoc analyses.

3.10.6. **Enhanced XOR activity in reversal ANGII mice treated with KCl compared to with KNO_3**

There were significantly lower levels of conventional XOR activity measured in reversal (P=0.004) study mice fed KNO_3 compared to KCl-fed mice under the same ANGII regimen (P=0.04, **Figure 3.34**).

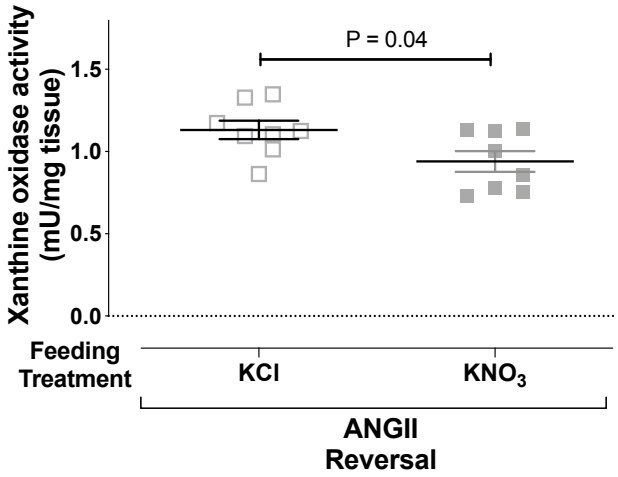

Figure 3.34 XO activity in liver homogenates from control, ANGII pre-treatment and reversal study mice.
Figure shows level of conventional XO activity present in mouse liver homogenates from control and ANGII infused mice with 15 mM KNO_3 or KCl reversal treatment. XO activity was measured by quantifying H_2O_2 generation using a commercially available kit. Data are represented as mean ± SEM with n = 8. Data were tested for statistical significance using Student's T-test, with P-value shown in the graph.

3.11. **Result One – Summary**

In summary, we have confirmed the ANGII model to be an effective method for producing a BP-dependent model of cardiac dysfunction in mice – inducing endothelial dysfunction, hypertension and a reduction in ejection fraction with a significant increase in heart weight, LVH and cardiac fibrosis and superoxide generation.

In this model, dietary nitrate pre-treatment significantly attenuated:

- Endothelial dysfunction ($P<0.01$) and hypertension ($P<0.002$).
- LVH as measured by echocardiography ($P<0.0001$) and LV:BW ratios ($P<0.05$).
- Cardiac CTGF mRNA expression ($P<0.05$) as measured by RT-PCR, and fibrosis ($P<0.001$) as measured by PSR staining.
- XOR-mediated H_2O_2 production ($P<0.01$) and superoxide generation ($P<0.05$).
- NADPH oxidase-mediated superoxide generation ($P<0.05$).

Furthermore, dietary nitrate pre-treatment increased nitrite reductase capacity in heart homogenate ($P<0.01$).

Dietary nitrate reversal treatment significantly attenuated:

- LVH as measured by echocardiography ($P<0.0001$), with borderline significance in LV:BW ratios ($P<0.06$).

However, there were no further significant differences when other parameters were compared.

CHAPTER FOUR -

The Effect of Dietary Nitrate on a BP-independent Model of Cardiac Dysfunction

4. CHAPTER FOUR - The effect of dietary nitrate on a BP-indepent model of cardiac dysfunction

Following our findings that dietary nitrate could significantly attenuate cardiac hypertrophy in a BP-dependent mouse model, as well as reducing oxidative stress, it was of particular interest to establish whether all of the benefits observed were attributed to BP reduction.

As one way in which many currently available treatments aim to reduce pathological hypertrophy is by reducing BP, it makes sense that the effects of nitrate on BP in the ANGII model could significantly attenuate cardiac hypertrophy. However, in clinical studies, not all anti-hypertensives reverse cardiac hypertrophy to the same degree, despite producing similar reductions in BP (Ferreira Filho et al. 2010).

With both animal and clinical studies having previously highlighted NO as a direct negative-modulator of cardiac hypertrophy (Buys et al. 2007; Hou et al. 1995; Ichinose et al. 2004; McNamara et al. 2003; Pechánová et al. 1999), independent of its actions as a vasodilator, we set out to investigate the potential of dietary nitrate in an isoprenaline (BP-independent) model of cardiac dysfunction.

4.1. BP-independent model of cardiac dysfunction – isoprenaline hydrochloride

In an identical study design to the ANGII pre-treatment model, mice were randomly assigned to one of 4 treatment groups – KNO_3 control, KCl control, isoprenaline + KNO_3 pre-treatment or isoprenaline + KCl pre-treatment (see **Figure 4.1**).

Controls - Mice received 15 mM KNO_3 or 15 mM KCl in drinking water *ad libitum* for 5 weeks.

Isoprenaline Pre-treatment - Mice received 15 mM KNO_3 or 15 mM KCl in drinking water *ad libitum* for 2 weeks prior to beginning a 3-week subcutaneous (SC) infusion of 15 mg/kg/day isoprenaline hydrochloride (Sigma® Life Science, UK) in 0.25% (w/v) ascorbic acid (Sigma Aldrich®, UK) from an ALZET® 1004 osmotic minipump (Durect Corporation, USA). Water feeding treatments were continued concomitantly for the remainder of the study, alongside isoprenaline infusion. In this study echocardiography was conducted sequentially at baseline (the day before minipump implantation surgery), and at weekly

intervals thereafter for 3 weeks. Another subset of mice underwent tail cuff BP measurements during the final week of isoprenaline infusion.

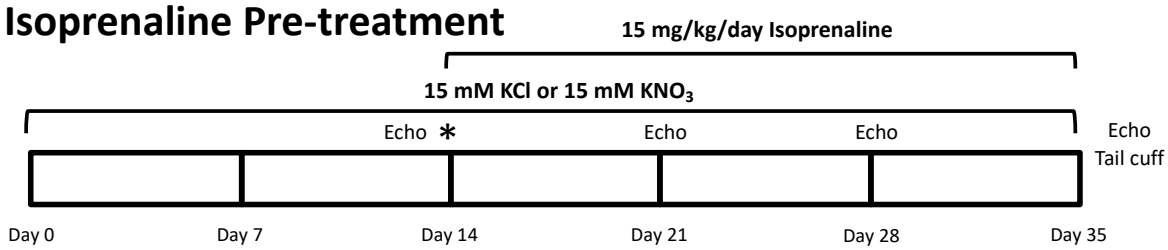

Figure 4.1 Experimental Design for isoprenaline studies.
Schematic illustrating the experimental design for isoprenaline pre-treatment studies. Schematics illustrate the duration of 15mM KCl (control) or 15mM KNO_3 (treatment) feeding and 15 mg/kg/day isoprenaline hydrochloride infusion. The points of osmotic minipump (*) implantation are marked, and days on which echocardiography (Echo) and tail cuff BP (tail cuff) measurements were taken are indicated.

4.2. Isoprenaline formulation

For the filling of osmotic minipumps, isoprenaline hydrochloride (Sigma® Life Science, UK) was weighed out and formulated in 0.25% ascorbic acid as required according to mouse weights and pump specifications. Ascorbic acid (Sigma Aldrich®, UK) was formulated in sterile saline. This isoprenaline hydrochloride solution was filtered using a 2 ml syringe and MILLEX® GP 0.22µm filter (Merck Millipore, UK) prior to minipump filling.

4.3. Isoprenaline oxidation assay

In preparation for isoprenaline formulation, 0.25%, 0.5%, 0.625%. 1.25%, 2.5% and 5% w/v solutions of ascorbic acid in saline were each used to formulate a 180 mg/ml isoprenaline hydrochloride solution (Sigma® Life Science, UK). These solutions were kept in 5 ml Eppendorf tubes for 12 days and tested periodically for oxidation measured by colour change by plating 150 µl of each sample in duplicate and measuring using a TECAN Sunrise 96 well plate reader at 405 nm light wavelength.

After analysing results from this assay after 12 days (**Figure 4.2A**), the assay was repeated with the two most optimal concentrations of ascorbic acid (0.25% and 5%) for 23 days (the length of time that the isoprenaline formulation would be in the mice in osmotic minipumps) - **Figure 4.2B**). Isoprenaline exhibited minimal oxidation (as measured by colour change) when formulated in 0.25% ascorbic acid. For this reason, 0.25% ascorbic acid was used for formulating isoprenaline in preparation for filling osmotic minipumps in this study.

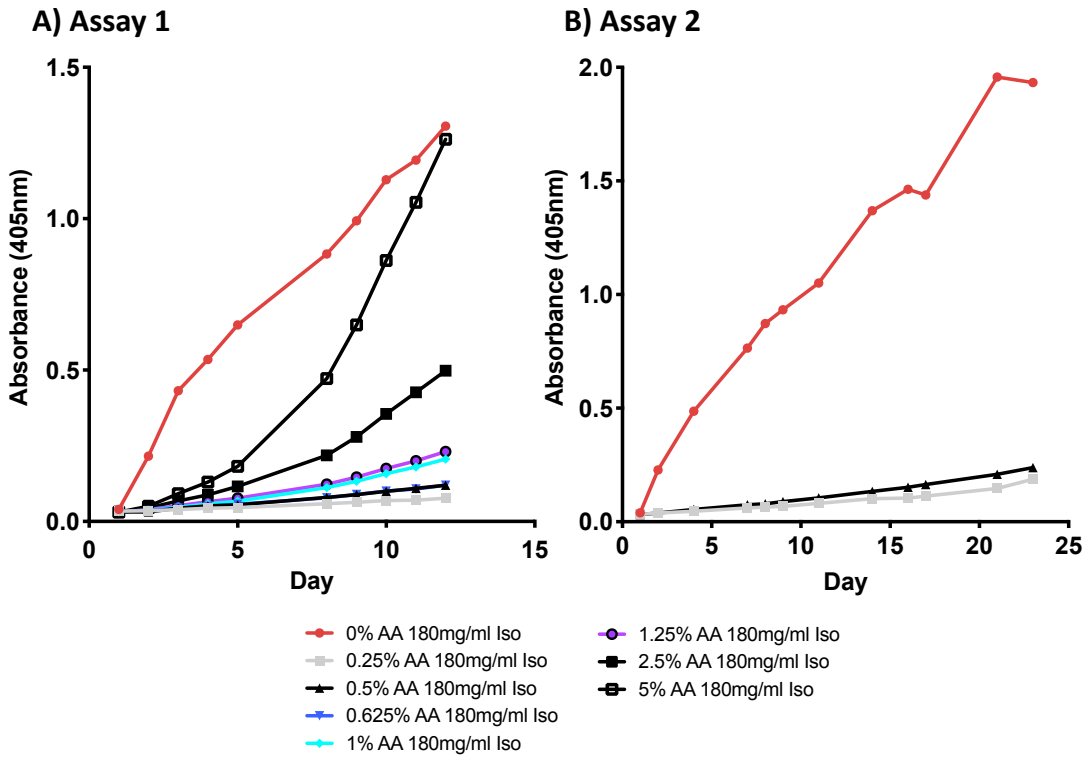

Figure 4.2 Isoprenaline oxidation following formulation in varying concentrations of ascorbic acid.
Graphs show oxidation of 180 mg/ml isoprenaline hydrochloride (Sigma® Life Science, UK) solution over time, when formulated in varying concentrations of ascorbic acid. Oxidation was quantified by measuring average colour change using a TECAN Sunrise 96 well plate reader at 405 nm light wavelength, with 150**µl** of each solution plated in duplicate. Assay 1 compared A) 0%, 0.25%, 0.5%, 0.625%. 1.25%, 2.5% and 5% and Assay 2 B) 0%, 0.25% and 0.5% w/v solutions of ascorbic acid in saline over a 12-day period and 23-day period respectively.

4.4. Model verification – the effects of isoprenaline on heart rate and BP

In order to confirm that isoprenaline induces a significant increase in heart rate, without a significant rise in BP (inducing a BP-independent model of cardiac hypertrophy), mouse heart rate was recorded during echocardiography imaging under light anaesthesia. Isoprenaline induced a significant increase in heart rate compared to control mice ($P<0.001$, **Figure 4.3A**), and this increase was maintained throughout the 3 weeks of isoprenaline infusion (**Figure 4.3B**). In addition to the fact that there was no significant rise detected in isoprenaline-infused BP (Controls: 143 ± 3 vs. Isoprenaline: 159 ± 4 mmHg see section 3.8), and cardiac hypertrophy was observed both visually (**Figure 4.3C**) and by increases in heart weights (see section 4.9), these results confirm the BP-independent nature of this model of cardiac hypertrophy.

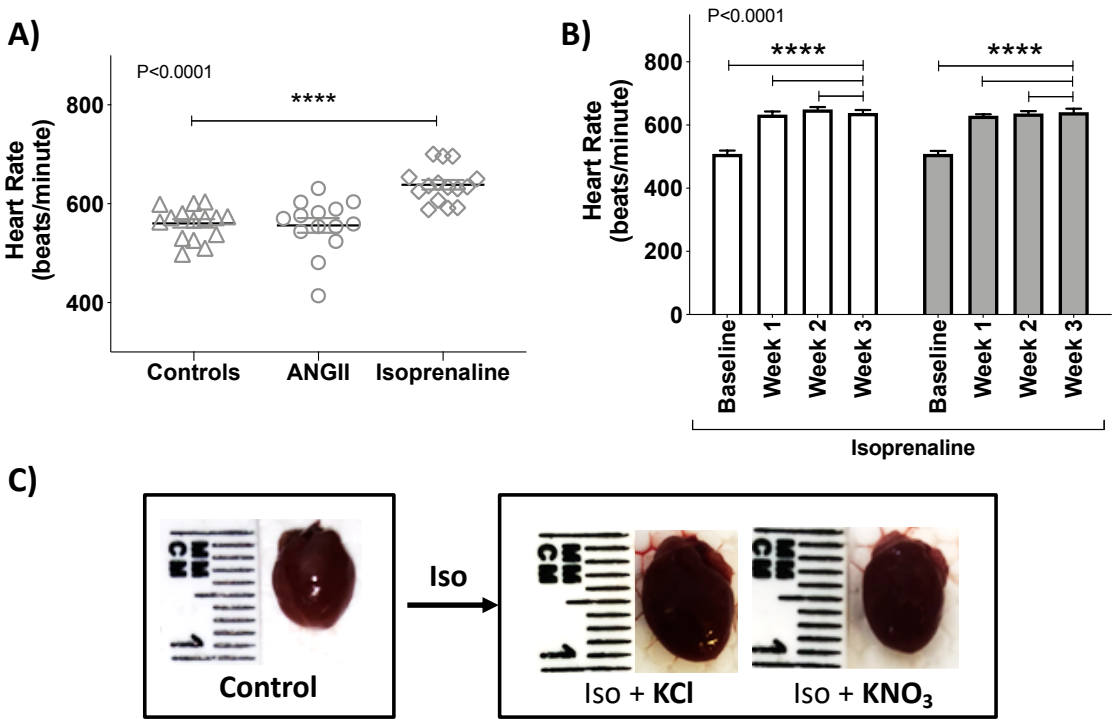

Figure 4.3 Heart rates recorded during echocardiography in isoprenaline study mice pre-treated with 15 mM KNO_3 or KCl and resulting heart images from harvesting after 3 weeks of isoprenaline infusion.
Figure shows A) average heart rates recorded during echocardiography on control mice and mice receiving 2 mg/kg/day or 15 mg/kg/day isoprenaline fed 15 mM KCl. Also shown are B) weekly heart rates recorded during echocardiography in isoprenaline-infused mice with 15 mM KNO_3 (Grey) or KCl (white) pre-treatment. Heart rates are shown at baseline (Week 0 – the day prior to isoprenaline minipump implantation) and an average of values recorded in subsequent weeks (Week 1-3 following minipump implantation). Heart rates were recorded while under ~2% isofluorane inhalation anaesthetic. Data are expressed as mean ± SEM with n = 14-15. Also shown are C) Photographs of hearts following harvesting from control and isoprenaline-infused mice, with KCl or KNO_3. Data are represented as mean ± SEM. Data were tested for statistical significance using one-way ANOVA with Sidak's post-hoc analysis. P-values for one-way ANOVA are shown in the graphs and stars represent statistical significance determined by post-hoc analyses: **** = P<0.0001.

4.5. Dietary nitrate increases plasma nitrite and nitrate in isoprenaline-infused mice

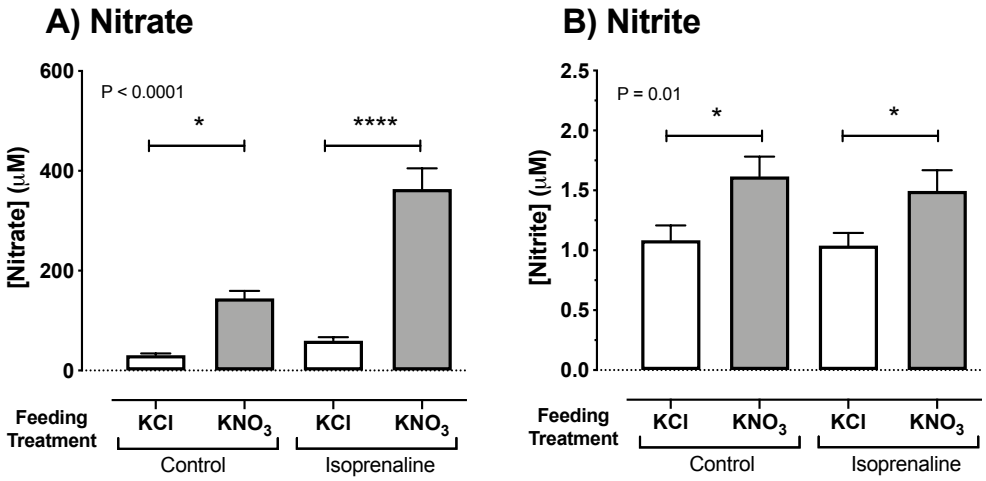

Figure 4.4 Nitrate and nitrite concentrations in plasma of isoprenaline pre-treatment and reversal study mice.
Graphs show A) nitrate (mM) and B) nitrite (μM) concentrations in plasma of control, isoprenaline pre-treatment mice, fed either 15 mM KNO_3 or KCl water. Data are represented as mean ± SEM with n ≥ 18. Data were tested for statistical significance using a one-way ANOVA with Sidak's post-hoc analysis. P-values for one-way ANOVAs are shown in the graphs. Stars represent statistical significance determined by post-hoc analyses:
* = P<0.05, **** = P<0.0001

Ad libitum 15 mM KNO_3 feeding through drinking water successfully raised plasma nitrate in both controls and isoprenaline infused mice (P<0.0001, **Figure 4.4A**). Furthermore, dietary nitrate feeding significantly increased plasma nitrite in controls (1.1 ± 0.1 vs. 1.6 ± 0.2, mean ± SEM, P<0.01) and isoprenaline infused mice (1.0 ± 0.1 vs. 1.5 ± 0.2, P<0.03) - **Figure 4.4B**.

4.6. The effect of isoprenaline infusion on mouse weight, and food and water consumption

4.6.1. Water and nitrate consumption

Water consumption was slightly, but significantly raised in KNO_3 and KCl fed isoprenaline study mice compared to control (P<0.01 and P<0.05 respectively, **Table 4.1**). Increased water consumption resulted in slightly increased doses of nitrate being received by the nitrate-fed isoprenaline-infused mice compared to KNO_3 controls (P<0.05, **Table 4.1**).

4.6.2. Body weight

There were no significant differences in the starting body weights of mice in any of the studies conducted (**Table 4.2**). However, isoprenaline infused mice had significantly greater rises in body weight compared to controls when end of study body weights were compared (P<0.05, **Table 4.2**). There was no significant difference in body weights between KNO_3 and KCl treatment groups.

4.6.3. Food consumption

Food consumption was significantly increased in isoprenaline-infused mice with both nitrate (P<0.05) and KCl (P<0.01) feeding compared to controls (**Table 4.2**). There was no significant difference in food consumption between KNO_3 and KCl treatment groups.

Treatment	Water Consumption (ml/day)			Nitrate Dose Estimation (mmol/kg/day)			Nitrate Dose Estimation (mg/kg/day)			n
	Average	Before Pump	With Pump	Average	Before Pump	With Pump	Average	Before Pump	With Pump	
KNO_3 Control	5.0 ± 0.2	5.2 ± 0.2	5.1 ± 0.3	3.3 ± 0.2	3.4 ± 0.2	3.3 ± 0.3	203.3 ± 13.0	209.5 ± 10.9	206.9 ± 15.9	15
KCl Control	5.0 ± 0.2	5.1 ± 0.1	5.1 ± 0.3	0.1 ± 0.00	0.1 ± 0.0	0.1 ± 0.0	8.3 ± 0.3	8.3 ± 0.3	8.4 ± 0.5	14
Iso + KNO_3 Pre	6.2 ± 0.2**	5.2 ± 0.2	6.9 ± 0.4**	3.9 ± 0.2*####	3.3 ± 0.1####	4.4 ± 0.3**####	243.4 ± 13.7*####	203.5 ± 8.5####	272.0 ± 19.4**####	15
Iso + KCl Pre	6.0 ± 0.3*	5.2 ± 0.2	6.5 ± 0.4*	0.2 ± 0.1	0.1 ± 0.0	0.2 ± 0.0	9.7 ± 0.7	8.4 ± 0.5	10.5 ± 0.9	14

Table 4.1 Table illustrating mouse water, and therefore resulting nitrate (NO_3^-), consumption of mice during isoprenaline studies.
Average water and nitrate consumption were calculated from water weights recorded 3 times weekly. Consumption is shown for KNO_3 and KCl control mice (with no isoprenaline) and isoprenaline + KNO_3 or KCl pre-treatment (Pre) mice. Data are broken down into average consumption, before pump consumption and with pump consumption. Data are represented as mean ± SEM with n ≥ 14.
Differences between treatment groups were tested for statistical significance using a one-way ANOVA and Sidak's post-hoc analysis.
* = significantly different from KNO_3 or KCl control mice with no isoprenaline infusion.
# = KNO_3 fed mice significantly different from KCl fed mice under the same isoprenaline regimen.
*/# = P<0.05, **/## = P<0.01, ***/### = P<0.001 and ****/#### = P<0.0001

Treatment	Mouse Weight (g)				Food Consumption (g/day)			n
	Average	Start of Study	End of Study	Weight Gain	Average	Before Pump	With Pump	
KNO_3 Control	23.9 ± 0.6	20.5 ± 0.7	25.6 ± 0.8	5.0 ± 0.4****	3.4 ± 0.1	3.3 ± 0.1	3.4 ± 0.1	15
KCl Control	24.0 ± 0.6	21.3 ± 0.5	25.7 ± 0.7	4.3 ± 0.6****	3.3 ± 0.1	3.3 ± 0.2	3.3 ± 0.1	14
Iso + KNO_3 Pre	24.8 ± 0.7	20.9 ± 0.6	28.0 ± 0.7*	7.1 ± 0.3	3.7 ± 0.1*	3.3 ± 0.1	3.9 ± 0.1****	15
Iso + KCl Pre	24.7 ± 0.6	21.0 ± 0.6	27.7 ± 0.6*	6.7 ± 0.3	3.7 ± 0.1**	3.3 ± 0.1	4.0 ± 0.1****	14

Table 4.2 Table illustrating mouse weights and food consumptions of mice during isoprenaline studies.
Average mouse weights are shown at the start and end of studies for KNO_3 and KCl control mice (with no isoprenaline) and Isoprenaline + KNO_3 or KCl pre-treatment (Pre) mice. Average food consumption was calculated both before and during isoprenaline infusion, from food weights recorded 3 times weekly. Data are represented as mean ± SEM with n ≥ 14.
Differences between treatment groups were tested for statistical significance using a one-way ANOVA and Sidak's post-hoc analysis.
* = significantly different from KNO_3 or KCl control mice with no isoprenaline infusion
# = KNO_3 fed mice significantly different from KCl fed mice under the same isoprenaline regimen
*/# = P<0.05, **/## = P<0.01, ***/### = P<0.001 and ****/#### = P<0.0001

4.7. cGMP Assay

In the cGMP enzymeimmunoassay, despite there being a significant increase in plasma nitrite concentrations measured using ozone chemiluminescence in all nitrate-fed mice, there was no detectable difference found when cGMP expression was compared in isoprenaline-infused mice fed KCl or KNO_3 pre-treatment (**Figure 4.5**).

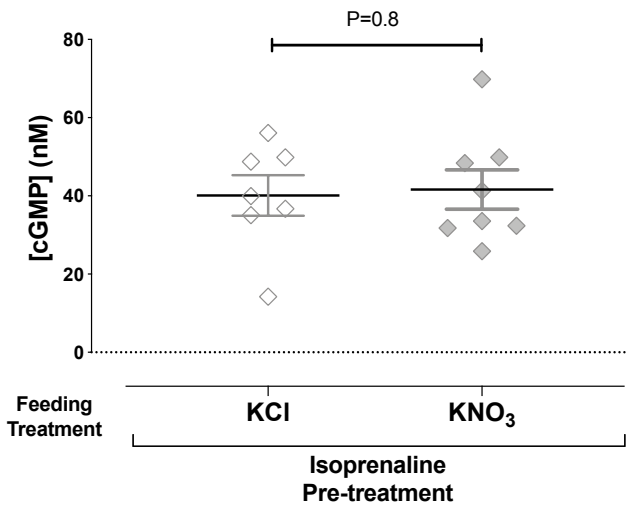

Figure 4.5 cGMP immunoassay results in isoprenaline-infused mice with KCl or KNO_3 pre-treatment.
Data are represented as mean ± SEM with n = 7-8. P-value shows there was no statistical significance of results when data were compared using Student's T-test.

4.8. Mortality

Overall mortality was reported as 21.5% and 14.3% for KCl and KNO_3 pre-treated isoprenaline-infused mice respectively. Deaths tended to occur within the first 5 days following minipump implantation. Mice did not present with overt health issues prior to death and were found unexpectedly dead in their cages. Importantly, survival curves were not significantly different when isoprenaline-infused mice with KCl or KNO_3 pre-treatment were compared using the Gehan-Breslow-Wilcoxon test (**Figure 4.6**).

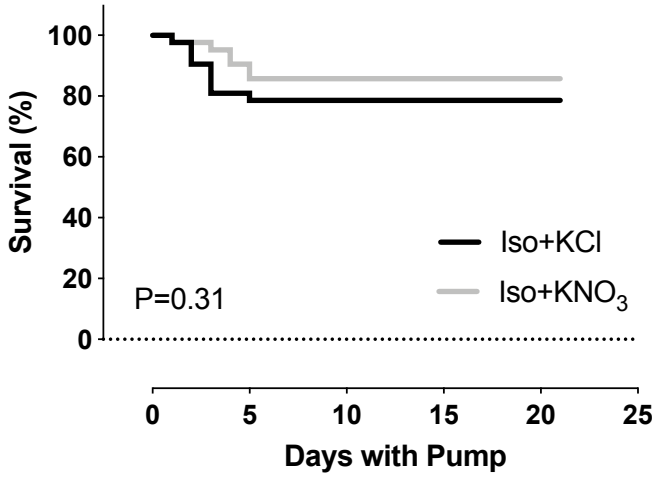

Figure 4.6 Mortality in isoprenaline-infused mice with KCl or KNO_3 pre-treatment.
Kaplan-Meier mortality curves for isoprenaline-infused mice with KCl or KNO_3 pre-treatment with n = 42. P-value shows there was no statistical significance of results when curves were compared using two-way ANOVA.

4.9. **Effect of nitrate on heart weights in isoprenaline-infused mice**

Isoprenaline infusion significantly increased overall heart weight (P<0.0001), HW:BW ratios (P<0.0001) and LV:BW ratios (P<0.01) in our model (**Figure 4.7A-C**). Overall heart weights were significantly attenuated by dietary nitrate pre-treatment (Iso+KCl: 179 ± 4 g; Iso+KNO_3 Pre: 166 ± 4 g, P<0.05, **Figure 4.7A**) as well as HW:BW ratios (Iso+KCl: 6.1 ± 0.1; Iso+KNO_3 Pre: 5.7 ± 0.1, P<0.05, **Figure 4.7B**). There were no significant effects on RV:LV ratios (**Figure 4.7D**).

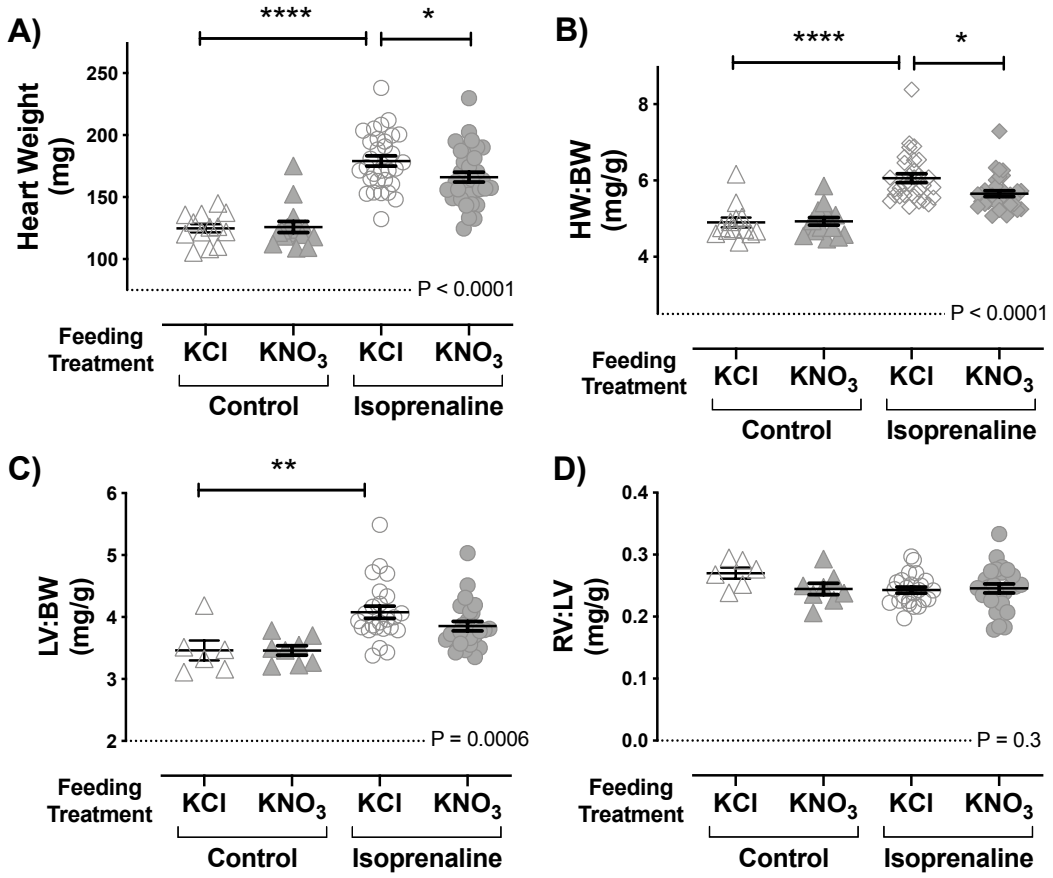

Figure 4.7 Heart weights data from isoprenaline study mice.
Figure shows A) whole heart weights as well as B) heart weight: body weight, C) left ventricle: body weight and D) right ventricle: left ventricle ratios for control mice and isoprenaline pre-treatment study mice fed either 15 mM KNO_3 or KCl. Data are represented as mean ± SEM. Data were tested for statistical significance using a one-way ANOVA with Sidak's post-hoc analysis. P-values for one-way ANOVA are shown in the graphs and stars represent statistical significance determined by post-hoc analyses:
* = P<0.05, ** = P<0.01, **** = P<0.0001.

4.10. **Oral nitrate improves cardiac ejection fraction in an isoprenaline model of cardiac dysfunction**

Echocardiography was performed at baseline and at 1, 2 and 3 weeks in control and isoprenaline infused mice fed KNO_3 or KCl pre-treatment. Ejection fraction was significantly reduced across the 3-week isoprenaline infusion period in KCl-fed isoprenaline-infused mice compared to KCl controls (P<0.001). However, KNO_3 pre-

treatment significantly preserved ejection fraction in isoprenaline-infused mice (P<0.0001, **Figure 4.8L** and **Figure 4.10G**).

Significant increases in LVIDd (P<0.01, **Figure 4.8I** and), LV end diastolic volume (P<0.01, **Figure 4.8J**) and LV mass (P<0.001, **Figure 4.8K**) were also observed in KCl fed mice following isoprenaline infusion. These effects were significantly attenuated by KNO_3 pre-treatment when compared across the 3-week infusion period **Figure 4.10C** (P=0.001), and **Figure 4.10E** (P=0.001) and **Figure 4.10I** (P=0.0005).

Slight, but significant increases in LVPW thickness were observed in KCl-fed isoprenaline-infused mice when compared to KCl controls (P<0.01, **Figure 4.8E**). There was no significant attenuation with dietary nitrate when curves from KNO_3 and KCl pre-treated mice were compared across the 3-week infusion period (P=0.3, **Figure 4.10A**).

There were no significant differences in IVSd, IVSs, LVIDd, LV end diastolic volumes or wall:lumen ratios when compared between treatment groups and there were no significant effects of KNO_3 compared to KCl feeding on cardiac structure and performance in controls (**Figure 4.9**).

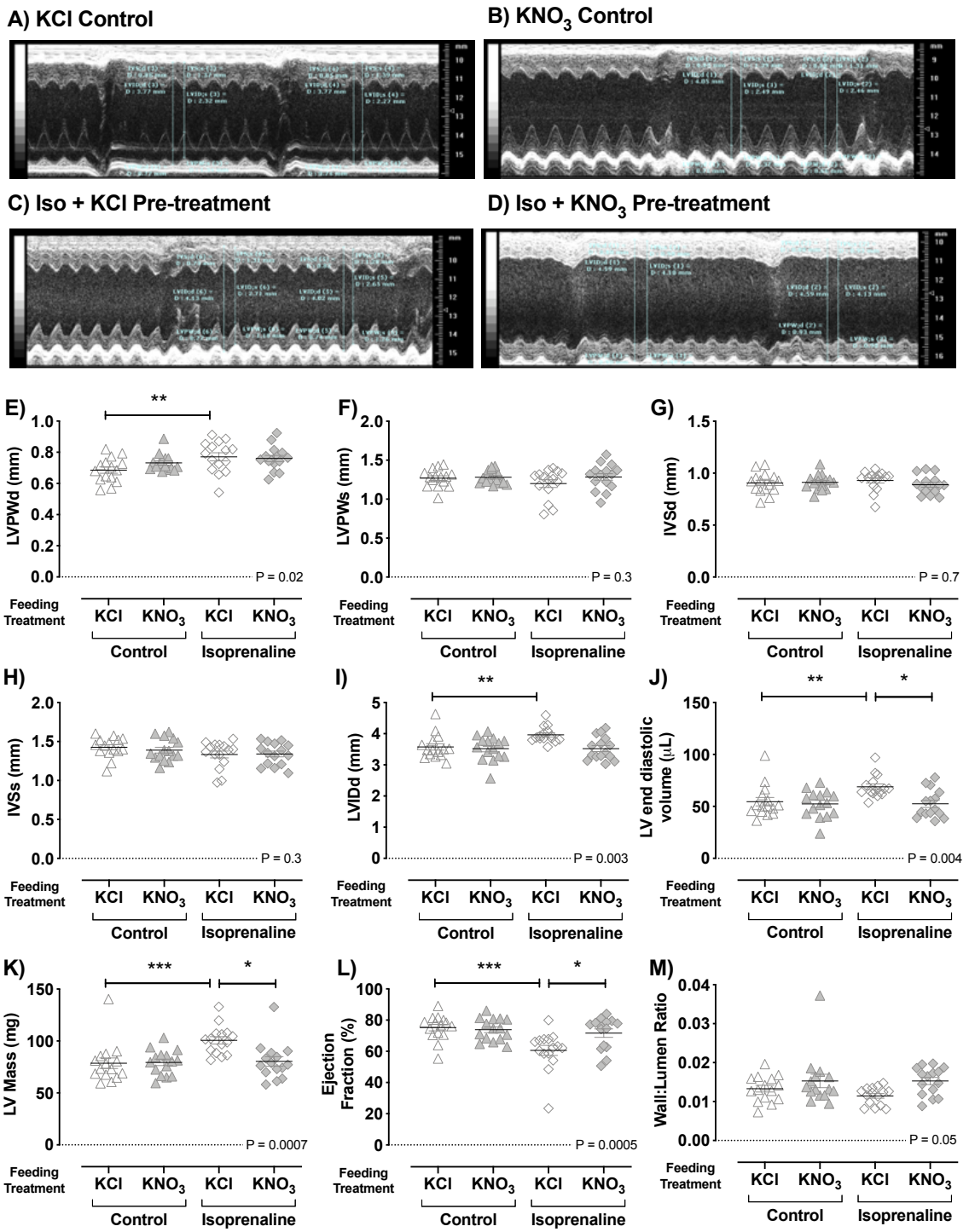

Figure 4.8 End of study echocardiography measurements from isoprenaline pre-treatment and control study mice. Figure shows representative M-mode images, acquired using Vevo 770 echocardiography software and equipment from A) KNO_3 control B) KCl control C) isoprenaline + KNO_3 pre-treatment and D) isoprenaline + KCl pre-treatment mice. Images were acquired under ~2% isofluorane inhalation anaesthetic. Measurements of the intra-ventricular septum (IVS), left ventricle posterior wall (LVPW) and left ventricle internal dimension (LVID) were taken during diastole (d) and systole (s). The image represents a total of 20ms of echocardiographic recording. Resulting LVPWd, LVPWs, IVSd, IVSs, LVIDd dimensions, LV end diastolic volume, LV mass, ejection fraction and wall:lumen ratios are shown in E), F) G), H), I) and J) respectively. Data are represented as mean ± SEM with n = 15. Data were tested for statistical significance using a one-way ANOVA with Sidak's post-hoc analysis. P-values for one-way ANOVA are shown in the graphs and stars represent statistical significance determined by post-hoc analyses: *= P<0.05, ** = P<0.01, *** = P<0.001.

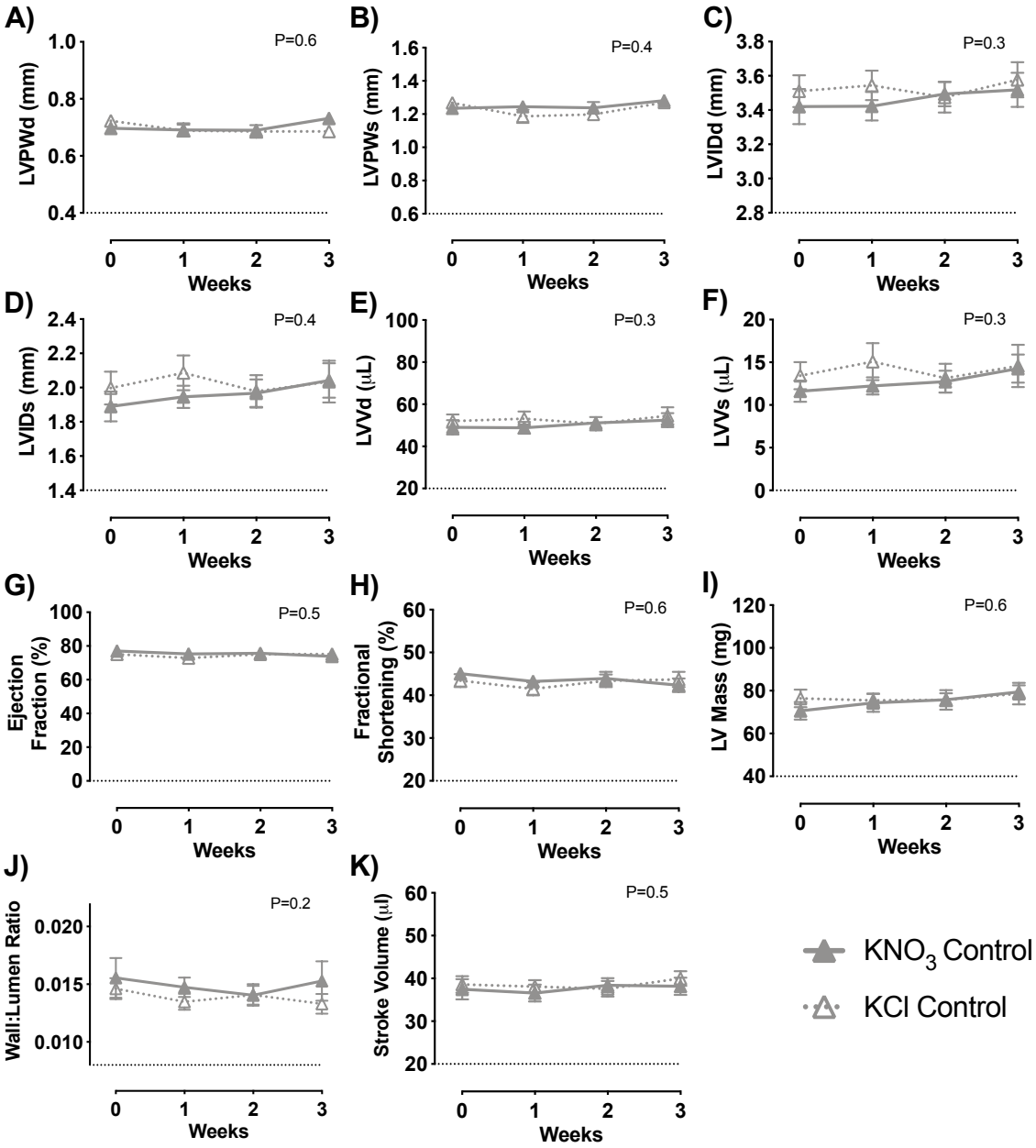

Figure 4.9 Echocardiography measurements from isoprenaline study control mice fed 15 mM KNO_3 or KCl.
Figure shows echocardiography data collected at baseline (0) and after 1, 2 and 3-weeks. Data were acquired using Vevo 770 echocardiography software and equipment in KNO_3 control and KCl control mice, fed 15mM KNO_3 or KCl for a total of 5 weeks (with 2 weeks of feeding prior to baseline Week 0 echocardiography session). Resulting A) LVPWd, B) LVPWs, C) LVIDd, D) LVIDs, E) LVVd, F) LVVs, G) Ejection fraction, H) Fractional shortening, I) LV mass, J) Wall:lumen ratios and K) Stroke volume are shown. Data are represented as mean ± SEM with n = 15. P-values show statistical significance when curves were compared with two-way ANOVA.

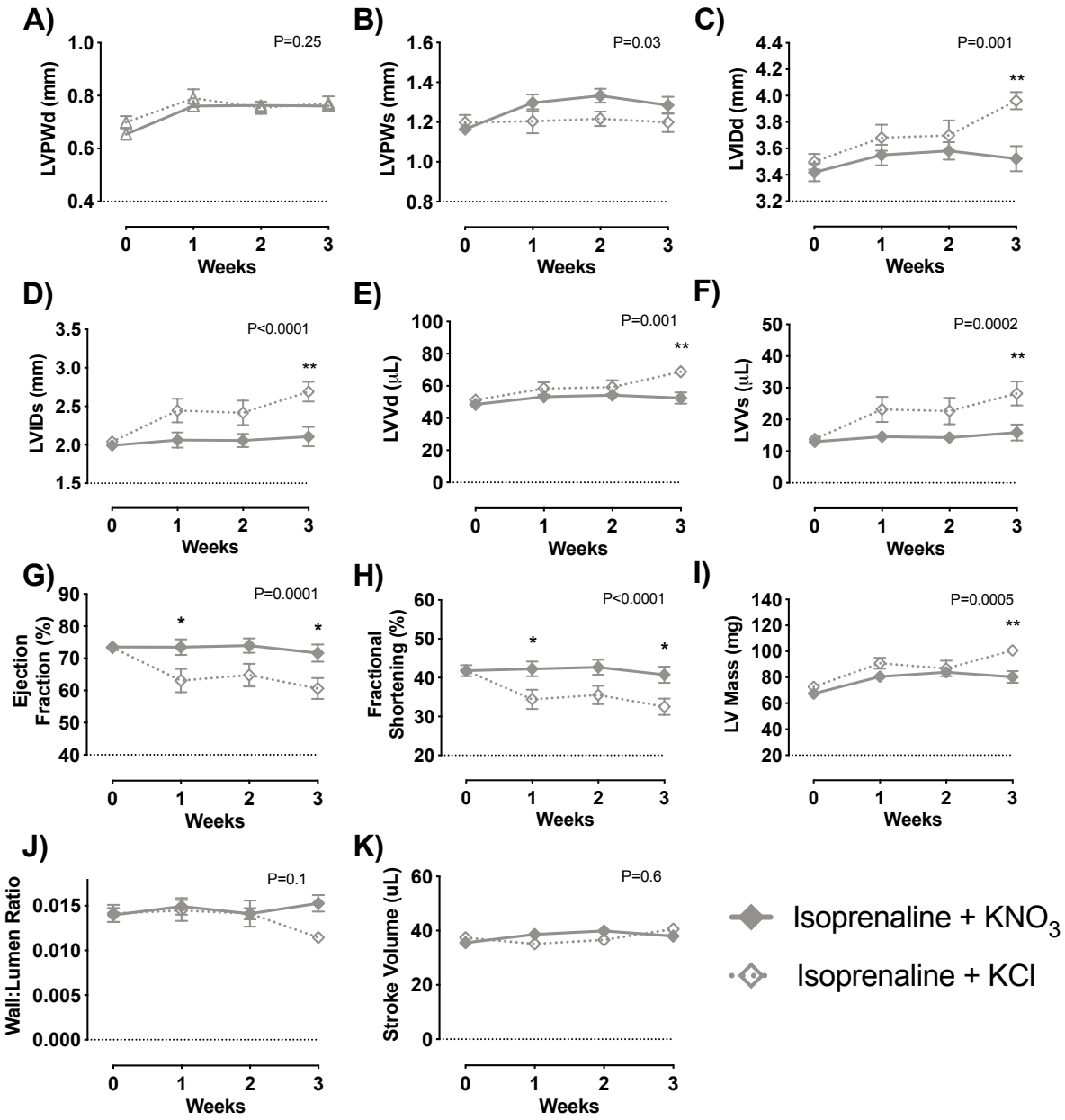

Figure 4.10 Echocardiography measurements from isoprenaline-infused mice fed 15 mM KNO_3 or KCl pre-treatment.

Figure shows echocardiography data collected at baseline (0) and after 1, 2 and 3-weeks of isoprenaline infusion. Data were acquired using Vevo 770 echocardiography software and equipment in isoprenaline + KNO_3 pre-treatment and isoprenaline + KCl pre-treatment mice. Resulting A) LVPWd, B) LVPWs, C) LVIDd, D) LVIDs, E) LVVd, F) LVVs, G) Ejection fraction, H) Fractional shortening, I) LV mass, J) Wall:lumen ratios and K) Stroke volume are shown. Data are represented as mean ± SEM with n = 15. P-values show statistical significance when curves were compared with two-way ANOVA. Stars shown statistical significance with Tukey's post-hoc comparisons: * = 0.05, ** = P<0.01

4.11. Effect of oral nitrate on cardiac fibrosis in isoprenaline treated mice, measured by PSR staining

3-week isoprenaline infusion caused a significant increase in fibrosis as measured by PSR staining in formalin-fixed mouse hearts (P<0.05, **Figure 4.11**). Although not statistically significant, dietary nitrate showed a trend towards attenuating fibrosis in isoprenaline-infused mice compared to KCl-fed isoprenaline controls (**Figure 4.11**).

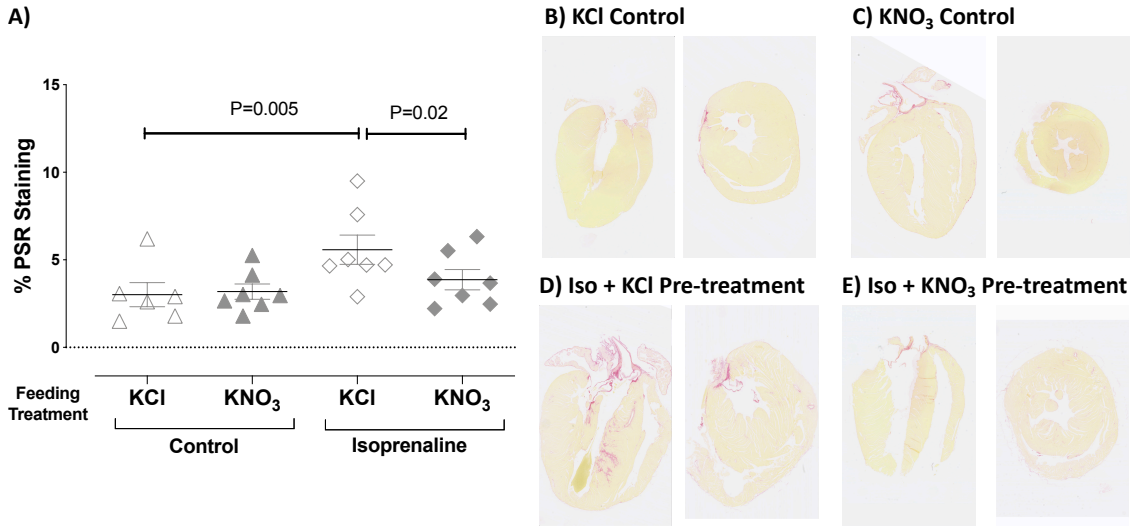

Figure 4.11 Level of collagen deposition as quantified by picrosirius red (PSR) staining.
Figure shows PSR staining carried out on 4 µm sections of formalin fixed hearts, embedded in paraffin. Hearts were randomly assigned to be sectioned in either the transverse or dorsal plane and stained with PSR to identify areas of connective tissue deposition. Images were acquired using a NanoZoomer slide scanner (Hamamatsu) and viewed using NDP View software. Three left ventricle, three intraventricular septum and three right ventricle fields of view were randomly selected at x20 magnification and PSR staining quantified using manual thresholding techniques in ImageJ software. Figure shows quantification of staining in controls and isoprenaline-infused mice with KNO_3 or KCl pre-treatment Sections B) – E) show representative staining images at x 1.25 magnification in all treatment groups. Data are represented as mean ± SEM with n = 6-7. Data were tested for statistical significance using one-way ANOVA with Sidak's post-hoc analysis. P-value for one-way ANOVA is shown in the graph, with stars representing statistical significance determined by post-hoc analyses: * = P<0.05.

4.12. Effect of oral nitrate on organ bath pharmacology in isoprenaline-infused mice

Organ bath assays were carried out to compare the effects of oral nitrate treatment on the vasoreactivity of mouse aortas from isoprenaline infused mice. KNO_3 pre-treatment had no significant effect on ACh or SNO concentration-response curves in isoprenaline infused mice (**Figure 4.12A** and **Figure 4.12B**). Dietary nitrate also had no significant effect on PE concentration-response curves in isoprenaline infused mice (**Figure 4.12C**).

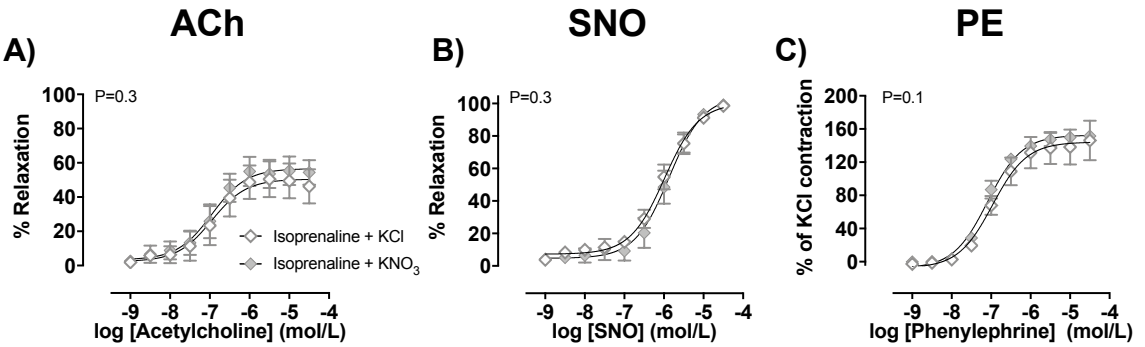

Figure 4.12 Organ bath vessel reactivity of thoracic aortas from isoprenaline study mice fed 15 mM KNO_3 or KCl pre-treatment.

Graphs show A) acetylcholine-induced (ACh) relaxation and B) spermine NONOate-induced (SNO) relaxation concentration-responses of aortic rings pre-contracted with 10^{-5} M phenylephrine (PE) and C) PE-induced contraction concentration-response of aortic rings from isoprenaline study mice fed either 15 mM KNO_3 (Grey) or 15 mM KCl (White) pre-treatment. Data are shown as mean ± SEM, with n ≥ 5. Mice were sacrificed aged 13-15 weeks. P-values show statistical significance of results when compared using two-way ANOVA.

4.13. Effect of nitrate on mRNA markers in isoprenaline-infused mice

4.13.1. TGFβ, CTGF, Col1 and Col3

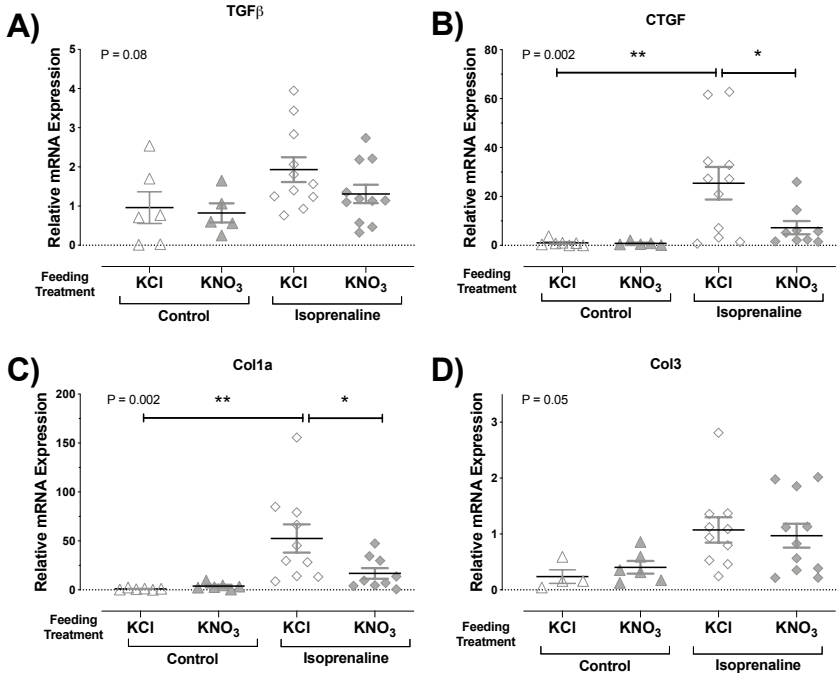

Figure 4.13 mRNA expression of TGBFβ, CTGF, Col1 and Col3 in heart tissue from isoprenaline study mice.

Figure shows mRNA expression of A) transforming growth factor β (TGFβ) B) connective tissue growth factor (CTGF), C) type I collagen (Col1a) and D) type III collagen (Col3) in whole heart homogenate from isoprenaline pre-treatment study mice treated with 15 mM KNO_3 or KCl. For RT-PCR, all samples were plated in duplicate, with gene expression measured relative to internal control 18S. Results are expressed relative to KCl fed controls using ΔΔCT analysis. Data are expressed as mean ± SEM with n = 6-10. Data were tested for statistical significance using one-way ANOVA with Sidak's post-hoc analysis. P-values for one-way ANOVA are shown in the graphs and stars represent statistical significance determined by post-hoc analyses: * = P<0.05, ** = P<0.01.

There was a significant increase in CTGF (P<0.01) and Col1a (P<0.01) mRNA expression in hearts from isoprenaline-infused mice compared to KCl controls. These increases were significantly attenuated by KNO_3 pre-treatment (P<0.05, **Figure 4.13A** and P<0.05, **Figure 4.13B**). There was a trend towards increased expression of Col3 in isoprenaline infused mice, but no clear effect with nitrate feeding. There was a trend towards

increased TGFβ expression following isoprenaline infusion, which was less pronounced in KNO_3-fed isoprenaline-infused mice (**Figure 4.13D**).

4.13.2. AT1Ra and BNP

There was no clear effect of isoprenaline infusion or KNO_3 feeding on AT1Ra mRNA expression (**Figure 4.14A**). There was a trend towards increased BNP expression following isoprenaline infusion, which was potentially more pronounced in KNO_3-fed isoprenaline-infused mice (**Figure 4.14B**).

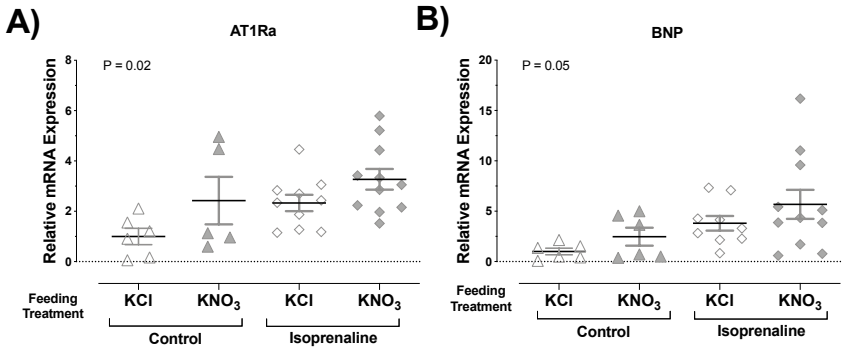

Figure 4.14 mRNA expression of AT1Ra and BNP in heart tissue from isoprenaline study mice.
Figure shows mRNA expression of A) angiotensin type 1 receptor (AT1Ra) and B) brain natriuretic peptide (BNP) in whole heart homogenate from isoprenaline pre-treatment study mice treated with 15 mM KNO_3 or KCl. For RT-PCR, all samples were plated in duplicate, with gene expression measured relative to internal control 18S. Results are expressed relative to KCl fed controls using ΔΔCT analysis. Data are expressed as mean ± SEM with n = 6-10. Data were tested for statistical significance using one-way ANOVA with Sidak's post-hoc analysis. P-values for one-way ANOVA are shown in the graphs and stars represent statistical significance determined by post-hoc analyses.

4.13.3. Xdh, NLRP1 and NLRP3

There was no statistically significant effect of either isoprenaline infusion or KNO_3 feeding on XDH mRNA expression (**Figure 4.15A**). There was no significant effect of either isoprenaline infusion or KNO_3 feeding on NLRP1 or NLRP3 mRNA expression (**Figure 4.15B** and **Figure 4.15C**).

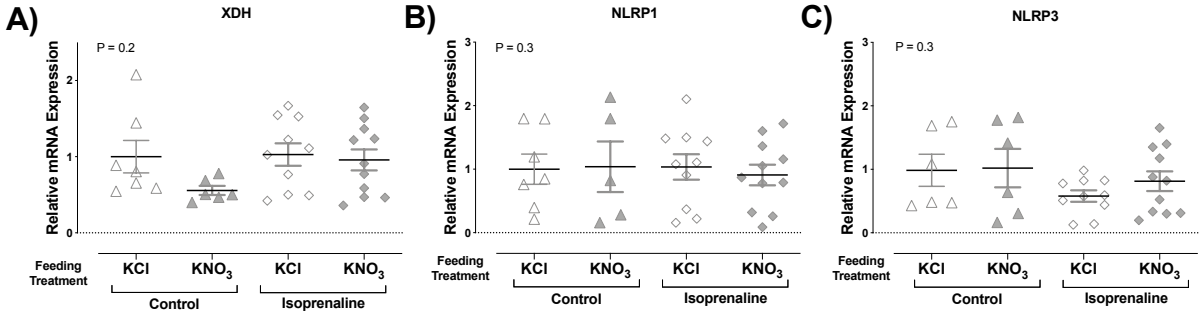

Figure 4.15 mRNA expression of XDH, NLRP1 and NLRP3 in heart tissue from isoprenaline study mice.
Figure shows mRNA expression of A) xanthine oxidoreductase (XDH), B) NLR family pyrin domain containing 1 (NLRP1) and C) NLR family pyrin domain containing 3 (NLRP3) in whole heart homogenate from isoprenaline pre-treatment study mice treated with 15 mM KNO_3 or KCl. For RT-PCR, all samples were plated in duplicate, with gene expression measured relative to internal control 18S. Results are expressed relative to KCl fed controls using ΔΔCT analysis. Data are expressed as mean ± SEM with n = 6-10. Data were tested for statistical significance using one-way ANOVA with Sidak's post-hoc analysis. P-values for one-way ANOVA are shown in the graphs and stars represent statistical significance determined by post-hoc analyses.

4.14. Effect of oral nitrate on oxidative stress in the isoprenaline-infused heart measured by lucigenin chemiluminescence

Whole heart homogenates from isoprenaline-infused mice were incubated with substrates including xanthine, NADPH and NADH, and resulting superoxide generation measured using lucigenin chemiluminescence quantification.

Nitrate feeding significantly reduced baseline superoxide generation (P=0.02, **Figure 4.16A**) as well as NADPH-driven superoxide formation (P=0.02). However, there was no significant effect on superoxide formation when heart homogenates were incubated with xanthine or NADH (**Figure 4.16B**).

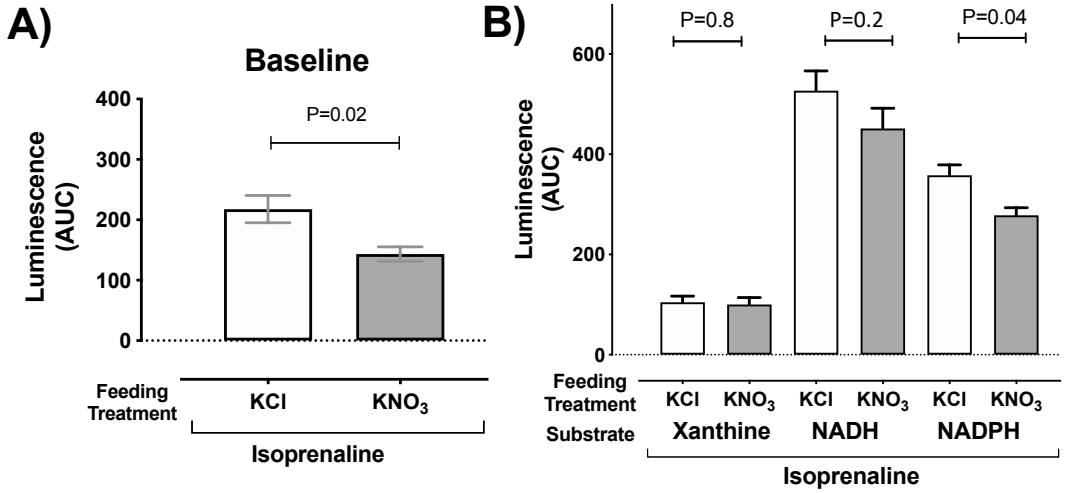

Figure 4.16 Superoxide generation quantified by lucigenin chemiluminescence in heart homogenates from isoprenaline study mice.
Figure shows superoxide generation in mouse heart homogenates from isoprenaline-infused mice with either 15 mM KNO_3 or KCl pre-treatment. Superoxide generation was measured by quantifying lucigenin chemiluminescence generated at baseline or upon homogenate incubation with substrates including Xanthine, NADPH, NADH. Data are represented as mean ± SEM with n = 5. P-values show statistical significance of results when data are compared to KCl fed mice under the same isoprenaline regimen using Student's T-tests.

4.15. The effects of dietary nitrate on XOR protein expression in control and isoprenaline-infused mice

There was no significant difference in XOR protein expression as measured by western blot immunoassay in livers from control and isoprenaline-infused mice. Furthermore, there was no difference in XOR expression between KNO_3 and KCl treatment groups (**Figure 4.17**).

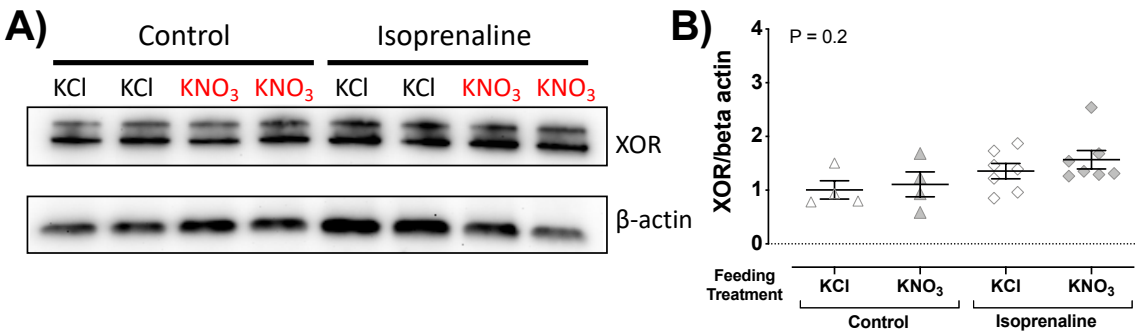

Figure 4.17 The effects of dietary nitrate on XOR protein expression in control and isoprenaline-infused mice
Figure shows XOR protein expression measured in liver homogenates by western blot analysis, normalised to beta actin expression. Data are expressed as mean ± SEM, with n = 4-7. Data were tested for statistical significance using one-way ANOVA with Sidak's post-hoc analysis. The P-value for one-way ANOVA is shown in the graph but there were no significant differences according to post-hoc analyses.

4.16. XOR activity in isoprenaline mice pre-treated with KCl compared to isoprenaline mice pre-treated with KNO_3

There was no significant difference in conventional XO activity measured in liver homogenates from isoprenaline-infused mice, fed KCl or KNO_3 pre-treatment (**Figure 4.18**).

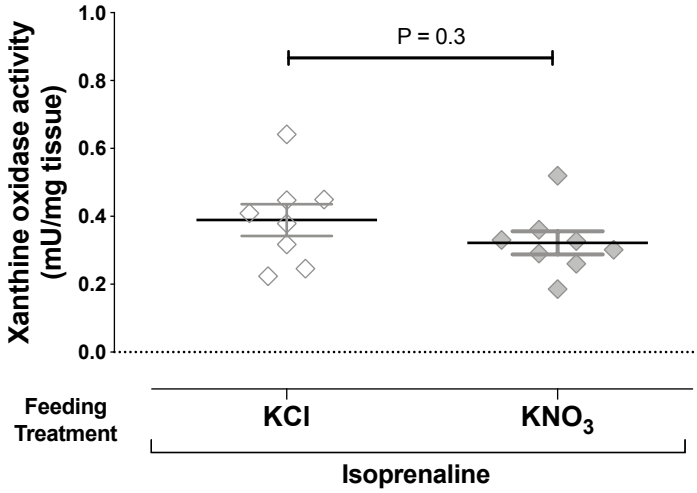

Figure 4.18 XO activity in liver homogenates from isoprenaline treated mice.
Figure shows level of conventional XO activity present in mouse liver homogenates from isoprenaline-infused mice with either 15 mM KNO_3 or KCl pre-treatment. XO activity was measured by quantifying H_2O_2 generation using a commercially available kit. Data are represented as mean ± SEM with n = 8. Data were tested for statistical significance using Student's T-test. The P-value for the T-test is shown in the graph.

4.17. The effects of dietary nitrate on nitrite reductase activity in isoprenaline-infused mice

Nitrite reductase capacity, as measured by gas phase ozone chemiluminescence in mouse heart homogenate, was significantly greater in isoprenaline-infused mice receiving dietary nitrate compared to KCl-fed mice (P<0.0001, **Figure 4.19**).

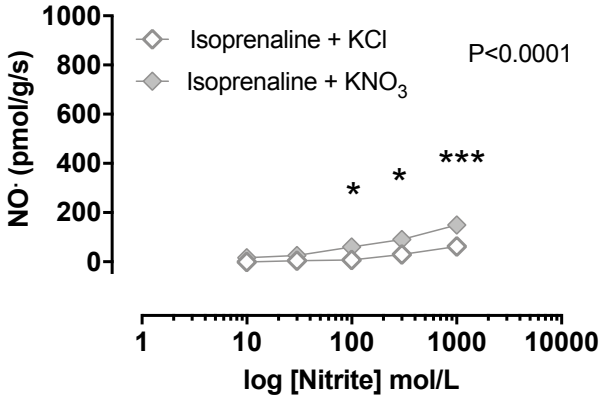

Figure 4.19 The effect of dietary nitrate on nitrite reductase capacity of heart tissue in an ozone chemiluminescence assay.

Cardiac nitrite reductase activity was measured by ozone chemiluminescence at pH 7.4 by incubating heart homogenate with nitrite at incremental doses. Data are represented as mean ± SEM with n = 6-7. P-values show statistical significance when curves were compared with two-way ANOVA. Stars represent statistical significance with Sidak's post-hoc analysis: * = P<0.05, *** = P<0.001

4.18. Result Two – Summary

In summary, we have confirmed the isoprenaline model to be an effective method for producing a BP-independent model of cardiac dysfunction in mice – inducing a significant and sustained increase in heart rate, reduction in ejection fraction, increases in heart weight, LVH, cardiac fibrosis and superoxide generation, but with no significant hypertension observed.

In this model, dietary nitrate pre-treatment significantly attenuated:

- Isoprenaline-induced decline in ejection fraction (P<0.0001).
- Cardiac hypertrophy as measured by HW:BW ratios (P<0.05), but with no effect on wall thickness.
- NADPH-oxidase mediated superoxide generation (P<0.05).
- Cardiac CTGF and Col1a mRNA expression as measured by RT-PCR (P<0.05), with a trend towards reduced cardiac fibrosis as measured by PSR staining.

Furthermore, dietary nitrate pre-treatment increased nitrite reductase capacity in heart homogenate (P<0.01).

CHAPTER FIVE -

Examining The Cardiovascular Phenotype of *Xdh* KO Mice

5. CHAPTER FIVE - Examining the cardiovascular phenotype of Xdh KO mice

Findings from both the ANGII and isoprenaline studies highlighted the potential of dietary nitrate to reduce oxidative stress in our models of cardiac dysfunction and identified XOR as one of the key sources of superoxide generation (particularly in the ANGII model of cardiac dysfunction). With XOR also capable of acting as a nitrite reductase, it has been previously hypothesised that this complex enzyme may have the potential to be 'repurposed,' acting as a beneficial nitrite reductase, as opposed to a detrimental superoxide generator when an abundance of nitrate/nitrite is provided as a substrate (Tripatara et al. 2007; Khambata et al. 2015). This hypothesis seemed to be supported by the findings of various experiments in mice supplemented with dietary nitrate in the ANGII study.

With the recent generation of *Xdh* KO mice, we therefore set out to further probe the importance of this complex enzyme in both cardiovascular health and disease, by examining the cardiovascular phenotypes of WT and Het mice, both with and without ANGII.

5.1. *Xdh* KO mice – generation and genotyping

The *Xdh* gene codes for XDH protein. *Xdh* KO mice were first reported in a paper in 2004 by Ohtsubo et al., where they were generated following disruption of exons 3 and 4, and intron 3, which were all replaced by a phosphoglycerate kinase/neo cassette (**Figure 5.1A**). Embryonic stem cells were deposited in the mutant mouse resource and research centres (MMRRC) following their initial development (Ohtsubo et al. 2004). Het breeding pairs were set up in-house, resulting in WT (+/+), Het (+/-) and KO (-/-) mice. Mouse colonies were maintained, and genotyping conducted, by Tipparat Parakaw and offspring allocated randomly to the various projects in the lab. To identify genotypes of offspring, ear clips were lysed overnight at 55^{o}C using proteinase K (0.3 mg/ml) in DirectPCR ear lysis buffer (Bioquote, UK). These samples were incubated at 85^{o}C for 45min and then kept at 4^{o}C. Two primers pairs were used to identify WT and KO gene sequences. WT primers; forward 5'-CCTATGCCTTCCACAGTTGT-3' and reverse 3'-CACCGTGATGATCTCCAAGT-5'. KO primers: forward 5'-ATGCGATGTTCGCTTGGTGG-3 and reverse 3'-CTATTCGGCTATGACTGGGC -5'. For each sample 2 different master mixes were used containing 12.5 µl 2x Biomix Red (Bioline, UK), 9.5 µl H_2O and 1 µl forward

and 1 µl reverse primers (10 µM) for either WT or KO primers. These were each added to 1 µl of DNA sample in PCR tubes. PCR conditions used: 94°C for 3 min, then 35 cycles

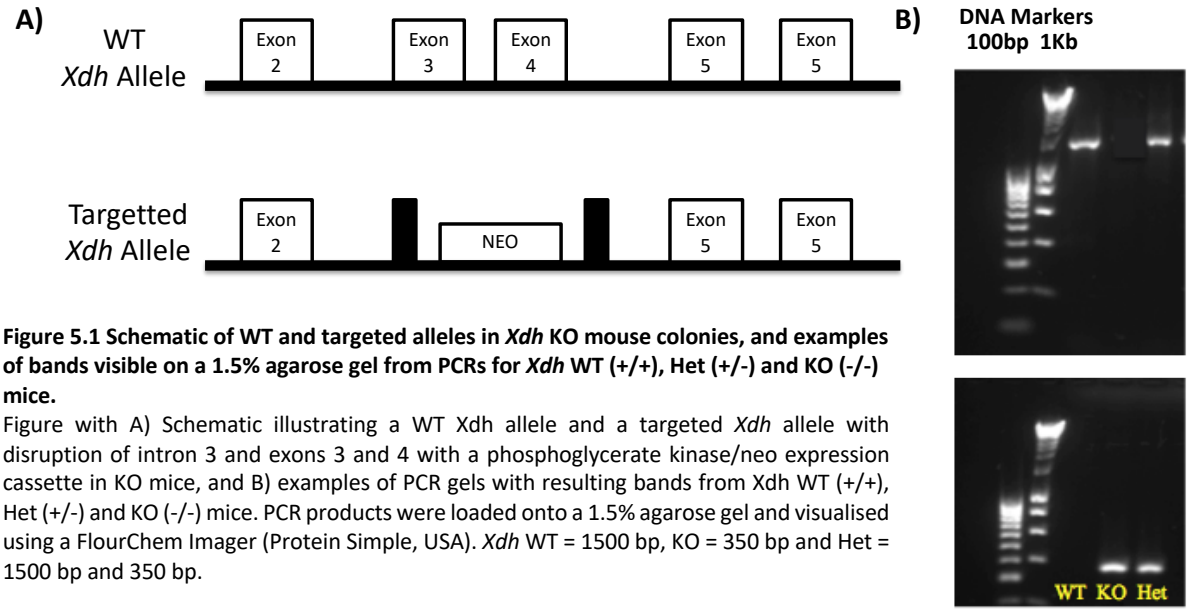

Figure 5.1 Schematic of WT and targeted alleles in *Xdh* KO mouse colonies, and examples of bands visible on a 1.5% agarose gel from PCRs for *Xdh* WT (+/+), Het (+/-) and KO (-/-) mice.
Figure with A) Schematic illustrating a WT Xdh allele and a targeted *Xdh* allele with disruption of intron 3 and exons 3 and 4 with a phosphoglycerate kinase/neo expression cassette in KO mice, and B) examples of PCR gels with resulting bands from Xdh WT (+/+), Het (+/-) and KO (-/-) mice. PCR products were loaded onto a 1.5% agarose gel and visualised using a FlourChem Imager (Protein Simple, USA). *Xdh* WT = 1500 bp, KO = 350 bp and Het = 1500 bp and 350 bp.

of 94°C for 30 s, 60°C for 30 s, and 72°C for 1 min, and 72°C for 7min. The amplified products (WT 1500bp and KO 350bp) were loaded and run on a 1.5% agarose gel. Resulting bands were visualised using a FlourChem Imager (Protein Simple, USA), see **Figure 5.1B**.

5.2. Study design – The impact of knocking out the *Xdh* gene on ANGII-induced hypertension and cardiac dysfunction

Full global *Xdh* KO mice do not survive past 5 weeks of age (Ohtsubo et al. 2004). Therefore, with the long-term nature of this study, Het mice (which exhibit ~50% *Xdh* transcript reduction compared to WT) were compared to WT littermate controls. Mice were randomly assigned to one of 4 treatment groups – WT control, Het control, WT + ANGII or Het + ANGII. Tail cuff BP measurements were carried out at 4, 8, 12, 14 and 16 weeks of age in these mice, as well as echocardiographic measurements at the 8, 12, 14 and 16-week timepoints (See

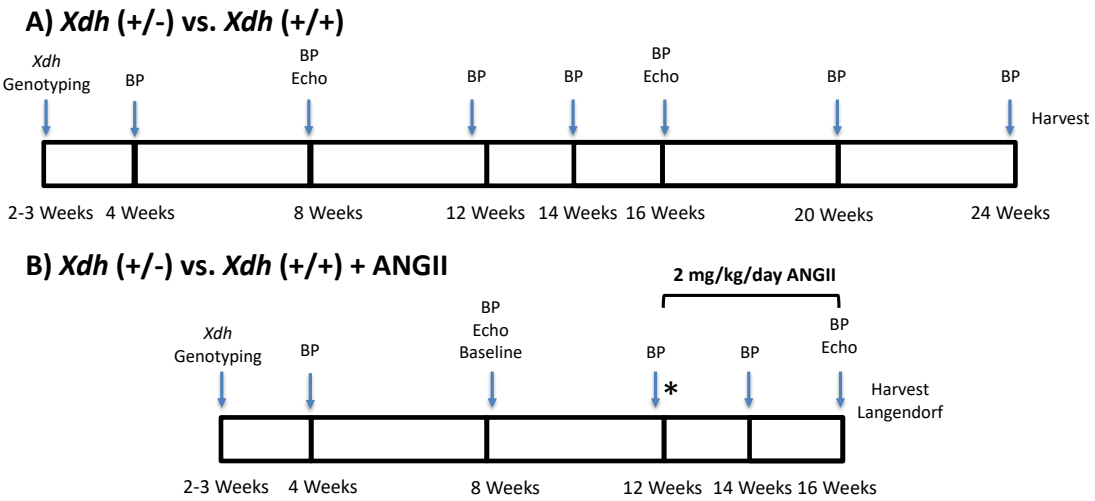

Figure 5.2). At 12 weeks of age some of the mice received a 4-week subcutaneous (SC) infusion of 2 mg/kg/day ANGII (Sigma Aldrich®, UK) in saline, from ALZET® 1004 osmotic minipumps (Durect Corporation, USA). The minipumps were implanted after the 12-week tail cuff and echo measurements had been taken, meaning the 4, 8 and 12-week data represents baseline, with 14 and 16-week data post ANGII infusion.

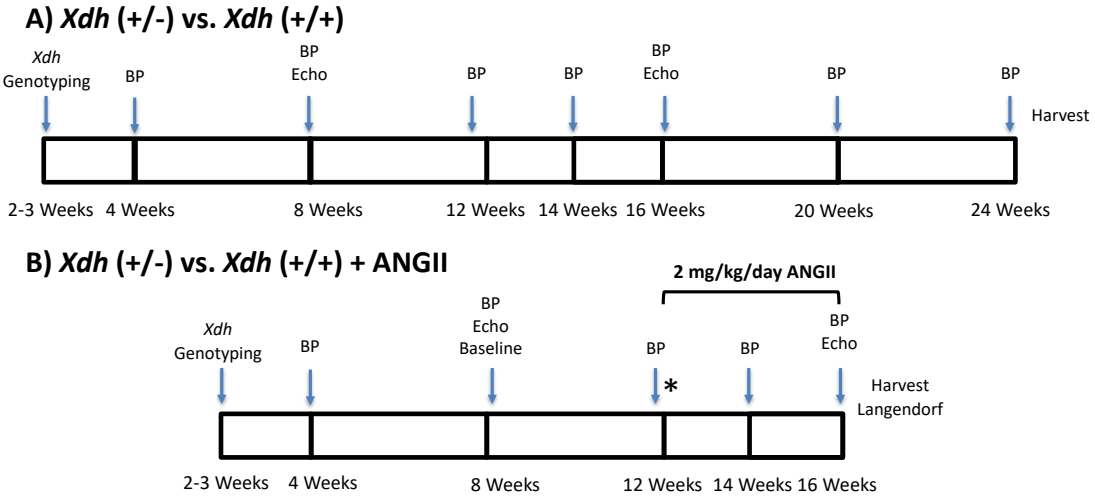

Figure 5.2 Experimental Design for *Xdh* KO mouse studies with and without ANGII.
Schematic illustrating the experimental design for A) *Xdh* Het (+/-) or WT (+/+) littermate control mice cardiovascular phenotyping and B) investigating the effects of 2 mg/kg/day ANGII for 4 weeks on *Xdh* Het (+/-) compared to WT (+/+) littermate control mice. The points of osmotic minipump (*) implantation are marked, and days on which tail cuff BP telemetry (BP) and echocardiography (Echo) measurements were taken are indicated.

5.3. ANGII formulation

For the filling of osmotic minipumps, ANGII (Sigma Aldrich®, UK) was dissolved under sterile conditions to yield a 25 mg/ml stock solution in sterile saline. This 25 mg/ml stock was then diluted accordingly in LoBind tubes (Eppendorf, UK) for minipump filling according to mouse weights and pump specifications. 25 mg/ml ANGII was stored at 4°C

for up to 3 days or at -20°C for up to 1 month. If stored at -20°C, ANGII was not freeze-thawed more than twice.

5.4. **Tail cuff BP in *Xdh* WT (+/+) and Het (+/-) mice**

When tail cuff BP was measured in *Xdh* WT (+/+) and Het (+/-) mice across a 24-week period, Het mice had significantly higher BP than WT littermate controls. This was observed in systolic, diastolic and mean BP (P<0.0001, **Figure 5.3**).

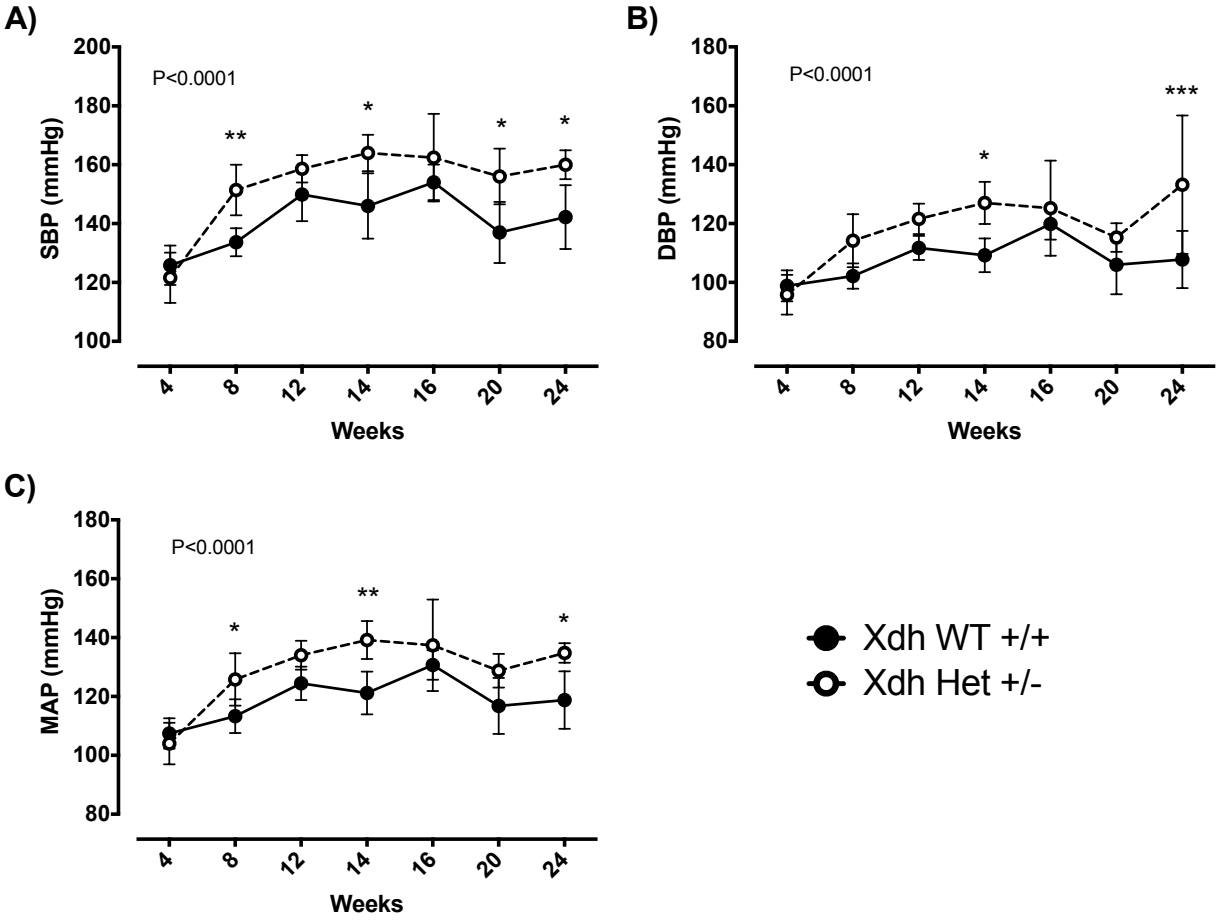

Figure 5.3 Tail cuff BP of Xdh Hets compared to WT littermate controls.
Figure shows A) Systolic B) Diastolic and C) Mean tail cuff BP measured in WT (+/+) and Het (+/-) *Xdh* mice at 4, 8, 12, 14, 16, 20 and 24 weeks of age. Tail cuff data was collected using a modified CODA tail cuff setup (Kent Scientific) with data for each time point averaged from 4 days of recording, with each day consisting of 5 acclimation cycles and 10 recorded data cycles. Data are represented as mean ± SEM (n=6-7) with p-values shown following comparison with two-way ANOVA. Stars represent statistical significance of points when Sidak's multiple comparisons post-hoc analysis is carried out:
* = P<0.05, ** = P<0.01, *** = P<0.001

5.5. **Tail cuff BP in ANG-infused *Xdh* WT and Het mice**

When tail cuff BP was measured in ANGII-infused *Xdh* WT and Het mice, ANGII-induced increases in BP were significantly attenuated in *Xdh* Het mice (**Figure 5.4**). This was

observed in systolic (P<0.0001), diastolic (P=0.0003) and mean BP (P=0.003) alike (**Figure 5.4**).

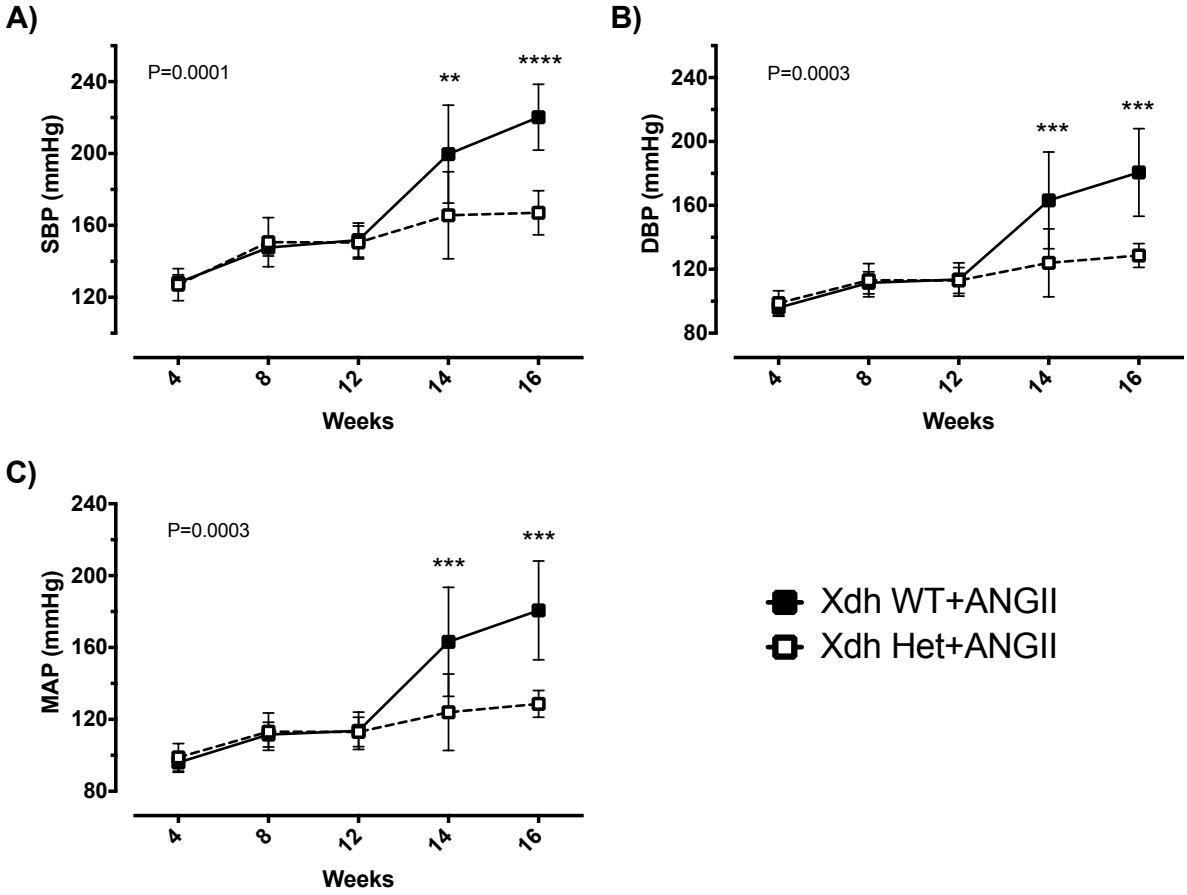

Figure 5.4 Tail cuff BP of Xdh Hets (+/-) compared to WT (+/+) littermate controls at baseline (4, 8 and 12 weeks) and following ANGII infusion (14 and 16 weeks).
Figure shows A) Systolic B) Diastolic and C) Mean tail cuff BP measured in WT (+/+) and Het (+/-) *Xdh* mice at baseline (4, 8, 12 weeks of age) and with ANGII 2 mg/kg/day infusion by osmotic minipump (14 and 16 weeks of age). Osmotic minipumps were implanted at 12 weeks of age following the 12-week baseline tail cuff measurements. Tail cuff data was collected using a modified CODA tail cuff setup (Kent Scientific) with data for each time point averaged from 4 days of recording, with each day consisting of 5 acclimation cycles and 10 recorded data cycles. Data are represented as mean ± SEM (n=6-7) with p-values shown following comparison with two-way ANOVA. Stars represent statistical significance of points when Sidak's multiple comparisons post-hoc analysis is carried out:
* = P<0.05, ** = P<0.01, *** = P<0.001

5.6. **Echocardiography in *Xdh* WT and Het mice**

At 8 weeks of age there were no significant differences detected in any echocardiographic parameters when *Xdh* WT and Het mice were compared (**Figure 5.5**). At 16 weeks of age there were trends observed towards increased LVID (**Figure 5.5C** and **Figure 5.5D**), LV Volume (**Figure 5.5E** and **Figure 5.5F**) and LV mass (**Figure 5.5I**) compared to 8 weeks in both WT and Hets. This increase may appeared somewhat more pronounced in *Xdh* Het mice.

There was also a possible trend towards reduced ejection fraction, fractional shortening and stroke volume in *Xdh* Het mice at 16 weeks old compared to WT age-matched controls (**Figure 5.5G**, **Figure 5.5H** and **Figure 5.5K**).

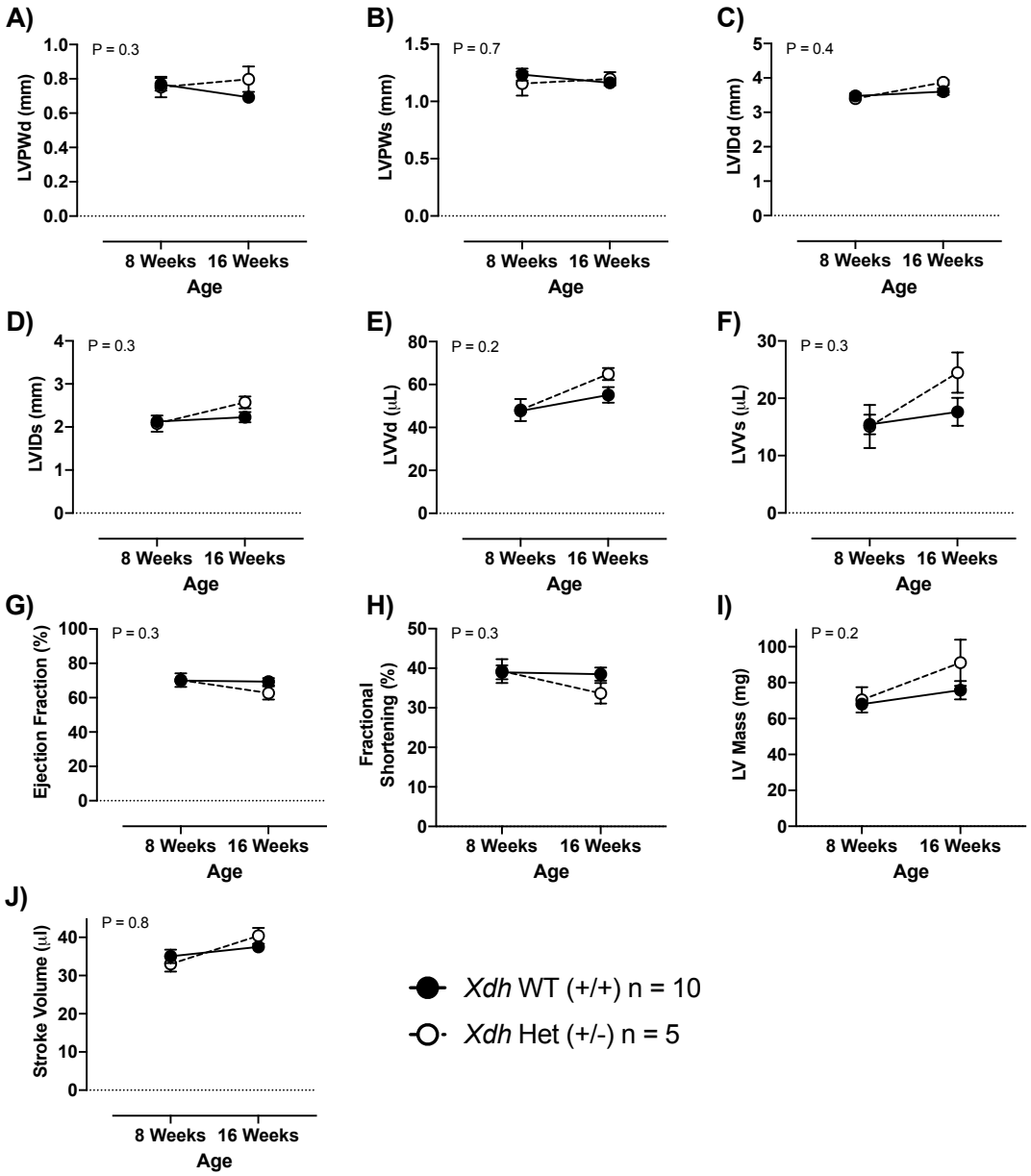

Figure 5.5 Echocardiography measurements at 8 and 16 weeks of age in Xdh WT and Het mice.
Figure shows *data* acquired using Vevo 3100 echocardiography software and equipment with A) LVPWd, B) LVPWs, C) LVIDd, D) LVIDs, E) LVVd, F) LVVs, G) Ejection fraction, H) Fractional shortening, I) LV mass, J) Wall:Lumen ratio, K) Stroke volume and L) E'A' Ratios shown for Xdh WT and Het mice at 8 and 16 weeks of age. Data are represented as mean ± SEM with n= 5-10. P-values show statistical significance of results when data are compared using two-way ANOVA.

Doppler flow data in *Xdh* WT and Het mice showed there was no clear difference between 8 and 16-week old mice. However, VTI was significantly greater in WT compared to *Xdh* Het mice (P=0.03, **Figure 5.6A**). Trends towards higher mean velocity, mean gradient, peak velocity and peak gradients were observed in WTs compared to age-matched *Xdh* Het mice (**Figure 5.6B-E**).

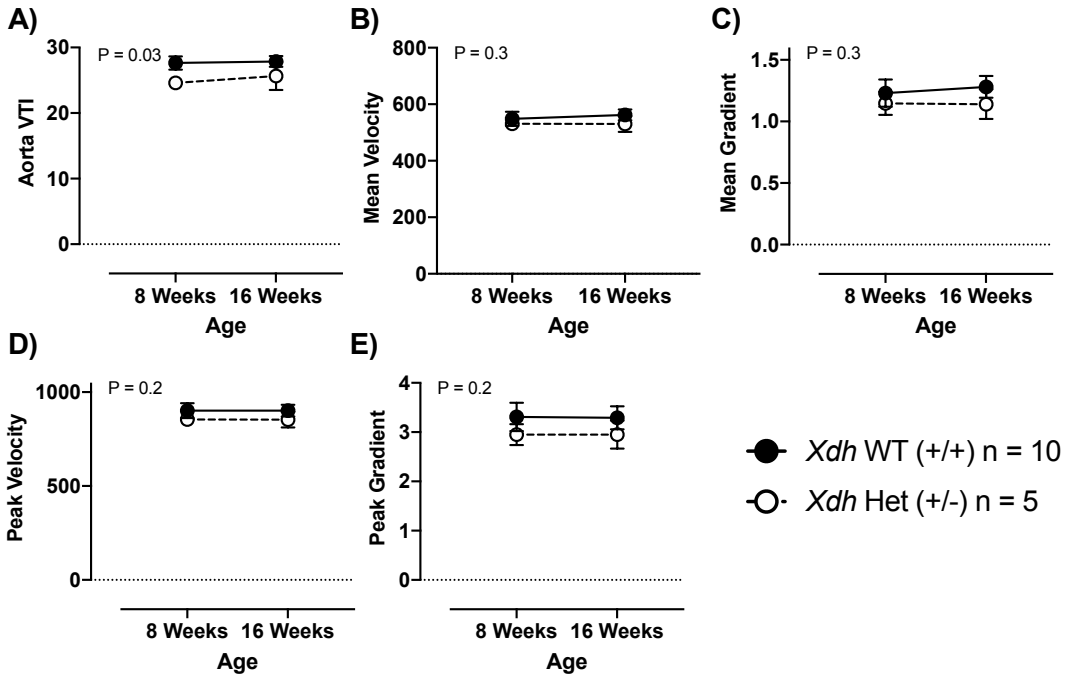

Figure 5.6 Aortic flow measurements obtained during echocardiography recording at 8 and 16 weeks of age in Xdh WT and Het mice.
Figure shows A) Aorta VTI, B) Mean velocity, C) Mean gradient, D) Peak velocity and E) Peak gradient data acquired using doppler flow on the Vevo 3100 echocardiography software and equipment. Data are shown for *Xdh* WT and Het mice at 8 and 16 weeks of age. Data are represented as mean ± SEM with n= 5-10. P-values show statistical significance of results when data are compared using two-way ANOVA.

5.7. **Echocardiography in ANG-infused *Xdh* WT and Het mice**

In the control mice from the ANGII *Xdh* KO study we observed the same trends in LVPW, LVID, LV volume, ejection fraction, fractional shortening and LV mass that had been seen in 16-week old *Xdh* WT and Het mice (**Figure 5.7**).

Following 3 weeks of ANGII infusion we saw a similar reduction in ejection fraction in both *Xdh* WT and Het mice (**Figure 5.7G**) and similar increases in LVPW dimensions (**Figure 5.7A** and **Figure 5.7B**). However, trends suggest that LVID and LV volume may be somewhat attenuated in *Xdh* Hets compared to WT mice.

Doppler flow data in control *Xdh* WT and Het mice from the ANGII *Xdh* KO study, exhibited the same differences as those seen previously in 16-week old mice (**Figure 5.8**). Following 3 weeks of ANGII infusion we observed a trend towards reduced VTI, mean gradient, mean velocity, peak gradient and peak velocity in both *Xdh* WT and Het mice. Both in controls and following ANGII infusion there were significantly reduced measures of aortic velocity in *Xdh* Het mice compared to WT littermate controls, with

reduced VTI (P=0.06), mean gradient (P=0.02), mean velocity (P=0.02), peak gradient (P=0.03) and peak velocity (P=0.03).

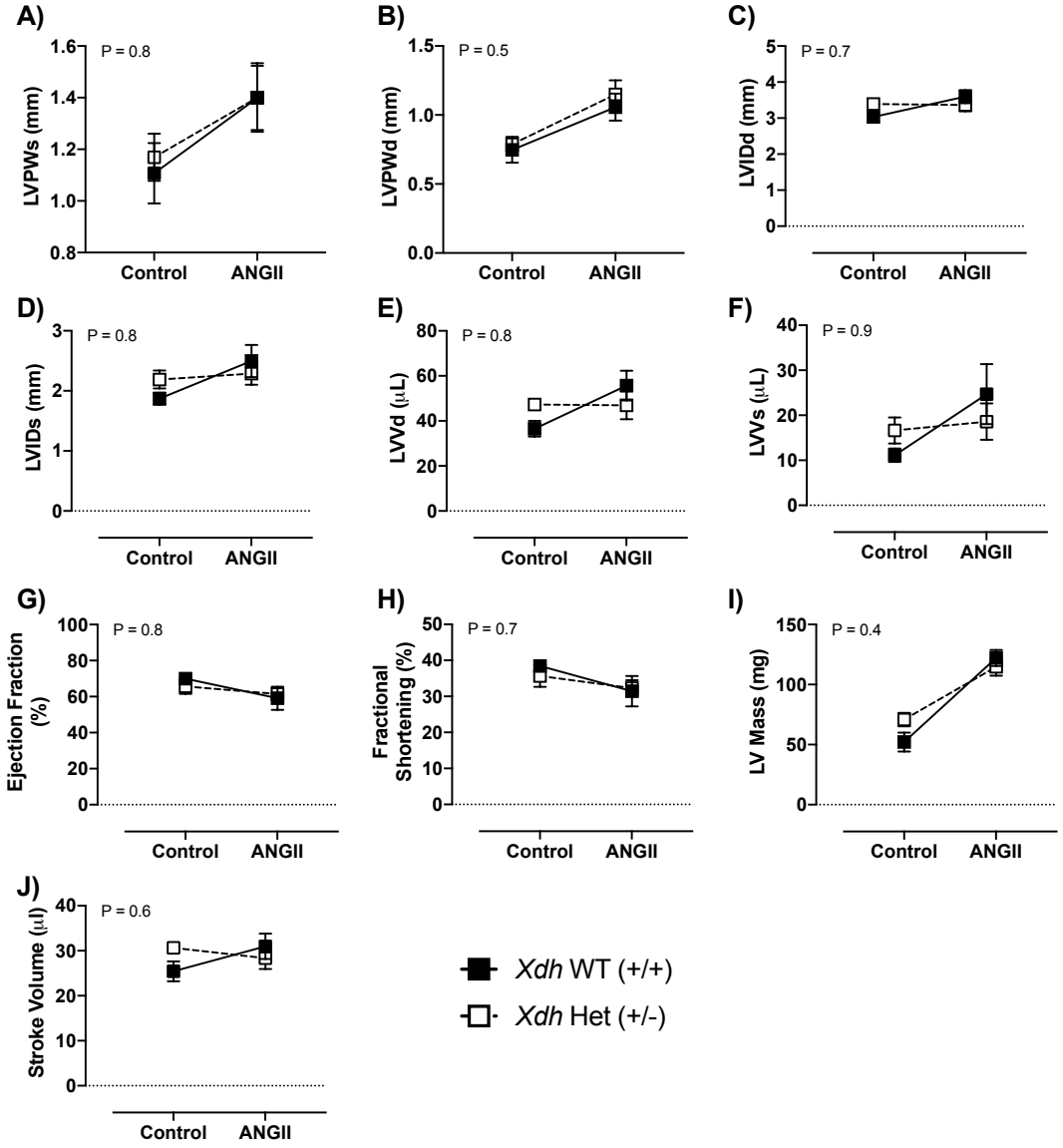

Figure 5.7 Echocardiography measurements in 16-week old control and ANGII-infused Xdh WT and Het mice.
Figure shows data acquired using Vevo 3100 echocardiography software and equipment with A) LVPWd, B) LVPWs, C) LVIDd, D) LVIDs, E) LVVd, F) LVVs, G) Ejection fraction, H) Fractional shortening, I) LV mass, J) Wall:Lumen ratio and K) Stroke volume shown for *Xdh* WT and Het mice at 16 weeks of age with or without ANGII 2 mg/kg/day. Data are represented as mean ± SEM with n= 4-6. P-values show statistical significance of results when data are compared using two-way ANOVA.

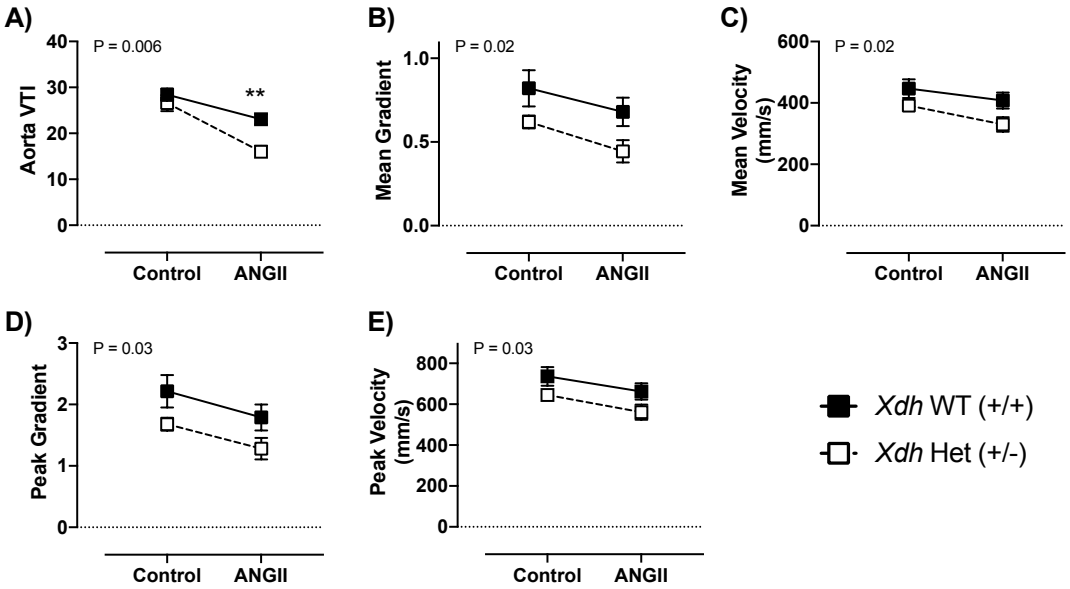

Figure 5.8 Aortic flow measurements obtained during echocardiography recording in 16-week old control and ANGII-infused *Xdh* WT and Het mice.

Figure shows A) Aorta velocity time interval (VTI), B) Mean velocity, C) Mean gradient, D) Peak velocity and E) Peak gradient data acquired using doppler flow on the Vevo 3100 echocardiography software and equipment. Data are shown for *Xdh* WT and Het mice at 16 weeks of age with or without ANGII 2 mg/kg/day. Data are represented as mean ± SEM with n= 4-6. P-values show statistical significance of results when data are compared using ANCOVA.

5.8. Langendorff cardiac function in *Xdh* WT and Het mice, with and without ANGII infusion

Ex vivo hearts from control and ANGII-infused mice, both *Xdh* WTs and Hets, were set up in a Langendorff preparation. Basal coronary perfusion pressures (CPP) in control mice (with no ANGII infusion) followed the same trends as BP data from these mice acquired at 16-weeks by tail cuff methodology, with higher CPP observed in Hets compared to WT (**Figure 5.9**). ANGII-infused mice also followed the same trends observed in BP data from ANGII-infused *Xdh* WTs and Hets, with WTs exhibiting raise BP compared to controls, but this effect attenuated in Hets (**Figure 5.9**).

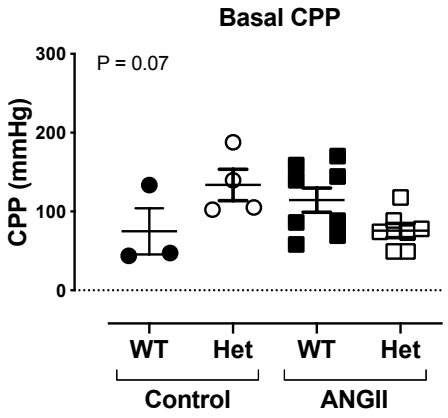

Figure 5.9 Coronary perfusion pressure data from ex vivo Langendorff hearts of 16-week old control and ANGII-infused Xdh WT (+/+) and Het (+/-) mice.

Figure shows A) Basal CPP and B) CPP AUC following L-NAME infusion. Data are shown for Xdh WT (+/+) and Het (+/-) mice at 16 weeks of age with or without ANGII 2 mg/kg/day. Data are represented as mean ± SEM with n= 4-8. P-values show statistical significance of results when data are compared using one-way ANOVA but there were no significant differences according to post-hoc analyses.

There was a significantly greater response to Bradykinin in *Xdh* Hets when concentration-response curves were compared in control mice (P=0.03, **Figure 5.10A**), but no significant difference in ANGII-infused mice (even perhaps a trend towards the opposite). There were potentially reduced responses to SNP when comparing *Xdh* Hets to WTs in both control and ANGII-infused mice. However, these results were not statistically significant.

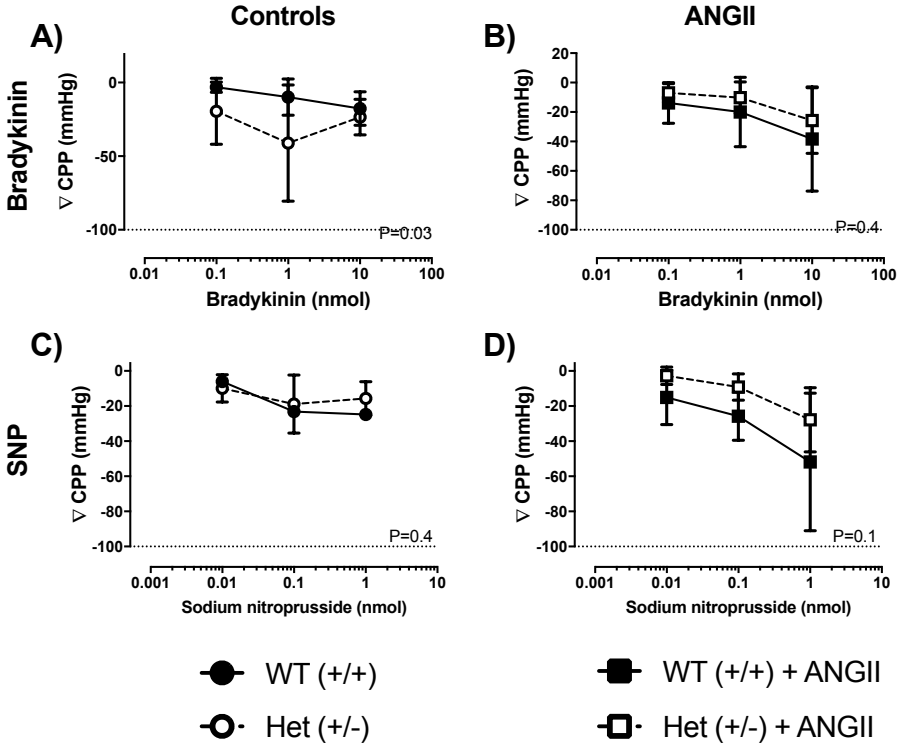

Figure 5.10 Concentration-response bradykinin and SNP data from ex vivo Langendorff hearts of 16-week old control and ANGII-infused Xdh WT and Het mice.
Figure shows bradykinin concentration-response curves in ex vivo Langendorff hearts from 16-week old controls (A) or ANGII-infused (B) mice. Also shown are SNP concentration-response curves in the same 16-week old mice either C) controls or D) ANGII-infused mice. Data are represented as mean ± SEM with n= 4-6. P-values shown following comparison with two-way ANOVA.

5.9. **Results Three - Summary**

In summary, *Xdh* Hets at baseline exhibited:

- Significantly higher BP measured by tail cuff (P<0.0001) and trends towards higher CPP in Langendorff when compared to their WT counterparts.
- Trends towards increased LVID, LV Volume and LV mass at 16 weeks of age compared to WTs.
- Trends towards reduced ejection fraction, fractional shortening and stroke volume at 16 weeks of age compared to WTs.

- Significantly reduced VTIs as measured by doppler flow in the descending aorta compared to WTs (P=0.03), with consistent trends towards lower mean and peak velocities and gradients.

Following 3 weeks of ANGII infusion, *Xdh* Hets exhibited:

- Significant attenuation of ANGII-induced hypertension compared to WTs (P<0.0001) and a trend towards attenuation in ANGII-induced increases in CPP.
- A trend towards attenuation in ANGII-induced increases in LVID, LV volumes and LV mass.
- No difference in ANGII-induced decline in ejection fraction or increases in LVPW dimensions compared to WTs.
- Significantly reduced measures of aortic velocity compared to WTs, with reduced VTI (P=0.06), mean gradient (P=0.02), mean velocity (P=0.02), peak gradient (P=0.03) and peak velocity (P=0.03).

		Xdh WT (+/+)	Xdh Het (+/-)
Control	**Blood pressure**	130 mmHg	137 mmHg
	LV Volume	37 µl	47 µl
	Ejection fraction	70%	65%
	LV mass	52 mg	71 mg
	Peak Velocity	736 mm/s	645 mm/s
	Basal CPP	75 mmHg	134 mmHg
ANGII	**Blood pressure**	180 mmHg	129 mmHg
	LV Volume	56µl	47µl
	Ejection fraction	59%	61%
	LV mass	122mg	114mg
	Peak Velocity	662 mm/s	561 mm/s
	Basal CPP	115 mmHg	76 mmHg

Table 5.1 Table highlighting the key BP and cardiac phenotyping observations noted which differed between *Xdh* Het and WT mice.

CHAPTER SIX -

Discussion

6. CHAPTER SIX – Discussion

6.1. Study background – Nitrate in HF and LVH

NO has long been recognised as a potent endogenous vasodilator, with constitutive production by eNOS in the vascular endothelium vital in mediating hormone-induced vasorelaxation and helping maintain healthy BP (Furchgott & Zawadzki 1980; Ignarro et al. 1987; Palmer et al. 1987; Huang et al. 1995). More recently, it has been discovered that inorganic nitrate (the end product of NO oxidative metabolism) can be reduced back to bioactive NO via the enterosalivary circuit (Webb, Milsom, et al. 2008; Lundberg, Weitzberg & Gladwin 2008b; Lundberg & Weitzberg 2010b). Furthermore, these studies (and those discussed below) highlight how it is possible to increase circulating nitrate/nitrite to physiologically relevant levels in the clinic through nitrate salt supplementation or a diet rich in green leafy vegetables such as spinach and beetroot (or their juices) thus providing a cheap, effective, long-term, exogenous source of NO.

Beneficial effects of dietary nitrate supplementation include reducing BP (Kapil et al. 2015; Webb et al., 2008b), platelet activity (Apostoli et al. 2014; Webb et al., 2008a) inflammation (Jädert et al. 2012; Raubenheimer et al. 2017; T. Yang et al. 2017) and oxidative stress (Ashor et al. 2016; Carlstrom et al. 2011; T. Yang et al. 2015), as well as improving endothelial function (D. A. Hobbs et al. 2013), mitochondrial efficiency (Larsen et al. 2011), exercise capacity (Eggebeen et al. 2016; A. M. Jones 2014; Zamani et al. 2014; Zamani et al. 2015) and muscle contractile function (Coggan et al. 2015; Zamani et al. 2014; Zamani et al. 2015).

These aforementioned benefits could potentially improve quality of life and clinical outcomes significantly for HF patients. Indeed, through chemical reduction to NO, dietary nitrate has already proven to be beneficial in HFpEF (Eggebeen et al. 2016; Zamani et al. 2015). However, the mechanisms resulting in these clinical observations are yet to be elucidated. The data presented in this thesis suggest that dietary nitrate can improve cardiac function by exerting direct effects upon cardiac structure as well as by mediating BP lowering (which leads to improvements in cardiac structure/function secondary to BP lowering). This data highlights that the beneficial cardiac effects relate to anti-hypertrophic mechanisms driven predominantly by reductions in XOR-derived ROS at the level of the blood vessel and within the heart when BP is the primary stumulus. However, in the absence of hypertension, the benefits of dietary nitrate, at

least in part, relate to reductions in NADPH oxidase driven ROS production as well as reductions in pro-fibrotic signalling pathways. Therefore, irrespective of the underlying cause of cardiac dysfunction, dietary nitrate treatment could potentially improve cardiac function through reductions in damaging ROS and cardiac fibrosis, in the clinical setting of cardiac disease.

In data soon to be published by the Ahluwalia lab, in patients with treated yet uncontrolled hypertension, significantly lower plasma nitrite levels were associated with pathological LVH compared to individuals without hypertrophy. Flow mediated dilatation was also significantly worse when LVH cases were compared to controls (unpublished Gee et al., 2020). With plasma nitrite concentration being inversely correlated to baseline BP (Kapil et al. 2013; Bondonno et al., 2015) and changes in plasma nitrite concentrations strongly correlated with changes in BP in both directions (Kapil et al. 2015), these findings further support our hypothesis that dietary nitrate provision in individuals with LVH would be clinically beneficial, particularly in those with treated, but uncontrolled blood pressure.

6.2. Clinical translation of dietary nitrate - circulating intermediates and metabolites

Dietary nitrate, as expected, caused an increase in circulating levels of nitrate and nitrite in both models of cardiac dysfunction; confirming that the enterosalivary circuit remains intact in these models. Interestingly, plasma nitrite and nitrate concentrations in ANGII-infused mice were ~2 and ~10-fold greater than those of nitrate-fed controls. Water consumption measured during the experimental protocol indicates that this increase relates to ANGII-induced polydipsia, likely due to stimulation of thirst receptors in the brain (Rowland & Fregly 1988). Importantly, the amount of water consumed was not different in mice receiving KNO_3 or KCl.

However, most importantly, the increases in plasma nitrite concentrations (the key intermediate responsible for the beneficial effects of dietary nitrate) demonstrated using 15 mM KNO_3 in drinking water available *ad libitum* are clinically translatable to a patient population. In clinical studies by Kapil et al., average increases in plasma nitrite concentrations, of 0.3 and 0.5 μM respectively, resulted in demonstrable clinical reductions in BP (Kapil et al. 2010; Kapil et al. 2015). The 15 mM dosing regimen used in

the present animal studies, provided between 3 and 10 mmol/kg/day KNO_3 dependent on treatment group, and resulted in increases of 0.6 µM, 1.8 µM, 3.0 µM and 0.5 µM in controls, ANGII pre-treatment, ANGII reversal and isoprenaline pre-treatment mice respectively. It should be noted that whilst the daily dose provided is 100-fold greater than the typical 0.07-0.8 mmol/kg/day given in a 5.5 or 6.4 mmol daily dose in the Kapil et al., clinical studies, it is shown both in our results and by other labs using animal models with dietary nitrate (e.g. Baliga et al., 2012) that the rises in plasma nitrite observed are comparable to those measured in in clinical studies. It is uncertain why in mice higher doses of nitrate are required, compared to those needed in humans, to achieve similar levels of circulating nitrite. It is possible that the pharmacokinetics of nitrite are slightly different between the species; relating perhaps to the renal clearance of nitrite, decreased capacity of the microbiome, or more avid oxidation of nitrite to nitrate. Further studies to investigate this are therefore required.

Further still, the dose of nitrate required to increase plasma nitrite to a clinically relevant level in humans is achievable by consumption of a diet rich in green leafy vegetables (Hord et al. 2009), and can provide an equivalent nitrate dose to those of beetroot juice regimens. Our intervention is therefore highly translatable to a human patient population, and it would be possible to increase plasma nitrite to a similar level in HF patients through dietary supplementation using beetroot juice, or a diet rich in green leafy vegetables.

Clinical studies, including those in our lab, have shown that raising circulating nitrite results in NO generation that is reflected by elevations in the downstream signalling molecules for NO, namely cGMP (Velmurugan et al., 2013). However, unlike the published human studies, in the mouse (despite elevations in circulating nitrite and clear biological activity of the dietary nitrate dosing regimen) no rise in plasma cGMP levels could be detected. With cGMP hypothesised to be a mediator of many of the beneficial effects of dietary nitrate/nitrite this is unfortunate, but not unprecedented. In a study by Baliga et al., despite having shown beneficial effects of 15 mM KNO_3 in a mouse hypoxia-induced model of pulmonary hypertension, increases in cGMP were not detectable. However, in mice with 45 mM KNO_3 feeding, a significant increase in cGMP was detectable with n=12-16 (Baliga et al. 2012). It is therefore possible, that with higher n-numbers we may have been able to uncover significant results. It is unclear exactly

why measurement of differences in cGMP concentrations in plasma has proven particularly difficult in mouse samples. It could be that PDE activity is significantly higher in mice compared to humans and despite the addition of IBMX to our samples, cGMP may be too rapidly metabolised for precise measurement to be feasible. As cGMP changes in cGMP expression have been detected in mouse platelets (Gambaryan et al. 2007) it could be possible that measurement in platelets in future may provide a more sensitive assessment of this parameter.

Additionally, it must be noted that although cGMP is highly likely to be a key mediator involved in the beneficial effects of dietary nitrate observed in our studies (particularly since pM concentrations of NO are capable of activating guanylyl cyclase (Batchelor et al. 2010)), it is by no means the only mechanism for NO signalling which may be occurring. Nitrosation of various proteins has been reported to underlie the biological effects of nitrite under various conditions. For example, nitrite exerts cardioprotective effects during ischaemia, that are associated with the selectively s-nitrosation of specific protein thiols. The s-nitrosation of mitochondrial proteins in particular has been highlighted by Couchani et al., and thought to influence mitochondrial energy metabolism in hypoxia and hence positive effects of nitrite. The methods employed by this group of identifying s-nitrosated thiols is a tool which could be extremely useful in future when searching for potential protein modifications of importance occurring in specific tissues and models following dietary nitrate/nitrite regimens (Chouchani et al. 2017). Chouchani et al., employed 'SNOxICAT' methodology on harvested mouse myocardial tissue following four *in vivo* interventions. The thiols in the samples were stabilized by homogenization in 20% TCA containing 0.5% sulphanilamide. Unmodified protein thiols were labelled with 'light' C_0-ICAT. *S*-nitrosated thiols were then chemically reduced in ascorbic acid and $CuSO_4$ and labelled with 'heavy' C_9-ICAT. The biotin tagging from ICAT allowed the tagged proteins to be isolated, separated by liquid chromatography, then analysed by mass spectrometry. Crucially, this enables distinction between identical proteins of different *S*-nitrosation states.

However, the theory that s-nitrosation of proteins in itself represents a stable change in protein regulation is a somewhat controversial topic. The reactivity of s-nitrosothiols (Broniowska & Hogg 2012) has been suggested to point towards the importance of these groups as transient intermediates prior to disulphide formation, as opposed to having

direct implications on protein function themselves (Wolhuter et al. 2018). Such advocates for the importance of disulphide bond formation in affected proteins are not disputing the existence or importance of s-nitrosation. However, they argue that the functional importance lies more-so with the resulting disulphide bond formation, rather than the transient protein s-nitrosation step. For some proteins, resistance to reduction and disulphide bond formation may occur due to the microenvironment they are found in (Paige et al. 2008). However, this is potentially the exception rather than the norm. Further assessment of s-nitrosation in the heart tissue of the experimental models used in this study would provide some insight into whether whether this pathway may be of importance in the setting of cardiac hypertrophy.

6.3. **Model verification and mouse mortality**

The ANGII (BP-dependent) and isoprenaline (BP-independent) models were each validated by measuring tail cuff BP and mouse heart rates during echocardiography and comparing to values from control mice. The results showed a significant increase in BP in ANGII-infused mice, with no significant increase in isoprenaline-infused mice. Furthermore, in ANGII-infused mice no change was evident in heart rate compared to control mice. But isoprenaline-infused mice (as expected) exhibited significantly increased heart rates, which were sustained throughout the 3-week duration of study. Although in both the ANGII and isoprenaline models some mouse deaths were observed within the first 1-7 days following minipump implantation, the mortality recorded from each treatment group was not significantly different between KCl and KNO_3-fed mice under each regimen. And importantly, the average mortality in the ANGII and isoprenaline studies were both under the 20% threshold deemed by the Home Office inspector to be worthy of re-assessing the methodology used. The use of osmotic mini-pumps for both models provided an excellent opportunity to compare pathways without the confounding of distinct methods of generating cardiac hypertrophy.

6.4. **Effects of dietary nitrate on BP, activity and endothelial function**

By measuring ambulatory BP, I was able to confirm that dietary nitrate significantly reduces BP both at baseline and in ANGII-infused mice. These findings are in accord with observations in healthy volunteers (Webb et al., 2008) and patients with hypertension (Kapil et al., 2015). However, the BP data was confounded by an increase in activity in

mice receiving nitrate. These experiments exposed an important aspect of measuring BP in mice receiving treatments that improve cardiac function i.e. that positive effects upon the heart may result in increased activity of mice and this in turn will result in 'apparent' increases in BP (Adlam et al. 2011). Thus, to account for this we normalized BP to activity and in doing this a clear BP-lowering effect of dietary nitrate is evident with respect to both SBP and DBP. Whilst in some mouse studies using BP telemetry, activity levels are reported by the authors to not differ between treatment groups (e.g. Labonté et al. 2008; Kawada et al. 2005), other studies do not reference activity levels recorded during BP telemetry recording (e.g. Forrester et al. 2017; Manhiani et al. 2015). The findings in our present study highlight how important activity levels are when measuring BP in freely moving, conscious animals. It must therefore be considered that in some studies which have not taken into account such potential differences in their analyses, it is possible that by normalising BP to activity levels, differences in BP may be evidenced.

Whilst in the ANGII model one can explain that the increased activity is due to improved cardiac health, the increased activity observed at baseline in the nitrate group (prior to ANGII infusion) indicates that other mechanisms are also likely involved. Indeed, dietary nitrate improves energy metabolism (Larsen et al. 2011), exercise capacity (Zamani et al. 2015; Eggebeen et al. 2016; Hirai et al. 2017; Zamani et al. 2017), as well as haemodynamic and muscle performance (Hernández et al. 2012; Ferguson et al. 2013; Coggan et al. 2015; Borlaug et al. 2016; Ferguson et al. 2016; Pironti et al. 2016). It should be considered that these improvements could in themselves be sufficient to stimulate mice to perform increased spontaneous activity in their home environment. It has also been previously reported that sildenafil (a selective phosphodiesterase 5 inhibitor) enhances activity in a cGMP-mediated manner in mice (Demirci et al. 2014). Additionally, NO inhibition by L-NAME also blocks phenylcyclidine-induced locomotor activity (Johansson et al. 1997). These findings, taken together with our data, suggest that NO likely underlies the observations. As increased activity can have a significant effect on mouse BP (Adlam et al. 2011), we therefore normalised BP values to their corresponding locomotor activity measured at all timepoints.

With ANGII infusion inducing such a severe BP phenotype, the reductions observed in this study may appear modest at ≈9 mm/Hg and ≈7 mm/Hg respectively. However, such

reductions would indeed be clinically significant if similar reductions were observed in hypertensive patients. For example, a meta-analysis investigating the effects of lowering BP on HF, determined that reducing SBP by just 5 mmHg reduced risk of HF development by ≈24% (Verdecchia et al. 2009). Furthermore, effectively controlling high BP by reducing it to a target of <140 mmHg, it is possible to reduce one's risk of developing heart failure by ≈52% (Meredith & Ostergren 2006). Thus, suggesting that a level of BP reduction similar to that observed in our study would indeed be of clinical benefit, and may have been enough to instigate some of the improvements in cardiac structure observed in our echocardiographic assessments.

The published findings of the SPRINT study in 2015 has emphasised the significance of BP lowering in HF development further still (SPRINT Research Group et al. 2015). With an intensive BP treatment strategy (to a target BP of <120 mmHg) having been shown to have a significant effect on the incidence of HF in this population over and above a traditional BP treatment target of <140 mmHg, clinicians should ultimately be looking towards utilising as many safe and effective BP lowering treatments as needed to reduce an individual's risk of developing or worsening cardiac function. If dietary nitrate has the potential to work independently of, or in concert with, currently used pharmacological interventions, the addition of dietary nitrate to a treatment regimen in order to push 'controlled' BP of ~ 140 mmHg towards a more intensive treatment threshold of 120 mmHg may indeed be of significant clinical benefit.

In the ANGII model, in addition to a shift in ACh concentration-dependent relaxation response curves, there was also a modest shift in SNO relaxation response curves in nitrate pre-treated mice. It is therefore possible that dietary nitrate targets recovery of basal endothelial NO generation and activity and not just agonist-stimulated activation of the endothelium. This in part could be related to the attenuation of oxidative stress observed (see below) and thus restoration of NO-mediated control of vascular tone. Previous findings have suggested that endothelium-independent relaxation via sGC signalling can be regulated by the presence/absence of NO in certain disease models (Hussain et al. 1999). Regardless, both findings highlight pathways which can contribute significantly to improved vasorelaxation, and reduced BP in this model. Moreover, as oxidative stress has been widely associated with direct and indirect impairment of endogenous NO production and a consequent increase in vascular tone, the reduction

of superoxide production in nitrate-fed mice may also contribute to improved endothelium- and NO-dependent vasodilation (Kojda & Harrison 1999).

In isoprenaline-treated mice the maximum PE response was increased and the maximum ACh response was reduced compared to control mice, however this effect was unaltered by dietary nitrate treatment. Isoprenaline is a selective β-adrenoceptor agonist with no α-agonist activity (Alexander et al. 2017). Studies with parotid cells have shown that prolonged treatment with isoprenaline results in an up-regulation of α-adrenoceptor signalling (Tanimura et al. 1999) through sensitization of IP_3 receptors and it is possible that this underlies the increased activity of phenylephrine in the experiments. Despite some change in vascular reactivity in this model, the prevailing view is that β_1 adrenoceptors primarily localized in the cardiomyocyte, rather than cells of the vasculature, are the target for isoprenaline-induced cardiac hypertrophy (Lohse et al. 2003; Puhl et al. 2016). The absence of any significant difference in BP between the treatment groups and echocardiographic evidence suggests no role for an afterload-mediated hypertrophy in this model, indicating that it is unlikely that changes in vascular resistance underlie this reduction in ACh responses. To our knowledge this phenomenon has not been previously reported and warrants further investigation.

6.5. **The effects of dietary nitrate on cardiac hypertrophy**

Dietary nitrate reduced cardiac hypertrophy to some degree in both the BP-dependent and BP-independent models as reflected by echocardiographic measures of LV mass, wall thickening and estimates of LV volumes. With ANGII-infusion prominent LV wall thickening was observed with reduced LV volume, indicating a maladaptive concentric hypertrophy. This was inhibited with nitrate pre-treatment, and even attenuated to some degree in the dietary nitrate reversal study.

That the impact upon cardiac structure occurs relatively rapidly is demonstrated by the fact that similar changes in LV mass and wall thickness occurred even when dietary nitrate was introduced only after ANGII-induced cardiac hypertrophy was in place. However, longer term treatment would likely be required to provide full restoration of cardiac muscle function in a non-prophylactic setting. These observations were supported further by reductions in HW:BW and LV:BW measured in our models - these reductions were mild, but consistent, and were evident irrespective of the model i.e. BP-

dependent or -independent. The fact that LV mass was reduced in all models suggests that whether the maladaptive hypertrophy is concentric (ANGII) or eccentric (isoprenaline), delivery of NO via dietary nitrate could still be clinically effective.

Since ANGII-induced LV wall thickening was so drastically attenuated by nitrate pre-treatment the modesty of reductions in heart weight data was somewhat surprising. However, it should be noted that with cardiac hypertrophy known to occur in two forms, eccentric and concentric (reflecting the multiple signalling pathways that can differently modulate the cardiac structure and performance) this may help explain our observations. Eccentric hypertrophy occurs when cardiac myocytes enlarge and grow in length (with sarcomeres added in series and LV volume increasing), as opposed to concentric hypertrophy where myocytes grow in width (with sarcomeres added in parallel and LV volume becoming smaller). Therefore, it may be that whilst ANGII-induced wall thickening is prevented/slowed with nitrate supplementation, the mass of the heart has still increased somewhat due to the development of eccentric rather than concentric hypertrophy. For that reason, in ANGII-infused mice with inorganic nitrate pre-treatment, cardiac hypertrophy may not have been entirely prevented *per se*, as cardiac mass still increased, but the type of remodelling occurring may be different.

In patients with pathological concentric hypertrophy, progression towards a dilated LV with wall thinning is often observed following a cardiac event, such as myocardial infarction, and accompanies transition from pathological cardiac hypertrophy to HF, with concurrent worsening of cardiac function (de Simone 2004). Therefore, a more dilated ventricle, with thinner walls, may be regarded by some as a sign of poorer clinical outcome. However, it should be noted that increased heart weight is not always detrimental and eccentric hypertrophy is different to dilated HF, where dilation occurs at the same time as cardiac output being compromised. Generally, eccentric hypertrophy results in dilation without compromised function, and it should be recognised that in terms of being a prognostic indicator for cardiac outcome, concentric hypertrophy has actually been associated with worse outcome. Regression of wall thickening (reverting back to eccentric hypertrophy), on the other hand, has been associated with improved prognosis (Muiesan et al. 2004).

Also, despite the fact that many assume that exercise-induced hypertrophy refers to reversible concentric adaptations, this occurs only in cases of resistance training. Intense aerobic exercise training is in fact known to induce eccentric hypertrophy, without reduction in cardiac function (Fernandes et al. 2011). In our study, we saw dilation occurring without wall thickening and without concurrent worsening of cardiac function, meaning LV diastolic chamber volume was increased – resulting in improved stroke volume. This type of adaptation would be more similar to changes observed during exercise-induced eccentric hypertrophy, rather than typical progression to HF. See **Figure 6.1** for schematic illustrating the differences between concentric and eccentric hypertrophy.

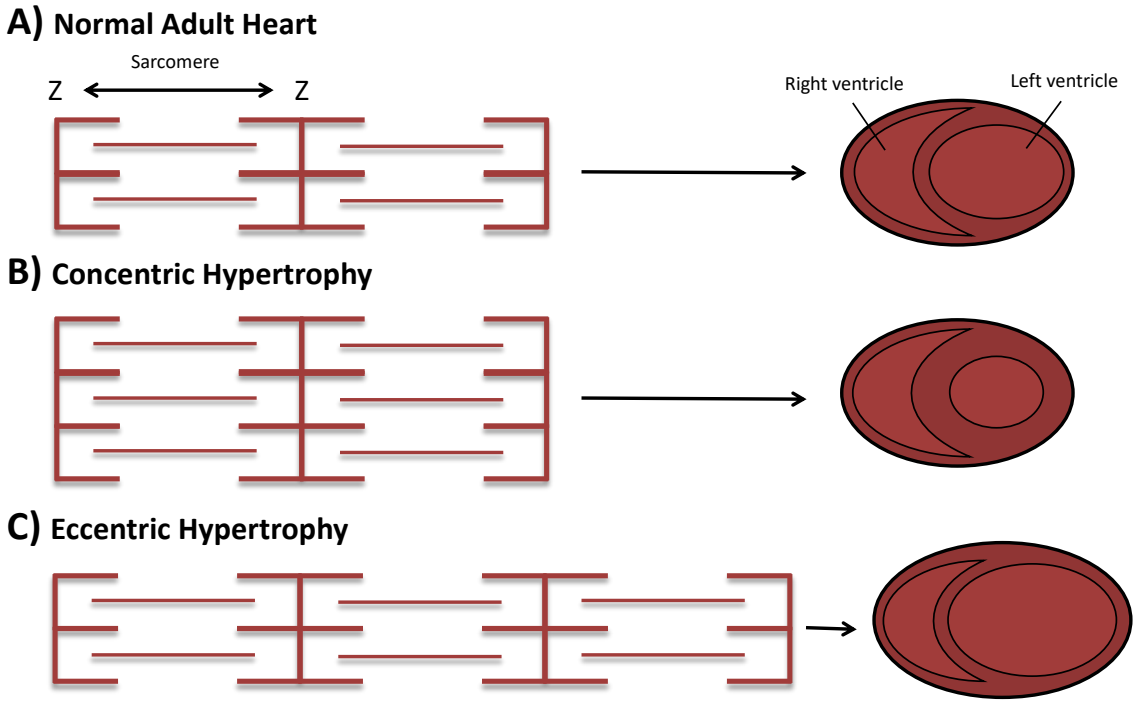

Figure 6.1 Differentiation between a normal adult heart, concentric hypertrophy and eccentric hypertrophy. Schematic illustrating fundamental structural differences between concentric and eccentric cardiac hypertrophy. Sarcomeres are added in parallel in concentric hypertrophy and in series in eccentric hypertrophy. Sarcomeres are represented as the individual units spanning the two "Z" markers (indicating Z-discs). Concentric hypertrophy (B) results in reduction in left ventricle diameter and an increase in wall thickness, apparent during intense resistance training. Eccentric hypertrophy (C) results in increased left ventricle diameter (dilation), occurring with or without wall thinning. Dilation occurs without wall thinning in exercise-induced eccentric hypertrophy, but with wall thinning in pathological eccentric hypertrophy.

6.6. The effects of dietary nitrate on cardiac function

ANGII infusion resulted in a significant reduction in ejection fraction measured by echocardiography in the BP-dependent model. Unfortunately, this was not significantly improved by nitrate pre-treatment. However, following a significant reduction in wall thickness, and a resultant increase in diastolic volume, stroke volume was preserved by nitrate pre-treatment in ANGII-infused mice - a finding which could be of significant

clinical benefit. In the clinical setting, dietary nitrate may have potential to provide symptomatic improvement relatively quickly, and thus restore LV volumes.

In contrast to the ANGII model, in the BP-independent isoprenaline model, ejection fraction was significantly improved in mice receiving nitrate as well as reductions in HW:BW. Recent studies have shown that nitrate supplementation can increase force of skeletal muscle contraction (Hernández et al. 2012; Coggan et al. 2015) and improve mitochondrial function (Larsen et al. 2011) – phenomena which would likely extend to being true for cardiac muscle. It is possible that s-nitrosation may be a key mechanism through which exogenous NO exerts beneficial effects with regards to maintaining ejection fraction, as reductions in protein s-nitrosation have been found in HF, and s-nitrosation of proteins such as the ryanodine receptor/calcium channel (RyR2) and L-type calcium channel have been associated with increasing/maintaining cardiac contractility (L. Xu et al. 1998; Sun et al. 2009). However, the question of why this observation was present in the isoprenaline model, but not ANGII makes this hypothesis less easy to support.

Interestingly, the increased presence of NO (via NO donors) in both animal and cellular models has also been associated with increased β-adrenergic receptor expression and prevention of agonist-induced downregulation of receptors by prevention of GPCR Kinase 2-mediated β-adrenergic receptor phosphorylation and recruitment of β-arrestin. This therefore results in attenuation of receptor desensitisation/internalisation (Whalen et al. 2007) and may therefore have helped sustain cardiac contractility during isoprenaline infusion in our mouse model. However, further molecular investigation is required to conclude which mechanisms are responsible for the physiological effects observed.

It has previously been recognized that reduced NO levels in the heart can result in increases in cytosolic Ca^{2+} and the occurrence of diastolic dysfunction. The study reporting these findings highlighted uncoupling of NOS as the principle mechanism responsible (Silberman et al. 2010), and therefore, we could hypothesise that by restoring NO and improving endothelial function in the ANGII model, it may be possible that whilst ejection fraction may not be significantly improved in the ANGII model, diastolic function may be preserved. Future investigations into cardiovascular

haemodynamics in these models is therefore warranted to further understand the implications of the structural cardiac changes observed.

6.7. The effects of dietary nitrate on cardiac fibrosis and the molecular pathways involved

The reduction of PSR staining suggests that fibrosis was significantly reduced by nitrate pre-treatment in the ANGII model, and this may also have some impact on diastolic function. CTGF expression is induced by ANGII (Ruperez et al. 2003) and in RT-PCR analysis of heart samples I discovered that CTGF was one of the genes significantly down regulated with dietary nitrate treatment in both the ANGII and isoprenaline models. CTGF has been investigated widely in many disease models with regards to fibrosis, including renal and skin models. In general an important balance exists with regards to CTGF and wound healing/fibrosis where in most tissues there is an importance in mediating physiological healing, but without causing excessive scarring (S. Liu et al. 2011). However, the findings from such studies should be extrapolated with care when attempting to translate to the heart – where any degree of fibrosis is likely to compromise function.

In vivo assays have shown TGFβ-induced collagen synthesis in both neonatal rat kidney and human foreskin fibroblasts to be blocked with anti-CTGF antibodies and by suppressing TGFβ-induced gene expression by elevating intracellular cAMP levels with adenylyl cyclase activator, cholera toxin (CTX). Elevated cAMP levels inhibited collagen synthesis induced by CTGF. In animal models, CTX injected intradermally in transgenic mice suppressed TGFβ activation of a human CTGF promoter/lacZ reporter transgene, and also blocked TGFβ-induced collagen deposition in a wound chamber assay (Duncan et al. 1999).

In an ANGII rat model it was shown that CTGF is upregulated extremely quickly following ANGII infusion and may be an important mediator in vascular fibrosis development (Ruperez et al. 2003). In an *in vitro* model of cardiac fibrosis, the importance of CTGF signalling has recently been placed on fibroblasts, particularly with regards to autocrine signalling in activated fibroblasts which worsens cardiac fibrosis. However, arguing against this is the finding that ANGII-stimulated CTGF expression by cardiomyocytes *in vitro* did not have any effect on fibroblasts and was not pro-fibrotic (Dorn et al. 2018).

One recent paper has in fact shown that transgenic mice over-expressing CTGF in general are protected from ANGII-induced hypertrophy (Yang et al. 2009). The exact reason for this is not made clear, and as the overexpression in this model is not tissue specific or temporal, it may be that overexpression of CTGF in certain tissues or in health/development is capable of over-riding its potential negative effects in fibroblasts. Further investigation in tissue-specific and/or temporal KO mouse models would be of particular benefit with regards to better understanding how this relates to the attenuated outcomes observed in our study.

Regardless, in in heart homogenates significant reductions in CTGF with dietary nitrate treatment was evidenced in ANGII- and isoprenaline-infused mice. NO has been shown previously to downregulate CTGF expression in a cGMP-mediated manner in cultured rat mesangial cells (Keil et al. 2002), and in a double transgenic rat model of HFpEF, NO-sensitive guanylyl cyclase simulation improved cardiac dysfunction and significantly reduced CTGF expression in this model (Wilck et al. 2018).

The canonical TGFβ signalling pathway is one that is strongly upregulated in cardiac dysfunction in both hypertensive heart disease, dilated and infarct-induced cardiomyopathy leading to heart failure (Dobaczewski et al., 2011; Liu et al., 2017). The lack of an effect of nitrate treatment upon TGFβ mRNA expression, an upstream modulator of CTGF signalling (Chen et al. 2000), indicated that this cytokine likely was not the target of NO. However, it has been previously shown that NO is capable of inhibiting TGFβ/SMAD signalling, but not necessarily via changing TBGβ expression but rather by altering TGFβ-triggered SMAD phosphorylation and signalling. NO has been shown to significantly attenuate TGFβ phosphorylation and downstream signalling via SMAD2/3, a process which was found to be cGMP dependent. These findings could be mimicked by a soluble cGMP analogue, and inhibiting protein kinase 1 (PKG-1), or overexpressing a dominant-negative version of PKG-1, was sufficient to inhibit NO-induced inhibition of TGFβ expression. Conversely, overexpression of PKG-1 blocked TGFβ/SMAD signalling. It was found that NO reduced SMAD2/3 phosphorylation and nuclear translocation, but L-NAME increased SMAD phosphorylation and signalling (Saura et al. 2005). Therefore, future experiments focused on phosphorylation of these proteins could be key in uncovering molecular pathways associated with the beneficial effects of dietary nitrate and NO. Furthermore, NO has been found suppress TGFβ-

induced epithelial-to-mesenchymal transition in mouse hepatocytes (a key stage in fibrosis development) as well as hepatocyte apoptosis (Pan et al. 2009). Whilst the model used here was an *in vitro* example of the cell transitions which occur during liver fibrosis pathogenesis, it is possible that similar pathways may be involved in cardiac fibrosis and could also benefit from nitrate/NO supplementation.

Interestingly, eNOS KO mice exhibit increased basal levels of TGFβ/SMAD signalling (Saura et al. 2005), but TGFβ/SMAD signalling has also been shown to be involved in regulating eNOS expression (Saura et al. 2002). These findings highlight the complexity of the relationship between eNOS/NO and TGFβ/SMAD and potential for the existence of negative feedback loops regulating expression and activity, further complicating interpretation of TGFβ/SMAD/CTGF expression being inherently good or bad. However, with CTGF and Col1a expression, as well as PSR staining all being reduced by dietary nitrate in our models, this suggests that dietary nitrate has had a generally beneficial impact on fibrosis development.

Similar findings have been reported in models of renal fibrosis where activators of cGMP signalling exerted protective effects by inhibiting SMAD phosphorylation (Schinner et al. 2017). Furthermore, in a model of pulmonary hypertension a significant reduction in lung fibrosis was observed following dietary nitrate intervention. Whilst this may be due, in part, to a reduction in pulmonary hypertension, it is also possible that direct NO signalling may have played a role in the protective benefits observed (Baliga et al. 2012). In L-NAME-induced hypertensive rats dietary nitrite reduced cardiac remodelling via reductions in TGFβ-mediated signalling (Sonoda et al. 2017). The authors hypothesised that this was due to supressed ANGII signalling, which may indeed be part of the story. However, we did not see a significant reduction in *AT1Ra* expression in our models and saw benefits of nitrate treatment even in an ANGII model where the RAAS system is pushed to the extreme. Therefore, whilst it is possible that there could be some impact of nitrate/nitrite/NO on RAAS signalling, there are other RAAS-independent pathways which are more likely to be responsible for the beneficial effects observed in our studies, for example reducing oxidative stress.

One other key mediator of fibrosis which may be altered by dietary nitrate is the nuclear transcription factor nuclear factor kappa-light-chain-enhancer of activated B cells (NFkB)

(Ma et al. 2018). It has been shown previously that NFkB binding can be significantly inhibited by NO (Matthews et al., 1996). Not only that, but ROS are also able to activate NFkB. With dietary nitrate having been shown to reduce the oxidative stress in both the ANGII and Isoprenaline models, it is possible that just via NFkB there are multiple pro-fibrotic pathways attenuated by treatment with dietary nitrate.

The lack of reduction in fibrosis in the reversal study is likely due to the fact that fibrosis can develop rapidly following hypertension, even prior to LVH development (Müller-Brunotte et al. 2007). In mice receiving 3 weeks of ANGII infusion prior to beginning nitrate intervention, it is likely that fibrosis developed prior to beginning nitrate feeding and could not be reversed by nitrate treatment. Even in clinical studies where marked reductions in CTGF and Col1a have been exhibited in response to pressure unloading, this has not been reflected in a marked reduction in fibrosis (Koshman et al. 2013). However, despite no reduction in fibrosis, it did appear that the progression of hypertrophy could be slowed to some degree, as wall thickening measured by echocardiography was significantly less than that of KCl-fed mice on the same ANGII regimen.

6.8. **Oxidative stress in our models of cardiac dysfunction**

Despite some seemingly disparate effects of dietary nitrate in the two models, one other key mechanism which was shared across the two models, in addition to the reduction in CTGF/fibrosis, was a reduction in oxidative stress. Over the last two decades, numerous clinical and experimental studies have shown that oxidative stress is implicated in the progression of a number of CVD pathologies, including cardiac hypertrophy (J.-M. Li et al. 2002; Satoh et al. 2006) and HF (Lakshmi et al. 2009; Tsutsui et al. 2011). Studies in isolated cardiomyocytes have shown that by reducing oxidative stress using treatments such as vitamin E, hydroxyanisole and catalase, the pro-hypertrophic effects of ANGII and TNF-α on neonatal cardiac myocytes could be prevented (Nakamura et al. 1998). Whilst translation of the use of antioxidants to the clinic has not been straightforward (Myung et al. 2013)**,** it should not be ruled out that reducing oxidative stress and accumulating superoxide damage via downstream mechanisms, with other specifically targeted treatments, may still be beneficial. In this regard, a large body of evidence have reported that targeting the nitrate-nitrite-NO

pathway therapeutically may be beneficial in models of renal and cardiovascular disease by reducing the oxidative stress (Carlstrom et al. 2011) and increasing NO bioavailability.

In light of these observations, in both models of cardiac dysfunction, we investigated the effects of dietary nitrate on oxidative stress, evaluating the individual contributions of XOR and NAD(P)H oxidase by measuring the superoxide production in presence of Xanthine, NADH and NADPH. In line with previous findings (Ling et al. 2018; Peleli et al. 2016) reporting that NO bioavailability can impact superoxide production, we showed that dietary inorganic nitrate attenuates basal superoxide production in both a BP-dependent and -independent model of cardiac dysfunction. ANGII-induced superoxide generation was found to be increased in the presence of Xanthine, NADH and NADPH. In the isoprenaline model, however, superoxide generation was primarily driven by NADPH and NADH substrates, with a much smaller contribution from xanthine. Inorganic nitrate in ANGII-infused mice significantly reduced both xanthine and NADPH-induced superoxide generation, with a similar trend when NADH was present. Whilst, unlike ANGII-infused mice, in the isoprenaline model, nitrate reduced only NADPH-mediated oxidative stress. Importantly, XOR and NADPH oxidative effects were prevented by enzymatic antagonists, allopurinol/febuxostat or DPI respectively.

Together, these findings clearly indicate that both models of HF are characterised by an increase of ROS production, and that XOR and NADPH oxidase can have a pivotal role in the development of oxidative stress in such conditions. However, whilst ANGII represents a stimulus for both enzymes, isoprenaline seems to primarily affect NADPH oxidase.

Differences in the enzymatic mediators of superoxide generation in the ANGII and isoprenaline models are likely to be as a result of the different pathophysiological mechanisms at play. ANGII drives cardiac pathology both in the vasculature and directly within the heart, but isoprenaline largely drives pathology from direct cardiac signalling and tachycardia. Differences in the triggers and sources of superoxide generation are also therefore likely to influence the improvement reported in response to nitrate treatment. Attenuating NADPH oxidase-mediated oxidative stress for example, may have a greater effect on direct cardiac signalling and cardiac output, whereas reducing XO-mediated oxidative stress may have more benefit in the vasculature, for example

improving endothelial function and subsequently BP-dependent wall thickening and fibrosis. However, regardless of the exact pathway(s) responsible, oxidative stress from a variety of sources has been widely implicated in the development and progression of cardiac hypertrophy and HF, and reductions in ROS generation are highly likely to be of benefit with regards to improving clinical outcome in patients (Tsutsui et al. 2011). Relating these types of molecular findings to the exact physiological improvements observed remains the main challenge, which is why using multiple cardiac dysfunction models (as we have done here) has proved invaluable as we look to tease apart both similarities and differences in the models and results observed.

However, in both models we detected a significant reduction in NADPH oxidase-driven oxidative stress. The fact that nitrate reduced NADPH oxidase-driven oxidative stress in both ANGII and isoprenaline models was particularly interesting as changes in this particular pathway may (at least in part) be directly driven by direct signalling in the heart, independent of vascular function and changes in BP.

Some may argue that as lucigenin can itself generate superoxide in some circumstances, and furthermore, superoxide is not the only radical that could react with lucigenin to induce the luminescence (e.g. hydrogen peroxide) that there are other, more reliable methods of measuring superoxide generation. For example, methods such as fluorescent staining of cells and tissues, using dihydroethidium (DHE) or dichlorodihydro fluorescein diacetate (DCFH-DA), or chromatography methods, may be preferable in some instances (Zhang et al., 2018).

However, due to the somewhat unique ability of the lucigenin assay to enable examination of the impact of particular enzymatic contributions to superoxide generation in tissues, the lucigenin method was used for these studies. It enabled us to probe the importance of specific enzymes of interest (namely NADPH oxidase and XOR) by adding substrates (xanthine, NADH and NADPH) to the assays, as well as inhibitors (DPI and allopurinol).

Although the reactivity between lucigenin and superoxide is quite low, and this is by no means a biological reflection of the in tissue level of superoxide produced, it enabled us to quantify the relative contributions of enzymes of interest to the oxidative stress

burden in cardiac tissue, and was therefore an appropriate method for use in our models.

6.9. **Dietary nitrate reduces XOR-mediated superoxide generation**

Due to the particular involvement of XOR in the ANGII model, XOR expression and activity was investigated further by measuring protein expression as well as H_2O_2 generating capacity. As expected, XOR protein expression was significantly increased following ANGII infusion. But with no significant reduction in expression in nitrate-fed mice. XO-mediated H_2O_2 generation was also increased following ANGII infusion, but contrary to changes in protein expression, this increase was significantly attenuated by nitrate feeding in both pre-treatment and reversal mice. In line with LECL findings, XOR expression and XOR-driven H_2O_2 production was much higher in the ANGII (BP-dependent) model compared to the isoprenaline (BP-independent) model.

With no reduction of XOR expression by dietary nitrate in the ANGII model, the question remained, how was XOR-dependent superoxide production being reduced by dietary nitrate if it wasn't having an effect on enzyme expression? XOR is an extremely complex enzyme, with varying activities depending on substrate/binding site, oxidation state and availability of terminal electron acceptors (Battelli et al. 2014). XOR exists in two interconvertible states - *XDH* (the reduced form of the enzyme) and XO. The principal form present under physiological conditions *in vivo* is *XDH*, but this can be converted to XO by either sulfhydryl oxidation (reversible) or proteolysis (irreversible) (Stirpe & Corte 1969; Enroth et al. 2000). The importance of this oxidation state is critical, as following the hydroxylation of purines at the molybdenum site, electrons are generated here and go on to be used at the FAD site. However, depending on the oxidation state of the FAD site, the resulting products will differ. *XDH* typically uses NAD^+ as its terminal electron acceptor (and molecular oxygen only in times of NAD^+ deficiency). However, XO utilizes only oxygen as a terminal acceptor, resulting in substantial superoxide formation (Hille & Massey 1981) and contributing to accumulating oxidative stress in pathological conditions, including HF (Tsutsui et al. 2011). However, of particular importance for this study, XO has also been known for some time to catalyse the reduction of nitrate to nitrite, and nitrite to NO (Millar et al. 1998; Zhang et al. 1998; Godber et al. 2000; H. Li et al. 2001), and the functional importance of this phenomenon has been demonstrated *in vivo* (Webb et al. 2004; Ghosh et al. 2013).

We have previously proposed that one particular benefit of dietary nitrate supplementation, may be the ability to encourage 'XOR repurposing' (Tripatara et al. 2007; Khambata et al. 2015). It is possible that the mechanism by which XOR-mediated oxidative stress is reduced in the ANGII model is simply through repurposing of already present XOR. One can speculate that XOR is being redirected by the increased concentrations of plasma nitrite to generate beneficial NO (via nitrite reduction) from the electron transport chain, instead of generating harmful superoxide. The fact that oxidative stress in the isoprenaline model is less XOR-driven and more by NADPH oxidase, may explain why XOR repurposing with nitrate has less of an impact in the LECL assay with isoprenaline-treated mice. In further support of this theory are the findings from the XO activity assay in which nitrate feeding in controls, ANGII pre-treatment and ANGII reversal study mice expressed significantly reduced H_2O_2 generation, but not in isoprenaline-treated mice. Additionally, our findings highlight that in cardiac tissue, when mice have been fed dietary nitrate, the nitrite reductase capacity of cardiac enzymes significantly increases. With no change in XOR expression following dietary nitrate, but a reduction in XOR-mediated superoxide generation and a concurrent increase in nitrite reduction, this supports the hypothesis that XOR activity may indeed be re-directed towards favourable nitrite reduction and away from generating harmful superoxide. Thus, the beneficial effects of dietary nitrate in the ANGII model in particular, may be two-fold. Not only could the resulting NO be of benefit in terms of encouraging blood vessel dilation and reducing hypertrophy via direct signalling, but with nitrite acting as a substrate for XOR, the ability of XOR to generate superoxide may also be reduced due to a 'repurposing' of the enzyme (discussed in Khambata et al. 2015).

6.10. Dietary nitrate reduces NADPH oxidase-mediated superoxide generation

The mechanisms behind the beneficial effects of dietary nitrate on NADPH oxidase activity remain to be fully elucidated. NOX2 and NOX4 subunits have been identified throughout the cardiovascular system (Bedard & Krause 2007), and along with XOR are considered the most probable sources of superoxide anion, which is one of the most reactive ROS. As previously reported from *in vivo*, *in vitro*, and clinical studies, ANGII represents one of the main stimuli of NADPH oxidase and XOR enzymes. Indeed, it has

been reported (Landmesser et al. 2007) that bovine endothelial cells exposed to ANGII (10-7 mol/l) show a time dependent increase of XOR expression and activity, followed by an increase in superoxide production. These effects were blocked by the AT_1 receptor antagonist losartan. Furthermore, as reported by Ling et al., immunoblotting in protein extract from aortas from ANGII-infused mice, showed an increase in NOX2 and NOX4 subunits. Such upregulation explains the increases in superoxide generation observed in the presence of xanthine and NADPH in this model should the same be true of cardiac tissue (Ling et al. 2018).

To begin investigating the possible mechanisms involved in attenuating NADPH oxidase-mediated superoxide generation we began by probing for NOX2 protein expression. With limited heart samples available for molecular analysis, aorta homogenates were used to investigate NOX2 protein expression in ANGII-infused mice. In western blot immunoassays probed for NOX2 protein expression, and tissues from nitrate-treated mice a trend towards reduced protein expression was seen, but this was not statistically significant. Such results are in accordance with the study by (Ling et al. 2018), where with dietary nitrite there was no detectable change in ANGII-induced NOX2 upregulation. In this study by Ling et al., they did however see a reduction in the NOX4 subunit – suggesting this may be an avenue to explore in further studies.

Furthermore, the protein kinase B (Akt)/mammalian target of rapamycin (mTOR) pathway has also been found to be attenuated by dietary nitrite (Guimaraes et al. 2018). NOX4 is a mediator of cardiac hypertrophy and remodelling via Akt/mTOR and NFkB signalling (Zhao et al. 2015), and these pathways have been shown to be upregulated in both pressure overload (Sciarretta et al. 2014) and spontaneous hypertension models (Soesanto et al. 2009). Further investigation of NOX4/Akt/mTOR signalling pathways would therefore be of particular interest in future, with regards to the reductions in NADPH oxidase-mediated oxidative stress in our models, and how this translates to reduced cardiac hypertrophy and fibrosis.

6.11. The *Xdh* KO mouse model – further understanding the complex roles of XOR in health and disease

Due to the apparent implications of XOR in the benefits of dietary nitrate on BP and cardiac dysfunction, the *Xdh* KO mouse model was used to further understand the

importance of this complex enzyme. It was of interest to characterise the cardiovascular phenotype of mice who lack, at least in part, the XOR enzyme and further understand the physiological role of XOR in cardiovascular health as a nitrite reductase. However, it was of equal interest to understand the implications of removing XOR with regards to superoxide generation in a model of cardiovascular disease, such as the ANGII model. Due to the lethal nature of the KO mouse model, *Xdh* Het (+/-) mice and WT (+/+) littermate controls were used. In other work conducted in our lab (yet to be published), it has been established that we have successfully generated a colony of *Xdh* KO mice - with XO activity (as measured by the XO assay discussed in Section 2.18) partially reduced in Hets and completely abolished in KOs (Khambata et al., unpublished). Furthermore, liver *Xdh* mRNA and XOR protein expression both demonstrated a substantial reduction, confirming that this observation was due to reduced XOR expression. Importantly, Hets exhibited a partial, but significant reduction in *Xdh* mRNA and XOR protein expression.

6.12. BP in *Xdh* Het and WT mice – with and without ANGII infusion

In unchallenged *Xdh* Het mice, BP (as measured using tail cuff methodology) was significantly increased compared to WT littermate controls. The nitrite reductase capacity of tissue homogenates in the *Xdh* KO mice has also been investigated in our lab, with results as of yet to be published. Nitrite reductase activity of liver homogenate was determined under physiological (pH 7.4), ischaemic (pH 6.8) and severe ischaemic (pH 5.5) conditions. Reduced nitrite reductase activity was observed in both Het and KO liver homogenates across all pHs and was most evident when the highest concentration of nitrite (1mM) was used. Furthermore, there was a significant increase in both liver and plasma nitrite and nitrate concentrations in KO mice, with a trend towards increased nitrite concentration in Hets, when compared using ozone chemiluminescence (Khambata et al., unpublished). Together, these finding support the notion that XOR acts as a nitrite reductase under physiological conditions and contributes towards maintaining low BP in health by reducing nitrite to bioactive NO. Reducing the expression of the *Xdh* gene in Hets therefore had a significant impact on cardiovascular phenotype, with an increase in DBP, SBP and MAP measured at baseline compared to WT controls.

However, interestingly, in Het mice which were infused with ANGII for 3 weeks, BP was significantly lower than that of WT controls under the same ANGII regimen. It can therefore be suggested that whilst *Xdh* expression is beneficial under physiological conditions, contributing to maintenance of healthy BP by reducing nitrite to NO, in diseased states XOR has the potential to contribute towards oxidative stress. It is therefore understandable that its absence (or reduction) in a disease model could be of benefit, helping reduce further vascular dysfunction/hypertension in the ANGII model.

6.13. Cardiac phenotyping *Xdh* Het and WT mice – with and without ANGII infusion

Due to the preliminary nature of the investigations into cardiac phenotypes of *Xdh* Het mice, this study was not powered to see significance in echocardiographic measures. However, using our findings as a basis to generate power calculations will provide an indication of the further work required to reach statistical significance in echocardiographic data for these studies.

When carrying out echocardiographic imaging in *Xdh* Het mice and WT littermate controls at 8 and 16 weeks of age, understandably there was a trend towards increased LV volume and LVID with age. This increase was present in both Het and WT mice. There However, this increase showed trends towards being somewhat greater in the Het group. In addition to this, there was a trend towards LV wall thickening and reduction in ejection fraction in the *Xdh* Het group at 16 weeks old. Whilst the data is not sufficiently powered to see statistical significance, should these findings be corroborated in subsequent mice, this may indicate some level of cardiac hypertrophy development alongside the hypertension measured by tail cuff methods.

In an *in vitro* cancer model XDH downregulation in cells has been found to increase TGFβ/SMAD signalling (G.-L. Chen et al. 2017). This could potentially be due to less NO being present, which (as previously discussed) can act as an inhibitor of this signalling pathway. Should similar patterns in expression be identified in *Xdh* Het cardiac tissue in future, along with the hypertension observed, this would go a long way towards helping explain increased levels of cardiac hypertrophy and dysfunction in *Xdh* Hets at baseline.

In experiments where *Xdh* Het and WT mice were challenged with ANGII and had echocardiographic parameters measured at 16 weeks of age, both Hets and WTs

exhibited LV wall thickening, increase in LV mass and reductions in ejection fraction. However, the LV volume increase was less pronounced in *Xdh* Hets. Comparing the values of ANG+Het and ANG+WT to those of Het and WT controls, it can be seen that the wall thickness of ANG+Het mice is not much different from Het controls. However, ANGII+WT mice exhibit more severe wall thickening compared to WT controls. This aligns with the fact that that ANGII infusion caused a much greater rise in BP in WT mice compared to Hets.

Doppler flow data, measured in the descending aorta of these mice, indicated that *Xdh* Het mice (regardless of age) have reduced mean and peak velocities in comparison to WT controls – potentially indicating reduced aortic stiffening, despite increased BP. This is particularly interesting, as with reduced *Xdh* expression we hypothesised that an increase in BP in *Xdh* Het mice would be due to a reduction in physiological nitrite reductase capacity. However, typically we would expect that along with raised BP and cardiac dysfunction would come aortic stiffening. However, it appears in the *Xdh* Het mice this may not necessarily be the case.

As previously discussed, XOR is a complex enzyme and can act both as a nitrite reductase and a generator of oxidative stress. It is therefore possible that in 16-week old *Xdh* Het mice, the loss of endogenous NO produced by XOR as a nitrite reductase is significant enough to raise BP and begin to initiate cardiac changes as a result of the raised BP and increased TGFβ signalling. However, with the absence of XOR in the setting of raised BP and cardiac dysfunction, it may be that superoxide generation, which is usually present in such disease states, is significantly reduced. Therefore, in the blood vessels for example the improved measures of aortic stiffening in mice who lack *Xdh* could potentially be a reflection of this. This is an area which warrants further investigation, for example using organ bath assays to explore the effects of vasoactive substances in an *ex vivo* set up. Unfortunately, in the Langendorf assays conducted thus far, the differences observed in basal CPP could mean that any potential differences in vasoreactivity to SNP and Bradykinin were confounded by this variable. This could make it difficult to detect any other potential differences.

It is also worth noting that in a study by Adelsperger et al., ANGII-infused mice were studied using echocardiography at the beginning and end of a 4-week period,

investigating the development of abdominal aortic aneurysms (AAA). In this study, greater peak velocity was associated with the development of AAA in the diseased group following ANGII infusion, with a lower velocity in the non-diseased group (Adelsperger et al. 2018). The non-diseased mice, which did not develop AAA, had a significantly reduced velocity at Day 28 compared to Day 0 baseline. Whereas the mice which developed AAA had significantly increased velocity at Day 28 compared to Day 0 baseline. With this in mind, it is possible that the lower velocities observed in our Xdh Hets both in controls and following ANGII infusion may indicate some level of vascular protection, for example against AAA development.

	Nondiseased		AAA	
Variable	Day 0	Day 28	Day 0	Day 28
n	27	N/A	16	N/A
Initial age (weeks)	15.0 ± 7.1	N/A	16.9 ± 8.9	N/A
Initial mass (g)	27.9 ± 4.0	N/A	29.5 ± 2.5	N/A
Mean diameter (mm)	0.968 ± 0.08	1.175 ± 0.17^	1.00 ± 0.07	2.215 ± 0.51*,^
Circumferential strain (mm/mm)	0.212 ± 0.03	0.141 ± 0.03^	0.200 ± 0.03	0.039 ± 0.01*,^
Peak blood flow velocity (mm/sec)	785 ± 169	521 ± 176^	825 ± 185	1188 ± 458*,^
Volume/Length (mm^2)	0.775 ± 0.12	1.180 ± 0.26^	0.783 ± 0.08	2.759 ± 1.15*,^

*Statistical differences ($P < 0.05$) shown as * when compared with the nondiseased group, ^ when compared with day 0 within same group. Data shown as mean ± SD.

Table 6.1 As published in Adelsperger et al.,2018 (Table 3) highlighting the longitudinal ultrasound metrics compared between Non-diseased and diseased (AAA) mice infused with 1000ng/kg/min ANGII for 28 days.

6.14. Future investigations of interest

In the ANGII and isoprenaline models, future investigations of particular interest to help elucidate the molecular mechanisms behind the phenotypic effects observed include:

- NOX4/Akt/mTOR protein expression in cardiac and vascular tissue.
- SMAD2/3p protein expression and phosphorylation in cardiac and vascular tissue.

Due to the preliminary nature of the *Xdh* KO mouse studies, it will be important in future to bring these n-numbers to those indicated by the power calculations below. Based on the preliminary data, it can be determined that n = 21 would be required to detect a significant difference in LV mass between *Xdh* Hets and WT with an effect size of 1.16, with 95% power (**Figure 6.2**). There were several suggestions of trends observed in directions which would support the hypothesis that XOR acts predominantly as a nitrite reductase in health, but as a superoxide generator in disease, and that this activity can be somewhat directed by the substrates and stimuli available. Having now calculated

the n-numbers required to reach statistical power, it will be important to complete these studies. In the *Xdh* mouse models, further to increasing n-numbers to power, future investigations of particular interest include:

- Comparing nitrite reductase activity in tissues from Hets and WTs (controls and ANGII-infused) and comparing superoxide generation using the XO assay and LECL. This will be particularly important in order to see whether the nitrite reductase/superoxide generation from XOR is impacted as hypothesized in the *Xdh* KO mice.
- Furthermore, the introduction of dietary nitrate to the *Xdh* KO mouse model would be of particular interest, to see whether the activity of XOR can be impacted either in health or under ANGII-infusion.

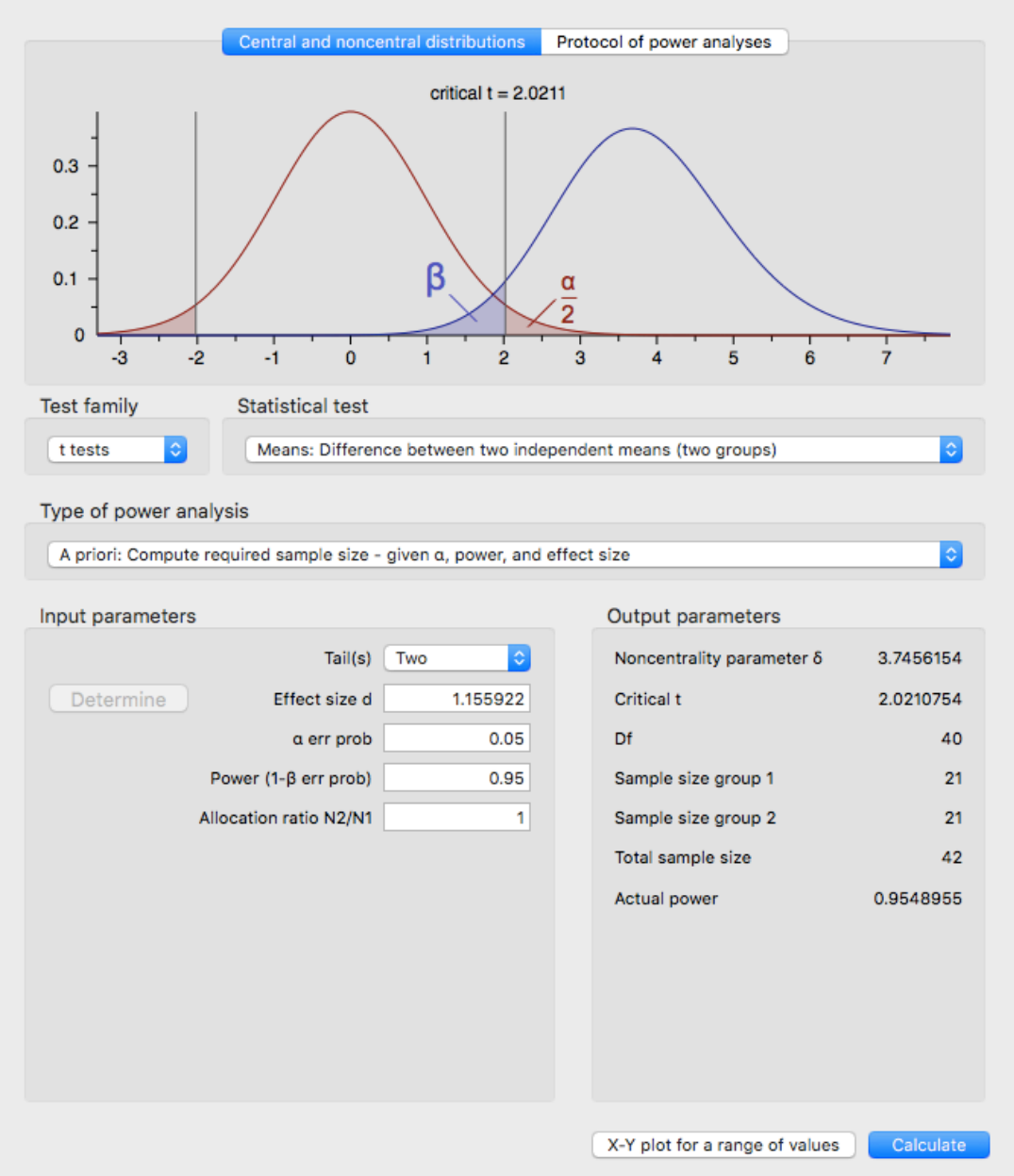

Figure 6.2 G*Power results for power calculations based on preliminary data from Xdh Het and WT mice.

6.15. Final Summary

In conclusion, data presented in this thesis supports the hypothesis that inorganic nitrate has the potential to attenuate both BP-dependent and -independent cardiac dysfunction. In the ANGII (BP-dependent) model, inorganic nitrate significantly attenuated endothelial dysfunction, hypertension, left ventricular (LV) hypertrophy and cardiac fibrosis. Furthermore, nitrate significantly reduced H_2O_2 and superoxide generation, whilst increasing nitrite reductase capacity of heart tissue. In the Isoprenaline (BP-independent) model, inorganic nitrate prevented isoprenaline-induced decline in ejection fraction, significantly reduced cardiac fibrosis and superoxide generation, and increased nitrite reductase capacity.

Molecular pathways of particular importance which we identified as being of interest for further investigation include:

- **cGMP signaling pathways** - Likely cGMP-dependent benefits of nitrate include vasodilation and BP reduction (which in turn can reduce the level of hypertrophy/cardiac dysfunction observed), as well as direct inhibition of fibrosis by reduction in TGFβ/SMAD/CTGF signaling.
- **XOR repurposing** - XOR-dependent benefits of nitrate include repurposing of XOR towards nitrite reductase activity (generating NO from nitrite) as opposed to superoxide generation.
- **NADPH oxidase-mediated superoxide generation** – dietary nitrate reduced NADPH oxidase-mediated superoxide generation. Whilst Nox2 protein expression was not significantly changed by dietary nitrate, Nox4 has yet to be measured in heart tissue from our studies and may represent the mechanism by which nitrate reduces this reduction in oxidative stress.
- **Protein nitrosation** – it is possible that nitrosation of various proteins, yet to be identified, could be impacting cardiac function in our models.
- **Mitochondrial and smooth muscle function** - Furthermore, potential improvements in mitochondrial function and muscle contractility in these models may also be of clinical benefit – whether by improving cardiac or skeletal muscle efficiency.

Furthermore, the importance of the enzyme XOR in both health and disease has been further emphasised by our studies in *Xdh* KO mice. We report evidence supporting its importance as a nitrite reductase enzyme in health, but with significant superoxide generating capacity in disease. It became apparent that XOR expression helps maintain physiological BP in WT mice (acting as a nitrite reductase), but upon ANGII infusion is detrimental (acting as a superoxide generator). Furthermore, despite higher baseline BPs in *Xdh* Hets, these mice were protected from ANGII-induced hypertension and associated worsening of cardiac function, truly highlighting the complexity of XOR's role in health and disease.

A summary figure highlighting particular pathways of relevance in the benefits of NO, and thus inorganic nitrate, on cardiac hypertrophy and dysfunction are shown in **Figure 6.3**. Our data supports the hypothesis that inorganic nitrate has the potential to improve cardiac remodelling both directly (by attenuating fibrosis and reducing superoxide generation) and indirectly (through BP-lowering). Thus, we have demonstrated in these animals models that dietary nitrate may indeed offer a relatively cheap, easily translatable and accessible therapeutic option for both BP-dependent and -independent HF, whether this be in isolation or in conjunction with existing therapies.

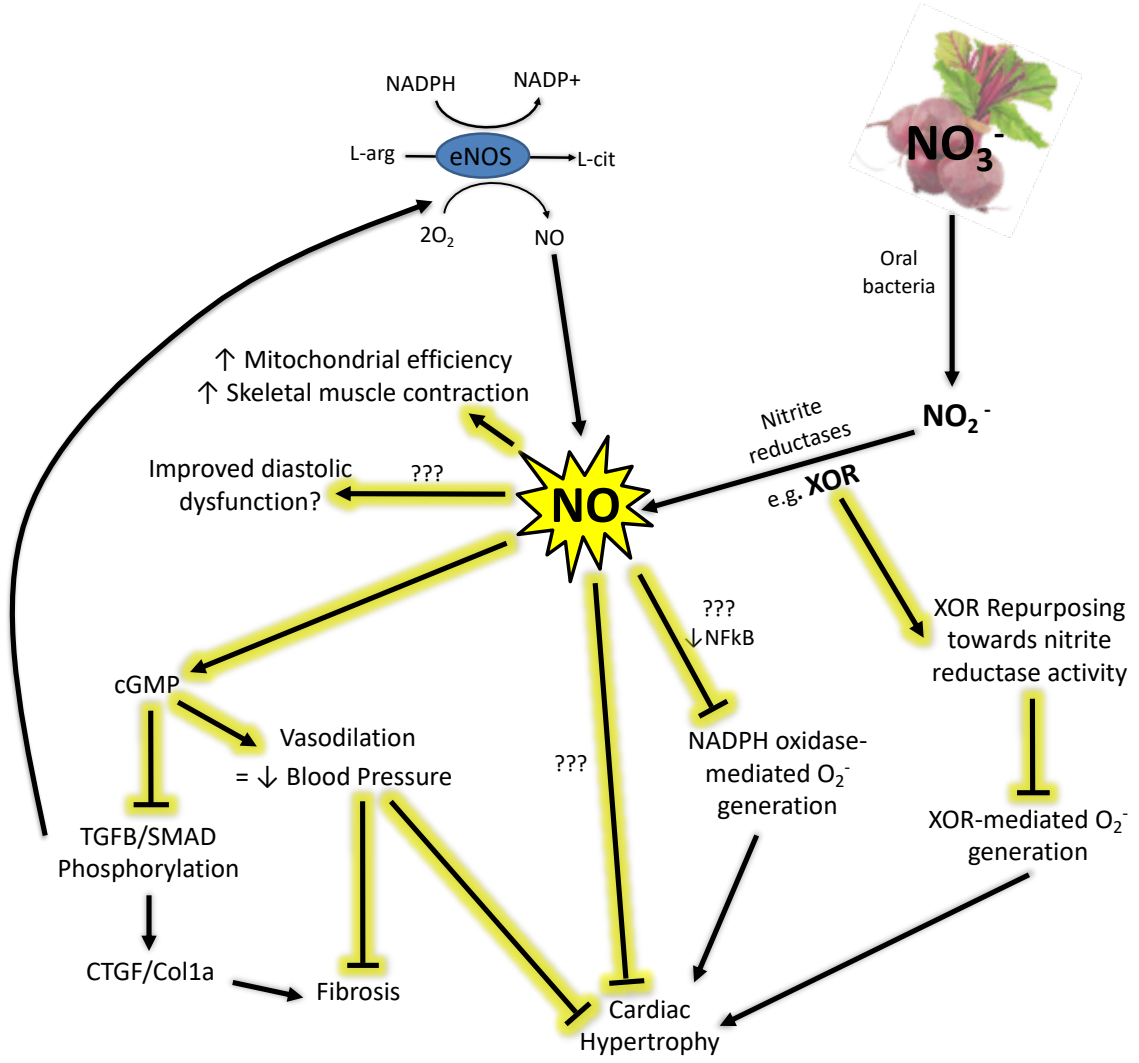

Figure 6.3 Schematic illustrating the key pathways in NO generation and the proposed pathways responsible for the observed effects on cardiac and vascular structure/function in our mouse models of cardiac dysfunction. Yellow lines/arrows highlight pathways in relation to cardiac hypertrophy/dysfunction which can be attenuated or activated by inorganic nitrate/NO.

7. References

Adelsperger, A.R. et al., 2018. Development and growth trends in angiotensin II-induced murine dissecting abdominal aortic aneurysms. *Physiological reports*, 6(8), p.e13668.

Adlam, D. et al., 2011. Telemetric analysis of haemodynamic regulation during voluntary exercise training in mouse models. *Experimental physiology*, 96(11), pp.1118–1128.

Al-Mohammad, A. et al., 2010. Diagnosis and management of adults with chronic heart failure: summary of updated NICE guidance. *BMJ (Clinical research ed.)*, 341, pp.450–452.

Alexander, S.P. et al., 2017. The Concise Guide to Pharmacology 2017/18: G protein-coupled receptors. *British journal of pharmacology*, 174 Suppl 1, pp.S17–S129.

ALLHAT Collaborative Research Group, 2002. Major outcomes in high-risk hypertensive patients randomized to angiotensin-converting enzyme inhibitor or calcium channel blocker vs diuretic: The Antihypertensive and Lipid-Lowering Treatment to Prevent Heart Attack Trial (ALLHAT). *JAMA : the journal of the American Medical Association*, 288(23), pp.2981–2997.

Alzahri, M.S., Rohra, A. & Peacock, W.F., 2016. Nitrates as a Treatment of Acute Heart Failure. *Cardiac failure review*, 2(1), pp.51–55.

ALZET 2019, *Formulating the solution,* viewed 15th November 2019 https://www.alzet.com/formulating-the-solution

Amado, L.C. et al., 2005. Xanthine oxidase inhibition ameliorates cardiovascular dysfunction in dogs with pacing-induced heart failure. *Journal of Molecular and Cellular Cardiology*, 39(3), pp.531–536.

Apostoli, G.L. et al., 2014. Role of inorganic nitrate and nitrite in driving nitric oxide-cGMP-mediated inhibition of platelet aggregation in vitro and in vivo. *Journal of thrombosis and haemostasis : JTH*, 12(11), pp.1880–1889.

Arakawa, K. & Urata, H., 2000. Hypothesis regarding the pathophysiological role of alternative pathways of angiotensin II formation in atherosclerosis. *Hypertension*, 36(4), pp.638–641.

Armstrong, P.W. et al., 2018. A Multicenter, Randomized, Double-Blind, Placebo-Controlled Trial of the Efficacy and Safety of the Oral Soluble Guanylate Cyclase Stimulator: The VICTORIA Trial. *JACC. Heart failure*, 6(2), pp.96–104.

Ashor, A.W. et al., 2016. Inorganic Nitrate Supplementation in Young and Old Obese Adults Does Not Affect Acute Glucose and Insulin Responses but Lowers Oxidative Stress. *The Journal of nutrition*, 146(11), pp.2224–2232.

Bachmanov, A.A. et al., 2002. Food intake, water intake, and drinking spout side preference of 28 mouse strains. *Behavior genetics*, 32(6), pp.435–443.

Baliga, R.S. et al., 2012. Dietary nitrate ameliorates pulmonary hypertension: cytoprotective role for endothelial nitric oxide synthase and xanthine oxidoreductase. *Circulation*, 125(23), pp.2922–2932.

Barouch, L.A. et al., 2003. Combined loss of neuronal and endothelial nitric oxide synthase causes premature mortality and age-related hypertrophic cardiac remodeling in mice. *Journal of Molecular and Cellular Cardiology*, 35(6), pp.637–644.

Barouch, L.A. et al., 2002. Nitric oxide regulates the heart by spatial confinement of nitric oxide synthase isoforms. *Nature*, 416(6878), pp.337–339.

Batchelor, A.M. et al., 2010. Exquisite sensitivity to subsecond, picomolar nitric oxide transients conferred on cells by guanylyl cyclase-coupled receptors. *Proceedings of the National Academy of Sciences*, 107(51), pp.22060–22065.

Battelli, M.G., Bolognesi, A. & Polito, L., 2014. Pathophysiology of circulating xanthine oxidoreductase: new emerging roles for a multi-tasking enzyme. *Biochimica et biophysica acta*, 1842(9), pp.1502–1517.

Becher, P.M. et al., 2012. Role of Heart Rate Reduction in the Prevention of Experimental Heart Failure: Comparison Between If-Channel Blockade and -Receptor Blockade. *Hypertension*, 59(5), pp.949–957.

Bedard, K. & Krause, K.-H., 2007. The NOX family of ROS-generating NADPH oxidases: physiology and pathophysiology. *Physiological reviews*, 87(1), pp.245–313.

Benjamin, E.J. et al., 2019. Heart Disease and Stroke Statistics-2019 Update: A Report From the American Heart Association. *Circulation*, 139(10), pp.e56–e528.

Bernardo, B.C. et al., 2010. Molecular distinction between physiological and pathological cardiac hypertrophy: experimental findings and therapeutic strategies. *Pharmacology and Therapeutics*, 128(1), pp.191–227.

Berry, C.E. & Hare, J.M., 2004. Xanthine oxidoreductase and cardiovascular disease: molecular mechanisms and pathophysiological implications. *The Journal of physiology*, 555(Pt 3), pp.589–606.

Bevan, E.G. et al., 1992. Candoxatril, a neutral endopeptidase inhibitor: efficacy and tolerability in essential hypertension. *Journal of Hypertension*, 10(7), pp.607–613.

BHF 2019, *Heart & Circulatory Disease Statistics 2019,* viewed 10th November 2019 https://www.bhf.org.uk/what-we-do/our-research/heart-statistics/heart-statistics-publications/cardiovascular-disease-statistics-2019

Bhushan, S. et al., 2014. Nitrite therapy improves left ventricular function during heart failure via restoration of nitric oxide-mediated cytoprotective signaling. *Circulation research*, 114(8), pp.1281–1291.

Blowey, D.L., 2016. Diuretics in the treatment of hypertension. *Pediatric nephrology (Berlin, Germany)*, 31(12), pp.2223–2233.

Bondonno, C.P. et al., 2014. Short-term effects of nitrate-rich green leafy vegetables on blood pressure and arterial stiffness in individuals with high-normal blood pressure. *Free radical biology & medicine*, 77, pp.353–362.

Bondonno, C.P., Liu, A.H., Croft, K.D., Ward, N.C., Shinde, S., Moodley, Y., Lundberg, J.O., Puddey, I.B., Woodman, R.J. & Hodgson, J.M., 2015a. Absence of an effect of high nitrate intake from beetroot juice on blood pressure in treated hypertensive individuals: a randomized controlled trial. *The American journal of clinical nutrition*, 102(2), pp.368–375.

Bondonno, C.P., Liu, A.H., Croft, K.D., Ward, N.C., Shinde, S., Moodley, Y., Lundberg, J.O., Puddey, I.B., Woodman, R.J. & Hodgson, J.M., 2015b. Absence of an effect of high nitrate intake from beetroot juice on blood pressure in treated hypertensive individuals: a randomized controlled trial. *The American journal of clinical nutrition*, 102(2), pp.368–375.

Borlaug, B.A., Melenovsky, V. & Koepp, K.E., 2016. Inhaled Sodium Nitrite Improves Rest and Exercise Hemodynamics in Heart Failure With Preserved Ejection Fraction. *Circulation research*, p.CIRCRESAHA.116.309184.

Brater, D.C., 1998. Diuretic therapy. *The New England journal of medicine*, 339(6), pp.387–395.

Broniowska, K.A. & Hogg, N., 2012. The chemical biology of S-nitrosothiols. *Antioxidants & redox signaling*, 17(7), pp.969–980.

Brunner, H. et al., 2005. Endothelial function and dysfunction. Part II: Association with cardiovascular risk factors and diseases. A statement by the Working Group on Endothelins and Endothelial Factors of the European Society of Hypertension*. *Journal of Hypertension*, 23(2), p.233.

Bueno, O.F. et al., 2002. Impaired cardiac hypertrophic response in Calcineurin Abeta - deficient mice. *Proceedings of the National Academy of Sciences of the United States of America*, 99(7), pp.4586–4591.

Buys, E.S. et al., 2007. Cardiomyocyte-restricted restoration of nitric oxide synthase 3 attenuates left ventricular remodeling after chronic pressure overload. *American journal of physiology. Heart and circulatory physiology*, 293(1), pp.H620–7.

Cai, H. & Harrison, D.G., 2000. Endothelial dysfunction in cardiovascular diseases: the role of oxidant stress. *Circulation research*, 87(10), pp.840–844.

Calderone, A. et al., 1998. Nitric oxide, atrial natriuretic peptide, and cyclic GMP inhibit the growth-promoting effects of norepinephrine in cardiac myocytes and fibroblasts. *Journal of Clinical Investigation*, 101(4), pp.812–818.

Callender, T. et al., 2014. Heart Failure Care in Low- and Middle-Income Countries: A Systematic Review and Meta-Analysis P. Byass, ed. *PLoS medicine*, 11(8), pp.e1001699–41.

Carlstrom, M. et al., 2011. Dietary nitrate attenuates oxidative stress, prevents cardiac and renal injuries, and reduces blood pressure in salt-induced hypertension. *Cardiovascular research*, 89(3), pp.574–585.

Cawley, S.M. et al., 2011. sGC{alpha}1 mediates the negative inotropic effects of NO in cardiac myocytes independent of changes in calcium handling. *AJP: Heart and Circulatory Physiology*, 301(1), pp.H157–63.

Chen, G.-L. et al., 2017. Xanthine dehydrogenase downregulation promotes TGFβ signaling and cancer stem cell-related gene expression in hepatocellular carcinoma. *Oncogenesis*, 6(9), pp.e382–e382.

Chen, M.M. et al., 2000. CTGF expression is induced by TGF- beta in cardiac fibroblasts and cardiac myocytes: a potential role in heart fibrosis. *Journal of Molecular and Cellular Cardiology*, 32(10), pp.1805–1819.

Chobanian, A.V. et al., 2003. Seventh Report of the Joint National Committee on Prevention, Detection, Evaluation, and Treatment of High Blood Pressure. *Hypertension*, 42(6), pp.1206–1252.

Chouchani, E.T. et al., 2017. Identification and quantification of protein S-nitrosation by nitrite in the mouse heart during ischemia. *The Journal of biological chemistry*, 292(35), pp.14486–14495.

Clayton, J.A. et al., 2006. Thiazide diuretic prescription and electrolyte abnormalities in primary care. *British journal of clinical pharmacology*, 61(1), pp.87–95.

Coggan, A.R. et al., 2015. Acute Dietary Nitrate Intake Improves Muscle Contractile Function in Patients with Heart Failure: A Double-Blind, Placebo-Controlled, Randomized Trial. *Circulation. Heart failure*, p.CIRCHEARTFAILURE.115.002141.

Cohn, J.N. et al., 1997. Report of the National Heart, Lung, and Blood Institute Special Emphasis Panel on Heart Failure Research. *Circulation*, 95(4), pp.766–770.

Conrad, N. et al., 2018. Temporal trends and patterns in heart failure incidence: a population-based study of 4 million individuals. *Lancet*, 391(10120), pp.572–580.

Crowley, S.D. et al., 2006. Angiotensin II causes hypertension and cardiac hypertrophy through its receptors in the kidney. *Proceedings of the National Academy of Sciences of the United States of America*, 103(47), pp.17985–17990.

Cushman, W.C. et al., 2000. Regional and racial differences in response to antihypertensive medication use in a randomized controlled trial of men with hypertension in the United States. Department of Veterans Affairs Cooperative Study Group on Antihypertensive Agents. *Archives of internal medicine*, 160(6), pp.825–831.

Daemen, M.J., Lombardi, D.M. & Bosman, F.T., 1991. Angiotensin II induces smooth muscle cell proliferation in the normal and injured rat arterial wall. *Circulation*, 68, pp.450–456.

Dahlöf, B., 2001. Left ventricular hypertrophy and angiotensin II antagonists. *American journal of hypertension*, 14(2), pp.174–182.

Dalzell, J.R. et al., 2014. Effects of neutral endopeptidase (neprilysin) inhibition on the response to other vasoactive peptides in small human resistance arteries: studies with thiorphan and omapatrilat. *Cardiovascular therapeutics*, 32(1), pp.13–18.

Dasgupta, C. & Zhang, L., 2011. Angiotensin II receptors and drug discovery in cardiovascular disease. *Drug discovery today*, 16(1-2), pp.22–34.

Dawson, D. et al., 2005. nNOS gene deletion exacerbates pathological left ventricular remodeling and functional deterioration after myocardial infarction. *Circulation*, 112(24), pp.3729–3737.

de Gasparo, M. et al., 2000. International union of pharmacology. XXIII. The angiotensin II receptors. *Pharmacological reviews*, 52(3), pp.415–472.

de Simone, G., 2004. Concentric or eccentric hypertrophy: how clinically relevant is the difference? *Hypertension*, 43(4), pp.714–715.

de Simone, G. et al., 2008. Left ventricular mass predicts heart failure not related to previous myocardial infarction: the Cardiovascular Health Study. *European heart journal*, 29(6), pp.741–747.

Demirci, D. et al., 2014. Sildenafil enhances locomotor activity in young mice and exerts anxiogenic effects in both young and aged mice. *Medical science monitor basic research*, 20, pp.15–21.

Devereux, R.B. et al., 1983. Left ventricular hypertrophy in patients with hypertension: importance of blood pressure response to regularly recurring stress. *Circulation*, 68(3), pp.470–476.

Dobaczewski, M., Chen, W. & Frangogiannis, N.G., 2011. Transforming growth factor (TGF)-β signaling in cardiac remodeling. *Journal of Molecular and Cellular Cardiology*, 51(4), pp.600–606.

Dorn, L.E. et al., 2018. CTGF/CCN2 is an autocrine regulator of cardiac fibrosis. *Journal of Molecular and Cellular Cardiology*, 121, pp.205–211.

Doughty, R.N. et al., 1997. Effects of beta-blocker therapy on mortality in patients with heart failure A systematic overview of randomized controlled trials. *European heart journal*, 18(4), pp.560–565.

Drazner, M.H. et al., 2004. Increased left ventricular mass is a risk factor for the development of a depressed left ventricular ejection fraction within five years: the Cardiovascular Health Study. *Journal of the American College of Cardiology*, 43(12), pp.2207–2215.

Duncan, M.R. et al., 1999. Connective tissue growth factor mediates transforming growth factor beta-induced collagen synthesis: down-regulation by cAMP. *FASEB journal : official publication of the Federation of American Societies for Experimental Biology*, 13(13), pp.1774–1786.

Dunlay, S.M. et al., 2009. Risk factors for heart failure: a population-based case-control study. *The American journal of medicine*, 122(11), pp.1023–1028.

Eggebeen, J. et al., 2016. One Week of Daily Dosing With Beetroot Juice Improves Submaximal Endurance and Blood Pressure in Older Patients With Heart Failure and Preserved Ejection Fraction. *JACC. Heart failure*.

Ekelund, U.E. et al., 1999. Intravenous allopurinol decreases myocardial oxygen consumption and increases mechanical efficiency in dogs with pacing-induced heart failure. *Circulation research*, 85(5), pp.437–445.

Enroth, C. et al., 2000. Crystal structures of bovine milk xanthine dehydrogenase and xanthine oxidase: structure-based mechanism of conversion. *Proceedings of the National Academy of Sciences of the United States of America*, 97(20), pp.10723–10728.

Exner, D.V. et al., 2001. Lesser response to angiotensin-converting-enzyme inhibitor therapy in black as compared with white patients with left ventricular dysfunction. *The New England journal of medicine*, 344(18), pp.1351–1357.

Ferguson, S.K. et al., 2016. Dietary nitrate supplementation: impact on skeletal muscle vascular control in exercising rats with chronic heart failure. *Journal of applied physiology (Bethesda, Md. : 1985)*, 121(3), pp.661–669.

Ferguson, S.K. et al., 2013. Effects of nitrate supplementation via beetroot juice on contracting rat skeletal muscle microvascular oxygen pressure dynamics. *Respiratory physiology & neurobiology*, 187(3), pp.250–255.

Fernandes, T., Soci, U.P.R. & Oliveira, E.M., 2011. Eccentric and concentric cardiac hypertrophy induced by exercise training: microRNAs and molecular determinants. *Brazilian journal of medical and biological research = Revista brasileira de pesquisas médicas e biológicas / Sociedade Brasileira de Biofísica ... [et al.]*, 44(9), pp.836–847.

Ferrario, C.M., 2016. Cardiac remodelling and RAS inhibition. *Therapeutic advances in cardiovascular disease*, 10(3), pp.162–171.

Ferrario, C.M. et al., 2014. An evolving story of angiotensin-II-forming pathways in rodents and humans. *Clinical science (London, England : 1979)*, 126(7), pp.461–469.

Ferreira Filho, C. et al., 2010. Anti-hypertensive drugs have different effects on ventricular hypertrophy regression. *Clinics (Sao Paulo, Brazil)*, 65(7), pp.723–728.

Flather, M.D. et al., 2000. Long-term ACE-inhibitor therapy in patients with heart failure or left-ventricular dysfunction: a systematic overview of data from individual patients. ACE-Inhibitor Myocardial Infarction Collaborative Group. *Lancet*, 355(9215), pp.1575–1581.

Fletcher, P.J. et al., 1981. Left ventricular diastolic pressure-volume relations in rats with healed myocardial infarction. Effects on systolic function. *Circulation research*, 49(3), pp.618–626.

Forrester, S.J. et al., 2017. Caveolin-1 Deletion Prevents Hypertensive Vascular Remodeling Induced by Angiotensin II. *Hypertension*, 69(1), pp.79–86.

Francois, H. et al., 2004. Role for thromboxane receptors in angiotensin-II-induced hypertension. *Hypertension*, 43(2), pp.364–369.

Friddle, C.J. et al., 2000. Expression profiling reveals distinct sets of genes altered during induction and regression of cardiac hypertrophy. *Proceedings of the National Academy of Sciences of the United States of America*, 97(12), pp.6745–6750.

Furchgott, R.F. & Zawadzki, J.V., 1980. The obligatory role of endothelial cells in the relaxation of arterial smooth muscle by acetylcholine. *Nature*, 288(5789), pp.373–376.

Fyhrquist, F., Metsärinne, K. & Tikkanen, I., 1995. Role of angiotensin II in blood pressure regulation and in the pathophysiology of cardiovascular disorders. *Journal of human hypertension*, 9 Suppl 5, pp.S19–24.

Gambaryan, S., Lohmann, S.M. & Walter, U., 2007. NO/cGMP/PKG pathway in platelets: inhibitory but not stimulatory. *BMC Pharmacology*, 7(S1), pp.77–1.

Gee, L.C. & Ahluwalia, A., 2016. Dietary Nitrate Lowers Blood Pressure: Epidemiological, Pre-clinical Experimental and Clinical Trial Evidence. *Current hypertension reports*, 18(2), pp.17–14.

Geleijnse, J.M., Kok, F.J. & Grobbee, D.E., 2003. Blood pressure response to changes in sodium and potassium intake: a metaregression analysis of randomised trials. *Journal of human hypertension*, 17(7), pp.471–480.

Gheorghiade, M. et al., 2015. Effect of Vericiguat, a Soluble Guanylate Cyclase Stimulator, on Natriuretic Peptide Levels in Patients With Worsening Chronic Heart Failure and Reduced Ejection Fraction: The SOCRATES-REDUCED Randomized Trial. *JAMA : the journal of the American Medical Association*, 314(21), pp.2251–2262.

Ghosh, S.M. et al., 2013. Enhanced vasodilator activity of nitrite in hypertension: critical role for erythrocytic xanthine oxidoreductase and translational potential. *Hypertension*, 61(5), pp.1091–1102.

Gibson, C.M. et al., 2008. Trends in reperfusion strategies, door-to-needle and door-to-balloon times, and in-hospital mortality among patients with ST-segment elevation myocardial infarction enrolled in the National Registry of Myocardial Infarction from 1990 to 2006. *American heart journal*, 156(6), pp.1035–1044.

Gilchrist, M. et al., 2013. Effect of dietary nitrate on blood pressure, endothelial function, and insulin sensitivity in type 2 diabetes. *Free radical biology & medicine*, 60, pp.89–97.

Godber, B. et al., 2000. Reduction of nitrite to nitric oxide catalyzed by xanthine oxidoreductase. *Journal of Biological ….*

Gori, T. et al., 2010. Tolerance to nitroglycerin-induced preconditioning of the endothelium: a human in vivo study. *American journal of physiology. Heart and circulatory physiology*, 298(2), pp.H340–H345.

Granata, L. et al., 1970. Beta adrenergic receptor activity in peripheral vascular beds of the unanesthetized dog. *Pflügers Archiv : European journal of physiology*, 320(1), pp.64–78.

Guimaraes, D.A. et al., 2018. Nitrite exerts antioxidant effects, inhibits the mTOR pathway and reverses hypertension-induced cardiac hypertrophy. *Free radical biology & medicine*, 120, pp.25–32.

Haddy, F.J., Vanhoutte, P.M. & Feletou, M., 2006. Role of potassium in regulating blood flow and blood pressure. *American journal of physiology. Regulatory, integrative and comparative physiology*, 290(3), pp.R546–R552.

Hammond, J. & Balligand, J.-L., 2012. Nitric oxide synthase and cyclic GMP signaling in cardiac myocytes: from contractility to remodeling. *Journal of Molecular and Cellular Cardiology*, 52(2), pp.330–340.

Harris, J.C. et al., 1979. Methemoglobinemia Resulting From Absorption of Nitrates. *JAMA : the journal of the American Medical Association*, 242(26), pp.2869–2871.

Heidenreich, P.A. et al., 2013. Forecasting the impact of heart failure in the United States: a policy statement from the American Heart Association. *Circulation. Heart failure*, 6(3), pp.606–619.

Hernández, A. et al., 2012. Dietary nitrate increases tetanic [Ca2+]i and contractile force in mouse fast-twitch muscle. *The Journal of physiology*, 590(15), pp.3575–3583.

Hezel, M.P. et al., 2015. Effects of long-term dietary nitrate supplementation in mice. *Redox biology*, 5, pp.234–242.

Hill, J.A. & Olson, E.N., 2008. Cardiac plasticity. *The New England journal of medicine*, 358(13), pp.1370–1380.

Hille, R. & Massey, V., 1981. Studies on the oxidative half-reaction of xanthine oxidase. *The Journal of biological chemistry*, 256(17), pp.9090–9095.

Hirai, D.M. et al., 2017. Dietary nitrate supplementation and exercise tolerance in patients with heart failure with reduced ejection fraction. *American journal of physiology. Regulatory, integrative and comparative physiology*, 312(1), pp.R13–R22.

Ho, K.K. et al., 1993. The epidemiology of heart failure: the Framingham Study. *Journal of the American College of Cardiology*, 22(4 Suppl A), pp.6A–13A.

Hobbs, D.A., George, T.W. & Lovegrove, J.A., 2013. The effects of dietary nitrate on blood pressure and endothelial function: a review of human intervention studies. *Nutrition research reviews*, 26(2), pp.210–222.

Hord, N.G., Tang, Y. & Bryan, N.S., 2009. Food sources of nitrates and nitrites: the physiologic context for potential health benefits. *The American journal of clinical nutrition*, 90(1), pp.1–10.

Hou, J. et al., 1995. Angiotensin II-induced cardiac fibrosis in the rat is increased by chronic inhibition of nitric oxide synthase. *Journal of Clinical Investigation*, 96(5), pp.2469–2477.

Houser, S.R. et al., 2012. Animal models of heart failure: a scientific statement from the American Heart Association. *Circulation research*, 111(1), pp.131–150.

Huang, P.L. et al., 1995. Hypertension in mice lacking the gene for endothelial nitric oxide synthase. *Nature*, 377(6546), pp.239–242.

Hussain, M.B., Hobbs, A.J. & MacAllister, R.J., 1999. Autoregulation of nitric oxide-soluble guanylate cyclase-cyclic GMP signalling in mouse thoracic aorta. *British journal of pharmacology*, 128(5), pp.1082–1088.

Ichiki, T. et al., 1998. Downregulation of angiotensin II type 1 receptor gene transcription by nitric oxide. *Hypertension*, 31(1 Pt 2), pp.342–348.

Ichinose, F. et al., 2004. Pressure overload-induced LV hypertrophy and dysfunction in mice are exacerbated by congenital NOS3 deficiency. *American journal of physiology. Heart and circulatory physiology*, 286(3), pp.H1070–5.

Ignarro, L.J. et al., 1987. Endothelium-derived relaxing factor from pulmonary artery and vein possesses pharmacologic and chemical properties identical to those of nitric oxide radical. *Circulation research*, 61(6), pp.866–879.

Ihara, M. et al., 1999. Increased chymase-dependent angiotensin II formation in human atherosclerotic aorta. *Hypertension*, 33(6), pp.1399–1405.

Iliești, A.M. & Hodorogea, A.S., 2018. Treatment of Heart Failure with Preserved Ejection Fraction. *Advances in experimental medicine and biology*, 1067(9), pp.67–87.

Ito, M. et al., 1995. Regulation of blood pressure by the type 1A angiotensin II receptor gene. *Proceedings of the National Academy of Sciences of the United States of America*, 92(8), pp.3521–3525.

Janssens, S. et al., 2004. Cardiomyocyte-specific overexpression of nitric oxide synthase 3 improves left ventricular performance and reduces compensatory hypertrophy after myocardial infarction. *Circulation research*, 94(9), pp.1256–1262.

Januzzi, J.L. et al., 2019. Association of Change in N-Terminal Pro-B-Type Natriuretic Peptide Following Initiation of Sacubitril-Valsartan Treatment With Cardiac Structure and Function in Patients With Heart Failure With Reduced Ejection Fraction. *JAMA : the journal of the American Medical Association*, 322(11), pp.1–11.

Jädert, C. et al., 2012. Decreased leukocyte recruitment by inorganic nitrate and nitrite in microvascular inflammation and NSAID-induced intestinal injury. *Free radical biology & medicine*, 52(3), pp.683–692.

JAX 2019, *Body weight information for C57Bl6l/6J (000664),* viewed 15th November 2019 https://www.jax.org/jax-mice-and-services/strain-data-sheet-pages/body-weight-chart-000664

Jian, Z. et al., 2014. Mechanochemotransduction during cardiomyocyte contraction is mediated by localized nitric oxide signaling. *Science signaling*, 7(317), pp.ra27–ra27.

Johansson, C., Jackson, D.M. & Svensson, L., 1997. Nitric oxide synthase inhibition blocks phencyclidine-induced behavioural effects on prepulse inhibition and locomotor activity in the rat. *Psychopharmacology*, 131(2), pp.167–173.

Jones, A.M., 2014. Dietary nitrate supplementation and exercise performance. *Sports medicine (Auckland, N.Z.)*, 44 Suppl 1(S1), pp.S35–45.

Jones, D.A. et al., 2015. Randomized phase 2 trial of intracoronary nitrite during acute myocardial infarction. *Circulation research*, 116(3), pp.437–447.

Kannel, W.B. & Belanger, A.J., 1991. Epidemiology of heart failure. *American heart journal*, 121(3 (Part 1)), pp.951–957.

Kapil, V. et al., 2014. Clinical evidence demonstrating the utility of inorganic nitrate in cardiovascular health. *Nitric oxide : biology and chemistry / official journal of the Nitric Oxide Society*, 38C, pp.45–57.

Kapil, V. et al., 2015. Dietary nitrate provides sustained blood pressure lowering in hypertensive patients: a randomized, phase 2, double-blind, placebo-controlled study. *Hypertension*, 65(2), pp.320–327.

Kapil, V. et al., 2010. Inorganic Nitrate Supplementation Lowers Blood Pressure in Humans. *Hypertension*, 56(2), pp.274–281.

Kapil, V. et al., 2013. Physiological role for nitrate-reducing oral bacteria in blood pressure control. *Free radical biology & medicine*, 55, pp.93–100.

Katholi, R.E. & Couri, D.M., 2011. Left ventricular hypertrophy: major risk factor in patients with hypertension: update and practical clinical applications. *International journal of hypertension*, 2011(1), pp.495349–10.

Kawada, N. et al., 2005. Cyclooxygenase-1-deficient mice have high sleep-to-wake blood pressure ratios and renal vasoconstriction. *Hypertension*, 45(6), pp.1131–1138.

Kawano, S. et al., 2005. Blockade of NF-kappaB ameliorates myocardial hypertrophy in response to chronic infusion of angiotensin II. *Cardiovascular research*, 67(4), pp.689–698.

Keil, A. et al., 2002. Nitric oxide down-regulates connective tissue growth factor in rat mesangial cells. *Kidney international*, 62(2), pp.401–411.

Khambata, R.S., Ghosh, S.M. & Ahluwalia, A., 2015. "Repurposing" of Xanthine Oxidoreductase as a Nitrite Reductase: A New Paradigm for Therapeutic Targeting in Hypertension. *Antioxidants & redox signaling*, 23(4), pp.340–353.

Kim, S. & Iwao, H., 2000. Molecular and cellular mechanisms of angiotensin II-mediated cardiovascular and renal diseases. *Pharmacological reviews*, 52(1), pp.11–34.

Knox, C.D. et al., 2016. Discovery and Clinical Evaluation of MK-8150, A Novel Nitric Oxide Donor With a Unique Mechanism of Nitric Oxide Release. *Journal of the American Heart Association*, 5(9), p.e003493.

Kojda, G. & Harrison, D., 1999. Interactions between NO and reactive oxygen species: pathophysiological importance in atherosclerosis, hypertension, diabetes and heart failure. *Cardiovascular research*, 43(3), pp.562–571.

Koshman, Y.E. et al., 2013. Regulation of connective tissue growth factor gene expression and fibrosis in human heart failure. *Journal of cardiac failure*, 19(4), pp.283–294.

Kurdi, M. & Booz, G.W., 2011. New take on the role of angiotensin II in cardiac hypertrophy and fibrosis. *Hypertension*, 57(6), pp.1034–1038.

Labonté, J. et al., 2008. Distinct modulation of the endothelin-1 pathway in iNOS-/- and eNOS-/- mice. *Canadian journal of physiology and pharmacology*, 86(8), pp.516–525.

Lakshmi, S.V.V. et al., 2009. Oxidative stress in cardiovascular disease. *Indian journal of biochemistry & biophysics*, 46(6), pp.421–440.

Landmesser, U. et al., 2007. Angiotensin II induces endothelial xanthine oxidase activation: role for endothelial dysfunction in patients with coronary disease. *Arteriosclerosis, thrombosis, and vascular biology*, 27(4), pp.943–948.

Larsen, F.J. et al., 2011. Dietary inorganic nitrate improves mitochondrial efficiency in humans. *Cell metabolism*, 13(2), pp.149–159.

Larsen, F.J. et al., 2006. Effects of dietary nitrate on blood pressure in healthy volunteers. *The New England journal of medicine*, 355(26), pp.2792–2793.

Lee, R. et al., 2012. Evaluating oxidative stress in human cardiovascular disease: methodological aspects and considerations. *Current medicinal chemistry*, 19(16), pp.2504–2520.

Levy, D. et al., 1990. Prognostic implications of echocardiographically determined left ventricular mass in the Framingham Heart Study. *The New England journal of medicine*, 322(22), pp.1561–1566.

Levy, D. et al., 1987. Risk of ventricular arrhythmias in left ventricular hypertrophy: the Framingham Heart Study. *The American journal of cardiology*, 60(7), pp.560–565.

Levy, D. et al., 1996. The progression from hypertension to congestive heart failure. *JAMA : the journal of the American Medical Association*, 275(20), pp.1557–1562.

Li, H. et al., 2001. Characterization of the magnitude and kinetics of xanthine oxidase-catalyzed nitrite reduction. Evaluation of its role in nitric oxide generation in anoxic tissues. *The Journal of biological chemistry*, 276(27), pp.24482–24489.

Li, J.-M. et al., 2002. Activation of NADPH oxidase during progression of cardiac hypertrophy to failure. *Hypertension*, 40(4), pp.477–484.

Liebson, P.R. et al., 1995. Comparison of five antihypertensive monotherapies and placebo for change in left ventricular mass in patients receiving nutritional-hygienic therapy in the Treatment of Mild Hypertension Study (TOMHS). *Circulation*, 91(3), pp.698–706.

Lijnen, P. & Petrov, V., 1999. Renin-angiotensin system, hypertrophy and gene expression in cardiac myocytes. *Journal of Molecular and Cellular Cardiology*, 31(5), pp.949–970.

Ling, W.C. et al., 2018. Chronic administration of sodium nitrite prevents hypertension and protects arterial endothelial function by reducing oxidative stress in angiotensin II-infused mice. *Vascular pharmacology*, 102, pp.11–20.

Liu, S. et al., 2011. CCN2 is required for bleomycin-induced skin fibrosis in mice. *Arthritis and rheumatism*, 63(1), pp.239–246.

Liu, G. et al., 2017. Transforming growth factor β and its role in heart disease. *Experimental and therapeutic medicine*, 13(5), pp.2123–2128.

Livak, K.J. & Schmittgen, T.D., 2001. Analysis of relative gene expression data using real-time quantitative PCR and the 2(-Delta Delta C(T)) Method. *Methods (San Diego, Calif.)*, 25(4), pp.402–408.

Lloyd-Sherlock, P., Ebrahim, S. & Grosskurth, H., 2014. Is hypertension the new HIV epidemic? *International Journal of Epidemiology*, 43(1), pp.8–10.

Lockette, W., Otsuka, Y. & Carretero, O., 1986. The loss of endothelium-dependent vascular relaxation in hypertension. *Hypertension*, 8(6 Pt 2), pp.II61–6.

Lohse, M.J., Engelhardt, S. & Eschenhagen, T., 2003. What is the role of beta-adrenergic signaling in heart failure? *Circulation research*, 93(10), pp.896–906.

Loscalzo, J., 2001. Nitric Oxide Insufficiency, Platelet Activation, and Arterial Thrombosis. *Circulation research*, 88(8), pp.756–762.

Lundberg, J.O. & Govoni, M., 2004. Inorganic nitrate is a possible source for systemic generation of nitric oxide. *Free radical biology & medicine*, 37(3), pp.395–400.

Lundberg, J.O. & Weitzberg, E., 2010a. NO-synthase independent NO generation in mammals. *Biochemical and biophysical research communications*, 396(1), pp.39–45.

Lundberg, J.O. & Weitzberg, E., 2010b. NO-synthase independent NO generation in mammals. *Biochemical and biophysical research communications*, 396(1), pp.39–45.

Lundberg, J.O., Weitzberg, E. & Gladwin, M.T., 2008a. The nitrate-nitrite-nitric oxide pathway in physiology and therapeutics. *Nature reviews. Drug discovery*, 7(2), pp.156–167.

Lundberg, J.O., Weitzberg, E. & Gladwin, M.T., 2008b. The nitrate-nitrite-nitric oxide pathway in physiology and therapeutics. *Nature reviews. Drug discovery*, 7(2), pp.156–167.

Ma, Z.-G. et al., 2018. Cardiac fibrosis: new insights into the pathogenesis. *International journal of biological sciences*, 14(12), pp.1645–1657.

Manhiani, M.M. et al., 2015. The role of IL-6 in the physiologic versus hypertensive blood pressure actions of angiotensin II. *Physiological reports*, 3(10), p.e12595.

Matsumoto, E. et al., 2013. Angiotensin II-induced cardiac hypertrophy and fibrosis are promoted in mice lacking Fgf16. *Genes to Cells*, 18(7), pp.544–553.

Mazzolai, L. et al., 1998. Blood pressure-independent cardiac hypertrophy induced by locally activated renin-angiotensin system. *Hypertension*, 31(6), pp.1324–1330.

McEwan, P.E. et al., 1998. Differential Effects of Angiotensin II on Cardiac Cell Proliferation and Intramyocardial Perivascular Fibrosis In Vivo. *Circulation*, 98(24), pp.2765–2773.

McMurray, J.J.V. et al., 2014. Angiotensin-neprilysin inhibition versus enalapril in heart failure. *The New England journal of medicine*, 371(11), pp.993–1004.

McNamara, D.M. et al., 2003. Effect of the Asp298 variant of endothelial nitric oxide synthase on survival for patients with congestive heart failure. *Circulation*, 107(12), pp.1598–1602.

Mehta, P.A. et al., 2009. Improving survival in the 6 months after diagnosis of heart failure in the past decade: population-based data from the UK. *Heart (British Cardiac Society)*, 95(22), pp.1851–1856.

Meredith, P.A. & Ostergren, J., 2006. From hypertension to heart failure -- are there better primary prevention strategies? *Journal of the renin-angiotensin-aldosterone system : JRAAS*, 7(2), pp.64–73.

Millar, T.M. et al., 1998. Xanthine oxidoreductase catalyses the reduction of nitrates and nitrite to nitric oxide under hypoxic conditions. *FEBS letters*, 427(2), pp.225–228.

Modin, A. et al., 2001. Nitrite-derived nitric oxide: a possible mediator of “acidic-metabolic” vasodilation. *Acta physiologica Scandinavica*, 171(1), pp.9–16.

Mori, J. et al., 2012. Agonist-Induced Hypertrophy and Diastolic Dysfunction Are Associated With Selective Reduction in Glucose Oxidation: A Metabolic Contribution to Heart Failure With Normal Ejection Fraction. *Circulation. Heart failure*, 5(4), pp.493–503.

Moser, M. & Frishman, W., 1998. Results of therapy with carvedilol, a beta-blocker vasodilator with antioxidant properties, in hypertensive patients. *American journal of hypertension*, 11(1 Pt 2), pp.15S–22S.

Mozaffarian, D. et al., 2016. Heart Disease and Stroke Statistics-2016 Update: A Report From the American Heart Association. *Circulation*, 133(4), pp.e38–360.

Muiesan, M.L. et al., 2004. Left ventricular concentric geometry during treatment adversely affects cardiovascular prognosis in hypertensive patients. *Hypertension*, 43(4), pp.731–738.

Müller-Brunotte, R. et al., 2007. Myocardial fibrosis and diastolic dysfunction in patients with hypertension: results from the Swedish Irbesartan Left Ventricular Hypertrophy Investigation versus Atenolol (SILVHIA). *Journal of Hypertension*, 25(9), pp.1958–1966.

Münzel, T., Daiber, A. & Mülsch, A., 2005. Explaining the Phenomenon of Nitrate Tolerance. *Circulation research*, 97(7), pp.618–628.

Myung, S.-K. et al., 2013. Efficacy of vitamin and antioxidant supplements in prevention of cardiovascular disease: systematic review and meta-analysis of randomised controlled trials. *BMJ (Clinical research ed.)*, 346(jan18 1), pp.f10–f10.

Nakamura, K. et al., 1998. Inhibitory effects of antioxidants on neonatal rat cardiac myocyte hypertrophy induced by tumor necrosis factor-alpha and angiotensin II. *Circulation*, 98(8), pp.794–799.

Nakayama, H. et al., 2009. α1G-dependent T-type Ca2+ current antagonizes cardiac hypertrophy through a NOS3-dependent mechanism in mice. *Journal of Clinical Investigation*, 119(12), pp.3787–3796.

Napoli, C. & Ignarro, L.J., 2001. Nitric Oxide and Atherosclerosis. *Nitric oxide : biology and chemistry / official journal of the Nitric Oxide Society*, 5(2), pp.88–97.

Napoli, C. et al., 2006. Nitric oxide and atherosclerosis: an update. *Nitric oxide : biology and chemistry / official journal of the Nitric Oxide Society*, 15(4), pp.265–279.

Nayak, A.S. et al., 1986. The Effect of Various Additives on the Stability of Isoproterenol Hydrochloride Solutions. 12(4), pp.589–601.

NICE, 2018. Diagnosis and management of adults with chronic heart failure: summary of updated NICE guidance. *BMJ (Clinical research ed.)*, 362, p.k4080.

NICE 2019, *Treating chronic heart failure with reduced ejection fraction,* viewed 10th November 2019 https://pathways.nice.org.uk/pathways/chronic-heart-failure#path=view%3A/pathways/chronic-heart-failure/treating-chronic-heart-failure-with-reduced-ejection-fraction.xml&content=view-node%3Anodes-surgical-interventions

O'Connor, C.M. et al., 2011. Effect of nesiritide in patients with acute decompensated heart failure. *The New England journal of medicine*, 365(1), pp.32–43.

Ohtsubo, T. et al., 2004. Xanthine Oxidoreductase Is an Endogenous Regulator of Cyclooxygenase-2. *Circulation research*, 95(11), pp.1118–1124.

Oudit, G.Y., 2003. Phosphoinositide 3-Kinase -Deficient Mice Are Protected From Isoproterenol-Induced Heart Failure. *Circulation*, 108(17), pp.2147–2152.

Packer, M. et al., 2015. Angiotensin receptor neprilysin inhibition compared with enalapril on the risk of clinical progression in surviving patients with heart failure. *Circulation*, 131(1), pp.54–61.

Paige, J.S. et al., 2008. Nitrosothiol reactivity profiling identifies S-nitrosylated proteins with unexpected stability. *Chemistry & biology*, 15(12), pp.1307–1316.

Palmer, R.M., Ferrige, A.G. & Moncada, S., 1987. Nitric oxide release accounts for the biological activity of endothelium-derived relaxing factor. *Nature*, 327(6122), pp.524–526.

Pan, X. et al., 2009. Nitric oxide suppresses transforming growth factor-beta1-induced epithelial-to-mesenchymal transition and apoptosis in mouse hepatocytes. *Hepatology (Baltimore, Md.)*, 50(5), pp.1577–1587.

Panza, J.A. et al., 1993. Role of endothelium-derived nitric oxide in the abnormal endothelium-dependent vascular relaxation of patients with essential hypertension. *Circulation*, 87(5), pp.1468–1474.

Panza, J.A., Quyyumi, A.A. & Brush, J.E., Jr, 1990. Abnormal endothelium-dependent vascular relaxation in patients with essential hypertension. *New England Journal …*, 323(1), pp.22–27.

Pechánová, O. et al., 1999. L-NAME-induced protein remodeling and fibrosis in the rat heart. *Physiological research*, 48(5), pp.353–362.

Peleli, M. et al., 2016. Enhanced XOR activity in eNOS-deficient mice: Effects on the nitrate-nitrite-NO pathway and ROS homeostasis. *Free radical biology & medicine*.

Pfeffer, M.A. et al., 1979. Myocardial infarct size and ventricular function in rats. *Circulation research*, 44(4), pp.503–512.

Pieske, B. et al., 2017. Vericiguat in patients with worsening chronic heart failure and preserved ejection fraction: results of the SOluble guanylate Cyclase stimulatoR in heArT failurE patientS with PRESERVED EF (SOCRATES-PRESERVED) study. *European heart journal*, 38(15), pp.1119–1127.

Pironti, G. et al., 2016. Dietary nitrate improves cardiac contractility via enhanced cellular Ca^{2+} signaling. *Basic Research in Cardiology*, 111(3), p.34.

Prabhu, S.D. et al., 2000. beta-adrenergic blockade in developing heart failure: effects on myocardial inflammatory cytokines, nitric oxide, and remodeling. *Circulation*, 101(17), pp.2103–2109.

Publication Committee for the VMAC Investigators (Vasodilatation in the Management of Acute CHF), 2002. Intravenous nesiritide vs nitroglycerin for treatment of decompensated congestive heart failure: a randomized controlled trial. *JAMA : the journal of the American Medical Association*, 287(12), pp.1531–1540. Available at: https://jamanetwork.com/journals/jama/fullarticle/194766.

Puhl, S.-L. et al., 2016. Assessing structural and functional responses of murine hearts to acute and sustained β-adrenergic stimulation in vivo. *Journal of pharmacological and toxicological methods*, 79, pp.60–71.

Qin, L. et al., 2012. Sialin (SLC17A5) functions as a nitrate transporter in the plasma membrane. *Proceedings of the National Academy of Sciences*, 109(33), pp.13434–13439.

Rahman, M., Douglas, J.G. & Wright, J.T., 1997. Pathophysiology and treatment implications of hypertension in the African-American population. *Endocrinology and metabolism clinics of North America*, 26(1), pp.125–144.

Ram, R. et al., 2011. New approaches in small animal echocardiography: imaging the sounds of silence. *AJP: Heart and Circulatory Physiology*, 301(5), pp.H1765–80.

Rapsomaniki, E. et al., 2014. Blood pressure and incidence of twelve cardiovascular diseases: lifetime risks, healthy life-years lost, and age-specific associations in 1·25 million people. *Lancet*, 383(9932), pp.1899–1911.

Raubenheimer, K. et al., 2017. Acute Effects of Nitrate-Rich Beetroot Juice on Blood Pressure, Hemostasis and Vascular Inflammation Markers in Healthy Older Adults: A Randomized, Placebo-Controlled Crossover Study. *Nutrients*, 9(11), p.1270.

Reungjui, S. et al., 2008. Do thiazides worsen metabolic syndrome and renal disease? The pivotal roles for hyperuricemia and hypokalemia. *Current opinion in nephrology and hypertension*, 17(5), pp.470–476.

Richards, A.M. et al., 1992. Effect of inhibition of endopeptidase 24.11 on responses to angiotensin II in human volunteers. *Circulation research*, 71(6), pp.1501–1507.

Rosamond, W.D. et al., 1998. Trends in the Incidence of Myocardial Infarction and in Mortality Due to Coronary Heart Disease, 1987 to 1994. *The New England journal of medicine*, 339(13), pp.861–867.

Rowland, N.E. & Fregly, M.J., 1988. Characteristics of thirst and sodium appetite in mice (Mus musculus). *Behavioral neuroscience*, 102(6), pp.969–974.

Ruperez, M. et al., 2003. Connective tissue growth factor is a mediator of angiotensin II-induced fibrosis. *Circulation*, 108(12), pp.1499–1505.

Sadoshima, J. et al., 1993. Autocrine release of angiotensin II mediates stretch-induced hypertrophy of cardiac myocytes in vitro. *Cell*, 75(5), pp.977–984.

Sakata, Y. et al., 1998. Decompensation of pressure-overload hypertrophy in G alpha q-overexpressing mice. *Circulation*, 97(15), pp.1488–1495.

Satoh, M. et al., 2006. Requirement of Rac1 in the development of cardiac hypertrophy. *Proceedings of the National Academy of Sciences of the United States of America*, 103(19), pp.7432–7437.

Saunders, E. et al., 1990. A comparison of the efficacy and safety of a beta-blocker, a calcium channel blocker, and a converting enzyme inhibitor in hypertensive blacks. *Archives of internal medicine*, 150(8), pp.1707–1713.

Saura, M. et al., 2005. Nitric oxide regulates transforming growth factor-beta signaling in endothelial cells. *Circulation research*, 97(11), pp.1115–1123.

Saura, M. et al., 2002. Smad2 mediates transforming growth factor-beta induction of endothelial nitric oxide synthase expression. *Circulation research*, 91(9), pp.806–813.

Schächinger, V., Britten, M.B. & Zeiher, A.M., 2000. Prognostic impact of coronary vasodilator dysfunction on adverse long-term outcome of coronary heart disease. *Circulation*, 101(16), pp.1899–1906.

Scherrer-Crosbie, M. et al., 2001. Endothelial nitric oxide synthase limits left ventricular remodeling after myocardial infarction in mice. *Circulation*, 104(11), pp.1286–1291.

Schinner, E. et al., 2017. Inhibition of the TGFβ signalling pathway by cGMP and cGMP-dependent kinase I in renal fibrosis. *FEBS open bio*, 7(4), pp.550–561.

Sciarretta, S., Volpe, M. & Sadoshima, J., 2014. Mammalian Target of Rapamycin Signaling in Cardiac Physiology and Disease. *Circulation research*, 114(3), pp.549–564.

Siervo, M. et al., 2013. Inorganic nitrate and beetroot juice supplementation reduces blood pressure in adults: a systematic review and meta-analysis. *The Journal of nutrition*, 143(6), pp.818–826.

Silberman, G.A. et al., 2010. Uncoupled cardiac nitric oxide synthase mediates diastolic dysfunction. *Circulation*, 121(4), pp.519–528.

Smith, C.J. et al., 1996. Reduced gene expression of vascular endothelial NO synthase and cyclooxygenase-1 in heart failure. *Circulation research*, 78(1), pp.58–64.

Soesanto, W. et al., 2009. Mammalian Target of Rapamycin Is a Critical Regulator of Cardiac Hypertrophy in Spontaneously Hypertensive Rats. *Hypertension*, 54(6), pp.1321–1327.

Sonoda, K. et al., 2017. Dietary nitrite supplementation attenuates cardiac remodeling in l-NAME-induced hypertensive rats. *Nitric oxide : biology and chemistry / official journal of the Nitric Oxide Society*, 67, pp.1–9.

Spiegelhalder, B., Eisenbrand, G. & Preussmann, R., 1976. Influence of dietary nitrate on nitrite content of human saliva: possible relevance to in vivo formation of N-nitroso compounds. *Food and cosmetics toxicology*, 14(6), pp.545–548.

SPRINT Research Group et al., 2015. A Randomized Trial of Intensive versus Standard Blood-Pressure Control. *The New England journal of medicine*, 373(22), pp.2103–2116.

Stirpe, F. & Corte, Della, E., 1969. The regulation of rat liver xanthine oxidase. Conversion in vitro of the enzyme activity from dehydrogenase (type D) to oxidase (type O). *The Journal of biological chemistry*, 244(14), pp.3855–3863.

Sun, Y. et al., 2009. Deletion of inducible nitric oxide synthase provides cardioprotection in mice with 2-kidney, 1-clip hypertension. *Hypertension*, 53(1), pp.49–56.

Tagawa, H. et al., 1998. Cytoskeletal role in the transition from compensated to decompensated hypertrophy during adult canine left ventricular pressure overloading. *Circulation research*, 82(7), pp.751–761.

Takimoto, E. et al., 2005. Oxidant stress from nitric oxide synthase-3 uncoupling stimulates cardiac pathologic remodeling from chronic pressure load. *Journal of Clinical Investigation*, 115(5), pp.1221–1231.

Tanimura, A. et al., 1999. Isoproterenol potentiates alpha-adrenergic and muscarinic receptor-mediated Ca2+ response in rat parotid cells. *The American journal of physiology*, 276(6), pp.C1282–7.

Tannenbaum, S.R., Weisman, M. & Fett, D., 1976. The effect of nitrate intake on nitrite formation in human saliva. *Food and cosmetics toxicology*, 14(6), pp.549–552.

Tesfamariam, B. & Halpern, W., 1988. Endothelium-dependent and endothelium-independent vasodilation in resistance arteries from hypertensive rats. *Hypertension*, 11(5), pp.440–444.

Treasure, C.B. et al., 1993. Hypertension and left ventricular hypertrophy are associated with impaired endothelium-mediated relaxation in human coronary resistance vessels. *Circulation*, 87(1), pp.86–93.

Tripatara, P. et al., 2007. Nitrite-derived nitric oxide protects the rat kidney against ischemia/reperfusion injury in vivo: role for xanthine oxidoreductase. *Journal of the American Society of Nephrology*, 18(2), pp.570–580.

Tsutsui, H., Kinugawa, S. & Matsushima, S., 2011. Oxidative stress and heart failure. *AJP: Heart and Circulatory Physiology*, 301(6), pp.H2181–90.

Velagaleti, R.S. et al., 2008. Long-term trends in the incidence of heart failure after myocardial infarction. *Circulation*, 118(20), pp.2057–2062.

Verdecchia, P. et al., 2009. Blood pressure reduction and renin-angiotensin system inhibition for prevention of congestive heart failure: a meta-analysis. *European heart journal*, 30(6), pp.679–688.

Vyssoulis, G.P. et al., 1995. Effect of beta-blockade on exercise capacity in hypertensive subjects: a one-year double-blind study of celiprolol and metoprolol. *Cardiovascular drugs and therapy / sponsored by the International Society of Cardiovascular Pharmacotherapy*, 9(1), pp.133–139.

Webb, A. et al., 2004. Reduction of nitrite to nitric oxide during ischemia protects against myocardial ischemia–reperfusion damage. 101(37), pp.13683–13688.

Webb, A.J., Milsom, A.B., et al., 2008. Mechanisms Underlying Erythrocyte and Endothelial Nitrite Reduction to Nitric Oxide in Hypoxia Role for Xanthine Oxidoreductase and Endothelial Nitric Oxide Synthase. 103(9), pp.957–964.

Webb, A.J., Patel, N., Loukogeorgakis, S., Okorie, M., Aboud, Z., Misra, S., Rashid, R., Miall, P., Deanfield, J., Benjamin, N., Macallister, R., Hobbs, A.J. & Ahluwalia, A., 2008a. Acute blood pressure lowering, vasoprotective, and antiplatelet properties of dietary nitrate via bioconversion to nitrite. *Hypertension*, 51(3), pp.784–790.

Webb, A.J., Patel, N., Loukogeorgakis, S., Okorie, M., Aboud, Z., Misra, S., Rashid, R., Miall, P., Deanfield, J., Benjamin, N., Macallister, R., Hobbs, A.J. & Ahluwalia, A., 2008b. Acute blood pressure lowering, vasoprotective, and antiplatelet properties of dietary nitrate via bioconversion to nitrite. *Hypertension*, 51(3), pp.784–790.

Weber, K.T., Brilla, C.G. & Janicki, J.S., 1993. Myocardial fibrosis: functional significance and regulatory factors. *Cardiovascular research*, 27(3), pp.341–348.

Whalen, E.J. et al., 2007. Regulation of β-Adrenergic Receptor Signaling by S-Nitrosylation of G-Protein-Coupled Receptor Kinase 2. *Cell*, 129(3), pp.511–522.

Whelton, P.K. et al., 1997. Effects of Oral Potassium on Blood Pressure: Meta-analysis of Randomized Controlled Clinical Trials. *JAMA : the journal of the American Medical Association*, 277(20), pp.1624–1632.

Wilck, N. et al., 2018. Nitric oxide-sensitive guanylyl cyclase stimulation improves experimental heart failure with preserved ejection fraction. *JCI insight*, 3(4), p.181.

Wolhuter, K. et al., 2018. Evidence against Stable Protein S-Nitrosylation as a Widespread Mechanism of Post-translational Regulation. *Molecular cell*, 69(3), pp.438–450.e5.

Xie, L. et al., 2009. Amelioration of experimental autoimmune encephalomyelitis by curcumin treatment through inhibition of IL-17 production. *International immunopharmacology*, 9(5), pp.575–581.

Xing, F. et al., 2017. Real role of β-blockers in regression of left ventricular mass in hypertension patients: Bayesian network meta-analysis. *Medicine*, 96(10), p.e6290.

Xu, J. et al., 2010. Local angiotensin II aggravates cardiac remodeling in hypertension. *American journal of physiology. Heart and circulatory physiology*, 299(5), pp.H1328–H1338.

Xu, L. et al., 1998. Activation of the cardiac calcium release channel (ryanodine receptor) by poly-S-nitrosylation. *Science (New York, N.Y.)*, 279(5348), pp.234–237.

Yang, F. et al., 2009. Angiotensin II induces connective tissue growth factor and collagen I expression via transforming growth factor-beta-dependent and -independent Smad pathways: the role of Smad3. *Hypertension*, 54(4), pp.877–884.

Yang, T. et al., 2017. Dietary nitrate attenuates renal ischemia-reperfusion injuries by modulation of immune responses and reduction of oxidative stress. *Redox biology*, 13, pp.320–330.

Yang, T. et al., 2015. Inorganic nitrite attenuates NADPH oxidase-derived superoxide generation in activated macrophages via a nitric oxide-dependent mechanism. *Free radical biology & medicine*, 83, pp.159–166.

Ye, Y. et al., 2001. High-energy phosphate metabolism and creatine kinase in failing hearts: a new porcine model. *Circulation*, 103(11), pp.1570–1576.

Yui, Y. et al., 2010. Reverse remodeling and improved function by antihypertensive treatment in hypertensive patients with coronary artery disease. *Journal of Hypertension*, 28(1), pp.178–185.

Zablocki, D. & Sadoshima, J., 2013. Angiotensin II and oxidative stress in the failing heart. *Antioxidants & redox signaling*, 19(10), pp.1095–1109.

Zafari, A.M. et al., 1998. Role of NADH/NADPH oxidase-derived H2O2 in angiotensin II-induced vascular hypertrophy. *Hypertension*, 32(3), pp.488–495.

Zamani, P. et al., 2015. Effect of inorganic nitrate on exercise capacity in heart failure with preserved ejection fraction. *Circulation*, 131(4), pp.371–80– discussion 380.

Zamani, P. et al., 2014. Inorganic Nitrate Supplementation Improves Exercise Capacity in Subjects with HF with Preserved EF - A Pilot Study. *Journal of cardiac failure*, 20(8 Suppl), p.S4.

Zamani, P. et al., 2017. Pharmacokinetics and Pharmacodynamics of Inorganic Nitrate in Heart Failure With Preserved Ejection Fraction. *Circulation research*, 120(7), pp.1151–1161.

Zhang et al., 1998. Generation of nitric oxide by a nitrite reductase activity of xanthine oxidase: a potential pathway for nitric oxide formation in the absence of nitric oxide synthase activity. *Biochemical and biophysical research communications*, 249(3), pp.767–772.

Zhang et al., 1997. Human xanthine oxidase converts nitrite ions into nitric oxide (NO).

Zhang, Y., Dai, M. & Yuan, Z., 2018. Methods for the detection of reactive oxygen species. *Analytical Methods*, 10(38), pp.4625–4638.

Zhao, Q.D. et al., 2015. NADPH oxidase 4 induces cardiac fibrosis and hypertrophy through activating Akt/mTOR and NFκB signaling pathways. *Circulation*, 131(7), pp.643–655.

Zhong, J. et al., 2010. Angiotensin-converting enzyme 2 suppresses pathological hypertrophy, myocardial fibrosis, and cardiac dysfunction. *Circulation*, 122(7), pp.717–28– 18 p following 728.